Studies of Fv1 binding and restriction

Ho Leung Wilson Li

February 2015

Division of Virology
MRC National Institute for Medical Research
The Ridgeway
Mill Hill, London
NW7 1AA

This thesis is submitted to University College London
for the degree of Doctor of Philosophy

I, Ho Leung Wilson Li, confirm that the work presented in this thesis is my own. Where information has been derived from other sources, I confirm that this has been indicated in the thesis.

Abstract

Host restriction factors such as Fv1 in mice and Trim5α in primates block retroviral infection through their interaction with capsids. One major form of Fv1, encoded by the $Fv1^b$ allele, restricts only N-tropic MLV (N-MLV) when expressed at the lower endogenous level, but also restricts B-tropic MLV (B-MLV) and NB-tropic MLV (NB-MLV) at the higher levels seen in cells transduced with $Fv1^b$-expressing retroviral vector. However, a previous pull-down study detected almost equal binding of $Fv1^b$ to all three MLV capsids. In this study, the relationships between Fv1 binding, restriction and expression level were studied in detail.

To study the restriction specificity of $Fv1^b$ at different expression levels, new Tet-On vectors were developed to allow doxycycline-inducible expression of Fv1. These vectors allowed restriction studies from a very low $Fv1^b$ level where no restriction could be observed, to a high level where inhibitions of B-MLV and NB-MLV are also observed. Similar phenomenon is also observed in other Fv1 mutants. By contrast, $Fv1^n$, even when over-expressed, restricted only B-MLV but not NB-MLV or N-MLV. The binding of $Fv1^b$ to different capsids at different Fv1 concentration were compared using a new pull-down assay performed on microtitre plates. $Fv1^b$ appears to bind to all MLV capsids at the lowest concentration of Fv1 where binding could be detected. The study was extended to include other Fv1 mutants, and as expected binding could be detected for all restrictive Fv1-MLV pairs. Interestingly, a few outliers including $Fv1^b$ vs B-MLV demonstrated strong binding but either weak or low restriction, suggesting there may be other factors causing the lack of restriction. Together, these data suggest that although $Fv1^b$ have very similar apparent binding affinities to different MLV capsids, different amount of $Fv1^b$ are required for the restriction of N-, B- and NB-MLV.

Dedication

I dedicate this thesis to my family, especially:

To my father, Thomas Li
To my mother, Shirley Leung
To my grandmother, Annie Wing-Mui Yung
To the memory of my late grandfather, Ho-Shiu Lee

For all their love, support, and encouragement.

Acknowledgements

I would like to express my sincere gratitude to my supervisor, Jonathan Stoye, for his guidance and mentorship. I would like to thank members of my thesis committee, Ian Taylor, Kate Bishop and Peter Rosenthal, for their advice and comments.

I would also like to thank many people, both past and present at the NIMR, for their assistance and support: Melvyn Yap, Ophélie Cosnefroy, Laura Hilditch, Victoria Felton, Marta Sanz-Ramos, Paula Ordonez, Sadayuki Ohkura, Alex Xiaoli Xiong, Seti Grambas, Graham Preece, Bhavik Patel, Neil Ball, David Goldstone, Rishi Matadeen, Madushi Wanaguru, Kate Holden-Dye, Darren Wight, Virginie Boucherit, Mirella Nader, Harriet Groom, Cécile Lemaître, Sam Fraser and Donna Brown.

I am also grateful to all my previous mentors in science, including Andrew Lever, Ulrich Desselberger, Stuart Siddell, Dan Quinton, John Jones, Keith Simpson, Damian Jones and Yuk-Chong Keung.

Lastly, I wish to thank my family and friends, especially John Elliott, for their support and encouragement.

Table of Content

List of figures

List of tables

Abbreviations

aa	Amino acid
AGM	African green monkey
ALV	Avian leukaemia virus
AIDS	Acquired immunodeficiency syndrome
APOBEC	Apolipoprotein C mRNA-editing enzyme catalytic polypeptide
B-MLV	B-tropic MLV
BCA	Bicinchoninic acid (assay)
BET	Bromodomain and extra-terminal
Bio PE	18:1 1,2-dioleoyl-sn-glycero-3-phosphoethanolamine-N-(biotinyl) (sodium salt)
BioCap PE	18:1 1,2-dioleoyl-sn-glycero-3-phosphoethanolamine-N-(cap biotinyl) (sodium salt)
BioPEG PE	1,2-distearoyl-sn-glycero-3-phosphoethanolamine-N-[biotinyl(polyethylene glycol)-2000] (ammonium salt)
BSA	Bovine serum albumin
CA	Capsid
CAE	Cytoplasmic accumulation element
Cβ	Beta-carbons
CCD	Catalytic core domain
cDNA	Complementary DNA
CMV	Cytomegalovirus
cppt	Central polypurine tract
CPSF6	Cleavage and polyadenylation specific factor 6
Cs	Cyclosporin
CTD	C-terminal domain
CTS	Central termination sequence
CypA	Cyclophilin A
DEST	Gateway destination cassette
DGS-NTA	1,2-dioleoyl-sn-glycero-3-[(N-(5-amino-1-carboxypentyl) iminodiacetic acid)succinyl]
DIS	Dimerisation initiation signal

DLS	Dimer linkage site
DMEM	Dulbecco’s Modified Eagle Medium
DMSO	Dimethyl sulfoxide
Dox	Doxycycline
DNA	Deoxyribonucleic acid
EDTA	Ethylenediaminetetraacetic acid
EGFP	Enhanced green fluorescent protein
EYFP	Enhanced yellow fluorescent protein
EIAV	Equine infectious anaemia virus
ELISA	Enzyme-linked immunosorbent assay
EMCV	Encephalomyocarditis virus
Env	Envelope precursor protein
ER	Endoplasmic reticulum
ESCRT	Endosomal sorting complexes required for transport
FACS	Fluorescence Activated Cell Sorter/ Flow cytometry
FCS	Foetal calf serum
FFV	Feline foamy virus
FIV	Feline immunodeficiency virus
Fv-MLV	Friend MLV
FV	Friend Virus
Fv1	Friend virus susceptibility-1
Fv1Cyp	Fv1(20-200) CypA fusion protein
Gag	Group-specific antigen precursor protein
GalCer	Galactosylceramide
GFP	Green fluorescent protein
GOI	Gene of interest
GPCR	G-Protein-Coupled Receptor
GPI	Glycophospatidylinositol
HERV	Human endogenous retrovirus
HIV	Human immunodeficiency virus
HSV	Herpes simplex virus
HTLV	Human T-cell lymphotropic virus
HuT5	Human Trim5α
HuT5HA	Human Trim5α with C-terminal HA-tag
IFITM	Interferon inducible transmembrane (protein)

IN	Integrase
IPTG	Isopropyl β-D-1-thiogalactopyranoside
IRES	Internal ribosome entry site
kD	Kilodalton
L1	Linker-1
L2	Linker-2
LB	Luria Broth
L-domain	Late assembly domain
LTR	Long terminal repeat
MA	Matrix
MERV	Murine endogenous retrovirus
MHR	Major homology region
Miip	Migration and invasion inhibitory protein
MOI	Multiplicity of infection
MLV	Murine leukaemia virus
MMTV	Mouse mammary tumour virus
MPMV	Mason-Pfizer monkey virus
MDTF	*Mus dunni* tail fibroblast
MWCO	Molecular weight cut off
Mx2	Myxovirus resistance 2
N-MLV	N-tropic MLV
NB-MLV	NB-tropic MLV
NC	Nucleocapsid
NES	Nuclear export signal
NLS	Nuclear localisation signal
NMR	Nuclear magnetic resonance
NPC	Nuclear pore complex
NTD	N-terminal domain
OMK	Owl monkey
ORF	Open reading frame
PAGE	Polyacrylamide gel electrophoresis
PBMC	Peripherial blood mononuclear cells
PBS	Phosphate buffered saline
PBS-T	PBS supplemented with 0.1% Tween-20
pbs	Primer binding site

PCR	Polymerase Chain Reaction
PE	Phosphatidylethanolamine
PERV	Porcine endogenous retrovirus
PFV	Prototypic foamy virus
PIC	Pre-integration complex
PIP_2	Phosphatidyl inositol (4,5) bisphosphate
PKCα	Protein kinase Cα
Pol	Polymerase precursor protein
ppt	Polypurine tract
PR	Protease
PS	Phosphatidyl serine
PVDF	Polyvinylidene fluoride
qPCR	Quantitative PCR
R	Repeated element of LTR
RBCC	RING, B-box 2 and coiled-coil
REAF	RNA-associated early-stage anti-viral factor
RhT5	Rhesus Trim5α
RhT5HA	Rhesus Trim5α with C-terminal HA-tag
RIPA	Radioimmunoprecipitation assay (buffer)
RNA	Ribonucleic acid
RNP	Ribonucleoprotein
RRE	Rev-responsive element
RSV	Rous sarcoma virus
RT	Reverse transcriptase
RTC	Reverse transcription complex
rtTA	Reverse tetracycline-controlled transactivator
SA	Splice acceptor
SAMHD1	SAM domain and HD domain containing protein 1
SCC	Single cell lone
SD	Splice donor
SDS	Sodium dodecyl sulfate
SFFV	Spleen focus forming virus
SFV	Simian foamy virus
SIN	Self-inactivating (vector)
SIV	Simian immunodeficiency virus

SIV_{cpz}	SIV from chimpanzee
SIV_{mac}	SIV from rhesus macaque
SIV_{sm}	SIV from sooty mangabey
SP1	Short spacer 1
SP2	Short spacer 2
SU	Surface subunit of Env
T5	Trim5α
T5-21R	Trim5α with RING domain of Trim21
T5HA	Trim5α with C-terminal HA-tag
TAR	Trans-activation response
TCyp	Trim5-CypA
TEMED	Tetramethylethylenediamine
tetO	Tet operator
TM	Transmembrane subunit of Env
TNPO3	Transportin 3
TRE	Tetracycline-responsive element
Trim	Tripartite motif
TYMV	Turnip yellow mosaic virus
tRNA	Transfer RNA
WDSV	Walleye dermal sarcoma virus
U3	Unique 3’ element of LTR
U5	Unique 5’ element of LTR
VSV-g	Vesicular stomatitis virus glycoprotein
XMRV	Xenotropic MLV-related virus
YFP	Yellow fluorescent protein
ψ	Packaging signal

Chapter 1

Introduction

Retroviruses are enveloped viruses which involve two important features in their life cycles: the synthesis of complementary DNA (cDNA) from viral RNA template (reverse transcription), and the insertion of viral cDNA into the genomes of infected cells to form a provirus (integration). As pathogens to many animal species, retroviruses have important implications for human and animal health. This literature review focuses on the biology of two retroviruses, murine leukaemia virus (MLV) and human immunodeficiency virus type 1 (HIV-1). The intrinsic mechanisms used by the host cells to defend against these retroviruses and the counteracting strategies developed by these retroviruses will be discussed in detail, with emphases on two capsid-binding restriction factors, Friend virus susceptibility-1 (Fv1) and Trim5α (T5).

1.1 Retroviruses

1.1.1 Classification

Early retrovirus classification systems assigned virus particles into type A, B, C and D based on the morphology of viral particles observed using thin-section electron microscopy techniques (Vogt, 1997). In the later classification system, the family of retroviridae is divided into two sub-families (Figure 1.1) – orthoretrovirinae and spumaretrovirinae (Stoye et al., 2011). Orthoretrovirinae consists of 6 different genera of retroviruses – alpha-retroviruses such as Rous sarcoma virus (RSV), beta-retroviruses such as mouse mammary tumour virus (MMTV), gamma-retroviruses such as MLV, delta-retroviruses such as human T-cell lymphotropic virus type 1 (HTLV-1), epsilon-retroviruses such as walleye dermal sarcoma virus (WDSV), and lentiviruses such as HIV-1. Particles of orthoretroviruses contain an RNA genome, which is reverse-transcribed into

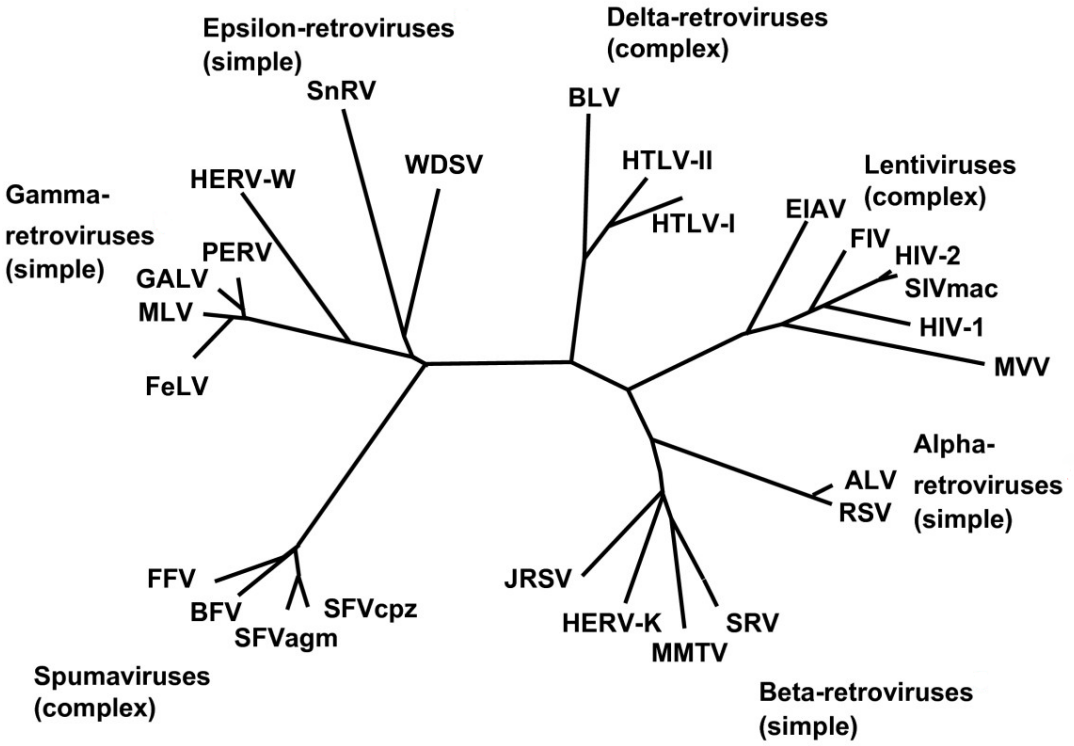

Figure 1.1 Phylogeny of retroviruses

A phylogenetic tree showing the approximate relatedness in sequences from different retroviral genera. Reproduced from (Weiss, 2006), with permission under BioMed Central open access policy and the Creative Commons Attribution (CC BY) license.

cDNA upon entry into the target cell. Spumavirinae comprise a single genus of spumaviruses such as Prototypic foamy virus (PFV). In contrast to orthoretroviruses, spumaviruses display features resembling hepadnaviruses including a DNA genome resulted from the completion of reverse transcription in the producer cell (Moebes et al., 1997) and the budding of nascent particles through intracellular compartments (Hutter et al., 2013).

Retroviruses could also be classified as complex or simple retroviruses based on their genome organisations and gene regulations (Cullen, 1991). Simple retroviruses consist of members from alpha-retroviruses, gamma-retroviruses, epsilon-retroviruses (Weiss, 2006) and some beta-retroviruses including Mason-Pfizer monkey virus (MPMV) (Hayward et al., 2013). These viruses contain a relatively simple genomic structure with viral proteins expressed from unspliced and singly spliced viral RNAs. In contrast, complex retroviruses including members of delta-retroviruses, lentiviruses, spumaviruses (Weiss, 2006) and some beta-retroviruses including MMTV (Hayward et al., 2013; Mertz et al., 2005) encode viral proteins for transcriptional regulation and for nuclear export of viral RNA. Many complex retroviruses also regulate the expression of some viral proteins through multiply spliced viral RNAs.

1.1.2 History of retrovirus discovery

Discovery of RNA tumour viruses

The discovery of retroviruses began in the early 20th century, when equine infectious anaemia was found to be transmittable between horses via a filterable agent (Vallée and Carré, 1904), later identified as the lentivirus equine infectious anaemia virus (EIAV). This was followed by numerous observations of transmission of tumours between animals by infectious agents in cell-free filtrates. These included the transmission of leukaemia in chicken by avian leukaemia virus (ALV) in filtered cell extract (Ellermann and Bang, 1908); the transmission of spindle-cell sarcoma in chicken by RSV in filtered cell extract (Rous, 1911); the transmission of mammary carcinoma in mice by MMTV in filtered milk (Bittner, 1936); the transmission of leukaemia by MLV in filtered cell extract (Gross, 1951); and the transmission of epidermal hyperplasia in fish by WDSV (Walker, 1969). The infectious agents were found to be viruses

containing RNA (Crawford and Crawford, 1961), and were known as RNA tumour viruses. Reverse transcriptase activity, a hallmark of retroviruses, was later detected in RNA tumour viruses (Baltimore, 1970; Temin and Mizutani, 1970).

First isolations of primate and human retroviruses

Isolation of retrovirus from primates was first described when "foamy viral agents", later known as simian foamy virus (SFV), was isolated from rhesus monkey kidney cells (Enders and Peebles, 1954; Rustigian et al., 1955). PFV was subsequently isolated from human nasopharyngeal carcinoma cells (Achong et al., 1971). However, genetic analyses showed that PFV is not a human retrovirus, but most likely a variant of SFV in chimpanzees resulted from a zoonotic transmission (Brown et al., 1978). A human retrovirus was first described in 1980, when HTLV-1 was isolated as the causative agent of adult T-cell leukaemia/lymphoma (ATLL) (Poiesz et al., 1980). A related virus, HTLV-2, was isolated shortly after (Kalyanaraman et al., 1982). More recently, HTLV-3 (Calattini et al., 2005; Wolfe et al., 2005) and HTLV-4 (Wolfe et al., 2005) have also been identified.

Discovery of human and simian immunodeficiency viruses

The global epidemic of acquired immunodeficiency syndrome (AIDS) was first recognised in 1981, when clustered cases of opportunistic infections and Kaposi's sarcoma were reported in the USA (Gottlieb et al., 1981). In 1983, a retrovirus was isolated from lymphatic tissue of a French AIDS patient (Barre-Sinoussi et al., 1983), and this virus is now known as HIV-1. A related virus, simian immunodeficiency virus (SIV_{mac}), was isolated from a rhesus macaque with simian AIDS (Daniel et al., 1985). A second human virus, HIV-2, was isolated from a West African AIDS patient (Clavel et al., 1986). Subsequent genetic analyses revealed different origins of HIV-1 and HIV-2. While SIV_{mac} and HIV-2 were closely related to SIV from sooty mangabey (SIV_{sm}) (Hirsch et al., 1989), HIV-1 appears to be derived from chimpanzee SIV (SIV_{cpz}) (Huet et al., 1990). While HIV-1 is responsible for most infections in the global AIDS pandemic, HIV-2 infection remains rare outside West Africa (Sharp and Hahn, 2011).

Discovery of endogenous retrovirus

While exogenous retroviruses described above were transmitted “horizontally” from host to host, endogenous retroviruses were transmitted “vertically” through genetic inheritance of provirus after infection of gamete cells such as oocytes (Weiss, 2006). The insertion of endogenous retroviruses to the host genome is often detrimental to the host (Stoye, 2012). Although some copies of endogenous retroviruses are replication-competent, most of them are defective due to deletions or point mutations in their genomes. Endogenous retroviruses have been identified in all vertebrate species (Stoye, 2012). The description of endogenous retroviruses began in late 1960s with an observation that ALV group-specific antigen (Gag) could be inherited in ALV-free chicken as a dominant gene following Mendelian genetics (Payne and Chubb, 1968). This was followed shortly by the detection of retroviral particles resembling MLV (Aaronson et al., 1969; Lowy et al., 1971) and MMTV (Bentvelzen and Daams, 1969; Bentvelzen et al., 1970) released from inbred laboratory mice. Endogenous retroviruses in the human genome have been problematic for the identification of infectious human retroviruses due to the high background of PCR signals from endogenous sequences. This contributed to the numerous reports of human “rumour” viruses with suspected disease etiologies, many have never been confirmed (Voisset et al., 2008). Porcine endogenous retroviruses (PERVs, a gamma-retrovirus) released from pig cells (Armstrong et al., 1971) were found to be able to infect human cell lines (Patience et al., 1997), causing concerns on whether zoonotic infection of PERVs could be resulted from xenotransplantation of pig cells or organs to human. However, later studies found no evidence of human infection from pig xenografts *in vivo* (Elliott et al., 2000; Gu et al., 2008; Heneine et al., 1998; Paradis et al., 1999; Patience et al., 1998; Scobie et al., 2013). Endogenous spurmavirus sequences have been identified in genomes of human, lemur, sloth and fish (Cordonnier et al., 1995; Han and Worobey, 2012a, b; Katzourakis et al., 2009; Rethwilm and Bodem, 2013). Different lineages of endogenous lentiviruses have been identified in the genomes of rabbits and hares (Katzourakis et al., 2007; Keckesova et al., 2009; van der Loo et al., 2009), weasels (Cui and Holmes, 2012; Han and Worobey, 2012c), lemurs (Gifford et al., 2008; Gilbert et al., 2009) and colugos (Han and Worobey, 2015; Hron et al., 2014). It has been estimated that human endogenous retroviruses (HERVs) comprise almost 8%

of the human genome (Denner, 2010). HERVs identified in the human genome were related to beta-retroviruses (e.g. HERV-K), gamma-retroviruses (e.g. HERV-H, HERV-W, HERV-FRD) or spumaviruses (e.g. HERV-L, HERV-S) (Blikstad et al., 2008). While most HERVs open reading frames (ORFs) became defective after accumulation of mutations, some had evolved with the host genome to become functional genes (Stoye, 2012). For example, the *env* genes of HERV-W and HERV-FRD, known as *syncytin-1* (Blond et al., 2000; Mi et al., 2000) and *syncytin-2* (Blaise et al., 2003), mediate cell-to-cell fusion events during human placental development (Dupressoir et al., 2012).

1.1.3 Genome organisation and gene expression

Long terminal repeats and untranslated regions

Each orthoretrovirus particle contains a dimer of genomic RNAs, which are capped at the 5' end (Beemon and Keith, 1977) and polyadenylated at the 3' end (Guntaka, 1993). The genome organisation of proviruses of a simple retrovirus (MLV) and a complex retrovirus (HIV-1) is shown in Figure 1.2. Identical long terminal repeats (LTR) are found at 5' and 3' ends of integrated retroviral genomes (Bannert et al., 2010). Each LTR contains the unique 3' element (U3), followed by the repeated element (R), and finally the unique 5' element (U5). In the provirus, sequences within the U3 region of the 5' LTR functions as a promoter for the transcription of viral RNA. The transcription of retroviral RNA starts at the beginning of the R region of the 5' LTR, and the polyadenylation signal in the 3' LTR marks the end of the R region. The transcribed viral RNA contains the R-U5 sequence at the 5' end, and the U3-R sequence before the poly-A tail at the 3' end. The R sequences at the 5' and 3' ends are essential for the transfer of DNA strands during reverse transcription. Binding sites for trans-activating proteins encoded by complex retroviruses can also be found within the LTR. The primer binding site (pbs) is found immediate downstream of the U5 region, and serves as the binding site for cellular tRNA primer required for the initiation of reverse transcription. The 5' untranslated region (UTR) also contains sequence responsible for genome dimerisation known as dimer linkage sites (DLSs). Sequences found to confer RNA encapsidation into virions (ψ-site) are present within the 5' UTR, often overlapping with the DLS, and may extend into the *gag* coding region. The 3'

UTR contains a polypurine tract (ppt) upstream of the 3' LTR for priming of plus strand synthesis during reverse transcription. Some complex retroviruses including lentiviruses contain a second plus strand priming site known as central polypurine tract (cppt) (Charneau and Clavel, 1991).

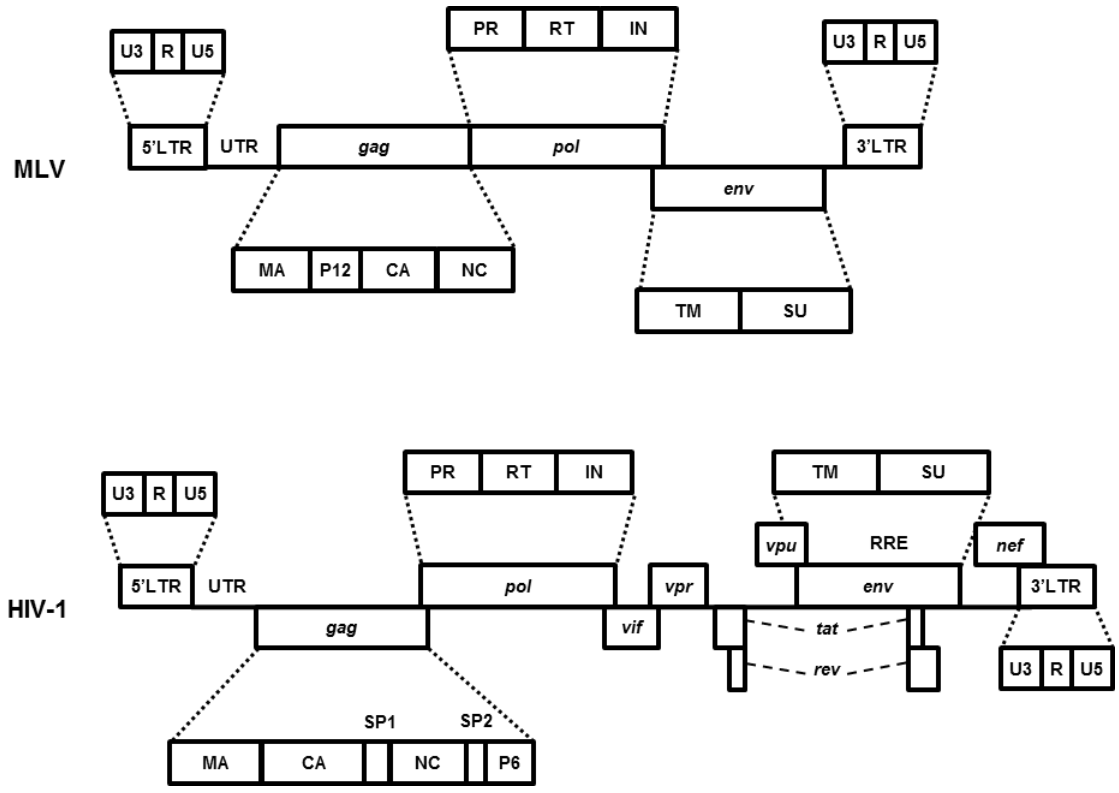

Figure 1.2 Genome organisations of MLV and HIV-1

Schematic diagrams of the untranslated and coding regions of MLV and HIV-1 proviral genomes. LTR, long terminal repeat; UTR, untranslated region; MA, matrix; CA, capsid; NC, nucleocapsid; PR, protease; RT, reverse transcriptase; IN, integrase; TM, transmembrane domain; SU, surface domain; RRE, Rev-responsive element. Gag and Gag-Pol are synthesised as precursor polyproteins, and processed into individual proteins and small peptides by the viral protease during maturation. In MLV, Gag-Pol is expressed by ribosome read-through of the *gag* stop codon into the in-frame *pol* ORF. In HIV-1, the translation of Gag-Pol involves a -1 ribosomal frame shift at the boundary of *gag* and *pol* ORFs. Env is processed into TM and SU by a cellular protease. HIV-1 also expresses accessory genes for functions including gene regulation and antagonism of host restriction factors.

Expression of Gag, Pol and Env

All retroviral genomes contain at least 3 genes: *gag*, *pol* and *env*. The Gag precursor protein contains subunits which are important for virus assembly and integrity of viral core, including matrix (MA), capsid (CA) and nucleocapsid (NC). With the exception of spumaviruses, these subunits are released as individual proteins upon cleavage by the viral protease during maturation. In many retroviruses, other small proteins are also released from Gag during maturation. MLV Gag is processed into MA, p12, CA and NC proteins, while HIV-1 is processed into MA, CA, SP1, NC, SP2 and p6 proteins (Bannert et al., 2010). In MLV, an alternative form of Gag known as Glyco-Gag is synthesised by translational initiation from an upstream CUG codon (Prats et al., 1989). The resulting 80kD protein includes a leader peptide in the N-terminus, which directs the protein to the Golgi complex for glycosylation. The *pol* gene is expressed in the form of a Gag-Pol precursor protein, which in MLV was produced by the translational read-through of the UAG amber stop-codon of the *gag* ORF using the cellular suppressor $tRNA^{Glu}$ (Yoshinaka et al., 1985), facilitated by a pseudoknot structure of the viral RNA (Wills et al., 1991). The ribosomal read through occurs at 5-10% efficiency (Jamjoom et al., 1976). In HIV-1, the synthesis of Gag-Pol involves a -1 ribosomal frameshift at 5-10% efficiency (Jacks et al., 1988). The processing of Gag-Pol yields three important enzymes: protease (PR), reverse transcriptase (RT) and integrase (IN). The Env precursor protein is translated from a spliced mRNA lacking most of Gag-Pol sequence. This transcript results from a splicing event between a splice donor (SD) in the 5' UTR and a splice acceptor (SA) close the start codon of *env* gene. The precursor protein undergoes extensive co- and post-translational modification in the endoplasmic reticulum (ER) and the Golgi complex, and cleaved into an N-terminal surface subunit (SU) and a C-terminal trans-membrane subunit (TM).

Expression of accessory genes

In addition to the expression of *gag*, *pol* and *env* genes, complex retroviruses such as HIV-1 also encode a large number of accessory proteins namely Vif, Vpr, Vpu, Tat, Rev and Nef. These accessory genes are found towards the 3' end of the genome, on either side of the *env* gene. In HIV-1, some accessory genes such as *vif*, *vpr* and *vpu* are from a singly spliced transcript, with *vpu* and

env expressed from the same bicistronic transcript (Schwartz et al., 1990). The trans-activator *tat*, the RNA nuclear export protein *rev*, and *nef* are expressed from multiply spliced transcripts. The Rev responsive element (RRE), an RNA element which interacts with Rev, is present in the *env* coding region between the introns of *tat* and *rev*. The RRE is present in unspliced and singly spliced HIV-1 transcripts, but not in multiply spliced transcripts encoding Tat and Rev. In the late stage of gene expression, Rev mediates the selective nuclear export of RRE-containing unspliced and singly spliced transcripts. This leads to a switch from the translation of gene regulatory proteins from multiply spliced RNA, to the expression of structural proteins and packaging of unspliced genomic RNA.

1.1.4 Retroviral particles

Retrovirus particles are roughly spherical with diameters ranging from 100 to 150nm (Bannert et al., 2010). Structures of typical retrovirus particles are shown in diagrammatic form in Figure 1.3. The outermost layers of retrovirus particles consist of an envelope with lipid bilayer and Env complexes. These Env complexes contain heavily glycosylated SU trimers joined to TM trimers on lipid bilayer by disulphide bonds (Opstelten et al., 1998). Orthoretrovirus particles can contain either mature or immature cores, while only immature cores can be found in spumavirus particles. Electron microscopy studies of immature cores showed electron-dense radial striations beneath the lipid membrane (Fuller et al., 1997; Yeager et al., 1998). These striations are formed by polymerised Gag and Gag-Pol proteins, with the N-terminal MA domain attached to the lipid bilayer and the C-terminus NC domain of gag bound to viral RNA. The maturation of retroviral particles is triggered by the proteolytic processing of Gag precursor protein (de Marco et al., 2010b). Mature retroviral cores are more condensed than immature cores, and are formed by processed Gag subunits. The morphologies of mature cores vary from roughly spherical core of MLV, tubular core of MPMV, to conical core of HIV-1 (Yeager, 2011). In mature particles, MA proteins are bound to the lipid bilayer, CA proteins form a condensed capsid shell, and NC proteins form a condensed ribonucleoprotein (RNP) complex with genomic RNA dimers inside the capsid shell.

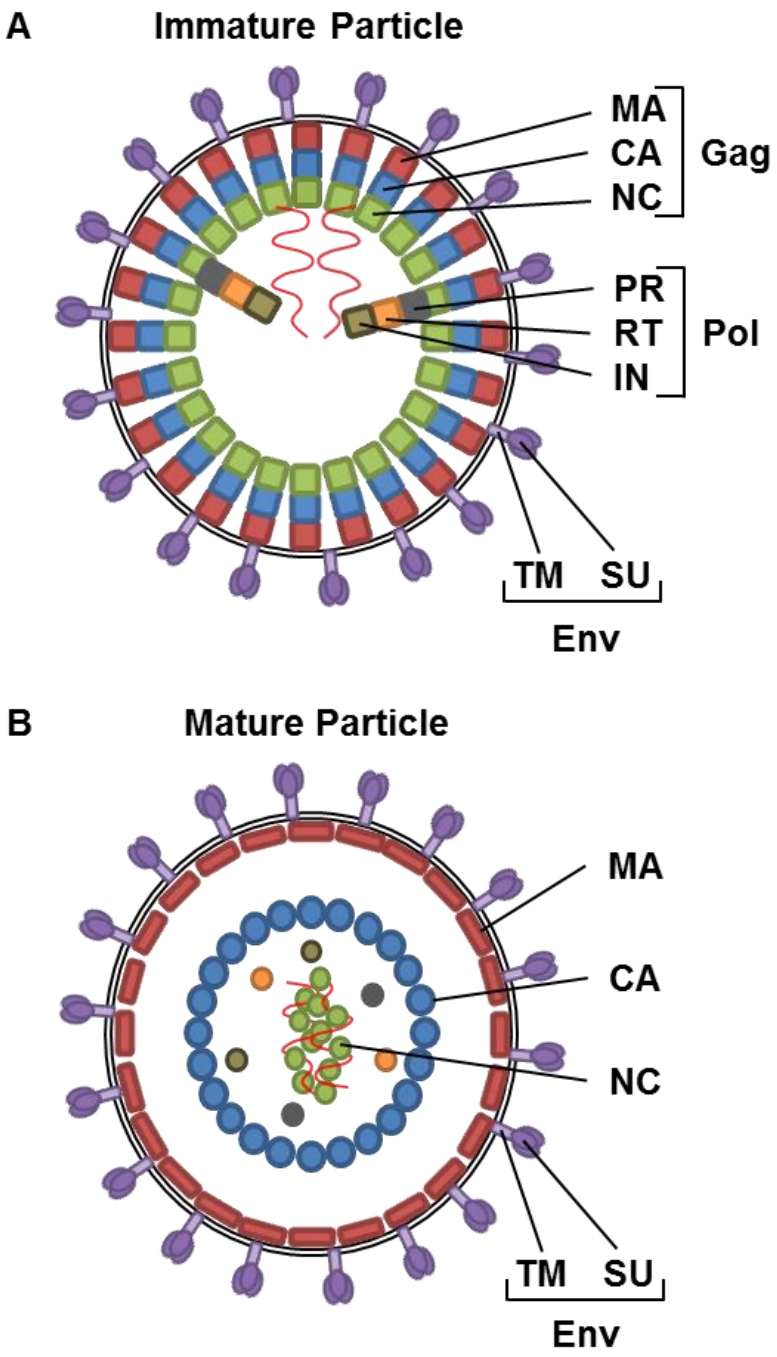

Figure 1.3 Typical immature and mature retroviral particle structures

(A) A typical immature retroviral particle with an envelope consists of lipid bilayer and envelope proteins, and an immature core consists of Gag, Gag-Pol and dimeric RNA genome. (B) A typical mature retroviral particle formed after the processing of Gag and Gag-Pol precursor proteins. The MA layer remains tethered to the viral membrane, the CA proteins form the capsid shell of the mature core, while the NC protein forms a ribonucleoprotein (RNP) complex with genomic RNAs. In addition, retrovirus particles incorporate many host proteins, lipids and RNA molecules (Bannert et al., 2010).

1.1.5 Retroviral proteins

Matrix

The key function of the MA subunit is to target Gag to lipid membrane during virus assembly. Despite the lack of sequence conservation, all retroviral MA subunits have similar topologies with a globular core formed by 4 helices (Conte and Matthews, 1998). The HIV-1 MA subunit has been crystallised as trimers (Hill et al., 1996), while the MLV MA subunit has been crystallised as dimers (Riffel et al., 2002). Membrane-bound HIV-1 MA has also been found to assemble into hexamers of trimers, suggesting the presence of two interfaces for multimerisation (Alfadhli et al., 2009a; Alfadhli et al., 2007). The N-terminus of MA subunit in gag is modified cotranslationally by the removal of Met1 and the attachment of the myristic acid, a 14-carbon saturated fatty acid, to the second amino acid of MA in many retroviruses including MLV and HIV-1 (Bryant and Ratner, 1990; Rein et al., 1986). The myristoylation of Gag is essential for the interaction between Gag and lipid bilayer. A patch of surface exposed basic residues is found close to the N-terminus of all retroviral MA, and has been hypothesised to participate in the membrane targeting of Gag through interactions with acidic head groups of phospholipids (Murray et al., 2005). In addition to lipid binding, there are some evidence of interactions between HIV-1 MA and RNA (Alfadhli et al., 2009b; Chukkapalli et al., 2013; Chukkapalli et al., 2010).

Capsid

A number of roles in multiple stages of retroviral life cycle has been suggested for CA proteins, including the formation of a curved polymerised lattice of Gag during budding (Carlson et al., 2008), the assembly of the capsid shell of condensed cores during maturation (de Marco et al., 2010b), the protection of viral nucleic acids from the detection by innate sensors (Rasaiyaah et al., 2013), as well as the recruitment of host factors for nuclear entry (Schaller et al., 2011). CA consists of two largely α-helical structural domains, the N-terminal domain (CA-NTD) and the C-terminal domain (CA-CTD). CA either as a subunit of Gag or as an individual protein forms hexameric rings, which are the main building blocks of the retroviral capsid shell (Burns, 2009; Ganser-Pornillos et al., 2007; Mortuza et al., 2008; Mortuza et al., 2004; Pornillos et al., 2009). CA

is also the target of many host restriction factors such as Fv1, T5 and Mx2 (Bock et al., 2000; Goujon et al., 2014; Yap et al., 2004). Details on the structure and function of CA will be discussed in the next section.

Nucleocapsid

Through its nucleic acid binding and chaperone activities, NC is important for multiple steps of the retroviral life cycle including assembly, maturation, reverse transcription, and possibly integration. Orthoretroviral NC contains one (MLV) or two (HIV-1) Cys-X_4-Cys-X_4-His-X_4-Cys zinc fingers (Summers et al., 1992), which has been shown to form tight interactions with the exposed residues of ψ-sites present on full-length genomic RNA (D'Souza and Summers, 2004; Dannull et al., 1994; De Guzman et al., 1998; Schuler et al., 1999). In addition to the zinc fingers, many basic residues also contribute towards RNA binding (Dannull et al., 1994). The abilities of Gag to bind genomic RNA through its NC subunit and to multimerise through its CA subunits are crucial for core assembly. In addition to the strong affinity for ψ-sites, Gag-NC subunits also display non-specific binding and chaperone activities towards nucleic acids (reviewed in Rein, 2010). Gag-NC subunits have been proposed to facilitate the dimerisation of genomic viral RNA and annealing of tRNA primer to pbs in producer cells through its chaperone activity. After Gag processing, the non-specific nucleic acid binding activity of NC is important for condensation of RNA or DNA. During maturation, NC binds to viral genomic RNA to form a condensed RNP complex. Binding of NC to DNA has also been shown to induce DNA condensation *in vitro* (Krishnamoorthy et al., 2003). The exact role of RNA and DNA condensation by NC is unclear, but may include the protection of nucleic acids from nuclease attack and innate sensing.

Envelope

The retroviral Env complex mediates receptor binding and membrane fusion during viral entry. Env undergoes a number of modifications including glycosylation (Bernstein et al., 1994; Pinter and Honnen, 1988) and sulfation (Bernstein and Compans, 1992), and is processed by cellular proteases during its transit through the ER and the Golgi network. The resulting Env complex consists of a SU trimer anchored to a TM trimer by disulphide bonds (Opstelten et al., 1998). In HIV-1, the SU subunit is known as gp120, while the TM subunit

is known as gp41. Presented on the exterior of the Env complex, the SU subunit is heavily glycosylated and is mediates binding to cellular receptors. The TM subunit contains a fusion peptide which is inserted into target membranes upon receptor binding for membrane fusion (Mothes and Uchil, 2010). In addition to SU and TM subunits, the MLV Env precursor contains a 16aa C-terminal R-peptide which inhibits membrane fusion activity of Env before viral bidding (Bobkova et al., 2002; Loving et al., 2011; Loving et al., 2008).

Protease

PR is required for the processing of Gag and Gag-Pol precursors into individual proteins during maturation. Retroviral aspartic proteases form homodimers, with catalytic aspartic acids inside the substrate binding pocket (Lapatto et al., 1989; Li et al., 2005; Miller et al., 1989; Navia et al., 1989; Weber et al., 1989). The processing of Gag and Gag-Pol is carried out sequentially, due to differences in cleavage rates at different processing sites (Erickson-Viitanen et al., 1989).

Reverse transcriptase

RT carries out reverse transcription of the viral genomic RNA. The structure and organisation of RT gene products differs among retroviruses. The MLV RT is a monomeric protein with an N-terminal polymerase domain and a C-terminal RNaseH domain (Das and Georgiadis, 2004). The polymerase domain synthesises DNA using either RNA or DNA as template, while the RNaseH domain degrades RNA from DNA/RNA hybrids. HIV-1 RT is a heterodimer of p66 and p51 subunits (Sarafianos et al., 2001). The two HIV-1 RT subunits were generated from Gag-Pol using different C-terminal cleavage sites, with p51 lacking the RNaseH domain.

Integrase

IN catalyses the insertion of viral DNA into host chromosome. IN contains 3 functional domains; an N-terminal domain (IN-NTD) containing a zinc finger motif, a catalytic core domain (IN-CCD) and the C-terminal domain (IN-CTD). Complex formation of HIV-1 IN and viral DNA involves tetramerisation of IN (Li et al., 2006a). Although the structure of full length HIV-1 IN has not been solved, crystal structure of complexes with full length PFV IN and viral DNA has

revealed a “dimer of dimer”, with DNA binding surfaces and catalytic sites at the dimer-dimer interface (Hare et al., 2010). IN also interacts with chromatin tethering factors, such as LEDGF which binds lentiviral IN (Cherepanov et al., 2005; Hare et al., 2009), and BET proteins which bind MLV IN (De Rijck et al., 2013; Gupta et al., 2013; Sharma et al., 2013).

MLV p12

p12 is located between MA and CA subunits in the Gag of MLV. Nuclear magnetic resonance (NMR) studies of Gag fragments containing p12 and CA-NTD showed that p12 domain is unstructured (Kyere et al., 2008). Purified p12 is monomeric (Wight et al., 2012). Functional motifs have been identified in p12, including the PPPY late domain which recruits an endosomal sorting complexes required for transport (ESCRT) protein HECT ubiquitin ligase for budding (Martin-Serrano et al., 2005; Yuan et al., 1999) and a clathrin binding domain (Zhang et al., 2011). Regions close to the N-terminus (p12-NTD) and the C-terminus (p12-CTD) of p12 are required for the infectivity of MLV (Yuan et al., 1999). p12-CTD is required for the localisation of p12 to mitotic chromatin (Prizan-Ravid et al., 2010), and loss of infectivity by mutations in p12-CTD could be rescued by heterologous chromatin-binding sequence (Elis et al., 2012; Schneider et al., 2013; Wight et al., 2012). The exact function of p12-NTD is not known, but cores with mutations in this region were not recognised by capsid-binding restriction factors, suggesting a defect in core morphology (Wight et al., 2012).

HIV-1 SP1 and SP2

Processing of HIV-1 gag releases two spacer peptides (SP1 and SP2) and a small protein p6. The SP1 links CA-CTD to NC in Gag. The SP1 peptide contains a hypothetical α-helix (Morellet et al., 2005), which has been proposed to form a 6-helix bundle under each CA hexamers in HIV-1 Gag (de Marco et al., 2010b; Wright et al., 2007). The temporal control of the processing of the 14aa SP1 and 16aa SP2 from adjacent domains have important roles in maturation, evident from the impaired core morphologies of cleavage site mutants (de Marco et al., 2012; de Marco et al., 2010b).

HIV-1 p6

The HIV-1 p6 protein is derived from the C-terminus of Gag. NMR studies showed that p6 consists of two helices joined by a flexible linker (Fossen et al., 2005), and both helices have been found to interact with lipid membrane (Solbak et al., 2013). Two late domains are present in p6 for recruitment of ESCRT proteins for budding, including the PTAP motif near the N-terminus which binds Tsg101; and the YPXL motif in the C-terminal helix which binds Alix (Demirov et al., 2002; Solbak et al., 2013; Strack et al., 2003). The helices of p6 also contain motifs for the recruitment of the accessory protein, Vpr (Salgado et al., 2009; Zhu et al., 2004).

HIV-1 p6*

The transframe protein p6*, encoded by the N-terminal sequence of the *pol* gene, is one of the cleavage products of GagPol precursor protein. p6* is involved in the regulation of the activity of PR (Paulus et al., 1999; Zybarth and Carter, 1995).

HIV-1 Tat and Rev

Complex retroviruses encode transactivator proteins to stimulate transcription of viral RNA, these include Tat of HIV-1 (Muesing et al., 1987), Tax of HTLV-1 (Felber et al., 1985; Fujisawa et al., 1985; Sodroski et al., 1984) and Tas of SFV (Campbell et al., 1996). Tat interacts with a stem-loop structure known as trans-activation response (TAR) at the 5’ end of the viral RNA for transactivation (Chun and Jeang, 1996; Feng and Holland, 1988). Complex retroviruses also encode viral proteins for selective nuclear export of full length and singly spliced RNA containing the RRE, leading to a switch from the expression of accessory genes to the translation of structural proteins (Cullen, 1991). These nuclear export proteins include Rev of HIV-1 (Malim et al., 1989), Rex of HTLV-1 (Hanly et al., 1989) and Rem of MMTV (Mertz et al., 2005). For simple retroviruses such as MLV and MPMV, the nuclear export of viral RNA depends on cis-acting RNA elements, and requires only host proteins but not viral proteins (Pasquinelli et al., 1997; Sakuma et al., 2014).

HIV-1 Vif, Vpu, Vpr and Nef

Vif was found to counteract restriction by multiple members of the APOBEC3 family (Desimmie et al., 2014). Vpu, which forms ion channels at lipid membranes, antagonises the restriction by tetherin (McNatt et al., 2013; Neil et al., 2008). Env, Nef and Vpu have all been found to downregulate the HIV-1 receptor CD4 on cell surface, which has been hypothesised to avoid superinfection of cells which may increase immune sensing (Wildum et al., 2006). Nef also downregulates a number of cell surface immune proteins (Basmaciogullari and Pizzato, 2014). The HIV-1 vpr, which is incorporated into viral particles via p6, has been shown in a large number of studies to cause cell cycle arrest and apoptosis (Guenzel et al., 2014).

1.2 Capsid structure and core assembly

1.2.1 Sequence and structural elements of CA

Retroviral CA consists of two largely α-helical structural domains, CA-NTD and CA-CTD. Structures of CA-NTD of many retroviruses had been solved by crystallography or NMR, and were found to be highly similar despite of the lack of sequence conservation (Bailey et al., 2012; Cornilescu et al., 2001; Ganser-Pornillos et al., 2007; Gitti et al., 1996; Jin et al., 1999; Mortuza et al., 2008; Mortuza et al., 2009; Mortuza et al., 2004; Pornillos et al., 2009). Among the structures of the CA-NTD is the β-hairpin, which is present at the N-terminus of CA. In crystal structures of CA-NTD, the β-hairpin is stabilised by a salt bridge between Pro1 and Asp54 in MLV (Mortuza et al., 2004), and between Pro1 and Asp51 in HIV-1 (Gitti et al., 1996). The rest of CA-NTD contains 6 (MLV) or 7 (HIV-1) α-helices, and a flexible loop between α4 and α5 which in HIV-1 CA interacts with the host protein cyclophilin A (CypA) (Gamble et al., 1996). A stretch of sequence highly conserved among all retroviruses, known as the major homology region (MHR), is found in the CA-CTD. Many conserved residues of MHR were found to be essential for virus assembly and infectivity (Chang et al., 2007; Ganser-Pornillos et al., 2004; von Schwedler et al., 2003). At the C-terminus of MLV CA, a stretch of 41aa highly charged residues has been predicted to form α-helical structure, termed the charged assembly helix (Cheslock et al., 2003). The charged assembly helix is essential for infectivity and virus assembly, although it can tolerate deletion of up to 22aa (Cheslock et al., 2003). The HIV-1 equivalent of the charged assembly helix is thought to be the SP1 peptide, which can form an α-helix under certain conditions and is important for the assembly of viral core (Datta et al., 2011; de Marco et al., 2010b).

1.2.2 The CA hexamer

Early crystal structures of HIV-1 CA-NTD and CA-CTD suggested that both domains may form dimers (Gamble et al., 1996; Gamble et al., 1997; Worthylake et al., 1999). However, electron cryo-tomography studies of N-terminally His-tagged HIV-1 and MLV CA immobilised on lipid monolayer containing a nickel-chelating lipid revealed a regular capsid array formed of hexameric symmetry units (Barklis et al., 1998; Barklis et al., 1997). *In vitro* capsid assemblies can be formed by CA or CA-NC at a high salt concentration (1M NaCl), or by mixing CA-NC with RNA (Campbell and Vogt, 1995; Ehrlich et al., 1992). These assemblies form a mixture of conical and tubular structures, and mutations have been identified to favour the formation of tubes (Ganser-Pornillos et al., 2004; Ganser et al., 1999). The regularity of tubular capsid assemblies allowed high resolution (9Å) electron cryo-microscopy studies of the HIV-1 CA array, and docking of known CA-NTD and CA-CTD crystal or NMR structures to generate structural models of the CA hexamer (Ganser-Pornillos et al., 2007). This model (Figure 1.4) shows extensive contacts between CA-NTD of each CA monomer, and led to identification of pairs of cysteine mutations in CA-NTD which could mediate disulphide crosslinking between monomers for stabilisation of CA hexamer (Pornillos et al., 2010). It also shows potential CTD-CTD inter-hexameric interactions, from which mutations can be identified to destabilise this interaction to assist structural studies by x-ray crystallography (Ganser-Pornillos et al., 2007). These crosslinking mutations, together with mutations for destabilisation of interaction between CTD domains, were introduced to CA to solve the crystal structure of full length HIV-1 CA hexamer (Pornillos et al., 2009). This hexamer structure is formed by two concentric rings: the CA-NTD forms the inner ring with β-hairpin at the central pore; the CA-CTD contains 4 α-helices, forms the outer ring, and mediates inter-hexameric interactions. CA-NTD of each monomer interacts with both CA-NTD and CA-CTD of the neighbouring monomer to form intra-hexameric interactions.

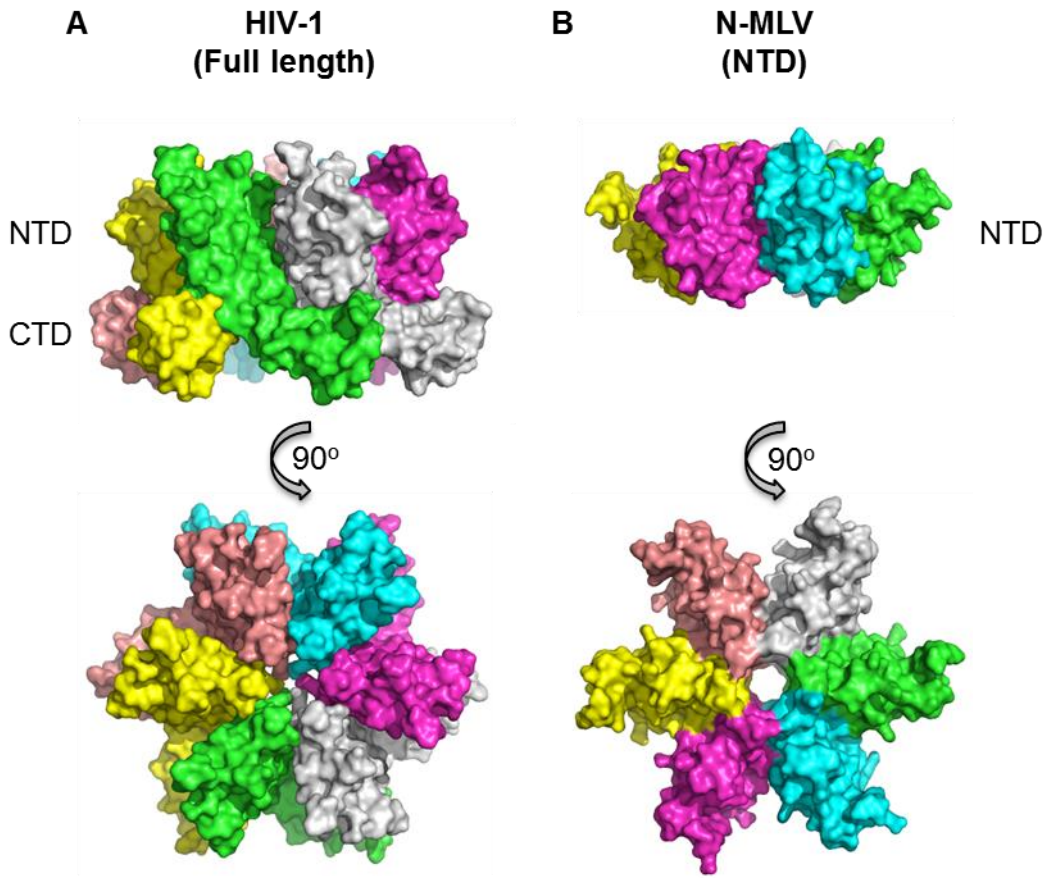

Figure 1.4 Hexameric structures of HIV-1 and MLV CA

(A) Crystal structure of full-length HIV-1 CA A14C/E45C/W184A/M185A crosslinked hexamer, PDB: 3H47 (Pornillos et al., 2009). (B) Crystal structure of N-MLV CA-NTD hexamer, PDB: 1U7K (Mortuza et al., 2004). Each individual CA monomer is labelled in different colour in both structures using PyMol. The bottom panels show the structures of CA hexamers as viewed from exterior of virus particles.

CA-NTDs from different strains of MLV have been crystallised as hexamers without the need of disulphide stabilisation (Burns, 2009; Mortuza et al., 2008; Mortuza et al., 2004). Like HIV-1, CA-NTD monomers form a hexameric ring with the β-hairpin at the centre (Figure 1.4), held by NTD-NTD interactions. The structure of full length MLV CA with deletion of the charged assembly helix has been solved (Burns, 2009). In this structure, the CA-CTD contains 5 α-helices, and forms an outer hexameric ring. Similar to HIV-1 CA, hexamers are stabilised by interactions between CA-NTD and both NTD and CTD of the neighbour CA monomer. These studies showed that despite the many differences between HIV-1 and MLV, their CA form conserved hexameric CA structures which serve as building blocks of retroviral cores.

1.2.3 Structure of the mature capsid shell

The cores of HIV-1 mature particles are typically conical in shape, with a thinner shell compared to cores of immature particles. Electron cryo-tomography studies suggested that like the *in vitro* CA assemblies, natural cores are also formed of hexamers (Briggs et al., 2003). Models on how CA hexamers can be arranged into conical core have been proposed and refined (Ganser et al., 1999; Li et al., 2000; Pornillos et al., 2011; Zhao et al., 2013). The formation of cores would require contacts between hexamers. Since HIV-1 CA-CTD is present in the outer ring, inter-hexameric interactions are likely to be between CA-CTDs (Pornillos et al., 2009). Because CA-CTD has been crystallised as dimers, it has been proposed that HIV-1 CA-CTD are linked through interactions at a dimer interface (Gamble et al., 1997; Ivanov et al., 2007; Worthylake et al., 1999). This is consistent with the apparent CTD-CTD contacts observed from high resolution electron cryo-tomography studies of *in vitro* CA tubular assemblies (Byeon et al., 2009; Ganser-Pornillos et al., 2007; Li et al., 2000). Some of these studies also suggested an additional trimer interface forming inter-hexameric contacts, and mutations at this trimer interface leads to loss of infectivity (Byeon et al., 2009; Zhao et al., 2013). Therefore, the linkage between HIV-1 hexamers requires CTD-CTD linkage at both dimer and trimer interfaces. Early modelling of the HIV-1 core suggested that the insertion of 12 CA pentamers in addition to hexamers would be required to form the conical core (Ganser et al., 1999). The formation of HIV-1 CA pentamers can be

stabilised by disulphide crosslinking, and the crystal structures of pentamer and hexamer show high similarity in the inter-molecular interactions (Pornillos et al., 2011). The most recent structural model of the HIV-1 core was generated with CA hexamers and pentamers joined by interactions at the CTD-CTD dimer and trimer interfaces (Zhao et al., 2013). In contrast to HIV-1, mature MLV cores are polygonal in a roughly spherical shape, and may not require the need of pentamers (Yeager et al., 1998). Crystal structures of MLV CA suggested that CA hexamers are joined by CTD-CTD dimerisation (Burns, 2009). The formation of CTD-CTD interactions between hexamers is in agreement from data from study of N-terminally His-tagged MLV CA (Ganser et al., 2003).

1.2.4 Comparison of mature and immature capsid lattice

Immature particles contain electron-dense radial striations beneath the lipid membrane composed mainly of polymerised Gag (Fuller et al., 1997; Yeager et al., 1998). In an immature core, both the N- and C-termini of CA in Gag are tethered to other Gag subunits, and the organisations of CA-NTD and CA-CTD are different from those in the mature lattice. Electron cryo-tomography studies of HIV-1 immature particles revealed that the CA-SP1 region are arranged in a "Y-shape" (Figure 1.5), with the six CA monomers of each hexamer interconnected and forming a rod-like structure at the SP1 region (de Marco et al., 2010b; Wright et al., 2007). The immature lattice can be mimicked by *in vitro* assemblies of Gag fragment in which CA is tethered at one or both ends. The Y-shape arrangement of such immature lattice was also observed in *in vitro* assemblies of a Gag fragment (MA-SP2 with internal MA deletion) with nucleic acids (de Marco et al., 2010a). High resolution electron cryo-tomography study of HIV-1 CA-NC tubes suggested that in the immature lattice, CA-CTD forms hexamers, with SP1 forming a bundle of 6 helices underneath (Bharat et al., 2014). The organisation of the CA-CTD layer in immature core is unknown in MLV, but the charged assembly helix has been proposed to function in a similar way to SP1 (Cheslock et al., 2003). A recent study of *in vitro* assembly of xenotropic MLV-related virus (XMRV) CA-NC with a 10aa N-terminal deletion did show a rod-like structure between folded domains of CA-CTD and NC (Hadravova et al., 2012).

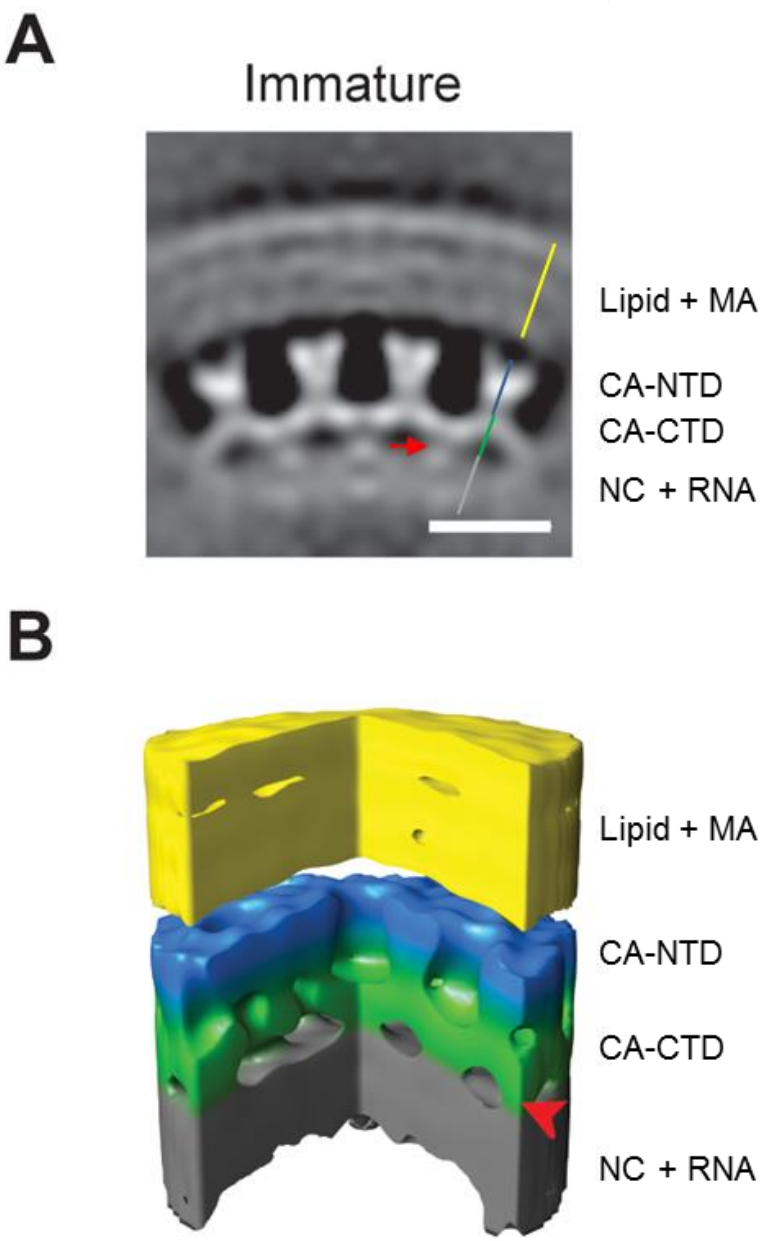

Figure 1.5 The HIV-1 immature gag lattice

A) Reconstruction of the HIV-1 immature gag lattice from averaged electron tomogram of immature particles. Red arrow indicates the position of a rod-like protrusion which may be formed by SP1. Scale bar is 10nm. B) Surface rendering of the reconstruction shown in (A). The lipid membrane and MA layers in yellow, CA-NTD in blue, CA-CTD and SP1 in green, and NC-RNA in grey. Rod-like protrusions, which may be formed by SP1, are indicated by the red arrow. Modified from (de Marco et al., 2010b), with permission under PLOS open-access license and the Creative Commons Attribution (CC BY) license.

The processing of the N-terminus of Gag is also important for the transition from immature to mature lattice. NMR studies have shown that the β-hairpin is unfolded in Gag of both MLV and HIV-1 (Kyere et al., 2008; Tang et al., 2002), but stabilised by a salt bridge in the structure of CA-NTD (Burns, 2009; Mortuza et al., 2008; Mortuza et al., 2004; Pornillos et al., 2009). Disruption of the salt bridge by mutagenesis blocks virus assembly and leads to changes in the morphologies of *in vitro* CA or CA-NC assemblies from tubular to spherical structures (Abdurahman et al., 2007; Cortines et al., 2011; Gross et al., 1998; Hadravova et al., 2012; von Schwedler et al., 1998). One study compared the crystal structures of MLV CA with or without insertion of a 4aa sequence in the N-terminus to mimic immature and mature CA, respectively (Burns, 2009). In the structure with an N-terminal extension, the β-hairpin is unfolded, and interactions are formed between NTD hexamers at 2-fold and 3-fold interfaces. In the structure with an authentic N-terminus, the β-hairpin is stabilised, and the inter-hexamer spacing increases from 79Å in immature-like structure to 99Å in mature-like structure. The NTD-NTD inter-hexameric interactions are lost due to the increased inter-hexameric spacing. Similar increases in inter-hexamer spacing from 80Å in immature lattices to 96Å in mature lattices have also been observed in HIV-1 particles (Briggs et al., 2004). These studies suggested processing at the boundary of the CA domain can lead to the rearrangement of CA-NTD and CA-CTD, including an increase in the inter-hexameric spacing.

1.3 Retroviral replication

The retroviral life cycle can be divided into two phases: the early phase (Figure 1.6) begins with viral entry and ends after integration, while the late phase (Figure 1.7) begins with the transcription of viral RNA and ends after the maturation of virus particle.

1.3.1 Entry

Receptor binding

Retrovirus particles are first attached to the cell surface via weak interactions with cell surface molecules such as heparan sulphate for HIV-1 (Saphire et al., 2001) and heparin for MLV (Walker et al., 2002), before encountering their cellular receptor. In MLV, the use of receptor varies among different strains, which contributes to the MLV tropism. Based on their host range, MLV strains can be classified into ecotropic, xenotropic, polytropic and amphotropic subgroups (Hunter, 1997). Ecotropic MLVs only infects mouse or rat cells, and includes exogenous viruses such as N-tropic MLV (N-MLV), B-tropic MLV (B_MLV), and NB-tropic Moloney MLV (NB-MLV). Ecotropic MLV use the mouse cationic amino acid transporter (mCAT-1) as the receptor (Albritton et al., 1989). Polytrophic, xenotropic and amphotropic MLVs can infect a broad range of mammalian cells with slight differences in their host ranges. Amphotropic MLVs use the sodium-dependent phosphate transporter Pit-2 as the receptor (Kavanaugh et al., 1994). Polytrophic and xenotropic MLVs use different alleles of the cell surface protein Xpr1 as receptor (Kozak, 2010). Xpr1 functions as an atypical G-Protein-Coupled Receptor (GPCR) in mammalian cells (Vaughan et al., 2012). HIV-1 uses CD4, a glycoprotein found on the surface of many immune cells including $CD4^+$ T-cells, as the primary receptor (Klatzmann et al., 1984). In addition, entry of HIV-1 requires either CXCR4 (Feng et al., 1996) or CCR5 (Alkhatib et al., 1996) as co-receptor.

Membrane fusion

The MLV SU subunit of Env contains a CXXC motif, in which one of the cysteine residue forms intermolecular disulphide bond with the TM subunit

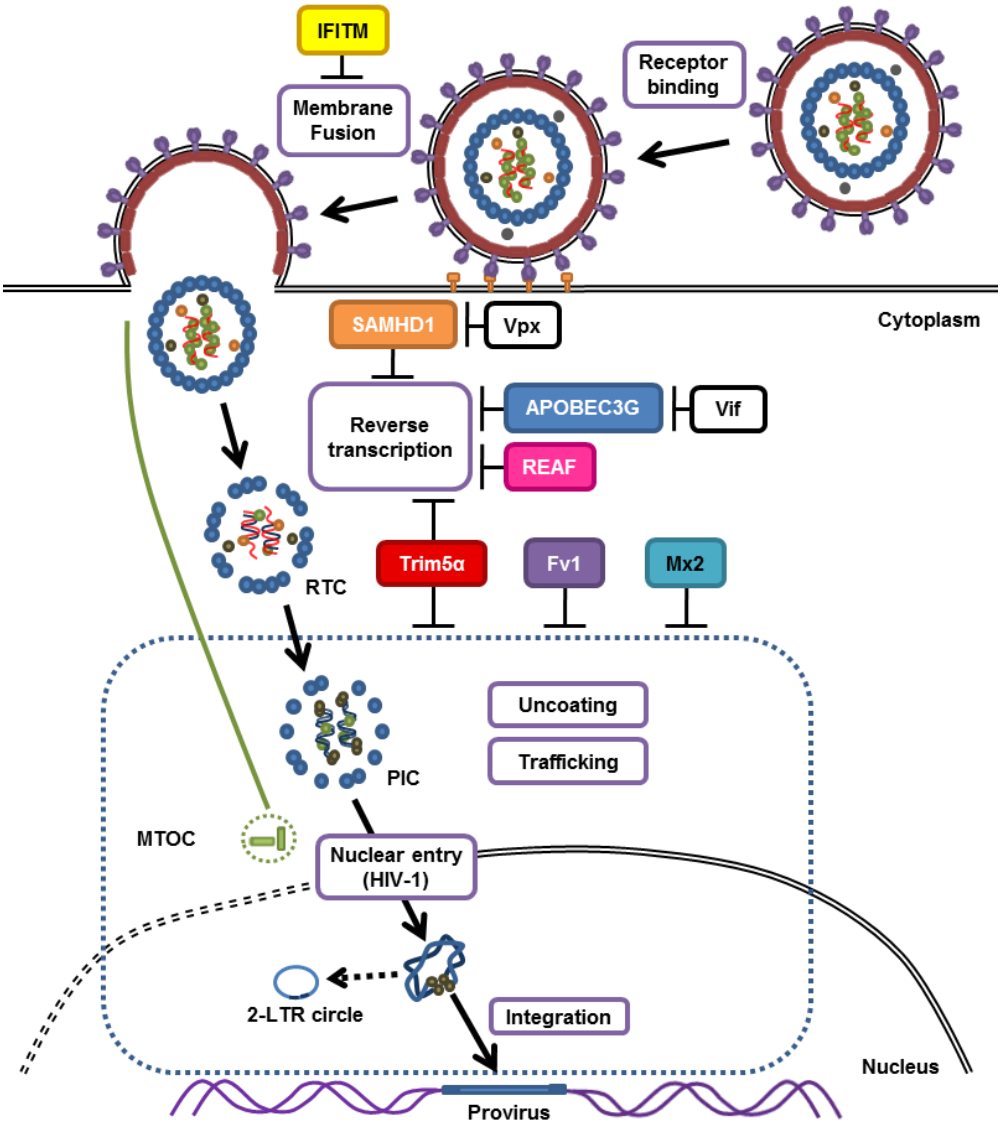

Figure 1.6. The early stage of the retrovirus life cycle

A schematic diagram showing steps in the early stage of retroviral life cycle (boxes with purple border), host restriction factors which target these steps (coloured boxes), and viral antagonists which counteract restrictions by these restriction factors (boxes with black border). Binding of mature retroviral particles leads to fusion between viral and host membranes, a process which can be inhibited by IFITM. Reverse transcription of viral DNA occurs once the viral core is released to the cytoplasm. Many restriction factors including APOBEC3G, SAMHD1, REAF and T5 inhibit reverse transcription. The complex in which reverse transcription occurs is defined as reverse transcription complexes (RTC). The RTC is transformed into an integration-competent pre-integration complex (PIC) during its transit on microtubule network towards the microtubule organising centre (MTOC) at the periphery of the nuclear envelope. Uncoating of the capsid shell occurs at some point between the viral entry and nuclear entry. HIV-1 PIC is actively transported into the nucleus, while MLV PIC only enters the nucleus after the disassembly of nuclear envelope during mitosis. Integration of viral DNA into the host genome occurs after nuclear entry. Capsid-targeting restriction factors Fv1, T5 and Mx2 all impose a block after reverse transcription and before integration.

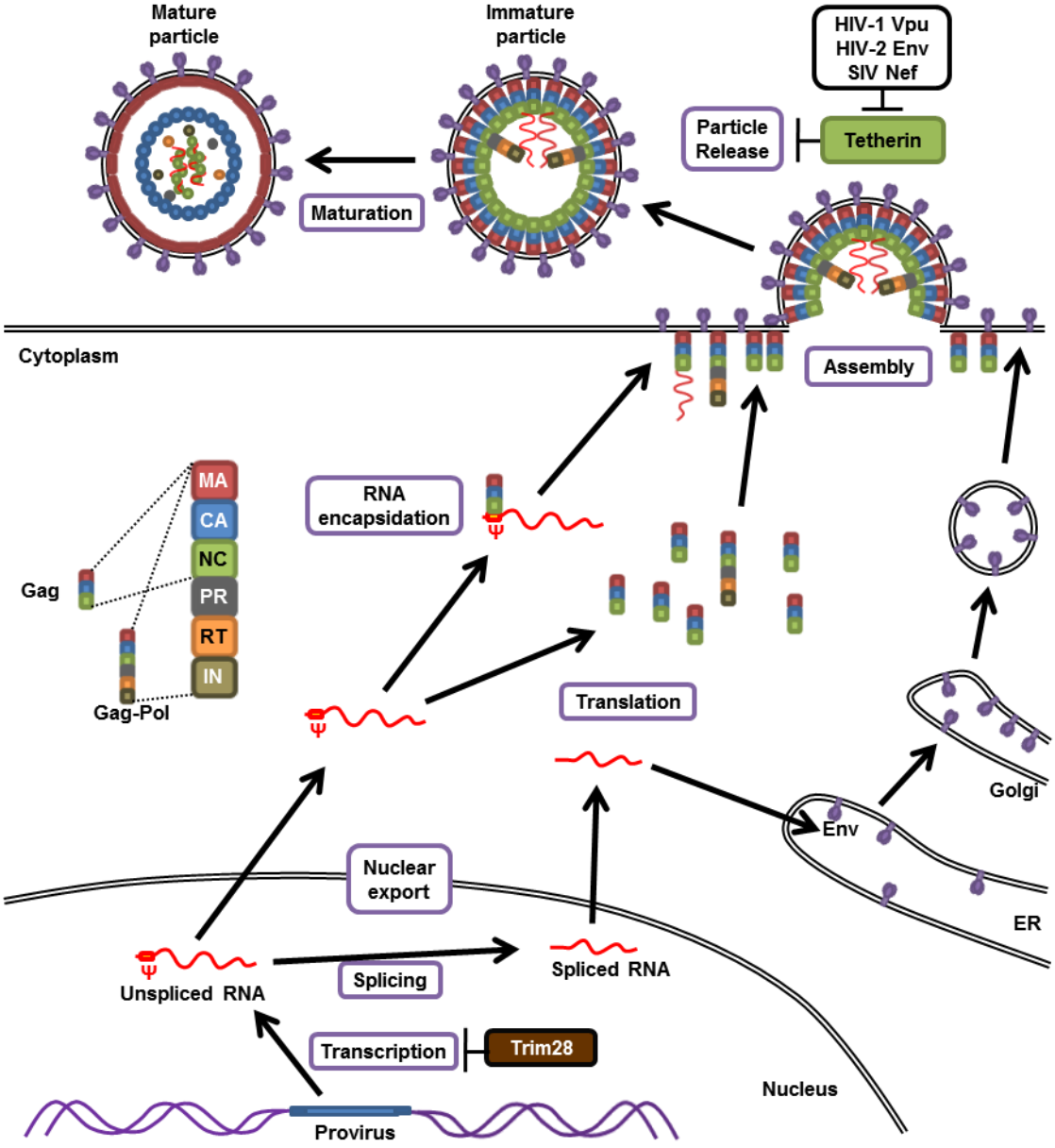

Figure 1.7. The late stage of the retrovirus life cycle

A schematic diagram showing steps in the late stage of retroviral life cycle (boxes with purple border), host restriction factors which target these steps (coloured boxes), and viral antagonists which counteract restriction by these restriction factors (boxes with black border). Full length retroviral RNA is transcribed using the promoter activity in the U3 region of 5' LTR. The restriction factor Trim28 together with other cellular cofactors inhibit the transcription of retroviral RNA. Full length transcripts are either exported to cytoplasm directly, or spliced before export. Gag and Gag-Pol are translated from full length transcripts, while Env and HIV-1 accessory proteins are translated from spliced transcripts. Two copies of full length genomic RNAs are packaged into each virion. The assembly of immature particles involves the polymerisation of Gag and Gag-Pol. After membrane fission facilitated by the ESCRT machinery, the release of immature particles is blocked by the restriction factor tetherin. Immature particles undergo maturation, in which the proteolytic processing of Gag triggers the formation of a mature core consisting of polymerised CA, and the formation of a condensed RNP consisting of NC and genomic RNA.

(Pinter et al., 1997). Binding of SU to receptor leads to conformational changes in both SU and TM subunits, triggering the exchanges of disulphide bonds and insertion of fusion peptides of TM to the target membrane. This results in the formation of intramolecular bonds within the CXXC motif, and the release of SU from TM (Wallin et al., 2004). TM trimers then fold back to form a 6-helix bundle, forcing the viral and cellular membranes together for fusion (White et al., 2008). The binding of gp120 to CD4 triggers a conformational change, allowing binding of co-receptor (Chen et al., 2005; Kwong et al., 1998). Binding of co-receptor triggers membrane fusion in a similar way to ecotropic MLV involving isomerisation of disulphide bonds (Abrahamyan et al., 2003; Markovic et al., 2004).

Sites of viral entry

The entry of ecotropic MLV occurs in endosomes and can be blocked by inhibitors of endosome acidification (Kubo et al., 2012; McClure et al., 1990). This is supported by the observation of ecotropic MLV endocytosis through a clathrin-dependent pathway (Lee et al., 1999). There are contradicting evidences on whether HIV-1 entry requires an endocytotic (Miyauchi et al., 2009) or non-endocytotic pathway (Maddon et al., 1988; McClure et al., 1988). It should be noted that viruses used in this study are pseudotyped with the vesicular stomatitis virus glycoprotein (VSV-g) envelope, which interacts with cellular LDL receptors for entry via a clathrin-dependent endocytic pathway (Aiken, 1997; Finkelshtein et al., 2013; Soneoka et al., 1995; Sun et al., 2005).

1.3.2 Reverse transcription and uncoating

After the fusion of viral and cellular membranes, the retroviral core is released into the cytoplasm of the target cell. Between viral entry and integration, a number of events take place including reverse transcription, uncoating of viral cores, and the transport of pre-intergation complex (PIC) to the site of integration in the nucleus. While MLV infects dividing cells only, HIV-1 can also infect non-dividing cells (Lewis et al., 1992; Weinberg et al., 1991) and therefore requires nuclear import of PIC. The exact order of these events is not known, and it is likely that many of these events occur simultaneously and may influence each other.

Reverse transcription

Reverse transcription (Figure 1.8) involves a complex procedure involving multiple strand transfer steps and the synthesis of cDNA using both RNA and DNA as templates (Hu and Hughes, 2012). The first step of reverse transcription involves the binding of tRNA primers to pbs. Different retroviruses use different tRNA primers, with MLV utilises $tRNA_{pro}$ (Peters et al., 1977) and HIV-1 uses $tRNA_{lys3}$ (Ratner et al., 1985). tRNA primers are packaged into virion, and the RNA chaperone activity of Gag-NC has been proposed to facilitate the annealing of tRNA primer before viral entry (Cen et al., 2000; Crawford and Goff, 1985). The tRNA primer initiates the synthesis of minus strand cDNA by the polymerase domain of RT, while the RNase H domain of RT degrades the RNA strand in DNA/RNA hybrid. The resulting minus strand strong stop DNA contains sequence complementary to the R and U5 elements, and is transferred to and hybridised to the R sequence at the 3' end of the viral RNA. Minus strand synthesis is continued while the RNA template is degraded, except for the ppt (and also cppt in the case of HIV-1) which is resistant to RNase H. The ppt sequence now serves as the primer for synthesis of plus strand strong stop DNA. After the degradation of tRNA sequence, the plus strand strong stop DNA is transferred and hybridised to pbs at the 3' end of minus strand cDNA. Elongation of both plus and minus strands results in a double strand DNA copy of the viral RNA with complete LTR on both 5' and 3' ends. In HIV-1, plus strand synthesis is initiated at both the ppt and the cppt (Charneau and Clavel, 1991). After the transfer of plus strand cDNA initiated from the ppt, the elongation of this plus strand cDNA is terminated at the central termination sequence (CTS), which is located at 100nt downstream of the cppt (Charneau et al., 1994). The 100nt overlapping between the two fully elongated plus strand DNA results in a triple strand structure at the centre of the reverse transcribed HIV-1 cDNA known as the "DNA flap".

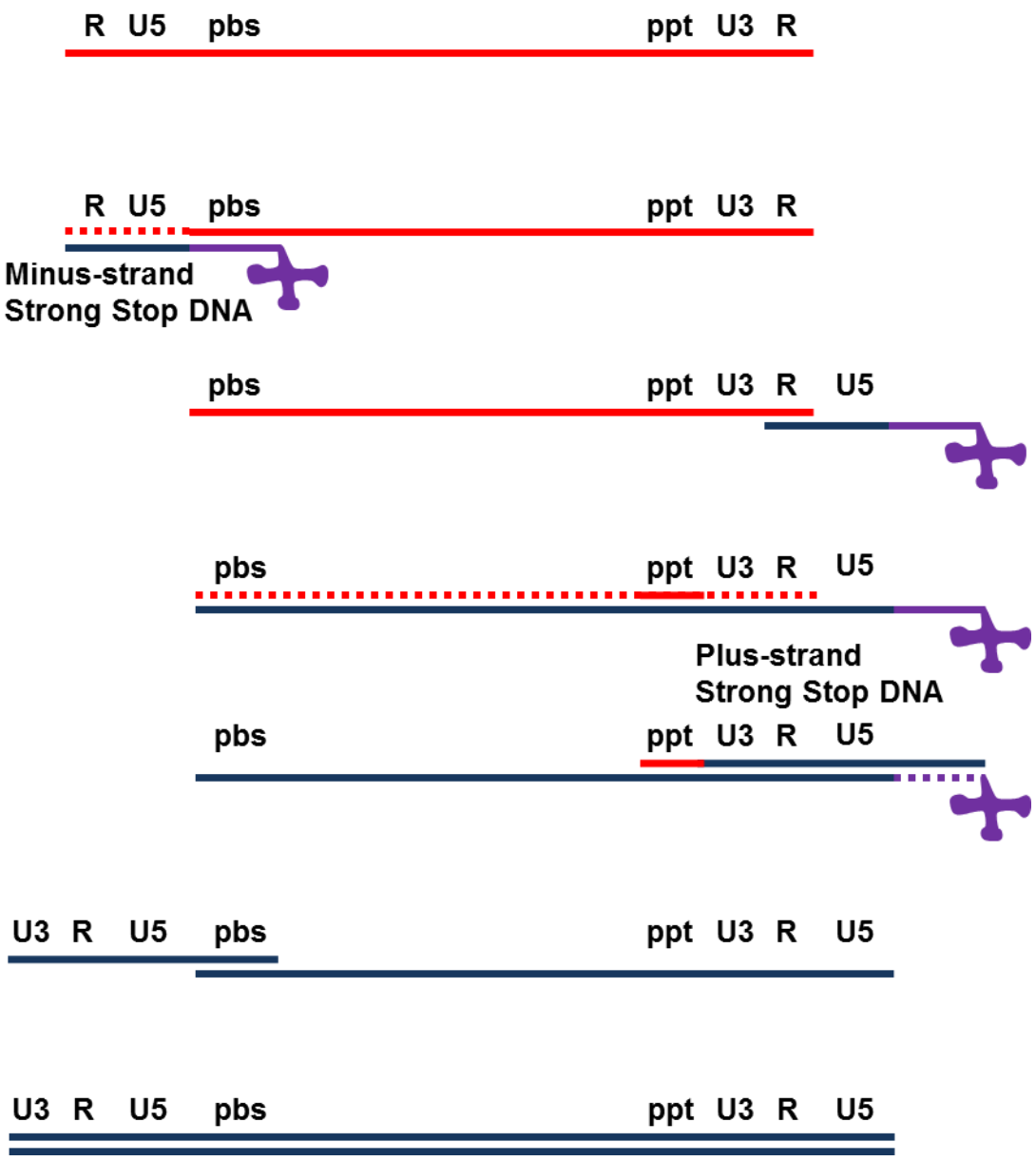

Figure 1.8 Reverse transcription

RNA is shown in red, DNA is shown in blue, tRNA is shown in purple. tRNA is annealed to the primer binding site (pbs) by the chaperone activity of Gag-NC before viral entry. The tRNA primer initiates the synthesis of minus strand cDNA by the polymerase domain of RT, while the RNase H domain of RT degrades the RNA strand in the DNA/RNA hybrid. The resulting minus strand strong stop DNA contains sequence complementary to R and U5, and is transferred to and hybridised to R at the 3' end of the viral RNA. Minus strand synthesis is continued while the RNA template is degraded, except for the ppt which is resistant to RNase H. The ppt sequence now serves as the primer for synthesis of plus strand strong stop DNA. After the degradation of tRNA sequence, the plus strand strong stop DNA is transferred and hybridised to pbs at the 3' end of minus strand cDNA. Elongation of both plus and minus strands results in a double strand DNA copy of the viral RNA with complete LTR on both 5' and 3' ends.

Uncoating

In order to integrate the reverse transcribed viral DNA into host genome, the viral DNA and the associated proteins including IN need to be released from the CA core. This uncoating process has been hypothesised to involve the gradual conversion of the reverse transcription complex (RTC), where DNA synthesis occurs, to PIC, which is capable of integration (Hu and Hughes, 2012). The timing and location of CA uncoating appears to be very different between MLV and HIV-1 (Fassati, 2012). MLV RTC/PIC contains viral DNA, RT, NC, IN, CA and p12 (Bowerman et al., 1989; Fassati and Goff, 1999; Prizan-Ravid et al., 2010; Risco et al., 1995).

CA remained associated with the RTC/PIC for at least 7h post-infection, but CA is disassociated from the PIC before entering the nucleus (Elis et al., 2012; Fassati and Goff, 1999). HIV-1 RTC/PIC isolated from infected cells contained viral DNA, NC, MA, RT, IN and vpr, but not CA (Bukrinsky et al., 1993; Farnet and Haseltine, 1991; Fassati and Goff, 2001; Gallay et al., 1995; Iordanskiy et al., 2006; Karageorgos et al., 1993; Miller et al., 1997). Many imaging studies showed CA colocalisation with RTC/PIC, with most studies suggested that HIV-1 uncoating occurs shortly after entry within 1h post-infection (Hulme et al., 2011; Jun et al., 2011; Xu et al., 2013), although there has been report of detection of HIV-1 core at the nuclear pore (Arhel et al., 2007). The RTC/PIC is transported towards the nucleus by cytoplasmic dynein on microtubules (McDonald et al., 2002).

Relationship between reverse transcription and uncoating

A number of recent studies have identified links between reverse transcription and uncoating of HIV-1 (Ambrose and Aiken, 2014). The observation that the disassociation of CA from RTC/PIC precedes the completion of reverse transcription suggested that both events occur simultaneously (Hulme et al., 2011). Blocking of reverse transcription with RT inhibitors has been reported to increase HIV-1 core stability *in vitro* and decrease the rate of uncoating *in vivo* (Hulme et al., 2011; Yang et al., 2013). Mutations that either increase or decrease core stability were found to inhibit reverse transcription (Forshey et al., 2002).

1.3.3 Nuclear localisation and integration

Nuclear entry

A key difference between HIV-1 and MLV is the ability of HIV-1 to infect non-dividing cells (Lewis et al., 1992; Weinberg et al., 1991). MLV particles only enter the nucleus during mitosis when the nuclear envelope is dissolved (Roe et al., 1993a), and p12 has been shown to target PIC to chromatin during mitosis (Elis et al., 2012; Prizan-Ravid et al., 2010; Schneider et al., 2013; Wight et al., 2012). The entry of HIV-1 into nucleus of non-dividing cells would involve active transport mechanism across the nuclear envelope. The main determinants for nuclear import lies within the HIV-1 CA domain (Yamashita and Emerman, 2004). Many host proteins, including components of the nuclear pore complex (NPC), have been identified through siRNA screens to promote HIV-1 nuclear entry, (Brass et al., 2008; Konig et al., 2008; Yeung et al., 2009; Zhou et al., 2008). Nuclear import mediated by Nup153, Nup358 or TNPO3 appears to be important for optimal integration site selection, depletion of these proteins leads to reduced infectivity and switching of integration site from high to low gene density regions (Koh et al., 2013; Matreyek and Engelman, 2011; Ocwieja et al., 2011; Schaller et al., 2011).

Recent studies have been focused on the roles of Nup153, Nup358, TNPO3, CPSF6 and CypA on nuclear entry and their interactions with CA (Hilditch and Towers, 2014; Matreyek and Engelman, 2013). Nup153 contains a NTD, which is a structural component of the nuclear basket in the NPC (Enarson et al., 1998), and a flexible CTD which interacts with CA-NTD and IN (Matreyek et al., 2013; Woodward et al., 2009). Nup358/RanBP2 forms long filaments on the cytoplasmic side of nuclear pore, and is involved in the regulation of protein import through NPC (Wu et al., 1995; Yokoyama et al., 1995). The C-terminal sequence of Nup358 is similar to that of the peptidyl-propyl isomerase CypA (Bosco et al., 2002; Lin et al., 2013). Both CypA and the CypA-like domain of Nup358 directly interact with the cyclophilin binding loop of CA, between α-helices 4 and 5 of CA-NTD (Bichel et al., 2013; Gamble et al., 1996; Luban et al., 1993; Schaller et al., 2011). Cleavage and polyadenylation specific factor 6 (CPSF6), an mRNA splicing protein, binds to CA-NTD (Lee et al., 2012; Price et al., 2012). CPSF6 also contains a C-terminal nuclear localisation signal (NLS) formed of RS repeats, which interacts with transportin

3 (TNPO3) (Maertens et al., 2014). TNPO3 is a member of the karyopherin-β protein family, mediating the import of splicing factors across NPC (Lai et al., 2001). Karyopherin-β shuttles between the cytoplasmic and nuclear sides of the NPC, transporting cargo using the RanGTPase cycle (Chook and Suel, 2011). Karyopherin-β binds to its cargo protein at the cytoplasmic side of NPC, which include Nup153 and other components. At the nuclear side, it binds to Ran-GTP with high affinity while releasing its cargo. Once back to the cytoplasmic side, the RanGTPase activity is activated by a complex of RanGAP, RanBP1 and Nup358, and the RanGDP is released from karyopherin-β for the next round of cargo binding.

The role of CypA and Nup358 in nuclear import have been studied using the small molecule cyclosporine (Cs) that abolish CypA but not Nup358 binding to CA (Luban et al., 1993; Schaller et al., 2011), and CA mutations (G89V and P90A) that abolish binding of both CypA and Nup358 (Schaller et al., 2011). Cs treatment or non-binding mutations both caused a switch of integration sites to region with higher density, using a nuclear entry pathway still dependent of TNPO3 (Matreyek and Engelman, 2011; Schaller et al., 2011). In contrast, a CA mutation (N74D) which abolishes binding between CA and CPSF6 led to random integration of provirus, using a nuclear entry pathway independent Nup153, Nup358 and TPNO3 (Matreyek and Engelman, 2011; Schaller et al., 2011). These studies suggested the presence of multiple nuclear entry pathways that can be used by HIV-1, but only some pathways could lead to optimal integration site selection.

Chromatin targeting

Although the choice of nuclear entry pathway has a strong influence on HIV-1 integration site selection, a host protein LEDGF has also been shown to target HIV-1 integration to transcriptionally active sites (Ciuffi et al., 2005; Marshall et al., 2007; Shun et al., 2007). LEDGF binds IN through its C-terminal domain, and causes nuclear localisation and chromatin tethering of IN through its NLS and chromatin-binding PWWP domain (Maertens et al., 2003). Bromodomain and extra-terminal (BET) family proteins Brd2, Brd3 and Brd4 have been shown to bind MLV IN and target MLV integration to transcription start sites (De Rijck et al., 2013; Gupta et al., 2013; Sharma et al., 2013). These proteins contain

two chromatin-interacting bromodomains which bind acetylated histone tails, and a conserved ET domain found in BET proteins interacts with the C-terminus of IN. The chromatin binding domains in BET proteins and LEDGF are the key determinants in integration site targeting. MLV infection in cells expressing a fusion protein with LEDGF chromatin binding domain and the ET domain of BET leads to HIV-like integration targeting pattern (De Rijck et al., 2013). Although MLV p12-CTD also contains sequences required for tethering of p12 to chromatin (Elis et al., 2012; Prizan-Ravid et al., 2010; Schneider et al., 2013; Wight et al., 2012), p12 does not alter integration site selection (Schneider et al., 2013).

Integration

Integration (Figure 1.9) occurs in a tight complex of IN homotetramer and linear viral dsDNA (Hare et al., 2010). In addition to linear dsDNA, two types of circular viral DNA can also be found in the nucleus: 1-LTR circles are formed by intramolecular homologous recombination between the LTRs on the same linear dsDNA, while 2-LTR circles are formed by non-homologous end joining between the blunt ends of a linear dsDNA. Only linear viral dsDNA can be used for integration (Brown et al., 1989). 2-LTR circles are frequently used as a marker for nuclear entry. The first step of integration, known as 3' processing, involves the removal of 2 nucleotides from 3' end of each viral DNA strand by IN (Craigie and Bushman, 2012). 3' processing converts the RTC into the integration-competent PIC, and probably occurs in the cytoplasm (Fassati and Goff, 1999). With the help of nuclear transport proteins and chromatin targeting factors, intasomes are transported to the integration sites. In the second step, known as strand transfer, the 3' hydroxyl groups exposed from 3' processing are used by IN to attack a pair of phosphodiester bonds in the target DNA, during which the 3' end of viral DNA is joined to the 5' end of host DNA. The sites of attack on the two strands of DNA are separated by 4 (MLV) or 5 (HIV-1) nucleotides. This resulted in a 4 or 5 nucleotide single strand region and a dinucleotide 5' overhang at both attack sites, which are repaired by cellular enzymes. Proviral DNAs integrated into host genome are flanked by 4 or 5 nucleotides of duplicated sequence.

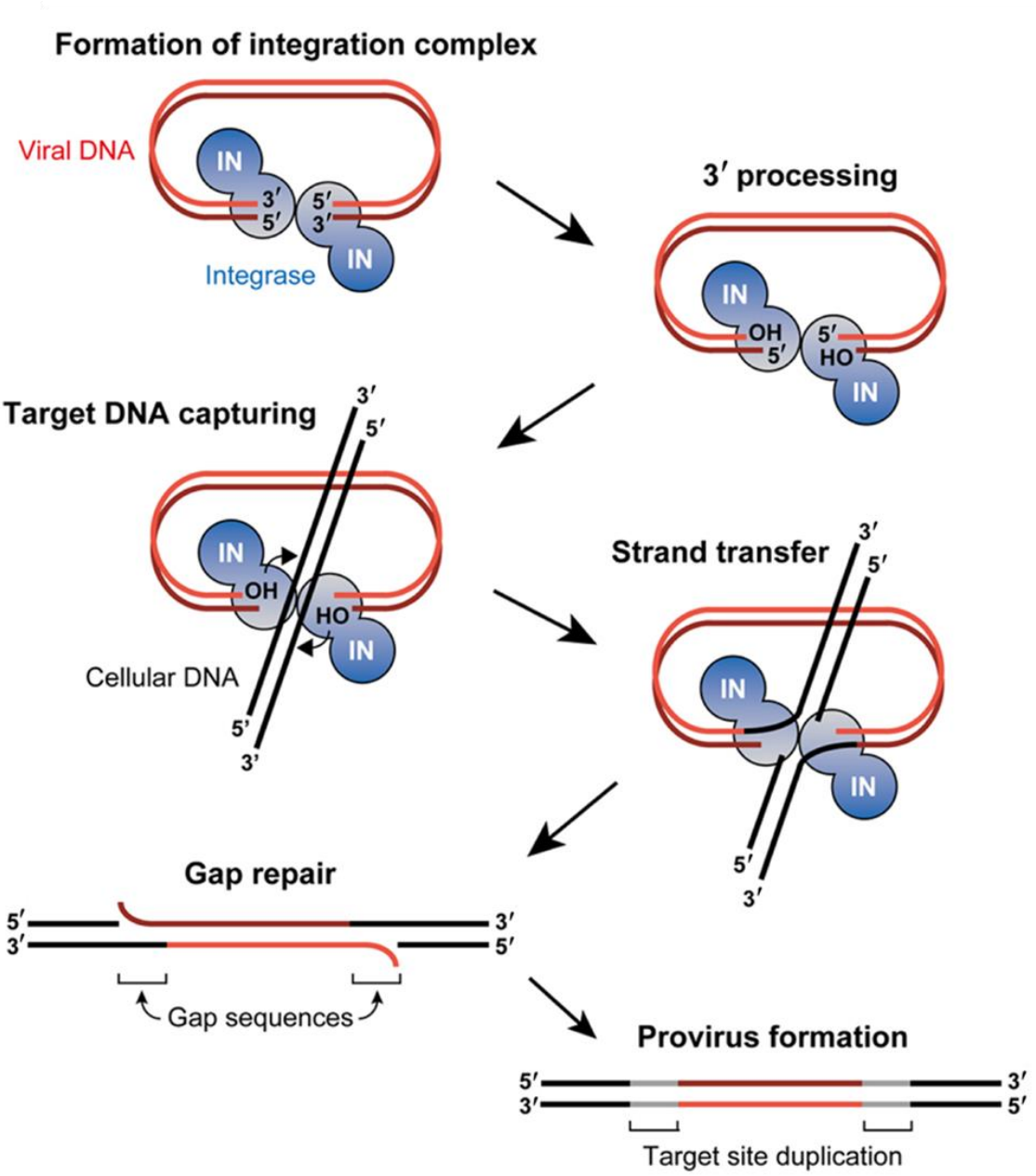

Figure 1.9 Integration

During 3’ processing, 2 nucleotides from 3’ end of each viral DNA strand are removed by IN. During strand transfer, the 3’ hydroxyl groups exposed from 3’ processing are used by IN to attack a pair of phosphodiester bonds in the target DNA, during which the 3’ end of viral DNA is joined to the 5’ end of host DNA. The sites of attack are separated by 4 (MLV) or 5 (HIV-1) nucleotides. This resulted in a 4 or 5 nucleotide single strand region and a dinucleotide 5’ overhang at both attack sites, which are repaired by cellular enzymes. Proviral DNAs integrated into host genome are flanked by 4 or 5 nucleotides of duplicated sequence. Reproduced from (Suzuki et al., 2012), permitted under open access license.

1.3.4 Transcription, splicing and nuclear export

Transcription

The U3 sequence of proviral LTR acts as a promoter for the transcription of viral RNA. Transcription of retroviral RNA starts at the U3-R boundary of the 5' LTR, and terminates within the U3 region of the 3' LTR. Each retroviral genomic RNA contains a 5o 7-Methylguanosine CAP and a 3' poly(A) tail. Simple retroviral U3 promoters are efficient and constitutively active. Complex retroviruses, particular those which enter latency, tightly regulate the U3 promoter activity. In HIV-1, the transactivator protein Tat is involved in the activation of transcription (Karn and Stoltzfus, 2012). Tat binds to the TAR stem-loop at the 5' end of viral RNA (Dingwall et al., 1990; Dingwall et al., 1989), and the P-TEFb protein complex consisting of CDK-9 and CycT1 (Wei et al., 1998). Tat binding activates P-TEFb, which in turns phosphorylate RNA polymerase II and a number of elongation factors to stimulate transcription elongation (Karn and Stoltzfus, 2012). Binding sites for the transcription factor NF-κB are found in the enhancer region of the U3 promoter of HIV-1, and are required for the activation of transcription (Alcami et al., 1995; Nabel and Baltimore, 1987).

Splicing

Splicing of mRNA involves the removal of introns between a 5' splice site and a 3' splice site, and requires a large RNP complex known as spliceosome. The MLV RNA contains only one 5' splice site and one 3' splice site, resulting in just unspliced and singly spliced RNA. In contrast, splicing of HIV-1 viral RNA is highly complex, involving four 5' splice sites, eight 3' splice sites and more than potential 40 splice variants. However, the relative abundance of different splice variants is very different (Purcell and Martin, 1993), with a number of sequence and structural RNA elements controlling the strengths of individual splice sites (Karn and Stoltzfus, 2012).

Nuclear export

Complex retroviruses such as HIV encode proteins for control of RNA export and HIV-1 Rev protein mediates the export of RRE-containing unspliced and spliced RNA (Malim et al., 1989). At the early phase of RNA expression, viral RNAs are subjected to rapid and multiple splicing in the nucleus, so that the majority of the exported viral RNAs would be multiply spliced RNA lacking the RRE sequence. These multiply spliced RNA leads to expression of Tat, Rev and Nef. At the late phase, the accumulation of Rev in the nucleus leads to the binding of Rev to RRE. As a result, RRE-containing viral RNAs are exported before splicing is complete. These RRE-containing RNAs include the unspliced genomic RNA which is packaged into nascent particles and is required for the translation of Gag and GagPol; as well as incompletely spliced RNAs required for the translation of Env, Vif, Vpr and Vpu. The Rev-RNA complexes are exported across the NPC through the binding of its nuclear export signal (NES) to the karyopherin Crm1, and re-enter the nucleus through interaction of its NLS with importin-β (Henderson and Percipalle, 1997; Neville et al., 1997). Like TNPO3, the transport of cargo by Crm1 and importin-β are driven by the Ran GTPase cycle. Although MLV does not express any viral protein for nuclear export, it contains a cis-acting cytoplasmic accumulation element (CAE) towards the end of the *pol* gene to mediate nuclear export of both spliced and unspliced RNA by the NXF1/TAP karypherin (Pessel-Vivares et al., 2014; Sakuma et al., 2014).

Translation

The translation of many cellular mRNA requires the recruitment of ribosome at the 5’ CAP structure. The ribosome then scans along the mRNA until it encounters an initiation codon flanked by a good Kozak sequence (Kozak, 1986). Despite the close proximity of start codons to the 5’ CAP, the translation of MLV Gag, Glyco-Gag and Env all require CAP-independent mechanisms. Two separate internal ribosome entry sites (IRES) have been identified in MLV, with the first IRES present immediately upstream of the initiation codon of the *gag* gene for the translation of Gag, Glyco-Gag and GagPol proteins, and the second IRES present between the splice junction and the initiation codon of the *env* gene for the translation of Env protein (Berlioz and Darlix, 1995; Deffaud and Darlix, 2000). Two IRES have been proposed to be involved in the translation of HIV-1 Gag, one in the 5’ untranslated region (Brasey et al., 2003; Gendron et al., 2011), and one in the *gag* coding region (Buck et al., 2001). While both CAP-dependent and CAP-independent initiation mechanisms can drive the translation of HIV-1 Gag and GagPol, the translation of other HIV-1 proteins requires a CAP-dependent initiation mechanism (Amorim et al., 2014; Monette et al., 2013). Many aspects of the translation of HIV-1 and MLV proteins were also discussed earlier in section 1.1.3.

1.3.5 Assembly and budding

RNA packaging and dimerisation

Orthoretroviral particles contain dimers of genomic RNA and mostly Gag proteins. The packaging of viral genomic RNA into particles requires interaction Gag-Gag and Gag-RNA interactions. This is supported by the *in vitro* assembly of CA-NC gag fragments with RNA (Ganser et al., 1999; Zuber et al., 2000). Importantly, full length genomic RNA needs to be specifically packaged from a mixture of cellular RNA and spliced viral RNA in the cytoplasm. This packaging specificity is mediated by the selective binding of Gag-NC domain to the packaging signal (ψ-site) in genomic RNA, and in often coupled to the dimerisation of genomic RNA (Nikolaitchik et al., 2013; Rasmussen and Pedersen, 2004). In MLV, the ψ-site is required for both dimerisation and packaging, and is absent in spliced viral RNA (D'Souza and Summers, 2005). The MLV ψ-site contains two stem-loops responsible for the initiation of dimerisation (DIS-1 and DIS-2) (Ly and Parslow, 2002), and two additional stem-loop important for packaging (SL-C and SL-D) (D'Souza et al., 2004). Gag-NC causes conformation change in ψ-site, probably through its RNA chaperone activity, stabilising an alternative form of the RNA (D'Souza et al., 2001; D'Souza and Summers, 2004). In this conformation a 4nt palindromic sequence in the loop region of DIS-1 and DIS-2 are exposed, leading to inter-molecular “kissing interactions” between equivalent loop regions of monomers, eventually forming extensive dimer linkage during maturation (D'Souza et al., 2001; Girard et al., 1995; Tounekti et al., 1992). The RNA dimer conformation is stabilised by the binding of NC to high affinity sites with the unpaired guanidine of UCUG elements, which are exposed in the dimeric conformation (D'Souza et al., 2001; Dey et al., 2005). SL-C and SL-D, although not necessary for dimerisation, also forms kissing interactions between the conserved palindromic GACG tetraloop of RNA monomers (Kim and Tinoco, 2000).

In HIV-1, RNA packaging and dimerisation occurs in the cytoplasm (Moore et al., 2009). The HIV-1 ψ-site at the 5’ leader sequence includes four stem-loops: SL1, SL2, SL3 and SL4 (Sakuragi et al., 2007) SL1 and SL3 are most important for packaging and dimerisation. SL1 contains a 6nt palindromic dimerisation initiation signal (DIS), and form kissing interaction between

monomeric RNA and can drive dimerisation *in vitro* (Clever et al., 1996; Laughrea and Jette, 1994). The kissing loops are converted into extensive dimer linkage structure during maturation with NC as a chaperone (Kafaie et al., 2008; Ohishi et al., 2011). SL2 contains the 5' major splice donor site, and is dispensable for packaging (Purcell and Martin, 1993). SL3 is the major packaging signal, and contains a GGAG tetraloop which forms tight interaction with gag-NC (De Guzman et al., 1998). As SL2 precedes SL3, spliced RNAs are not packaged.

Membrane targeting

While core assembly of some retroviruses such as MPMV and MMTV can occur in cytoplasm, others including MLV and HIV-1 require attachment to lipid membranes. The membrane targeting of Gag-MA allows the transport of HIV-1 and MLV Gag to lipid membranes enriched in cholesterol and several lipids including sphingomyelin, phosphatidyl serine (PS), phosphatidyl ethanolamine (PE) and phosphatidyl inositol (4,5) bisphosphate (PIP_2) (Chan et al., 2008). N-terminal myristoylation is essential for stable attachment of Gag to membrane and for assembly of MLV and HIV-1 (Bryant and Ratner, 1990; Rein et al., 1986; Spearman et al., 1994). A switch mechanism has been recently proposed between RNA and lipid binding activities of HIV-1 MA (Alfadhli and Barklis, 2014). Surface basic residues on HIV-1 MA form overlapping binding sites for both RNA and lipid with acidic head groups (Alfadhli et al., 2011; Jones et al., 2011). Gag binds to RNA through both NC and MA subunits (Jones et al., 2011). Once this complex reaches the plasma membrane, acidic phospholipids such as PIP_2 compete with RNA for MA binding (Alfadhli et al., 2011; Jones et al., 2011). The electrostatic interaction between MA and lipid induces the extrusion of N-terminal myristoyl group in MA, allowing stable lipid anchoring of gag (Saad et al., 2006). This allows the tethering of gag to lipid membrane via MA, and to genomic RNA via NC.

Gag polymerisation

Once the Gag-RNA complex is tethered to the site of assembly on the plasma membrane, polymerisation of Gag begins. The immature gag lattice consists of 1100-1800 Gag molecules for MLV (Yeager et al., 1998), and 2500 Gag molecules for HIV-1 (Briggs et al., 2004; Carlson et al., 2008). Gag molecules in

the lattice are organised into regular symmetric units, and held by strong Gag-Gag interactions. Electron cryo-tomography analyses of native budding sites (Carlson et al., 2010) and native immature particles (Wright et al., 2007; Yeager et al., 1998) have shown that Gag proteins of MLV and HIV-1 are arranged into regular arrays, with hexagonal symmetry. MA also appears to form inter-hexameric contacts with its trimer interface (Alfadhli et al., 2007; Huseby et al., 2005). In addition, there are indirect contacts between NC subunits through the binding of viral RNA.

Budding

Budding of retroviruses involves membrane deformation, followed by membrane fission (Votteler and Sundquist, 2013). The membrane deformation transforms the planar plasma membrane into a spherical shape in the immature particle. The polymerisation of HIV-1 gag into an immature lattice leads to the formation of an almost complete spherical particle, which still connects to the cell through a neck region (Carlson et al., 2008). The next step, membrane fission, resolves this neck region leading to release of the immature particle. Membrane fission requires the ESCRT machinery, which contains multiple protein complexes. The ESCRT pathway mediates membrane fission during cytokinesis and during the formation of intraluminal vesicles in multivesicular bodies (McCullough et al., 2013). Many retroviruses contain late assembly (L-)domains for the recruitment of proteins from the ESCRT pathway. There are 3 types of L-domains: P(T/S)AP, LYPX_nL and PPXY. The P(T/S)AP motif binds to the UEV domain of Tsg101, which is a subunit of the heterotetrameric ESCRT-I complex. This motif is found in the MA region of MLV Gag (Segura-Morales et al., 2005) and in the p6 region of HIV-1 Gag (Garrus et al., 2001). The LYPX_nL motif binds the V domain of the ESCRT-associated protein Alix. This motif is found at the junction between MA and p12 in MLV (Segura-Morales et al., 2005), in the p6 region of HIV-1 (Strack et al., 2003). The HIV-1 NC domain also interacts with the Bro1 domain of Alix, but this interaction is dependent on RNA-binding (Sette et al., 2012; Strack et al., 2003). Both ESCRT-I and Alix can activate the ESCRT-III proteins such as the CHMP2 and CHMP4 complex (Sundquist and Krausslich, 2012). Activated ESCRT-III complex generates long filament which coil into a dome shape at the neck of the budding virus. The recruitment of the Vps4 ATPase terminates membrane fission through hydrolysis of ATP, releasing the

virus and ESCRT-III proteins. Lastly, the PPXY motif binds to WW motif of Nedd4 family ubiquitin ligases. This motif can be found in the p12 region of Gag, and mutation of the PPPY motif leads to the formation of tubular particles (Yuan et al., 2000). Although little is known about the incorporation of retroviral Env, clustering of HIV-1 Env around budding sites containing HIV-1 gag have been reported (Muranyi et al., 2013). This recruitment of Env requires the cytoplasmic tail of TM, and is sensitive to mutations in MA.

1.3.6 Maturation

Nascent orthoretroviral particles contain an immature core consist of Gag, Gag-Pol and viral RNA. Retroviral maturation is controlled by the proteolytic processing of Gag and Gag-Pol precursor proteins, leading to the formation of a condensed capsid core. The transition from immature to mature core involves rearrangements of CA, triggered by the stabilisation of β-hairpin at the N-terminus, and removal of NC (and SP1) on the C-terminus. This leads to an increase in inter-hexameric distance and formation of inter-hexameric interactions between CA-CTD. In addition to changes in capsid core, maturation also leads to the formation of stable dimer linkages, the annealing of tRNA primer, and the activation of Env for fusion through the cleavage of R-peptide from Env by PR (Loving et al., 2012; Rein, 2010; Sundquist and Krausslich, 2012; Wyma et al., 2004).

In HIV-1, the timing of maturation is tightly controlled by the sequential cleavage of different processing sites by PR, with up to 400-fold difference in cleavage rates (Figure 1.10) (Pettit et al., 1994). Studies of core morphology of HIV-1 processing site mutants by transmission electron microscopy (TEM) have led to the evaluation of the effects of each cleavage event (de Marco et al., 2012; de Marco et al., 2010b; Sundquist and Krausslich, 2012). The first cleavage event occurs at the SP1/NC junction forming the MA-SP1 and the SP1-p6 products, this triggers the condensation of NC-RNA complex and activates Env for fusion (de Marco et al., 2010b; Wyma et al., 2004). At this stage, the CA layer remains tethered to the membrane through the MA domain (de Marco et al., 2010b). Next, the cleavage at the MA/CA junction releases the CA-SP1 product from the lipid membrane. This leads to the stabilisation of β-hairpins in CA-NTD. Although CA-SP1 is released from membrane tethering, at this stage mature core structures are not yet formed, with fragments of capsid shell observed in some particles (de Marco et al., 2010b). Finally, the cleavage of the SP1 bundle from CA leads to the destabilisation of CA-CTD hexamers, allowing the rearrangement of CA-CTD to form interactions at trimer and dimer interfaces (Meng et al., 2012). Further processing of the NC-SP2-p6 precursor also releases NC, which acts as a chaperone to facilitate the formation of stable dimer linkages (Kafaie et al., 2008; Ohishi et al., 2011). Some studies suggested that MLV processing sites are cleaved at similar efficiencies (Feher et al., 2006; Oshima et al., 2004), but the slower cleavage at the MA/p12 junction has been reported (Wight et al., 2012). The control of maturation is not well understood, although it is known that the formation of mature core requires cleavage at the p12/CA junction but not at the MA/p12 junction (Oshima et al., 2004).

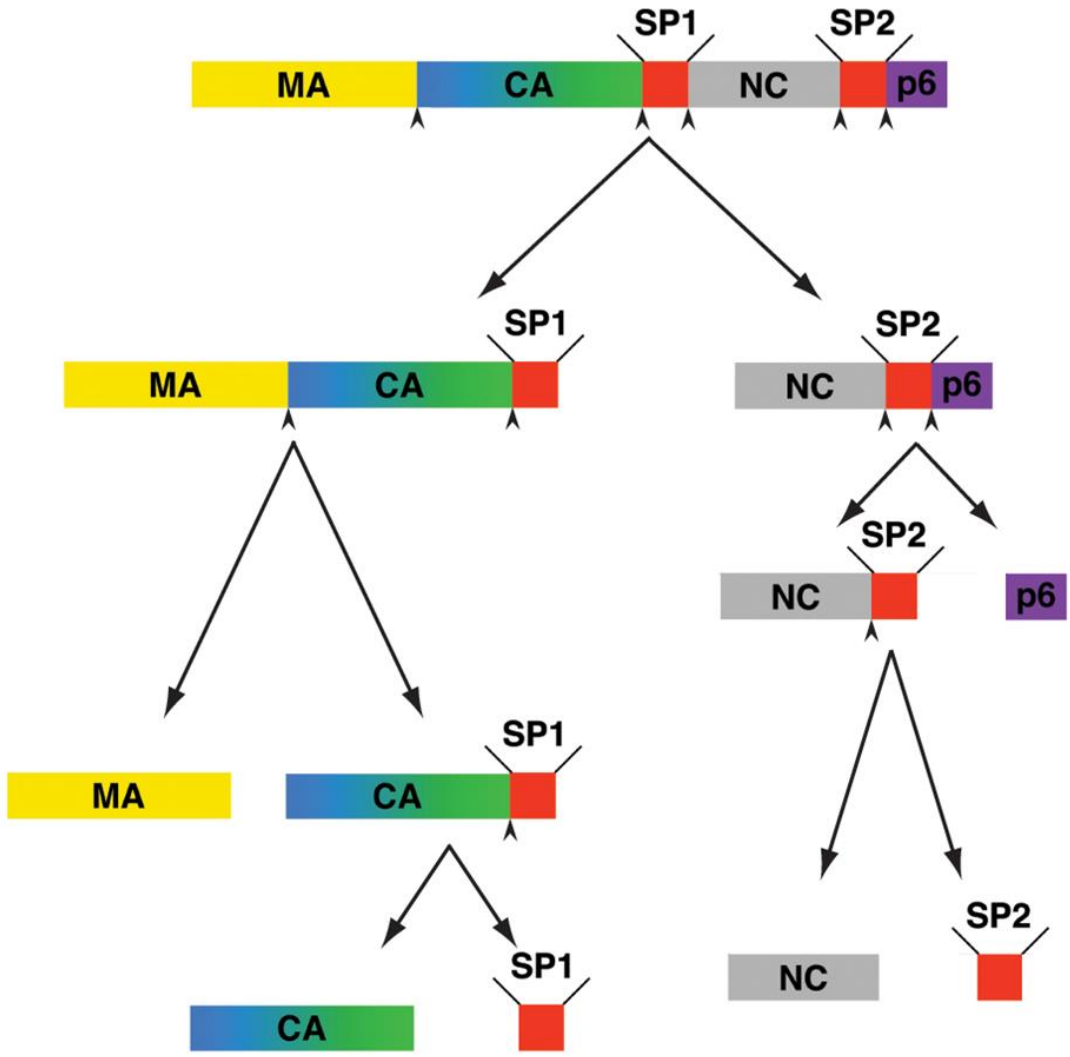

Figure 1.10 Sequential processing of HIV-1 gag

In HIV-1, the timing of maturation is tightly controlled by the sequential cleavage of different processing sites by PR, with up to 400-fold difference in cleavage rates. The first cleavage event occurs at the SP1/NC junction forming MA-SP1 and SP1-p6 products. Cleavage at the MA/CA junction releases CA-SP1 from the lipid membrane, but at this stage mature core structures are not yet formed. Final cleavage at the CA/SP1 junction leads to the formation of mature capsid core. In parallel to the processing of CA, p6 and SP2 are sequentially released from the NC-SP2-p6 fragment, allowing the formation of RNP between NC and RNA. Reproduced from (de Marco et al., 2010b), with permission under PLOS open-access license and the Creative Commons Attribution (CC BY) license.

1.4 Retroviral restriction factors

The coevolution between host and retrovirus has led to the emergence of host cellular defence mechanisms, as well as viral counteracting mechanisms. In recent years, many host proteins have been found to restrict retroviral infection by targeting various steps of the retroviral life cycle (Figure 1.6, Figure 1.7). These host proteins, termed restriction factors, are often under positive selection for their antiviral role (Fay and Wu, 2000). To evade from restriction, retroviruses can either mutate viral proteins targeted by restriction factors, or encode viral proteins, termed viral antagonists, to mediate the degradation of restriction factors. The presence of entry receptors, restriction factors and viral antagonists all contributes to the specificity of retroviruses in host cells, or retroviral tropism.

1.4.1 Restriction factors targeting viral entry

Some restriction factors inhibit viral infection by blocking envelope mediated entry mechanisms. The interferon inducible transmembrane (IFITM) proteins, including IFITM1, IFITM2 and IFITM3, restrict a broad range of viruses including HIV-1 but not MLV (Brass et al., 2009; Lu et al., 2011; Perreira et al., 2013). These IFITM proteins have evolved under positive selection (Everitt et al., 2012; Zhang et al., 2012b). IFITM is anchored to the cytosolic side of the plasma membrane through two intramembrane domains (Perreira et al., 2013), and blocks membrane fusion driven by viral envelope proteins (Li et al., 2013), It has been hypothesised that IFITM remodels and strengthens the plasma membrane to resist action of viral fusion peptides (John et al., 2013).

1.4.2 Restriction factors targeting reverse transcription

Several restriction factors are known to target reverse transcription by retroviruses through different mechanisms. The interferon-inducible apolipoprotein C mRNA-editing enzyme catalytic polypeptide 3G (APOBEC3G) is a cytidine deaminase which introduce C to U conversion in DNA through the nucleophilic attack of the amine group at position 4 of the pyrimidine ring, and has been found to inhibit infection by HIV-1 harbouring deletion of Vif (Chen et

al., 2006; Sheehy et al., 2002). APOBEC3G has evolved under strong positive selection (Sawyer et al., 2004). During reverse transcription, APOBEC3G causes CC to CU deamination in the viral minus-strand DNA, leading to GG to AG hypermutations in the viral genome (Lecossier et al., 2003). This introduces lethal mutations including introduction of in-frame stop codons through TGG to TAG mutations (Mangeat et al., 2003). APOBEC3G can also inhibit many steps of reverse transcription without introducing hypermutations (Bishop et al., 2008; Iwatani et al., 2007). The HIV-1 accessory protein Vif binds APOBEC3G and recruits an E3-ubiquitin ligase complex involving cullin 5, elongin B, elongin C, RBX1 and CBF-β (Jager et al., 2012; Kobayashi et al., 2005; Yu et al., 2003), leading to polyubiquitination and subsequent degradation of APOBEC3G by proteasome (Yu et al., 2003).

Another restriction factor, SAM domain and HD domain containing protein 1 (SAMHD1), inhibits reverse transcription during HIV-1 infection in differentiated myeloid cells (Laguette et al., 2011a). SAMHD1 has evolved under positive selection (Zhang et al., 2012a). SAMHD1 hydrolyses dNTP into dN and triphosplates, and is thought to restrict reverse transcription by depletion of the cellular dNTP pool (Goldstone et al., 2011). The active form of SAMHD1 is a tetramer consists of 4 catalytic sites and 8 allosteric sites (Ji et al., 2013). The restriction of SAMHD1 is abolished by the expression of Vpx from HIV-2 or SIV_{mac} (Hrecka et al., 2011; Laguette et al., 2011b). Similar to the antagonism of APOBEC3G by Vif, Vpx binds SAMHD1 and recruits an E3-ubiquitin ligase complex involving cullin 4A, DDB1 and DCAF1 for polyubiquitination and proteasomal degradation of SAMHD1 (Schwefel et al., 2014).

Although the exact restriction mechanism is not known, the RNA-associated early-stage anti-viral factor (REAF) blocks infection by HIV-1, HIV-2 and SIV during reverse transcription (Marno et al., 2014). REAF is a phosphatase which binds the CTD of RNA polymerase II, and is involved in the control of transcription cycle (Ni et al., 2011; Ni et al., 2014). Determinants of restriction were found on CA and Env (Schmitz et al., 2004); restriction is controlled by the pathway of endocytosis used for virus internalisation (Harrison and McKnight, 2011; Marchant et al., 2005). Since REAF binds DNA and is degraded by proteasome during reverse transcription, it has been hypothesised

to restrict retrovirus by targeting reverse transcription products for degradation (Marno et al., 2014).

1.4.3 Capsid-targeting restriction factors

Several restriction factors including Fv1, T5, Trim5Cyp (TCyp), Trim1 and Mx2 restrict retroviral infection by specifically targeting the capsid core. While Fv1 restricts retrovirus infection after reverse transcription but before integration (Huang et al., 1973; Jolicoeur and Baltimore, 1976); T5, TCyp and Trim1 can also block reverse transcription (Keckesova et al., 2004; Nisole et al., 2004; Sayah et al., 2004; Stremlau et al., 2004; Yap et al., 2004). Fv1, T5 and TCyp will be discussed in detail later. More recently, the interferon-inducible myxovirus resistance 2 (Mx2) has been found to restrict HIV-1 (Goujon et al., 2013; Kane et al., 2013; Liu et al., 2013). Some sites on Mx2 have evolved under positive selection (Busnadiego et al., 2014; Sironi et al., 2014). Similar to Fv1 and T5, Mx2 contains an N-terminal domain which defines specificity, and a C-terminal domain which can mediates dimerisation (Fricke et al., 2014). Mx2 binds to CA polymers and causes stabilisation of core, and has been proposed to restrict HIV-1 by block uncoating (Fricke et al., 2014).

1.4.4 Restriction factors targeting transcription

Some other restriction factors target the late stage of retroviral life cycle, such as transcription of viral RNA. Trim28 causes transcriptional silencing of MLV in mouse embryonic cells (Wolf et al., 2008). MLV provirus is sensed by different zinc finger proteins including ZPF809 which binds specifically to the pbs of ecotropic MLV proviruses, and YY1 which binds to the MLV LTR (Schlesinger et al., 2013; Wolf and Goff, 2009). Trim28 then recruits a large number of chromatin modifiers to form a large silencing complex (Wolf et al., 2008).

1.4.5 Restriction factors targeting particle release

Other restriction factors target the release of retrovirus particle from the cell surface after viral fission. The interferon-inducible tetherin protein restricts HIV-1 with Vpu deletions (Neil et al., 2008). The tetherin has a transmembrane domain near the N-terminus and a C-terminal glycophospatidylinositol (GPI) anchor, and a long coiled-coil helix for dimerisation (Hinz et al., 2010; Kupzig et al., 2003; Schubert et al., 2010; Yang et al., 2010). When the two lipid anchors are on different membranes, tetherin links virus particles to each other and to the plasma membrane (Neil et al., 2008). Different lentiviruses have evolved to use different viral antagonists, including HIV-1 Vpu, HIV-2 Env and SIV Nef, all appear to sequester tetherin away from the cell surface (Hauser et al., 2010; Serra-Moreno et al., 2013).

1.4.6 Innate sensing

In addition to their primary role, some restriction factors including T5 and tetherin also act as sensors which activate innate signalling pathways upon detection of virus. Upon sensing retroviral CA, the E3 ubiquitin ligase activity T5 generates K63-linked polyubiquitin chains, which activate TAK1 and the NF-κB pathway (Pertel et al., 2011). A long isoform of tetherin has also been bound to activate the NF-κB pathway (Cocka and Bates, 2012; Hotter et al., 2013). The presence of replicating virus is also sensed by DNA sensors present in the cytoplasm. Two cytoplasmic DNA sensors, IFI16 and cGAS, have been found to activate STING, which in turn activate IRF3 and NF-κB (Gao et al., 2013; Jakobsen et al., 2013; Lahaye et al., 2013; Sun et al., 2013; Thompson et al., 2014; Towers and Noursadeghi, 2014). The transcription factors IRF3 and NF-κB activate the production of type 1 interferon and other genes, leading to the activation of many interferon-inducible restriction factors including APOBEG3G, T5, SAMHD1, tetherin and Mx2 (Towers and Noursadeghi, 2014).

Recently, it has been proposed that CA recruits host proteins to protect its DNA against innate sensing (Towers and Noursadeghi, 2014). Abortion of CPSF6 or CypA binding to CA through mutations or Cs leads to reduced core stability, and stimulation of type 1 interferon production in monocyte-derived

macrophages (Briones et al., 2010; Fricke et al., 2013a; Fricke et al., 2013b; Rasaiyaah et al., 2013; Tipper and Sodroski, 2014). It has been hypothesised that the binding of CypA and CPSF6 suppress the detection of reverse transcription products by cytosolic DNA sensors by interfering with the uncoating process (Towers and Noursadeghi, 2014). A host DNase, TREX1, has also been shown to protect against innate sensing of HIV-1 by digestion of excess viral DNA (Yan et al., 2010). The host restriction factors and innate sensors form a complex defense system to detect and block retroviral infection. Retroviruses counteract these restriction mechanisms in several ways such as encoding proteins to degrade or sequester restriction factors, recruiting host proteins prevent innate detection, or by mutating the viral target of restriction factors.

1.5 Fv1 and Trim5α (T5)

1.5.1 The discovery of Fv1

The discovery of Fv1 began in the 1960s when certain strains of inbred mice displayed variable susceptibility to spleen focus formation by Friend Virus (FV) (Odaka, 1969; Odaka and Yamamoto, 1965). FV was later found to be a complex of two retroviruses: the replication defective spleen focus forming virus (SFFV), and the replication competent helper virus Friend MLV (Fr-MLV). The variable susceptibility was found to be due to two independently segregating genes, Fv1 and Fv2, of which Fv1 was found to target Fr-MLV (Lilly, 1970). Simultaneously, MLV strains had been classified into three subgroups based on their ability to replicate in embryonic cells derived from NIH Swiss or Balb/c mice (Hartley et al., 1970). MLV strains which replicate well in NIH Swiss but not Balb/c cells were designated N-tropic MLV (N-MLV), while those which replicate well in Balb/c but not NIH Swiss cells were designated B-tropic MLV (B-MLV). MLV strains which replicated well on both strains were classified as NB-tropic MLV (NB-MLV), and in this thesis NB-MLV refers to Moloney MLV. Studies on MLV infection in cells from crossbred mice led to the suggestion of a

single locus dominant factor conferring resistance to MLV infection (Pincus et al., 1971). Since then a number of alleles of Fv1 have been identified in mice, including $Fv1^n$ from NIH Swiss mice which restricts B-MLV but not N-MLV, $Fv1^b$ from Balb/c mice which restricts N-MLV but not B-MLV, and $Fv1^{nr}$ which restricts B-MLV and some N-MLV (Lilly and Steeves, 1973; Steeves and Lilly, 1977). $Fv1^o$ (null) alleles which do not restrict any MLV were identified in some wild mice (Hartley and Rowe, 1975; Kozak, 1985). These include the $Fv1^o$ allele in *Mus dunni* which was later found to contain a premature stop codon (Lander and Chattopadhyay, 1984; Qi et al., 1998a). Genetic linkage studies mapped Fv1 to chromosome 4 (Rowe and Sato, 1973). The screening of a yeast artificial chromosome library of the mouse genome for MLV restriction activity revealed the exact location of Fv1, and enabled the subsequently cloning of the $Fv1^n$ and $Fv1^b$ alleles in 1996 (Best et al., 1996). Sequencing of $Fv1^n$ and $Fv1^b$ alleles revealed that the Fv1 gene contains an MHR motif, and is a distant relative of the Gag protein of an endogenous retrovirus MERV-L (Benit et al., 1997; Best et al., 1996). Since then, many wild mice Fv1 alleles have been cloned and studied (Yan et al., 2009; Yap et al., 2014).

1.5.2 Functional domains and restriction determinants of Fv1

The Fv1 protein consists of two structural domains (Figure 1.11): an N-terminal domain (Fv1-NTD) and a C-terminal domain (Fv1-CTD), joined by a flexible linker (Bishop et al., 2001; Bishop et al., 2006). A fragment of Fv1-NTD comprising of residues 20-200 could be bacterially expressed and purified, and was found to form dimers (Bishop et al., 2006). A coiled-coil (aa88-115) in the Fv1-NTD mediates the tight binding between Fv1-NTD to form antiparallel homodimer (Goldstone et al., 2014). Mapping of regions in Fv1 required for restriction revealed that Fv1 can tolerate large deletions (aa123-250) in the region between the coiled-coil and the Fv1-CTD without abolishing restriction activity, while point mutations at the MHR (aa267-286) or large truncations at the N- and C-termini abolish restriction (Bishop et al., 2001).

The determinants for $Fv1^n$, $Fv1^b$ and $Fv1^{nr}$ restriction specificity are all present in the Fv1-CTD, suggesting that the Fv1-CTD may be a specificity domain (Bock et al., 2000; Stevens et al., 2004). $Fv1^n$ and $Fv1^b$ differ at

positions 358, 399 and the C-terminus, all of which are present in the Fv1-CTD. The $Fv1^n$ allele, which only restricts B-MLV, contains the residues K358, V399 and a short 3aa C-terminal tail (Best et al., 1996). The $Fv1^b$ allele, which appears to restrict only N-MLV in mice, contains the sequence E358, R399 and a long 22aa C-terminal tail (Best et al., 1996). Restriction studies suggested that sequence at positions 358, 399 and C-terminus can all influence Fv1 restriction specificity, with the strongest effect exerted by the charged residue at position 358 (Bock et al., 2000). However, mutations at these variable residues do not always lead to predictable phenotypes, instead the restriction specificities of Fv1 mutants are determined by complex and combinatorial effects the of sequences at all 3 positions (Bishop et al., 2001).

A study of wild mice Fv1 showed that like $Fv1^n$ and $Fv1^b$, these alleles display different restriction specificities towards different MLV strains (Yap et al., 2014). In addition to MLV restriction, some Fv1 alleles can restrict non-gamma-retroviruses including spumavirus and lentivirus (Yap et al., 2014). These alleles include Fv1CAR (from *M. caroli*) which restricts feline foamy virus (FFV) only; Fv1SPR1 (from *M. spretus*) which restricts N-MLV, B-MLV and EIAV; and Fv1MAC (from *M. macedonicus*) which restricts N-MLV and EIAV. Four variable regions have been identified in Fv1-CTD, with MHR, aa358, aa399 and the C-terminus each in a distinct variable region. Like $Fv1^n$ and $Fv1^b$, the restriction determinants of wild mice Fv1 alleles are complex, and the swapping of restriction phenotypes between alleles often require changes in sequence at multiple residues. Residues important for specificity were found across the 4 variable regions, which have evolved under positive selection (Yan et al., 2009; Yap et al., 2014). The study of wild mice Fv1 alleles confirmed the role of Fv1-CTD as a specificity domain, and suggested that the interaction with CA may involve a large surface on Fv1-CTD. It has also revealed the complexity of the viral recognition by Fv1, where one Fv1 allele can recognise multiple retroviruses from different retroviral genera, at the same time one MLV strain can be recognised by many but not all Fv1 alleles.

A

B

	352	358	399	C-Terminus
Fv1 n	S	K	V	TKL
Fv1 b	S	E	R	GLTSVGSVGVLSLSPWKHQSNS
Fv1 nr	F	K	V	TKL

Figure 1.11 Sequence and structural features of Fv1

A) Structural domains on Fv1. CC, coiled-coil; MHR, major homology region. Variable sites are indicated with blue triangles. B) Sequence variation of major Fv1 alleles.

1.5.3 Viral target of Fv1

Shortly after the initial identification of the *Fv1* gene, there was evidence suggesting that Fv1 restrict MLV by targeting CA. Virus susceptible to both $Fv1^n$ and $Fv1^b$ could be prepared by co-infection of cells with N-MLV and B-MLV (Kashmiri et al., 1977; Rein et al., 1976). This suggested that the determinant for Fv1 restriction is a component that is mixed in virions, such as proteins. NB-tropic virus could be obtained by forced passage of B-MLV in cells expressing $Fv1^n$, and the change in tropism was found to be associated with a genetic change mapping to the gag region (Faller and Hopkins, 1977). By testing the tropism of chimeric MLV containing sections of gag sequence from both N-MLV and B-MLV, it was found that mutations at residues 109 and 110 are sufficient to swap between N and B tropism (DesGroseillers and Jolicoeur, 1983). The charged residue at position 110 was subsequently identified as the most important determinant for N and B tropisms, while R110 of N-MLV is positively changed, E110 of B-MLV is negatively charged (Kozak and Chakraborti, 1996). Since K358 of $Fv1^n$ is positively charged and E358 of $Fv1^b$ is negatively charged, it has been hypothesised that aa358 of Fv1 forms a salt bridge with aa110 of CA. Detailed studies of NR and NB tropisms revealed that in addition to positions 109-110, many other residues on CA including aa 82, 92, 95, 105, 114 and 117 can influence Fv1-mediated MLV tropism (Jung and Kozak, 2000; Lassaux et al., 2005; Stevens et al., 2004). Residues within the β-hairpin including positions 7 and 8 also have strong influence on N and B tropisms (Ohkura and Stoye, 2013). These residues cover a large exposed area of the MLV CA-NTD hexamer (Figure 1.12), suggesting that Fv1 may interact with CA through a large binding surface.

1.5.4 Mechanism of Fv1 restriction

Although it has been well established that Fv1 targets MLV CA, the mechanism by which Fv1 restrict MLV is not clear. Early infection studies showed that Fv1 restriction is independent of the choice of pseudotype envelope and rate of virus adsorption, but requires the presence of MLV cores (Huang et al., 1973; Krontiris et al., 1973). These observations suggested that Fv1 inhibits MLV

infection after viral entry. It was also found that while Fv1 restriction did not affect synthesis of viral linear DNA, the amount of integrated DNA detected was reduced (Jolicoeur and Baltimore, 1976; Sveda and Soeiro, 1976). This suggested that Fv1 restriction affects a step after reverse transcription but before integration. A study of Fv1 localisation showed that Fv1 is present in the cytoplasm and is associated with the trans-golgi network, while a non-restricting mutant is mislocalised to the ER (Yap and Stoye, 2003). The block of MLV by Fv1 occurs in the cytoplasm. In a process known as abrogation, Fv1 can be saturated by pre-exposure to a restrictive virus, leading to loss of restriction towards a second virus which is normally restricted (Duran-Troise et al., 1977). The saturability of restriction is an important property shared by Fv1 and other capsid-targeting restriction factors.

1.5.5 The discovery of Ref1 and Lv1 activities

Early studies have shown that despite the lack of an Fv1-like gene, restriction of N-MLV but not B-MLV is observed in cell lines from human and African green monkey (AGM) (Towers et al., 2000). This activity was termed Ref1, and is associated with many Fv1-like properties including the sensitivity to aa110 of CA, and the abrogation of restriction by pre-treatment with a restrictive virus (Towers et al., 2002). Meanwhile, HIV-1 was found to be restricted in human but not rhesus peripheral blood mononuclear cells (PBMC), and like Fv1 the viral determinants of restriction has been mapped to the gag-pol region (Himathongkham and Luciw, 1996; Shibata et al., 1991). HIV-1 was also found to be restricted in many cell lines derived from old world monkeys, while SIV_{mac} is restricted in many cell lines derived from new world monkeys (Hofmann et al., 1999). One exception among the new world monkeys was owl monkeys, cell lines derived from owl monkeys (OMK cells) restrict HIV-1 instead of SIV_{mac} (Hofmann et al., 1999). This restriction activity against lentiviruses was named Lv1, and like Fv1 this activity is dominant, saturable, and determined by CA sequence (Cowan et al., 2002; Munk et al., 2002). In contrast to Fv1, both Ref1 and Lv1 were found to act before reverse transcription (Besnier et al., 2002; Cowan et al., 2002; Munk et al., 2002).

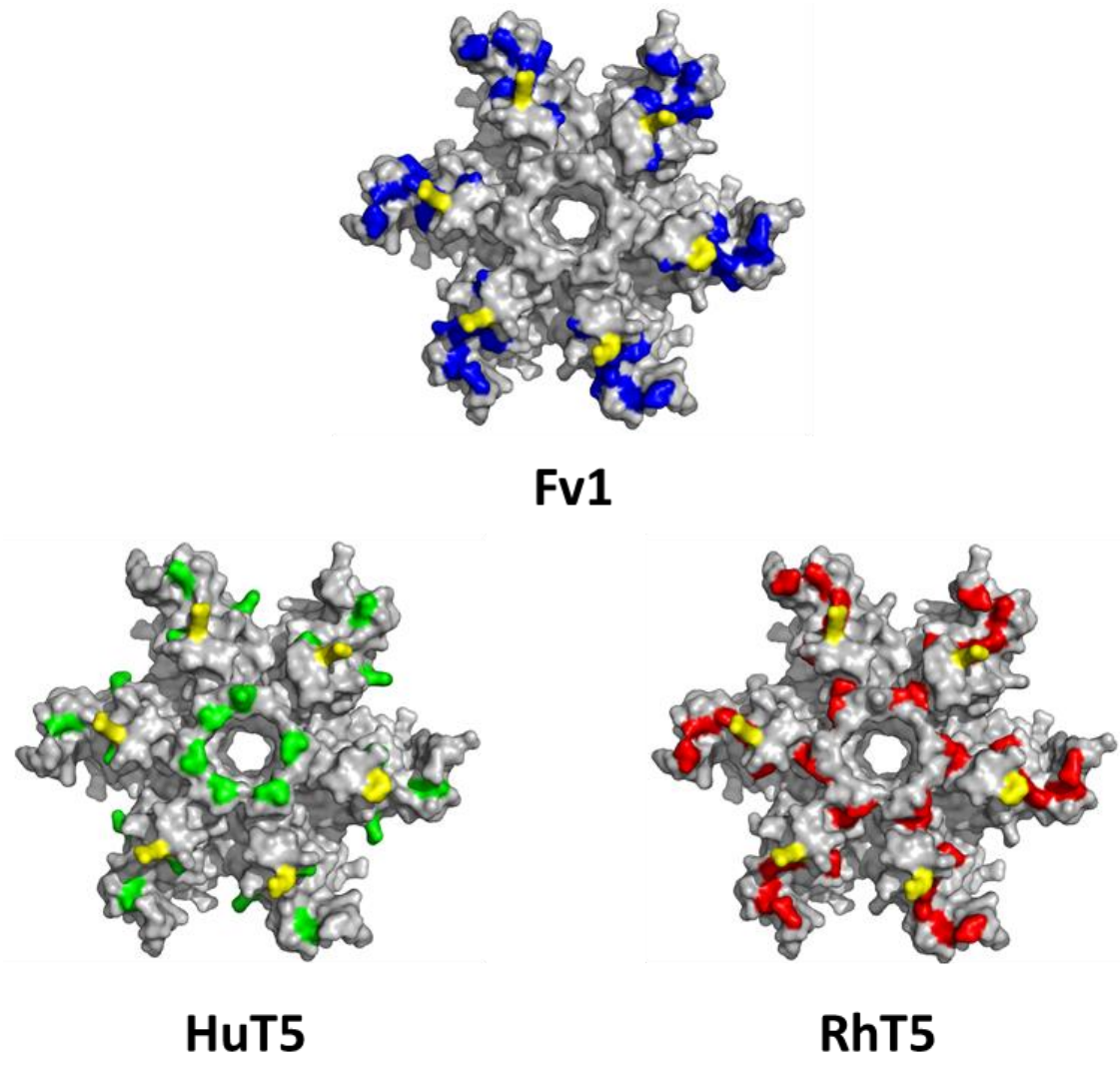

Figure 1.12. Viral determinants for Fv1 and T5 restriction

Top: Determinants of Fv1 restriction (Stevens et al., 2004) are shown on the hexamer structure of N-MLV CA-NTD, PDB: 1U7K (Mortuza et al., 2004). Bottom left: residues involved in HuT5 escape mutations (Ohkura and Stoye, 2013) are labelled in green. Bottom right: residues involved in RhT5 escape mutations (Ohkura et al., 2011) are labelled in red. The residue 110, which affects MLV N and B tropisms in both Fv1 and T5, is labelled in yellow in all structures.

HIV-1 and SIV_{mac} were both found to be restricted in AGM cells, and these activities saturable by pre-treatment with either HIV-1 or SIV_{mac} (Besnier et al., 2002). This suggested that the HIV-1 and SIV_{mac} restriction activities were due to the presence of the same factor, although the restriction specificity varies between alleles (Besnier et al., 2002). Similarly, Ref1 and Lv1 activities were found to be due to the same restriction factor after the discoveries of the restriction of N-MLV and EIAV in human cells, and the restriction of HIV-1, SIV_{mac}, N-MLV and EIAV in AGM cells (Hatziioannou et al., 2003). The hypothesis was strengthened by the fact that in these cells, both Lv1 and Ref1 activities can be abrogated by restrictive lentiviruses and gamma-retroviruses (Hatziioannou et al., 2003).

1.5.6 The identification of T5 and TCyp

By screening a rhesus monkey cDNA library for genes which confer HIV-1 restriction activity in human cells, T5 was identified to be responsible for Lv1 activity (Stremlau et al., 2004). This was soon confirmed by a number of groups, and T5 was found to be restriction factor for both Ref1 and Lv1 activities (Hatziioannou et al., 2004; Keckesova et al., 2004; Perron et al., 2004; Yap et al., 2004). These studies showed that expression of T5 in non-restricting cells can confer resistance, while depletion of endogenous T5 by siRNA can abolish restriction. T5 is a tripartite motif family protein and contains the RING, B-box 2, coiled-coil (RBCC) domain in the N-terminal region, and a B30.2 domain in the C-terminal region (Figure 1.13).

As mentioned earlier, although cells from new world monkey mostly restrict SIV_{mac} but not HIV-1, OMK cells restrict HIV-1 but not SIV_{mac} (Hofmann et al., 1999). Interestingly, the HIV-1 restriction in OMK cells can be abolished by treatment of Cs, which blocks the interaction between the host protein CypA and the CypA binding loop of HIV-1 CA (Towers et al., 2003). Subsequent cloning of the OMK T5 locus revealed the OMK TCyp allele, which is expressed as a fusion protein with RBCC domain of T5 and CypA instead of B30.2 domain (Figure 1.13) (Nisole et al., 2004; Sayah et al., 2004). The OMK TCyp allele is formed by the retrotransposition of CypA pseudogene into the T5 locus of OMK genome (Nisole et al., 2004; Sayah et al., 2004). Since the discovery of OMK

TCyp, many other TCyp alleles resulted from separate retrotransposition events have been identified. These include a TCyp allele found in old world monkeys (Brennan et al., 2007; Newman et al., 2008; Virgen et al., 2008; Wilson et al., 2008), an ancient but decayed primate TCyp allele (Malfavon-Borja et al., 2013), a TCyp allele found in zebrafish and pufferfish (Boudinot et al., 2011), and more recently a TCyp allele found in tree shrews (Mu et al., 2014). The *CypA* gene is frequently duplicated by retrotransposition, which resulted in over 60 copies of defective *CypA* pseudogenes in the human genome (Zhang et al., 2003). These TCyp alleles are unique among other CypA duplications due of the expression of a chimeric T5-CypA fusion protein. The fact that this unusual fusion event occurred on 4 independent occasions in different species suggested a strong evolutionary advantage for the expression of TCyp, most likely by allowing the recognition and restriction of HIV-1 by T5 using the CypA domain. There are 17 cyclophilin proteins in human (Davis et al., 2010). There has not been any report of retrotransposition events which resulted cyclophilin fusion genes apart from T5-CypA fusions. The convergent evolution of TCyp fusion proteins, as well as the sensitivity of restriction to the abolishment of CypA-CA interaction, suggested that the B30.2 domain in T5 could also be involved in the interactions between T5 and CA in other alleles.

1.5.7 The T5 RBCC domain

T5 contains the RBCC domain in the N-terminal region, and the B30.2 domain in the C-terminal region (Figure 1.13). Two flexible linker regions are also found in T5, with Linker-1 (L1) present between the RING and B-Box2, and Linker-2 (L2) between the coiled coil and B30.2. The RBCC domain is conserved among members of the tripartite motif (Trim) protein family, and is required for many properties of T5, including dimerisation, high order self-association, formation of cytoplasmic bodies, turnover, and E3-ubiquitination activity. Like Fv1, T5 forms antiparallel dimers (Goldstone et al., 2014). Crystal structure of a fragment of T5 B-Box2 and coiled-coil showed that the dimerisation is mediated by extensive interactions between the long continuous α-helices of coiled coil domains (Goldstone et al., 2014). The coiled-coil of Trim25 was also crystalised and

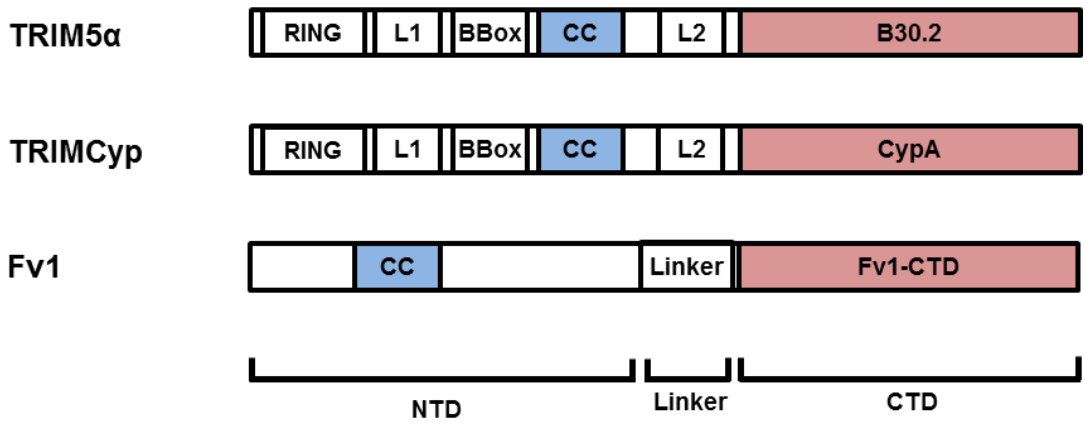

Figure 1.13 A comparison of domain organisations of Fv1, T5 and TCyp

The coiled-coil (CC) domains are highlighted in blue, while the capsid-targeting domains are highlighted in pink.

showed similar structure (Sanchez et al., 2014). In the T5 dimer, B-box2 domains are located on each end of the rod shape coiled-coil (Goldstone et al., 2014). T5 dimers also form higher order assemblies, and studies of chemically crosslinked T5 mutants suggested that this requires the RING domain, the B-Box2 domain, the L2 region but not the B30.2 domain (Diaz-Griffero et al., 2009; Li and Sodroski, 2008; Liberatore and Bieniasz, 2011). The formation of higher order assembly correlates with stronger binding to HIV-1 CA-NC assemblies *in vitro* (Diaz-Griffero et al., 2009; Li and Sodroski, 2008; Liberatore and Bieniasz, 2011). A recombinant T5 protein with a Trim21 RING domain (T5-21R) was found to self-assembly into regular hexagonal lattice, this led to the proposal that the higher order self-association of T5 may allow the formation of a T5 super-lattice, which lays on top of the CA hexagonal lattice during restriction (Ganser-Pornillos et al., 2011).

Some T5 alleles can also form cytoplasmic bodies (Stremlau et al., 2004). The determinants for cytoplasmic body formation has been mapped to the L2 region (Sastri et al., 2010). The functional importance of T5 cytoplasmic bodies remains controversial. Blocking the formation of these cytoplasmic bodies with inhibitors did not appear to affect viral restriction (Song et al., 2005a). In contrast, L2 mutants which do not form cytoplasmic body but still multimerise, fail to restrict HIV-1 (Sastri et al., 2010). Co-localisation of T5 cytoplasmic bodies with viral core and proteasome subunit has also been observed during viral infection (Lukic et al., 2011). The RING and B-box2 domains mediate the rapid turnover of T5 through proteasomal degradation, and increased turnover of T5 has been observed in infected cells (Diaz-Griffero et al., 2006). E3-ubiquitin ligase activity of RING domain also leads to self-ubiquitination, this leads to mono-ubiquitination of T5 for translocation which signal the translocation of T5 from cytoplasmic body to cytoplasm (Yamauchi et al., 2008). E3-ubiquitin ligase also acts with other proteins to synthesise unattached K63-linked polyubiquitin chains, which then activate TAK1 kinase and transcription factors NF-κB and AP-1, leading to activation of the type 1 interferon pathway (Pertel et al., 2011).

1.5.8 The T5 B30.2 domain and restriction specificity

The restriction specificities of many primate T5 alleles have been studied (Ohkura et al., 2006; Song et al., 2005c; Stremlau et al., 2005; Yap et al., 2008). Like Fv1, some primate T5 alleles restrict retroviruses across gamma-retroviruses, lentivirus, and spumavirus genera, yet display high specificities within the same genus. For example, the Orang-utan T5 can restrict HIV-1, SIV_{mac}, N-MLV and FFV, but neither N-MLV nor PFV (Ohkura et al., 2006; Yap et al., 2008). Two alleles, human T5 (HuT5) and rhesus T5 (RhT5), are important to this thesis. HuT5 restricts N-MLV and EIAV but does not inhibit B-MLV and NB-MLV, with weak inhibition of HIV-1, SIV_{mac} and the lentivirus feline immunodeficiency virus (FIV) reported in some studies; RhT5 restricts HIV-1, N-MLV, EIAV and FIV but does not inhibit B-MLV and NB-MLV, with weak inhibition of SIV_{mac} reported in some studies (Hatziioannou et al., 2004; Keckesova et al., 2004; Ohkura et al., 2006; Perron et al., 2004; Saenz et al., 2005; Song et al., 2005c; Stremlau et al., 2004; Yap et al., 2004).

The specificity determinants of T5 restriction are mostly found on the B30.2 domain. The restriction specificity of T5 is defined by many residues in 3 variable regions of B30.2 domain, with many showing evidence of positive selection indicated by a high ratio of non-synonymous to synonymous mutations (Kono et al., 2009; Maillard et al., 2007; Ohkura et al., 2006; Perron et al., 2006; Pham et al., 2013; Rahm et al., 2011; Sawyer et al., 2005; Song et al., 2005b; Stremlau et al., 2005). An example of these important residues is the R332 residue in human T5 (HuT5), mutation at this residue such as R332P allows HuT5 to fully restrict HIV-1 (Li et al., 2006c; Yap et al., 2005). Residues of these regions are present as flexible loops located one side of the core B30.2 structure, which is formed of a β-sandwich containing two 7-stranded antiparallel β-sheets (Biris et al., 2012; Ohkura et al., 2006; Yang et al., 2012). These studies suggested that the recognition of retrovirus by T5 involves a large binding surface comprising of loops.

1.5.9 Viral target of Trim5α

Like Fv1, the E110R mutation leads to the gain of T5 restriction by B-MLV, and aa110 was once considered as the primary determinant for Fv1 and T5 restriction (Figure 1.12) (Perron et al., 2004). Studies of N-MLV escape mutants, which were selected through passaging in cells, led to identification of many escape mutations (Ohkura et al., 2011; Ohkura and Stoye, 2013). Some escape mutants have reduced infectivity, indicating that the escape from T5 restriction may come with a fitness cost. These escape mutations, many of which involved charged residues, are found on the exposed surface of CA-NTD hexamer (Figure 1.12). This suggested that the interaction between T5 and CA may involve electrostatic interactions between B30.2 and CA-NTD hexamer. Since many of these mutations not only alter the sensitivity to T5 but also alter the sensitivity to Fv1, there may be significant overlap between the binding sites of Fv1 and T5 on MLV CA. A study of HIV-1 escape mutants selected in RhT5-expressing cells also yielded mutations across the exposed surface of the CA-NTD hexamer (Soll et al., 2013). In contrast, the restriction of TCyp is sensitive to only a few mutations on the CypA binding loop.

1.5.10 Mechanism of Trim5α restriction

In contrast to Fv1, T5 also inhibits reverse transcription (Stremlau et al., 2004). Inhibition of proteasome can remove the block in reverse transcription, but not the viral restriction (Anderson et al., 2006; Wu et al., 2006). There has been suggestion that this early proteasome-dependent block is caused by the accelerated uncoating of viral core upon T5 binding (Perron et al., 2007; Stremlau et al., 2006). This is supported by the observation of HIV-1 CA-NC tube disassembly when mixed with cell lysates containing RhT5 (Zhao et al., 2011), and the fact that accelerated uncoating of core by T5 is also proteasome-dependent (Kutluay et al., 2013). In the presence of proteasome inhibitors such as MG132, T5 does not block reverse transcription but still blocks viral infection before integration, resembling the restriction by Fv1 and Mx2. This proteasome-independent block could be due to the formation of a T5 super-lattice surrounding the core (Ganser-Pornillos et al., 2011), thereby preventing binding of host factors required for trafficking or nuclear entry. Interestingly, proteasome inhibitors can partially relieve the restriction of HIV-1 and SIV_{mac} by HuT5 R332P but not by RhT5, suggesting that there are situations where both blocks are required to achieve full restriction (Maegawa et al., 2010).

1.6 Studies of Fv1 binding and restriction

1.6.1 The apparent $Fv1^b$ inhibition of NB-MLV and B-MLV

Early studies of Fv1 restriction specificity were carried out by measuring infectivity of different MLV strains in mice or cell lines which endogenously express Fv1, such as N-3T3 which expresses $Fv1^n$ and B-3T3 which expresses $Fv1^b$ (Kozak and Chakraborti, 1996; Pryciak and Varmus, 1992). However, the infectivity of MLV in these mice or cell lines is also affected by other factors unrelated to Fv1, and it is difficult to manipulate the Fv1 gene to study the effect of mutations and deletions on MLV replication. Therefore, there was a need for a reliable assay which allows study of the specific effect of a recombinant Fv1 on MLV growth, in order to study the Fv1 determinants of MLV tropism. In 2000, a flow cytometry based restriction assay was developed in our lab (Bock et al., 2000), and has since been used in many studies of Fv1 and T5 (Bishop et al., 2001; Nisole et al., 2004; Stevens et al., 2004; Yap et al., 2014; Yap et al., 2008; Yap et al., 2004).

In this assay (Figure 1.14), Fv1 is expressed in a retroviral vector which will be referred to as LxIG (or pLxIG for the vector plasmid) in this thesis (Bock et al., 2000). Infection of cells with this delivery vector virus leads to integration of provirus into the host genome. Transcription from the provirus is driven by the efficient MLV U3 promoter, synthesising a bicistronic mRNA with the Fv1 ORF close to the 5' end, followed by an internal ribosome entry site (IRES) originating from the genome of the encephalomyocarditis virus (EMCV) (Jang et al., 1988), and the enhanced green fluorescent protein (EGFP) reporter ORF close to the 3' end (Zhang et al., 1996). Translation initiated at the 5' CAP structure of the transcript allows expression of Fv1, while translation initiated at the IRES leads to expression of EGFP. This assay used a mouse cell line termed *Mus dunni* tail fibroblast (MDTF), that cannot express Fv1 due to a premature stop codon in its $Fv1^o$ allele (Lander and Chattopadhyay, 1984; Qi et al., 1998a). Transduction of MDTF cells with the LxIG-Fv1 vector at multiplicities of infection (MOI) of 1 or below allows the expression of both Fv1 and EGFP in a subpopulation of cells. The restriction caused by Fv1 can then be tested by comparing the infectivity of a MLV tester virus in the GFP^+ population to that of

the GFP^- population. These tester viruses were generated using gag sequence from N-MLV, B-MLV or NB-MLV (specifically Moloney MLV), and a genome which allows expression of EYFP under the MLV U3 promoter. FACS analysis allow the separation of cells into 4 populations based on GFP and YFP fluorescent signals, and restriction can be measured as a ratio of the percentage of YFP^+ cells in the GFP^+ population relative to the percentage of YFP^+ cells in the GFP^- population.

The study of $Fv1^n$ using this assay showed restriction of B-MLV by almost 20-fold, but neither N-MLV nor NB-MLV (Bock et al., 2000). However, the results for $Fv1^b$ were surprising, in addition to the restriction of N-MLV by almost 20-fold, $Fv1^b$ also appeared to restrict NB-MLV by more than 5-fold, and appeared to weakly inhibit B-MLV by about 30% (Bock et al., 2000). These results raised many questions about the Fv1-controlled N and B tropisms. Why was the observed restriction specificity of $Fv1^b$ different from previous reports that $Fv1^b$ does not restrict NB-MLV and B-MLV (Hartley et al., 1970)? One hypothesis was that due to the strong MLV U3 promoter, Fv1 could be overexpressed in MDTF cells compared to cells with endogenous expression of Fv1 (Bock et al., 2000). Can the over-expression of $Fv1^b$ leads to restriction of NB-MLV and B-MLV? If it can, why did $Fv1^n$ fail to restrict or inhibit N-MLV or NB-MLV in the same assay? The observed restriction activities of $Fv1^b$ appeared to be strongest against N-MLV, intermediate against NB-MLV, and weakest against B-MLV. It then seems reasonable to ask whether the differences between restriction activities of $Fv1^b$ towards MLV strains reflect differences in binding activities of $Fv1^b$ towards different MLV capsid core.

1.6.2 The complex determinants of Fv1 restriction specificity

In order to study the determinants of Fv1 restriction specificity, 6 Fv1 mutants, termed “mix-and-match” mutants, were generated by swapping the amino acid sequence between $Fv1^n$ and $Fv1^b$ at the variable sites aa358, aa399 and the C-terminus (Bock et al., 2000). The $Fv1^n$ allele contains the sequence K358, V399 and a short 3aa C-terminal tail; while the $Fv1^b$ allele contains the sequence E358, R399 and a long 22aa C-terminal tail (Best et al., 1996). In this thesis,

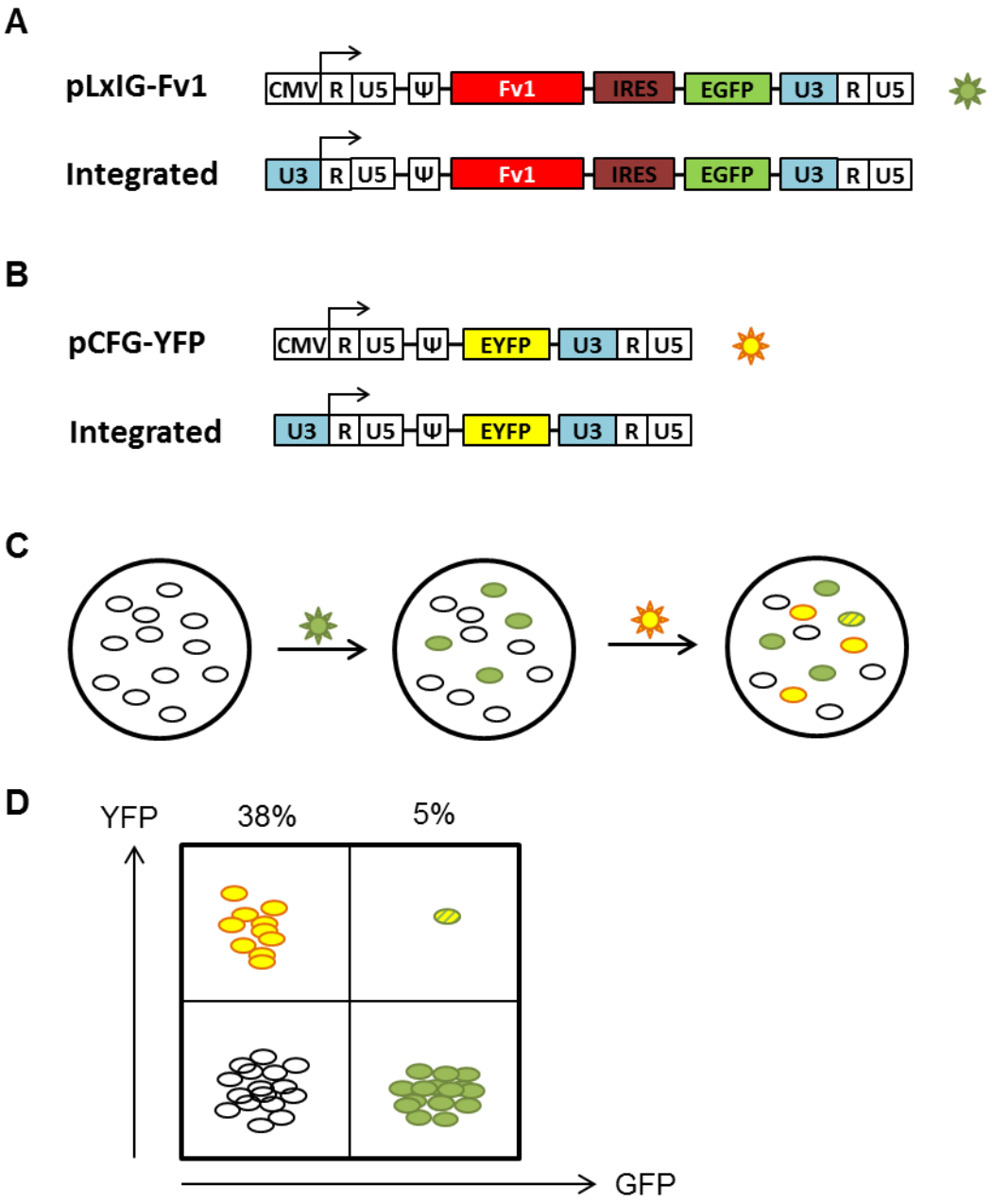

Figure 1.14 Study of Fv1 restriction using a 2-colour FACS assay

The 2-colour FACS assay was described in (Bock et al., 2000). (A) The pLxIG-Fv1 vector plasmid was used to generate delivery virus for transduction of MDTF cells. (B) The pCFG-YFP vector plasmid was used to generate tester virus for infection of transduced cells. (C) MDTF cells were first infected with delivery virus, allowing expression of Fv1 and EGFP in a subpopulation of cells. Subsequent infection with tester virus leads to expression of YFP in infected cells. (D) A hypothetical FACS plot showing a situation where the recombinant Fv1 leads to restriction of YFP tester virus.

the wild-type and mutant Fv1 variants will be identified by a 3-letter code, with the first, second and third letter corresponding to the source of sequence at aa358, aa299 and C-terminus, respectively. Illustrated in Table 1.1, the sequence at aa358 appeared to have the strongest influence on the restriction of N-MLV, since N-MLV appeared to be restricted by Fv1 variants with E358 but not R358 (Bock et al., 2000). Subsequent studies with alanine mutations suggested that A358 also leads to restriction of N-MLV, suggesting the positively charged R358 may be preventing N-MLV restriction (Bishop et al., 2001). For B-MLV, full or partial restriction was observed with all Fv1 variants except Fv1bbb and Fv1bnb, suggesting that the combination of E358 and a long C-terminal tail have inhibitory effect on Fv1 restriction (Bock et al., 2000). This was also confirmed by the fact that Fv1bAb (where A represent A399) did not restrict B-MLV (Bishop et al., 2001). However, partial restriction of B-MLV is observed with Fv1Abb but not Fv1Anb mutant suggesting that R399 also enhances B-MLV restriction, and similarly weak inhibition is observed in Fv1bbb but not Fv1bnb variants (Bishop et al., 2001; Bock et al., 2000). All variants which restrict NB-MLV has R399, although the mutant Fv1nbb did not restrict NB-MLV (Bock et al., 2000). The Fv1bAn mutant was also found to partially restrict NB-MLV, suggesting that several combinations of sequence at the variable sites can lead to NB-MLV restriction (Bishop et al., 2001).

These early studies revealed the complexity of the determinants of Fv1 restriction specificity. How do different Fv1 mutations lead to different restriction specificity against N-MLV, B-MLV and NB-MLV? It has been hypothesised that a mutation may change the binding affinities of Fv1-CTD to different MLV CA, leading to alteration of restriction specificity. However, other factors such as Fv1 expression level and localisation may also play a role. For example, the mutation may lead to an increase in Fv1 protein concentration, which may allow the gain of binding to CA without a change in the intrinsic binding affinity. The different concentration of endogenous $Fv1^n$ than $Fv1^b$ suggested that mutations may have an effect on Fv1 protein level, either at transcription or translation levels (Yap and Stoye, 2003). Mutations could also alter the intracellular localisation of Fv1, sequestering Fv1 from the incoming core. This is supported by the fact that an Fv1 mutation with internal deletions (Int1, aa109-118 deleted) was inactive (Bishop et al., 2001) and mis-localised from the trans-

Golgi network to ER (Yap and Stoye, 2003). Which of these effects were contributing to the Fv1 restriction specificity?

1.6.3 Fv1 and T5 binding require polymeric CA

In order to test the hypothesis that binding has a major role in determining the specificity of MLV restriction by Fv1, the development of an assay to study Fv1 binding to MLV CA would be needed. However, the demonstration of Fv1 to MLV binding was found to be difficult. Early attempts in our lab to demonstrate the interaction between Fv1 and CA using yeast two-hybrid or co-immunoprecipitation techniques were unsuccessful (cited in Dodding et al., 2005). However, in a process known as abrogation, Fv1 can be saturated by pre-exposure to a restrictive virus, leading to loss of restriction towards a second virus which is normally restricted (Duran-Troise et al., 1977). This strongly suggested an interaction between Fv1 and the viral core, and this must require a polymerised form of CA rather than monomeric CA. The human factor Ref1 which restricts N-MLV but not B-MLV is also sensitive to mutations at aa110 in a similar way to Fv1 (Towers et al., 2000). This also led to the question on whether Fv1 and Ref1 recognise MLV CA in a similar way. A study in our lab showed that the expression of properly processed, monomeric form of MLV CA cannot saturate Fv1 and Ref1 activities (Dodding et al., 2005). Furthermore, we showed that processing at both N-terminus and C-terminus of MLV CA, as well as the stabilisation of β-hairpin by the P1-D54 salt bridge, are essential for abrogation of Fv1 and Ref1 activities (Dodding et al., 2005). These data suggested that both Fv1 and T5 recognise the mature capsid shell consisting of polymerised MLV CA. Similar data on TCyp restriction were published by another lab (Forshey et al., 2005).

Since the cloning of T5, the specific pull-down of N-MLV CA by glutathione S-transferase (GST)-tagged HuT5 in cell lysate was reported (Sebastian and Luban, 2005). However, many attempts in our lab and other labs failed to reproduce such finding (Jonathan Stoye, personal communication). Shortly afterwards, Stremlau et al demonstrated the specific binding of T5 to HIV-1 CA-NC tubes (Stremlau et al., 2006). These tubular

Fv1	N-MLV	B-MLV	NB-MLV
bbb	+	(-)	(+)
bbn	+	+	+
bnb	+	-	-
bnn	+	(+)	-
nnn	-	+	-
nnb	(-)	+	-
nbn	-	+	+
nbb	-	+	-
nn_	-	+	-
bb_	+	(+)	+

Table 1.1 Complex restriction specificity of Fv1

Restriction phenotypes of "mix-and-match" and C-terminal tail truncation Fv1 mutants (Bishop et al., 2001; Bock et al., 2000). The mutants were named with a 3 letter code. The first, second and third letter represent the origin of sequence at positions 358, 399 and C-terminus, respectively. For example, wild-type $Fv1^n$, which has the sequence K358, V399 and short 3aa tail at C-terminus, is labelled as nnn; while wild-type $Fv1^b$, which has the sequence E358, R399 and a long 22aa tail at C-terminus, is labelled as bbb. Underscore indicates the truncation of C-terminal tail.

complexes were assembled by incubating HIV-1 CA-NC with a DNA oligonucleotide. Following incubation with lysate from cells transiently over-expressing T5, the CA-NC tubes together with bound T5 were separated from unbound T5 and cellular proteins by ultracentrifugation through a 70% sucrose cushion. This study demonstrated the specific binding of RhT5 but not HuT5 to HIV-1 CA-NC tubes (Stremlau et al., 2006). The binding was also found to require the coiled-coil and B30.2 domains but not the RING and B-box domains, suggesting that the basic requirement for restriction factor binding is the presence of a multimerisation domain and a capsid-binding domain. This idea was confirmed by the discovery that artificial restriction factor against HIV-1 could be generated by fusing various dimerisation domains to CypA (Yap et al., 2007). The R332P mutant of HuT5 which restricts HIV-1 was also found to bind HIV-1 CA-NC tubes, which confirms the role B30.2 in defining the binding and restriction specificity of T5 (Li et al., 2006c; Yap et al., 2005).

1.6.4 The apparent binding of $Fv1^b$ to NB-MLV and B-MLV

The demonstration of T5 binding to HIV-1 CA-NC suggested that a similar approach could be used to study binding of Fv1 and T5 to MLV CA. However, N-MLV and B-MLV CA-NC failed to polymerise in the presence of oligonucleotides, so other methods were explored (Hilditch, 2010). Other studies have described the assembly of hexameric array by N-terminally His-tagged MLV CA on planar monolayer lipid containing a Nickel-chelating lipid, which have proved useful for high resolution electron tomography studies as the averaging of symmetric units of the assay allows reduction of signal to noise ratio (Barklis et al., 1997; Ganser et al., 2003; Mayo et al., 2003). An alternative method known as helical crystallisation has also been developed to form protein arrays on lipid nanotubes (Wilson-Kubalek et al., 2010). These nanotubes involve a curvature forming lipid galactosylceramide (GalCer), and a lipid with functionalised head group such as the Nickel-chalating 1,2-dioleoyl-sn-glycero-3-[(N-(5-amino-1-carboxypentyl) iminodiacetic acid)succinyl] (DGS-NTA) (Dang et al., 2005a; Dang et al., 2005b). After incubation with C-terminally His-tagged MLV CA, lipid nanotubes can be observed to be coated with a regular protein layer by electron microscopy (Hilditch et al., 2011). Tomography studies showed that the protein array is organised as a hexagonal lattice (Hilditch et al.,

2011). Binding of Fv1 could be studied by incubation of CA-coated lipid nanotubes with lysate from cells over-expressing Fv1, followed by separation of nanotubes and bound Fv1 from unbound proteins by ultracentrifucation through a 40% sucrose cushion (Hilditch et al., 2011). This study showed the specific binding of $Fv1^n$ to B-MLV CA, but not to N-MLV or NB-MLV. This binding specificity matched the observed restriction specificity from our early study (Bock et al., 2000). Similar to the restriction specificity of $Fv1^n$, the binding specificity of $Fv1^n$ is also sensitive to mutation at aa110. While E110R mutation in B-MLV leads to loss of binding, the R110E mutation in N-MLV leads to gain of binding to $Fv1^n$. This binding can be abolished by either of two mutations, P1G and D54A, which disrupt the formation or stabilisation of β-hairpins. Electron microscopy showed disruption to the otherwise regular lattice on nanotubes coated with P1G and D54A CA. This confirmed the idea that Fv1 interacts with the mature form of CA, in which the β-hairpin is stabilised (Mortuza et al., 2004). While many $Fv1^n$ mutants that do not restrict B-MLV also failed to bind B-MLV CA, binding of Int1 mutant to B-MLV could be detected. Therefore, the defect in Int1 was most likely due to mis-localisation rather than loss of binding (Yap and Stoye, 2003).

The pattern of $Fv1^b$ binding observed using this assay was more surprising. $Fv1^b$ appeared to bind CA from N-MLV, B-MLV and NB-MLV equally (Hilditch et al., 2011). These $Fv1^b$ binding can be abolished by P1G and D54A mutation in CA, ruling out the non-specific interactions with lipids. Since $Fv1^b$ restriction showed strong restriction of N-MLV, intermediate restriction of NB-MLV and weak inhibition of B-MLV (Bock et al., 2000), differences between the apparent binding affinities of $Fv1^b$ to different MLV CA is expected if there is a direct restriction-binding correlation. Why was a differential binding of $Fv1^b$ to different MLV CA not observed using this binding assay? First, it is possible that $Fv1^b$ distinguishes between CA of different tropisms by recognising a structure that present on the mature capsid shell, but not on the CA lattice on lipid nanotubes. The curvature of the nanotubes is different from that of a mature MLV core. The C-terminus of CA is tethered to the lipids via the His-tag, which may have prevented some of the conformational changes required to complete the maturation. Secondly, it is possible that although $Fv1^b$ binds to all MLV CA with similar apparent affinity, there are differences in the amount of $Fv1^b$ binding

required to cause restriction. Lastly, it is possible that while $Fv1^b$ binds to all MLV CA, the small differences in apparent binding affinity can only distinguish at a small window of $Fv1^b$ concentrations.

1.6.5 Fv1 expression level and restriction

Restriction of NB-MLV and weak inhibition of B-MLV by $Fv1^b$ was observed in a previous study in our lab (Bock et al., 2000), but not in previous studies carried out in cell lines expressing $Fv1^b$ endogenously (Hartley et al., 1970). On the other hand, the binding of $Fv1^b$ to all MLV CA on lipid nanotubes appears to be similar (Hilditch et al., 2011). To explore the possibility that the apparent $Fv1^b$ restriction of NB-MLV and inhibition of B-MLV could be due to over-expression, an examination of the relationship between Fv1 concentration and restriction began in a previous study (Felton, 2012). First, the transcription and translation of endogenous $Fv1^n$ and $Fv1^b$ were studied. The core Fv1 promoter was identified within the 431bp upstream of the Fv1 ORF. This promoter is not interferon-inducible, but has bidirectional activities for transcription of both *Fv1* and the neighbouring gene *Miip*, which encode the Migration and invasion inhibitory protein. Despite having almost identical promoter sequences, quantitation of Fv1 transcripts revealed a 23-fold higher Fv1 mRNA level in N-3T3 cells endogenously expressing $Fv1^n$ than in B-3T3 cells which endogenously expressing $Fv1^b$. The protein level of $Fv1^n$ in N-3T3 was also reported to be higher than that of $Fv1^b$ in B-3T3. The protein level of Fv1 expressed by LxIG-Fv1 vectors in MDTF cells was also found to be higher than the endogenous level. This suggested that the MLV U3 promoter in the LxIG vectors is more efficient than the Fv1 promoter, and supports the hypothesis that the over-expression of Fv1 may affect the restriction specificity of $Fv1^b$.

Next, attempts were made to develop a system to express recombinant Fv1 at a level similar to the endogenous level of Fv1, and yet express sufficient amount of reporter proteins for FACS-based restriction assay. Despite many failed attempts, study of $Fv1^b$ restriction using one particular vector did show specific restriction of N-MLV without any measureable inhibition of B-MLV. This suggested that at low but unknown concentration of $Fv1^b$, no B-MLV inhibition is observed. To directly prove that the restriction of NB-MLV and inhibition of B-

MLV are linked to over-expression of $Fv1^b$, an attempt was made to develop a system for inducible expression of Fv1 for restriction study. This system employed the Tet-On inducible expression system, which allows dose-dependent induction of Fv1 and reporter expression by doxycycline. However, this system suffers from a number of problems, including the low expression level of reporter protein and the high basal expression of Fv1 even in the absence of the inducer. Study of $Fv1^b$ using this system did show that increase of $Fv1^b$ expression from the basal level to the maximally induced level can reduce infectivity of NB-MLV from 50% to 20%, and reduce infectivity of B-MLV from 100% to 70%. Analysis of $Fv1^b$ protein level suggested that the basal protein level is already much higher than the endogenous level. Data from this study suggested that an increase in $Fv1^b$ expression from an already over-expression level can lead to further increase in restriction. However, this did not provide direct evidence of how increasing the $Fv1^b$ concentration from the endogenous level to the overexpression level correlate with the change in restriction specificity.

1.6.6 Aims of project

In this thesis I aimed to address some of the unanswered questions on binding and restriction of two capsid-binding restriction factors, Fv1 and T5. These questions can be broadly summarised into two important questions.

Question 1: What controls the Fv1 restriction specificity?

Specifically, I wanted to dissect the relationships between Fv1 expression level and restriction specificity, between Fv1 concentration and binding specificity, and between binding and restriction specificities. I started by first attempting to address the question on whether $Fv1^b$ specifically bind N-MLV at low concentration. A binding assay which allows the comparison of Fv1 binding at multiple Fv1 concentrations was developed. However, the specific binding of $Fv1^b$ to N-MLV only could not be detected. I then attempted to address the question on whether an increase in $Fv1^b$ concentration from the endogenous level to an over-expression level can lead to emergence of NB-MLV and B-MLV restriction. This was studied using an optimised inducible expression system which allows inducible Fv1 expression from a very low basal level to an over-

expression level, while at the same time allows high expression of reporter gene for FACS-based assay. The results have demonstrated that the inhibition of NB-MLV and B-MLV was indeed caused by the over-expression level of $Fv1^b$. By correlating restriction with Fv1 protein level, I also demonstrated that even at the endogenous level, $Fv1^b$ imposes a weak inhibition against NB-MLV. Next I wanted to address the question on how sequences at the 3 variable sites influence the restriction specificity, using a total of 10 Fv1 variants which have different sequence at the 3 sites. I compared the over-expression level of different Fv1 alleles, and found that some residues have strong effects on Fv1 protein levels. I then used the new binding assay to compare the binding of all 10 variants to all 3 MLV CA, and found a good correlation between binding and restriction for N-MLV and NB-MLV. Interestingly, the Fv1bnb mutant does not seem to restrict B-MLV despite an apparently strong binding to B-MLV CA.

Question 2: Do Fv1 and T5 recognise the same structure on MLV CA?

Specifically, I wanted to develop a binding assay which allows recognition of both Fv1 and T5 to MLV CA, to allow the study of differences in the recognition mechanisms by these capsid-binding restriction factors. I first attempted to study binding of T5 to MLV CA using the binding assay developed for Fv1 binding. However, no binding of T5 to N-MLV could be observed. I explored other methods of generating binding CA assemblies that can be used for binding study *in vitro*. Since there has been report of success in generating HIV-1 hyperstable core and *in vitro* CA assemblies by introducing intra-hexameric disulphide crosslinking (Meng et al., 2012; Pornillos et al., 2010), MLV virus particles with double cysteine mutations were screened for evidence of crosslinking. Two mutants were form crosslinked CA without defects in gag processing, however abrogation studies in cells endogenously expressing $Fv1^b$ and HuT5 suggested that the cores of these mutants do not form a structure that can be recognised by restriction factors.

Chapter 2

Materials and Methods

2.1 Recombinant DNA

A list of plasmids purchased or obtained for use in this study is shown in Table 2.1 and Table 2.2.

2.1.1 Polymerase Chain Reaction (PCR)

A list of PCR products with their corresponding templates and primers is shown in Table 2.3. Amplification of DNA fragments from plasmids with introduction of new restriction sites was performed by PCR using custom made primers (Sigma). Each 50µl PCR reaction contained 50ng of plasmid template, 25pmol of forward primer, 25pmol of reverse primer, 200µM of each dNTP, 2.5U of PfuUltra high fidelity polymerase (Agilent Technologies) in the supplied buffer. PCR reactions were carried out using a PTC-100 thermal cycler (MJ research). Thermo cycling parameters typically consisted of 2min of initial denaturation at 95^{o}C; followed by 25 to 30 cycles of 1min denaturation at 95^{o}C, 1min annealing at 5^{o}C below the lowest melting temperature (T_m) of the primers, 2min extension at 72^{o}C; and a final 10min extension at 72^{o}C.

2.1.2 DNA separation by agarose gel electrophoresis

To analyse the size of DNA fragments, samples were mixed with a 6X DNA-loading buffer (0.25% bromophenol blue, 0.25% xylene cyanol FF, 30% glycerol) and analysed by electrophoresis on agarose gels at 100V along with SmartLadder DNA size marker (Eurogentec). Agarose gels were made with 0.8 to 1.2% agarose (Melford), 0.5µg/ml ethidium bromide (Biorad) and TBE buffer (0.09M Tris-HCl, 0.09M borate, 2mM EDTA, at pH 8.4).

Short name	Long name	Source/Reference
pQCXIX		ClonTech #631515
pTREPuro-DEST	pLenti-CMVTRE3G-Puro-DEST	Eric Campeau (Addgene #27565)
pCMVrtTA3G	pLenti-CMV-rtTA3-Blast	Eric Campeau (Addgene #26429)
pVSV-g		(Yee et al., 1994)
pHIT60		(Soneoka et al., 1995)
pCIGB		(Bock et al., 2000)
pCIGN		(Bock et al., 2000)
pCIGN-57	pCIGN-S57C	Ophélie Cosnefroy
pCIGN-44	pCIGN-V44C	Ophélie Cosnefroy
pCIGN-47	pCIGN-T47C	Ophélie Cosnefroy
pCIGN-48	pCIGN-H48C	Ophélie Cosnefroy
pCIGN-4457	pCIGN-V44C/S57C	Ophélie Cosnefroy
pCIGN-4757	pCIGN-T47C/S57C	Ophélie Cosnefroy
pCIGN-4857	pCIGN-H48C/S57C	Ophélie Cosnefroy
p8.91		(Naldini et al., 1996)
p8.91-1445	p8.91-A14C/E45C	Ophélie Cosnefroy
pLNCG		(Yap et al., 2004)
pCFG-YFP	pCFG2-fEYFPf	(Bock et al., 2000)
pCSGW		(Bainbridge et al., 2001)
pHIT111		(Soneoka et al., 1995)
pENTR-LUC		Eric Campeau (Addgene #17473)
pENTR-Fv1n		(Yap et al., 2004)
pENTR-Fv1b		(Yap et al., 2004)
pLxIG-Fv1n	pL-Fv1n-IRES-EGFP	(Bock et al., 2000)
pLxIG-Fv1b	pL-Fv1b-IRES-EGFP	(Bock et al., 2000)
pLxIG-Fv1bbn	pL-Fv1bbn-IRES-EGFP	(Bock et al., 2000)
pLxIG-Fv1nnb	pL-Fv1nnb-IRES-EGFP	(Bock et al., 2000)
pLxIG-Fv1bnb	pL-Fv1bnb-IRES-EGFP	(Bock et al., 2000)
pLxIG-Fv1nbn	pL-Fv1nbn-IRES-EGFP	(Bock et al., 2000)
pLxIG-Fv1bnn	pL-Fv1bnn-IRES-EGFP	(Bock et al., 2000)
pLxIG-Fv1nbb	pL-Fv1nbb-IRES-EGFP	(Bock et al., 2000)
pLxIG-Fv1nn_	pL-Fv1nn_-IRES-EGFP	(Bishop et al., 2001)
pLxIG-Fv1bb_	pL-Fv1bb_-IRES-EGFP	(Bishop et al., 2001)
pLxIY-HuT5	pL-HuT5-IRES-EYFP	(Yap et al., 2004)
pLxIY-RhT5	pL-RhT5-IRES-EYFP	(Yap et al., 2004)
pLxIY-HuT5HA	pL-HuT5-HA-IRES-EYFP	(Hilditch, 2010)
pLxIY-RhT5HA	pL-RhT5-HA-IRES-EYFP	(Hilditch, 2010)

Table 2.1 Plasmids obtained for transfection and cloning

Short name	Long name	Source/Reference
pET22-NCA	pET22-N-MLV-CA	(Hilditch et al., 2011)
pET22-NCA-P1G	pET22-N-MLV-CA-P1G	(Hilditch et al., 2011)
pET22-NCA-D54A	pET22-N-MLV-CA-D54A	(Hilditch et al., 2011)
pET22-NCA-R110E	pET22-N-MLV-CA-R110E	(Hilditch et al., 2011)
pET22-BCA	pET22-B-MLV-CA	(Hilditch et al., 2011)
pET22-BCA-P1G	pET22-B-MLV-CA-P1G	(Hilditch et al., 2011)
pET22-BCA-D54A	pET22-B-MLV-CA-D54A	(Hilditch et al., 2011)
pET22-BCA-E110R	pET22-B-MLV-CA-E110R	(Hilditch et al., 2011)
pET22-NBCA	pET22-NB-MLV-CA	(Hilditch et al., 2011)
pET22-HIVCAp2	pET22-HIV-1-CA-p2	(Hilditch, 2010)
pET22-Fv1NTD	pET22b-Fv1NTD(20-200)	(Bishop et al., 2006)

Table 2.2 Plasmids obtained for bacterial expression of recombinant proteins

PCR Product	Template	Primer	Sequence
PCR-TRE3G	pTREPuro-DEST	E178P3-F	GTATATATCGATCACGAGACTAGCCTCGAGAG
		E178P6-R	GTATATGCGGCCGCCCACCACACTGGACTAGTC
PCR-EGFP	pLxIG-Fv1n	E178P18-F	GTATATGCGGCCGCCATGGTGAGCAAGGGCGAGG
		E178P19-R	GTATATGAATTCTTACTTGTACAGCTCGTCC
PCR-EYFP	pLxIY-HuT5	E178P18-F	GTATATGCGGCCGCCATGGTGAGCAAGGGCGAGG
		E178P19-R	GTATATGAATTCTTACTTGTACAGCTCGTCC
PCR-TOPO-Fv1bbn	pLxIG-Fv1bbn	TOPO-Fv1-F	CACCATGAATTTCCCACGTGCGCTTG
		TOPO-Fv1n-R	TCGGAGTTTTGTAGCTGCTG
PCR-TOPO-Fv1nnb	pLxIG-Fv1nnb	TOPO-Fv1-F	CACCATGAATTTCCCACGTGCGCTTG
		TOPO-Fv1b-R	TTAACTGTTGCTTTGATGTTTC
PCR-TOPO-Fv1bnb	pLxIG-Fv1bnb	TOPO-Fv1-F	CACCATGAATTTCCCACGTGCGCTTG
		TOPO-Fv1b-R	TTAACTGTTGCTTTGATGTTTC
PCR-TOPO-Fv1nbn	pLxIG-Fv1nbn	TOPO-Fv1-F	CACCATGAATTTCCCACGTGCGCTTG
		TOPO-Fv1n-R	TCGGAGTTTTGTAGCTGCTG
PCR-TOPO-Fv1bnn	pLxIG-Fv1bnn	TOPO-Fv1-F	CACCATGAATTTCCCACGTGCGCTTG
		TOPO-Fv1n-R	TCGGAGTTTTGTAGCTGCTG
PCR-TOPO-Fv1nbb	pLxIG-Fv1nbb	TOPO-Fv1-F	CACCATGAATTTCCCACGTGCGCTTG
		TOPO-Fv1b-R	TTAACTGTTGCTTTGATGTTTC
PCR-TOPO-Fv1nn_	pLxIG-Fv1nn_	TOPO-Fv1-F	CACCATGAATTTCCCACGTGCGCTTG
		TOPO-Fv1-notail-R	TCAAGCTGCTGTTGGCTTTAAAC
PCR-TOPO-Fv1bb_	pLxIG-Fv1bb_	TOPO-Fv1-F	CACCATGAATTTCCCACGTGCGCTTG
		TOPO-Fv1-notail-R	TCAAGCTGCTGTTGGCTTTAAAC
PCR-TOPO-uORF-Fv1b	pLxIG-Fv1b	TOPO-uORF-Fv1-F	CACCATGGGTTGACACCATGAATTTCCCACGTGCGC
		TOPO-Fv1b-R	TTAACTGTTGCTTTGATGTTTC
PCR-TOPO-AGG-Fv1b	pLxIG-Fv1b	TOPO-AGG-Fv1-F	CACCAGGAATTTCCCACGTGCGC
		TOPO-Fv1b-R	TTAACTGTTGCTTTGATGTTTC

Table 2.3 Primers used for PCR reactions

2.1.3 Gel purification of DNA fragments

Bands containing the target DNA fragment are excised from agarose gels on a UV transilluminator using a scalpel. DNA fragments were purified from agarose gel using the MinElute Gel Extraction Kit (Qiagen, #28604) according to the manufacturer's instructions. DNA was eluted in 10µl of elution buffer.

2.1.4 DNA quantitation

Concentration of DNA in plasmids or purified PCR products were determined by measuring the absorbance at 260nm using a NanoDrop 2000 UV spectrophotometer.

2.1.5 Restriction digestion

Digestions of plasmid DNA and PCR products were performed with restriction enzymes from Roche using the supplied buffer. For double digestions, a buffer compatible to both restriction enzymes was chosen. A 20µl digestion reaction typically contained up to 1µg of DNA and 1U of restriction enzyme (or 0.5U in double digestions) in the appropriate buffer. Reactions were performed at 37^{o}C for at least 2h. To screen DNA clones, digested DNA was immediately analysed by agarose gel electrophoresis. To prepare digested vector or insert DNA for ligation, DNA was isolated by gel purification.

2.1.6 Blunting of 5'overhang

5' overhangs created by EcoR1 digestion of pQTGIX were filled in using the 5' to 3' synthesis activity of T4 DNA polymerase (New England Biolabs), to create a blunt end for downstream ligation reaction. A 50µl reaction contained 1µg of digested vector DNA, 100µg/ml of BSA and 100µM of each dNTP in NEBuffer 2. The blunting reaction was carried out at 12^{o}C for 30min, followed by inactivation at 75^{o}C for 10min. Blunt vector DNA was purified using the QIAquick PCR purification kit (Qiagen, #28104) according to the manufacturer's instructions.

2.1.7 Dephosphorylation

Dephosphorylation of digested vector DNA was carried out using the Rapid DNA Dephos and Ligation Kit (Roche, #04898117001). A 20µl dephosphorylation reaction contained up to 1µg of digested vector DNA, and 1U rARid Alkaline Phosphatase (Roche) in the supplied buffer. Dephosphorylation reaction was performed at 37^{o}C for 1h followed by 2min inactivation at 75^{o}C. Dephosphorylated vector DNA was used directly in ligation reactions without further purification.

2.1.8 DNA Ligation

Ligation between vector and insert DNA was carried out using the Rapid DNA Dephos and Ligation Kit (Roche). Dephosphorylated vector and digested insert were mixed at a 1:3 molar ratio to a final volume of 4µl. 1µl of 5X DNA dilution buffer was added, followed by addition of 5µl of 2X T4 DNA ligation buffer and 0.5µl of T4 DNA ligase (5U/µl). Ligation reactions were performed at 20^{o}C for 1h.

2.1.9 Transformation

Table 2.4 shows a list of chemically-treated competent cells used for transformation. Different strains of competent cells were used for different purposes. In a typical transformation, 50µl of competent cells was thawed on ice and mixed with up to 2µl of ligation reaction or 1ng of purified plasmid DNA. After 20min incubation on ice, competent cells were heat shocked at 42^{o}C for 30s and followed immediately by 2min incubation on ice. 250µl of SOC media (2% w/v tryptone, 0.5% w/v yeast extract, 8.55mM NaCl, 2.5mM KCl, 10mM $MgCl_2$ and 20mM glucose) was added and the cells were incubated at 37^{o}C with shaking. Transformed cells were spread on LB-agar (1.5% agar) plates supplemented with antibiotics (Table 2.5) and incubated at 37^{o}C overnight.

Competent cells	Function	Source
TOP10	General propagation of plasmids	Life Technologies #C4040
ccdB Survival 2 T1	Propagation of Gateway destination vectors	Life Technologies #A10460
dam-/dcm-	Propagation of pQCXIX for ClaI digestion	NEB #C2925
XL10 Gold	Propagation after QuikChange mutagenesis	Agilent #200315
Rosetta2 DE3	Expression of recombinant CA and Fv1NTD	Merck #71400

Table 2.4 Competent cells used for transformation

Chemical	Stock concentration	Final Concentration	Source
Nafcillin	50mg/ml in water	50µg/ml	Sigma #N3269
Ampicillin	50mg/ml in water	50µg/ml	Sigma #A9518
Kanamycin	50mg/ml in water	50µg/ml	Sigma #60615
Chloramphenicol	25mg/ml in ethanol	25µg/ml	Sigma #C0378
Puromycin	10mg/ml in water	10µg/ml	Sigma #P9620
Blasticidin	10mg/ml in water	10µg/ml	Sigma #15205
Penicillin Streptomycin	10000U 10mg/ml	100U/ml 100µg/ml	Sigma #P0781
Doxycycline	10mg/ml in water	1-1000ng/ml	Sigma #D9891
MG132	20mg/ml in DMSO	10nM	Sigma #C2211
IPTG	1M in water	500µM	Sigma #I6758
GalCer	5mg/ml in 1:1 chloroform:methanol		Avanti #790404
DGS-NTA(Ni)	5mg/ml in chloroform		Avanti #860546
Bio PE	5mg/ml in chloroform		Avanti #870282
BioCap PE	5mg/ml in chloroform		Avanti #870273
BioPEG PE	5mg/ml in chloroform		Avanti #880129

Table 2.5 List of antibiotics and chemicals

2.1.10 Propagation and purification of plasmid DNA

For small scale production of plasmid DNA, each colony of E coli from agar plate was cultured at 37^{o}C with shaking overnight in 3ml LB (1% tryptone, 0.5% yeast extract, 1% NaCl, pH 7.0) supplemented with antibiotic. Bacteria from 1.5ml of culture were pelleted by centrifugation at 13,000 x g for 3min for plasmid purification using the QIAprep Spin Miniprep Kit according to manufacturer's instructions. For large scale plasmid production, 50ml of LB with antibiotic was inoculated with 100µl of small scale culture, and incubated overnight at 37^{o}C with shaking. Bacterial cells were pelleted at 4000 x g for 15min for plasmid purification using the HiSpeed Plasmid Midi Kit (Qiagen, #12643) according to manufacturer's instructions.

2.1.11 Gateway cloning system

The Gateway cloning system (Life Technologies) has been implemented in our lab to allow efficient ligation-free cloning of restriction factors into destination vectors (Figure 2.1) (Yap et al., 2004). The system relies on recombination reactions between att sequences. Each entry clone consists of a Kanamycin-resistant backbone and a gene of interest (GOI) flanked by attL1 and attL2 sequences, while each destination vector consists of an ampicillin-resistant backbone and a DEST cassette containing the *ccdB* suicide gene and the chloramphenicol-resistant gene flanked by the attR1 and attR2 sequences. The LR reaction allows recombination between attL1 and attL2 sequences in the entry clone and attR1 and attR2 sequences in the destination vector, leading to the transfer of GOI insert from the entry clone to the destination vector. The resulting expression clone can be selected using ampicillin, while the by-product donor vector would be eliminated due to the expression of suicide gene. There are 3 ways from which entry clones can be obtained. First, entry clones can be obtained by BP recombination between an expression clone and a donor vector. Alternatively, entry clone can be obtained from BP reactions between a PCR product flanked with attB1 and attB2 sequences and a donor vector. Lastly, entry clones can be obtained from directional TOPO reaction between a blunt end PCR product with 5' CACC sequence and pENTR-D-TOPO vector (Life Technologies).

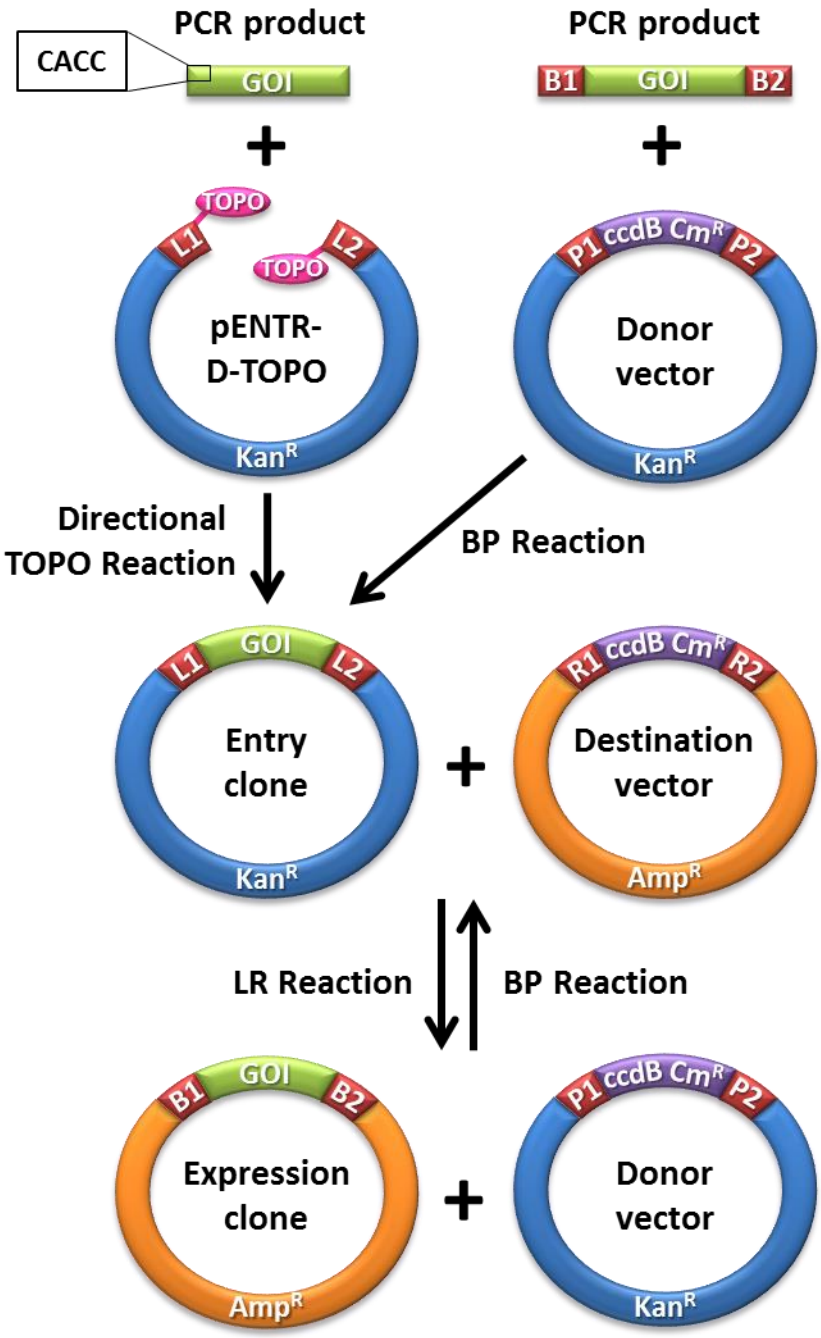

Figure 2.1 Gateway cloning system

2.1.12 Cloning of inducible destination vectors

Figure 2.2 shows the steps taken to generate two destination vectors, pTGx-DEST and pTGIx-DEST. All constructs made are listed in Table 2.6 and the PCR products generated are listed in Table 2.3. Briefly, the TRE3G promoter was amplified by PCR from pTREPuro-DEST and inserted between ClaI and NotI sites of the self-inactivating (SIN) retroviral vector pQCXIX. Since ClaI digestion is sensitive to dam methylation, pQCXIX was purified from a dam$^-$ *E. coli* strain (Table 2.4). This replaced the CMV promoter in pQCXIX with the inducible TRE3G promoter to generate the pQTXIX construct. EGFP sequence was amplified from LxIG-Fv1^n and inserted between NotI and EcoRI sites of pQTXIX. This led to the insertion of EGFP ORF between the TRE3G promoter and IRES element in the resulting pQTGIX construct. The blunt DEST cassette was obtained by digestion of pTREPuro-DEST with EcoRV. The pTGIx-DEST vector was constructed by insertion of the DEST cassette to the EcoRV site. To obtain the pTGx-DEST vector, the pQTGIX construct was digested with EcoRI and EcoRV followed by blunting of the 5' overhang to remove the IRES element. The DEST cassette was ligated to the blunt vector to obtain the IRES-free pTGx-DEST vector. Since the DEST cassette contains the *ccdB* suicide gene and the chloramphenicol resistant gene, ccdB Survival competent cells were used for transformed (Table 2.4) and selected with ampicillin, nafcillin and chloramphenicol (Table 2.5). The orientation of DEST cassettes in both vectors were screened by restriction digestion and confirmed by sequencing.

2.1.13 Cloning of entry clones by TOPO reaction

Fv1 entry clones shown in Table 2.6 were cloned using the pENTR-D-TOPO vector kit (Life Technologies, #K2400). PCR products of Fv1 ORFs with 5' CACC inserted sequence were inserted into the pENTR-D-TOPO vector by TOPO reaction. For pENTR-uORF-Fv1^b and pENTR-AGG-Fv1^b, insertion of uORF and mutation of start codon were introduced by the 5' primers used in the TOPO PCR reaction. A typical 3µl reaction contains 5µg of purified PCR product, 200mM NaCl, 10mM $MgCl_2$ and 0.5µl of pENTR-D-TOPO vector mix. The reaction was incubated at 25^{o}C for 1h before transformation using TOP10 (Table 2.4). Entry clones were selected with kanamycin (Table 2.5).

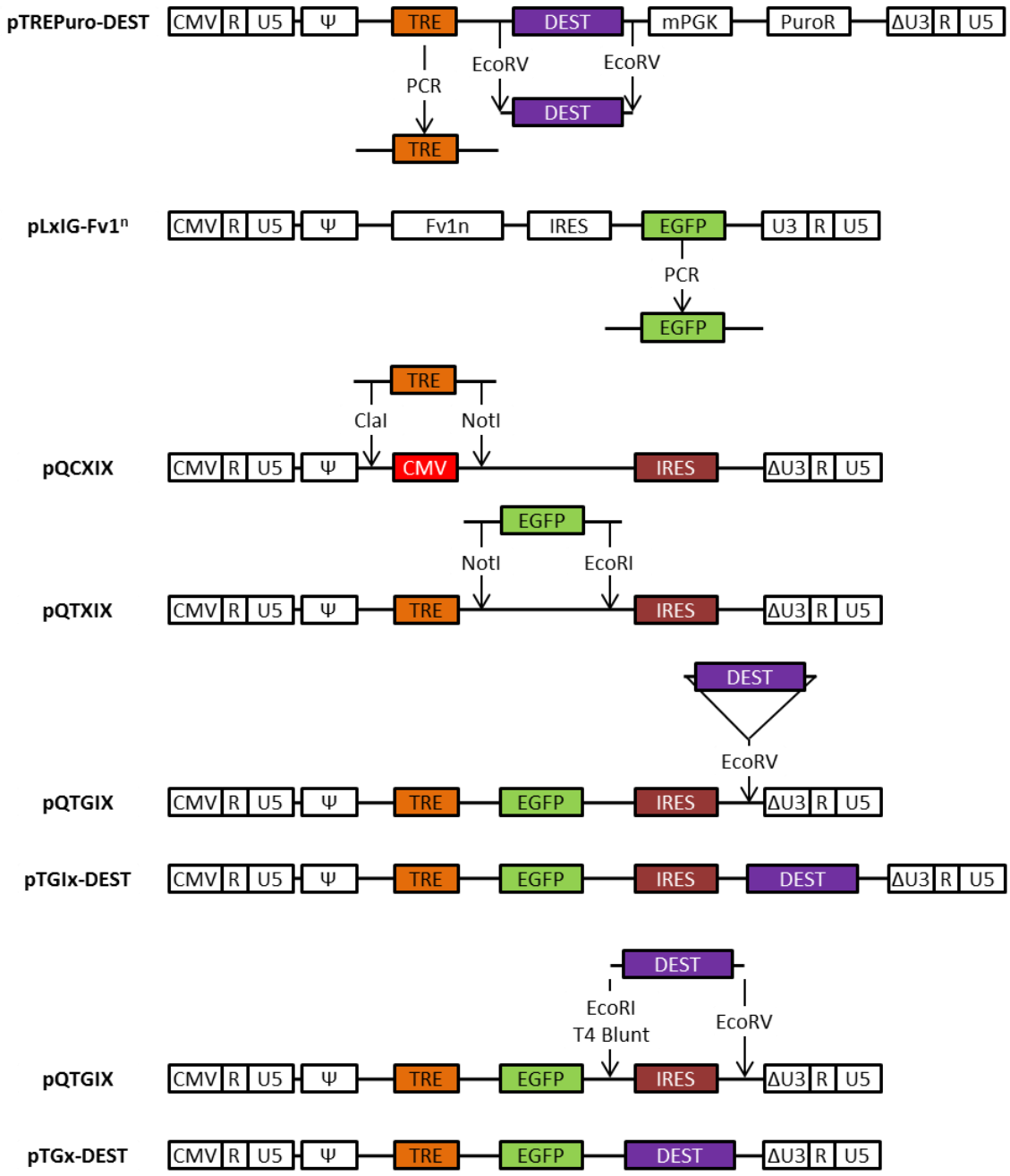

Figure 2.2 Cloning of pTGIx-DEST and pTGx-DEST vectors

Short name	Vector	Insert	Cloning method
pQTXIX	pQCXIX (dam-)	PCR-TRE3G	ClaI + NotI
pQTGIX	pQTXIX	PCR-EGFP	NotI + EcoRI
pTGIx-DEST	pQTGIX	DEST cassette	EcoRV
pTGx-DEST	pQTGIX	DEST cassette	EcoRI + EcoRV End blunting with T4 Pol
pQTYIX	pQTXIX	PCR-EYFP	NotI + EcoRI
pTYIx-DEST	pQTYIX	DEST cassette	EcoRV
pTYx-DEST	pQTYIX	DEST cassette	EcoRI + EcoRV End blunting with T4 Pol
pENTR-Fv1bbn	pENTR-D-TOPO	PCR-TOPO-Fv1bbn	TOPO reaction
pENTR-Fv1bbn	pENTR-D-TOPO	PCR-TOPO-Fv1nnb	TOPO reaction
pENTR-Fv1bnb	pENTR-D-TOPO	PCR-TOPO-Fv1bnb	TOPO reaction
pENTR-Fv1nbn	pENTR-D-TOPO	PCR-TOPO-Fv1nbn	TOPO reaction
pENTR-Fv1bnn	pENTR-D-TOPO	PCR-TOPO-Fv1bnn	TOPO reaction
pENTR-Fv1nbb	pENTR-D-TOPO	PCR-TOPO-Fv1nbb	TOPO reaction
pENTR-Fv1nn_	pENTR-D-TOPO	PCR-TOPO-Fv1nn_	TOPO reaction
pENTR-Fv1bb_	pENTR-D-TOPO	PCR-TOPO-Fv1bb_	TOPO reaction
pENTR-uORF-Fv1b	pENTR-D-TOPO	PCR-TOPO-uORF-Fv1b	TOPO reaction
pENTR-AGG-Fv1b	pENTR-D-TOPO	PCR-TOPO-AGG-Fv1b	TOPO reaction

Table 2.6 Cloning of Gateway destination vectors and entry clones

2.1.14 Cloning of expression vectors by Gateway LR reaction

A list of expression clones constructed by Gateway LR reactions is shown in Table 2.7. In a typical 2.5µl LR reaction, 37.5ng of destination vector with mixed with 37.5ng of entry clones, diluted to a total of 2µl with TE buffer (10mM Tris-HCl, 1mM EDTA, pH 8.0), followed by addition of 0.5µl of LR Clonase II enzyme mix (Life Technologies, #11791). After 1h incubation at 25^{o}C, 0.5µl of the supplied Proteinase K was added and the reaction was incubated at 37^{o}C for 10min. The LR reaction was transformed into TOP10 and selected with ampicillin and nafcillin.

2.1.15 Generation of cysteine mutants by Site-directed mutagenesis

Primers used for generation of cysteine mutations of pCIGN are listed in Table 2.8. Forward and reverse primers with the required point mutations flanked by complementary sequences were used to amplify mutant plasmid by PCR reaction according to the QuikChange site-directed mutagenesis protocol (Agilent Technologies). Each 50µl QuikChange PCR reaction contained 50ng of plasmid template, 10pmol of forward primer, 10pmol of reverse primer, 200µM of each dNTP, 2.5U of PfuUltra high fidelity polymerase (Agilent Technologies) in the supplied buffer. PCR reactions were carried out using a PTC-100 thermal cycler (MJ research). Thermo cycling parameters typically consisted of 5min of initial denaturation at 95^{o}C; followed by 12 cycles of 1min denaturation at 95^{o}C, 1.5min annealing at 55^{o}C, 15min extension at 68^{o}C; and a final 15min extension at 68^{o}C. 30U of DpnI was added to the reaction to digest the methylated template DNA but not the unmethylated PCR product, and the reaction was further incubated at 37^{o}C for 2h. Amplified mutant plasmids were concentrated by ethanol precipitation and transformed into XL10 Gold ultracompetent cells (Agilent Technologies). The introduction of mutations was verified by sequencing.

Short name	Long name	Destination vector	Entry clone
pTREPuro-Luc	pLenti-CMVTRE3G-Puro-Luc	pTREPuro-DEST	pENTR-Luc
pTGIx-Fv1n	pQ-TRE3G-EGFP-IRES-Fv1n	pTGIx-DEST	pENTR-Fv1n
pTGIx-Fv1b	pQ-TRE3G-EGFP-IRES-Fv1b	pTGIx-DEST	pENTR-Fv1B
pTGIx-Fv1bbn	pQ-TRE3G-EGFP-IRES-Fv1bbn	pTGIx-DEST	pENTR-Fv1bbn
pTGIx-Fv1nnb	pQ-TRE3G-EGFP-IRES-Fv1nnb	pTGIx-DEST	pENTR-Fv1nnb
pTGIx-Fv1bnb	pQ-TRE3G-EGFP-IRES-Fv1bnb	pTGIx-DEST	pENTR-Fv1bnb
pTGIx-Fv1nbn	pQ-TRE3G-EGFP-IRES-Fv1nbn	pTGIx-DEST	pENTR-Fv1nbn
pTGIx-Fv1bnn	pQ-TRE3G-EGFP-IRES-Fv1bnn	pTGIx-DEST	pENTR-Fv1bnn
pTGIx-Fv1nbb	pQ-TRE3G-EGFP-IRES-Fv1nbb	pTGIx-DEST	pENTR-Fv1nbb
pTGIx-Fv1nn_	pQ-TRE3G-EGFP-IRES-Fv1nn_	pTGIx-DEST	pENTR-Fv1nn_
pTGIx-Fv1bb_	pQ-TRE3G-EGFP-IRES-Fv1bb_	pTGIx-DEST	pENTR-Fv1bb_
pTGIx-uORF-Fv1b	pQ-TRE3G-EGFP-IRES-uORF-Fv1b	pTGIx-DEST	pENTR-uORF-Fv1b
pTGIx-AGG-Fv1b	pQ-TRE3G-EGFP-IRES-AGG-Fv1b	pTGIx-DEST	pENTR-AGG-Fv1b
pTGIx-Luc	pQ-TRE3G-EGFP-IRES-Luc	pTGIx-DEST	pENTR-Luc
pTGx-Fv1n	pQ-TRE3G-EGFP-Fv1n	pTGx-DEST	pENTR-Fv1n
pTGx-Fv1b	pQ-TRE3G-EGFP-Fv1b	pTGx-DEST	pENTR-Fv1B
pTGx-Fv1bbn	pQ-TRE3G-EGFP-Fv1bbn	pTGx-DEST	pENTR-Fv1bbn
pTGx-Fv1nnb	pQ-TRE3G-EGFP-Fv1nnb	pTGx-DEST	pENTR-Fv1nnb
pTGx-Fv1bnb	pQ-TRE3G-EGFP-Fv1bnb	pTGx-DEST	pENTR-Fv1bnb
pTGx-Fv1nbn	pQ-TRE3G-EGFP-Fv1nbn	pTGx-DEST	pENTR-Fv1nbn
pTGx-Fv1bnn	pQ-TRE3G-EGFP-Fv1bnn	pTGx-DEST	pENTR-Fv1bnn
pTGx-Fv1nbb	pQ-TRE3G-EGFP-Fv1nbb	pTGx-DEST	pENTR-Fv1nbb
pTGx-Fv1nn_	pQ-TRE3G-EGFP-Fv1nn_	pTGx-DEST	pENTR-Fv1nn_
pTGx-Fv1bb_	pQ-TRE3G-EGFP-Fv1bb_	pTGx-DEST	pENTR-Fv1bb_
pTGx-Luc	pQ-TRE3G-EGFP-Luc	pTGx-DEST	pENTR-Luc

Table 2.7 Cloning of Gateway expression vectors by LR reaction

Mutations	Primer	Sequence
S17C	F	GTACTGGCCGTTTTCCTGCTCTGATCTATATAAC
	R	GTTATATAGATCAGAGCAGGAAAACGGCCAGTAC
D19C	F	GTACTGGCCGTTTTCCTCCTCTTGTCTATATAACTGG
	R	CCAGTTATATAGACAAGAGGAGGAAAACGGCCAGTAC
N22C	F	GGCCGTTTTCCTCCTCTGATCTATATTGCTGGAAAAATAATAATCCTTCC
	R	GGAAGGATTATTATTTTTCCAGCAATATAGATCAGAGGAGGAAAACGGCC
Y21C	F	GGCCGTTTTCCTCCTCTGATCTATGTAACTGGAAAAATAATAATCCTTCC
	R	GGAAGGATTATTATTTTTCCAGTTACATAGATCAGAGGAGGAAAACGGCC
N26C	F	CTGATCTATATAACTGGAAAAATTGTAATCCTTCCTTCTCTGAGGATCC
	R	GGATCCTCAGAGAAGGAAGGATTACAATTTTTCCAGTTATATAGATCAG
N27C	F	GATCTATATAACTGGAAAAATAATTGTCCTTCCTTCTCTGAGGATCCAGG
	R	CCTGGATCCTCAGAGAAGGAAGGACAATTATTTTTCCAGTTATATAGATC
D53C	F	CACCCACCAGCCCACCTGGTGTGATTGCCAGCAATTATTAG
	R	CTAATAATTGCTGGCAATCACACCAGGTGGGCTGGTGGGTG
T46C	F	GATTGAATCTGTCCTCTGCACCCACCAGCCCAC
	R	GTGGGCTGGTGGGTGCAGAGGACAGATTCAATC
S17C S19C	F	GTACTGGCCGTTTTCCTGCTCTTGTCTATATAACTGG
	R	CCAGTTATATAGACAAGAGCAGGAAAACGGCCAGTAC
S17C N22C	F	GGCCGTTTTCCTGCTCTGATCTATATTGCTGGAAAAATAATAATCCTTCC
	R	GGAAGGATTATTATTTTTCCAGCAATATAGATCAGAGCAGGAAAACGGCC
Y21C N26C	F	CTGATCTATGTAACTGGAAAAATTGTAATCCTTCCTTCTCTGAGGATCC
	R	GGATCCTCAGAGAAGGAAGGATTACAATTTTTCCAGTTACATAGATCAG
Y21C N27C	F	GATCTATGTAACTGGAAAAATAATTGTCCTTCCTTCTCTGAGGATCCAGG
	R	CCTGGATCCTCAGAGAAGGAAGGACAATTATTTTTCCAGTTACATAGATC

Table 2.8 Primers used for site-directed mutagenesis of pCIGN

2.2 Cell culture

2.2.1 General cell culture

All cell lines used in this study (MDTF, 293T, TE671, N-3T3, B-3T3) were maintained at 37^{o}C in 5% $CO_{2,}$ using Dulbecco's Modified Eagle Medium (DMEM) (Life Technologies) supplemented with penicillin/streptomycin (Table 2.5) and 10% heat-inactivated foetal calf serum (FCS) (Perbio). Cells were typically passaged every 3 to 4 days by dislodging confluent monolayer of cells from culture flask with trypsin-Versene (0.05% w/v trypsin, 0.53mM EDTA in PBS) followed by transferring 10-20% of cells to a new flask.

2.2.2 Virus preparation

Preparation of retroviral or lentiviral vectors were carried by transient transfection of 293T with 3 plasmids providing vector, Gag-Pol and Env functions (Soneoka et al., 1995). 293T cells at log phase were counted using the Countess automatic cell counter (Life Technologies), and 2x10^{6} cells were seeded to each 6cm dish (Corning) in 5ml of medium. On the next day, cells were transfected 4h after a change of culture medium. 2µg of each plasmid was incubated with 600µl of serum-free DMEM and 12µl of Turbofect (Thermo Fisher) at room temperature for 20min, and the mixture was added drop wise to the cells. 16h later, transfected cells were incubated with medium supplemented with 10mM sodium butyrate for 6h to enhance expression of viral proteins by CMV promoter, followed by replacement of medium to 2.5ml of supplemented DMEM. Supernatant containing vector viruses was harvested 48h after transfection, and passed through a 0.45µm filter to remove cell debris. Virus stocks were stored as aliquot at -80^{o}C.

2.2.3 Transduction

Retroviral vector viruses used for transduction were prepared using pVSV-g (pseudotype envelope), pHIT60 (NB-MLV Gag-Pol) and a retroviral vector plasmid. Lentiviral vector viruses used for transduction were prepared using pVSV-g, p8.91 (HIV-1 Gag-Pol and accessory proteins) and a lentiviral vector

plasmid. MDTF cells were seeded at $5x10^4$/well (for 12 well plate) or $2.5x10^4$/well (for 24 well plate) 24h before addition of thawed viruses. In cases where the volume of viruses to be added exceeded 5% of the total volume of medium, an equal volume of medium was removed prior to the addition of viruses.

2.2.4 Generation of single cell clones (SCCs) from transduced MDTF cells

MDTF cells that were transduced with vectors without antibiotic resistance genes were counted and reseeded on 96 well plates at a concentration of 0.2 cells per well in DMEM with 20% FCS. After two weeks, SCCs were transferred to 24 well plates and allowed to grow until confluent. For selection of MDTF cells transduced with vector expressing rtTA3 and the blasticidin-resistance gene, blasticidin (Table 2.5) was added to transduced cells at 24h after transduction. Cells were seeded on 96-well plates at 7 days post transduction using the same procedure as above.

2.2.5 Freezing and resuscitation of cell stocks

To prepare cell stocks for long term storage, cells at 70% confluency were dislodged with 2ml of trypsin and 8ml of medium, pelleted by 300 x g centrifugation for 5min, and resuspended in 2ml of freezing mix (10% DMSO, 90% FCS). Cells were frozen as 1ml aliquots in cryovials (Nalgene) using a CoolCell FTS30 cell freezing container (Biocision) placed at -80^oC. Cells were transferred to liquid nitrogen for long term storage after at least 24h. To resuscitate cells from frozen stocks, cells were thawed at room temperature and pelleted through 10ml of medium to remove DMSO from the freezing mix. Cells were then resuspended in fresh medium and transferred to new culture flasks.

2.3 Protein expression and purification

2.3.1 Expression and purification of MLV CA and HIV-1 CA-p2

A list of pET22b vectors used for bacterial expression of recombinant proteins is shown in Table 2.2. The expression and purification of MLV CA-His and HIV CA-p2-His had been described in previous studies (Hilditch, 2010; Hilditch et al., 2011). Briefly, Rosetta 2 DE3 competent cells were transformed with pET22b vector and plated on ampicillin/nafcillin agar plates. A colony was used to inoculate 50ml of LB supplemented with ampicillin at 30^{o}C with shaking overnight. Overnight culture was diluted 1 in 100 into 1L of LB, and cells were grown at 37^{o}C with shaking. Expression of recombinant protein was induced at an optical density (OD) of 0.6 with 0.5mM IPTG for 3h. Cells were centrifuged at 2k x g for 30min, and the pellet was stored at -20^{o}C until purification.

Purification of His-tagged proteins was carried out using Nickel columns. The thawed cell pellet was resuspended in 50ml of lysis buffer (20mM Tris-HCl pH 7.5, 300mM NaCl, 5mM β-mercaptoethanol, 5mM imidazole, complete EDTA-free protease inhibitors (Roche), 4µl benzonase (Merck Millipore) and 1mM $MgCl_2$). Cells were lysed with 50mg of lysozyme (Sigma) for 30min at 4^{o}C, followed by sonication on ice. Insoluble materials were pelleted by centrifugation at 23000 x g for 30min at 4^{o}C. Soluble lysate was passed through a 5ml HisTrap FF column (GE Healthcare) that had been pre-equilibrated with wash buffer (20mM Tris-HCl pH 7.5, 300mM NaCl, 5mM β-mercaptoethanol, 5mM imidazole) using a P1 pump (GE Healthcare). The column was attached to the ÄKTAprime plus system (GE Healthcare), washed with 20ml of wash buffer. His-tagged proteins were eluted using a 5 to 300mM imidazole gradient, and collected as fractions. Peak fractions were pooled, analysed by SDS-PAGE, and concentrated using a Vivaspin column with a 10kDa molecular weight cut off (MWCO) (GE Healthcare). The concentration column allows the removal of buffer while retaining the recombinant capsid proteins. The samples were further purified by size-exclusion chromatography using on a HiLoad 16/600 Superdex 75 gel filtration column (GE Healthcare) in the gel filtration buffer (10mM Tris-HCl pH 8.0, 150mM NaCl, 5mM β-mercaptoethanol). Proteins of different sizes travel through the gel filtration column at different speed, so that

proteins of different molecular weight collected at different fractions at different elution volumes. Peak fractions corresponding to monomeric recombinant capsids were pooled and concentrated, and stored as aliquots at -80^{o}C.

2.3.2 Expression and purification of Fv1NTD

The expression of Fv1NTD with N-terminal His-tag had been described before (Bishop et al., 2006). The procedure for protein expression was the same as described for recombinant CA-His. For the purification procedure, thawed cells were lysed with lysis buffer (5mM β-mercaptoethanol, 5mM imidazole, complete EDTA-free protease inhibitors (Roche), 4µl benzonase (Merck Millipore) and 1mM $MgCl_2$ in Y-PER lysis buffer (Thermo Fisher)) for 30min at room temperature. Lysate was clarified by centrifugation at 23000 x g for 30min at 4^{o}C, and purified with HisTrap column as described above.

2.4 Protein quantitation and analyses

2.4.1 Quantitation of purified protein by A280 absorbance

The concentration of purified proteins was determined using the Biophotometer UV spectrophotometer (Eppendorf). The extinction coefficient value of each protein was calculated based on the Tryptophan and Tyrosine content (37410 cm^{-1} M^{-1} for MLV CA, 33570 cm^{-1} M^{-1} for HIV-1 CA-p2 and 26700 cm^{-1} M^{-1} for Fv1NTD), and the concentration of purified protein samples were calculated from absorbance at 280nm using the extinction coefficient.

2.4.2 Total protein quantitation by Bradford assay

Total protein concentrations of detergent-free lysate samples were determined using a microplate Bradford assay. 5µl of neat or 1/5 diluted lysate samples was added to 96-well plates along with BSA standards (Thermo Fisher) of 1000, 500, 250 and 125µg/ml. 200µl of 1/5 diluted Bradford reagent (Bio-Rad protein assay) was mixed with lysate or standard samples in each well. After 10min incubation at room temperature, the absorbance at 595nm was measured using the Synergy 2 (Biotek) plate reader and the Gen5 software. The protein concentration of lysate was interpolated from a standard curve from known BSA concentrations.

2.4.3 Total protein quantitation by BCA assay

Total protein concentrations of lysate samples in buffer containing detergent (such as RIPA buffer which contains NP40 and SDS) were determined using a microplate BCA assay. 5µl of 1/5 diluted lysate was added to 96-well plates along with BSA standards of 2000, 1000, 500, 250, 125, 62.5, 31.3 and 0µg/ml. 200µl of prepared BCA protein assay reagent (Thermo Fisher) was added to each well. After 30s of shaking, the plate was incubated at 37^{o}C for 30min. The absorbance at 562nm was measured using the Synergy 2 plate reader and the Gen5 software. The protein concentration of lysate was interpolated from a standard curve from known BSA concentrations.

2.4.4 Separation of proteins by SDS-PAGE

For most purposes, samples were separated with hand cast 10% polyacrylamide gels containing 33.3% of 30% Acrylamide/Bis 35.1:1 stock (Bio-rad), 375mM Tris-HCl pH 8.8, 0.1% SDS, 0.11 ammonium persulphate (Bio-Rad) and 8µl TEMED (Sigma). For analysis of crosslinked MLV capsid complexes, 4-20% Mini-Protean TGX Precast Gel (Bio-Rad) was used. Samples with Protein samples were mixed with 5X SDS-PAGE loading buffer (5X: 250mM Tris-HCl pH 6.8, 10% SDS, 12.5% β-mercaptoethanol, 0.1% w/v bromophenol blue, 50% glycerol) in 4:1 ratio, and boiled at 98^{o}C for 5min. Electrophoresis was carried at 150V in SDS running buffer (27.6mM Tris-HCl pH 8.8, 0.2M glycine, 0.1% SDS). Both the PageRuler Prestained Protein Ladder (Thermo Fisher) and the Spectra Multicolor High Range Protein Ladder (Thermo Fisher) have been used as molecular weight protein markers. For analysis of purified proteins, gels were stained with Imperial Protein Stain (Thermo Fisher).

2.4.5 Electro-transfer of proteins to PVDF membrane

For western blot analysis, proteins in polyacrylamide gels were transferred to PVDF membranes using the Trans-Blot SD semi-dry transfer cell (Bio-rad). SDS gel was placed above a methanol-activated PVDF membrane, and sandwiched between stacks of filter papers saturated with transfer buffer (48mM Tris, 39mM glycine, 20% methanol). Immobilon-P (Merck Millipore) PVDF membrane was used for chemiluminescent western blots, while Immobilon-FL (Merck Millipore) was used for LI-COR western blot. Transfer was carried out at 20V for 1.5h. The membrane was blocked with 5% non-fat dry milk (Marvel) in PBS at 4^{o}C overnight.

2.4.6 Western blot with chemiluminescent substrate

Antibodies used for western blot analyses are listed in Table 2.9. Blocked membrane was incubated with primary antibody diluted in 5% milk in PBS supplemented with 0.1% Tween-20 (PBS-T) for 1h, followed by four 5min washes with PBS-T. The membrane was then incubated with HRP-conjugated secondary antibody diluted in 5% milk in PBS-T, followed by four 5min washes with PBS-T. Protein bands were detected by adding ECL chemiluminescent substrate (Merck Millipore) to the membrane, followed by film exposure (Kodak).

2.4.7 LI-COR western blot

The LI-COR western blot procedure was similar to that for HRP western blot. This system allows the detection of two targets at the same blot, so in some cases rabbit anti-Fv1 and mouse anti-His primary antibodies were used simultaneously, together with IRDye800-conjugated anti-rabbit and IRDye680-conjugated anti-mouse secondary antibodies. 0.01% SDS was also added to the diluted secondary antibody mix to reduce non-specific binding of secondary antibodies. After the last wash with PBS-T, the membrane was washed for 5min with PBS before scanning using the Odyssey scanner (LI-COR) at 700nm and 800nm. Quantitation of signal in each protein band was carried out using the ImageStudio software (LI-COR), using median signal from pixels immediately above and below the band for background calculation. For absolute quantitation of Fv1, a standard curve was generated using the Prism 5 software (GraphPad) and fluorescent signals from bands of known quantity of Fv1NTD. The quantity of Fv1 in samples was determined by interpolation of measured fluorescent signal to the standard curve.

Antibody	Type	Source	Dilution
Anti-Fv1NTD (#6689)	Rabbit polyclonal	(Bishop et al., 2006)	1/1000
Anti-HA	Mouse monoclonal	Sigma #H9658	1/5000
Anti-His	Mouse monoclonal	QIAgen #34660	1/5000
Anti-p30	Rat monoclonal	ATCC #CRL-1912	1/5000
Anti-p24	Mouse monoclonal	Malim Lab	1/1000
Anti-mouse-HRP	Rabbit polyclonal HRP-conjugated	Thermo Fisher	1/5000
Anti-rat-HRP	Goat polyclonal HRP-conjugated	Thermo Fisher	1/5000
Anti-rabbit-HRP	Mouse monoclonal HRP-conjugated	Sigma #A2074	1/5000
Anti-mouse-680	Goat polyclonal IRDye680RD conjugated	LI-COR #926-68070	1/5000
Anti-mouse-800	Donkey polyclonal IRDye 800CW conjugated	LI-COR #926-32212	1/5000
Anti-rabbit-800	Goat polyclonal IRDye 800CW conjugated	LI-COR #926-32211	1/5000

Table 2.9 List of antibodies

2.4.8 Quantitation of Fv1 in cells

To determine the Fv1 expression level per cell, $7.5x10^5$ cells (3T3 cells, transduced cells, or SCCs) were seeded to each 10cm dish (Thermo Fisher) and treated with the required amount of doxycycline. 24h later, cells were harvested with trypsin, mixed with medium, and pelleted at 300 x g for 5min. Cell pellet was resuspended 2ml PBS, and pelleted again at 300 x g for 5min. The pellet was snap frozen with liquid nitrogen, and stored at -80^{o}C until analysis. 100µl RIPA buffer (Thermo Fisher) supplemented with complete EDTA-free protease inhibitors (Roche) was added to each cell pellet. Cells were lysed on ice for 30min, and then centrifuged at 13krpm for 10min at 4^{o}C to remove cell debris. The total protein concentrations of lysate samples were determined with the BCA assay, and the lysates were diluted to 1mg/ml before quantitation of Fv1 by LI-COR western blot. In a parallel experiment, it was determined that on average 120pg of total protein was extracted per MDTF cell, and this value was used to calculate the mean number of Fv1 molecules per cell. For mixed transduced cell populations, the percentage of $Fv1^+/GFP^+$ cells determined by FACS analysis was taken into account for the calculation of number of molecules per cell. The average number of Fv1 molecules per cell was calculated using the following equation:

$$Fv1\ per\ cell = \frac{[Fv1_{Lysate}] \times Yield \times N_A}{[Protein] \times f_{GFP+}}$$

$[Fv1_{Lysate}]$	The concentration of Fv1 in the 1mg/ml lysate sample, in mole L^{-1}, determined by the quantitative western blot analysis
$Yield$	The mass of total protein per cell in lysate of 120 x 10^{-12} g $cell^{-1}$
N_A	The Avogadro constant of 6.02214129 x 10^{23} $mole^{-1}$
$[Protein]$	The concentration of total protein in standardised lysate, 1 g L^{-1}
f_{GFP+}	The fraction of $GFP^+/Fv1^+$ cells in all sampled cells

2.4.9 Screening of SCCs with overexpression of Fv1 and T5HA

Confluent monolayers of SCC cells on a 10cm dish were scraped off in 10ml PBS and pelleted by centrifugation at 300 x g for 5min. Cells were resuspended in 500µl hypotonic buffer (10mM Tris-HCl pH 8.0, 10mM KCl) and incubated on ice for 10min. Cells were lysed by centrifugation through a QIAShredder column (Qiagen, #79654) at 13k x g for 2min at 4^{o}C. Supernatant was centrifuged again at 13k x g for 10min to remove cell debris. The total protein concentration of cell lysates was measured by Bradford assay and standardised to 0.5mg/ml. Standardised lysate samples were analysed by LI-COR western blot to compare the relative level of Fv1 or T5HA in different clones.

2.4.10 Analyses of crosslinked capsid complexes in virus particles of HIV-1 and N-MLV

Viruses with wt or mutant N-MLV capsid sequence were prepared using plasmids for pseudotype envelope (pVSV-g), Gag-Pol (wt or mutant pCIGN) and vector for GFP expression (pLNCG). Viruses with wt or mutant HIV-1 capsid sequence were prepared with plasmids for pseudotype envelope (pVSV-g), Gag-Pol (p8.91 or p8.91CC) and vector for GFP expression (pCSGW). Viruses were pelleted either by centrifugation at 14k x g at 4^{o}C (N-MLV) for 2h or by ultracentrifugation at 70k x g at 4^{o}C for 1h (HIV-1), and resuspended in 100µl 1X non-reducing SDS-PAGE loading buffer (50mM Tris-HCl pH 6.8, 2% SDS, 0.02% w/v bromophenol blue, 10% glycerol). The sample was divided into 2 x 50µl aliquots, and 1µl of β-mercaptoethanol was added to 1 aliquot for reduced sample. HIV-1 samples were analysed by LI-COR western blot with anti-p24, while N-MLV samples were analysed by chemiluminescent western blot with anti-p30.

2.5 RNA quantitation

2.5.1 Preparation of cell lysate

To determine the relative quantities of Fv1 mRNA in SCCs induced levels, $7.5x10^5$ cells were seeded to each 10cm dish and treated with the required amount of doxycycline. 24h later, cells were harvested with trypsin, mixed with medium, and pelleted at 300 x g for 5min. Cell pellet was resuspended 2ml PBS, and pelleted again at 300 x g for 5min. The pellet was snap frozen with liquid nitrogen, and stored at -80^{o}C until analysis.

2.5.2 RNA extraction

RNA purification was carried out using the RNeasy kit (Qiagen, #74104). Cell pellets were resuspended in 350µl RLT buffer, transferred to a QiaShredder column, and centrifuged at 14krpm for 2min. 300µl of supernatant was mixed with 300µl of 70% ethanol, added to an RNAeasy column, and centrifuged at 10krpm for 15s. The column was washed with 350µl of RW1, incubated with 80µl of DNase I mix (DNase:RDD = 1:7; Qiagen, #79254) at room temperature for 15min, and then washed again with 350µl RW1. The column was then washed with 500µl RPE first for 15s, then again for 2min. The column was centrifuged in a new collection tube for 1min to remove residual buffer. RNA was eluted by centrifuging 50µl of RNase-free water through the column for 1min using a new collection tube. The required amount of RNA sample was transferred to PCR tubes, and the rest were stored at -80oC.

2.5.3 Reverse transcription

Generation of cDNA was carried out using the High-capacity cDNA reverse transcription kit (Life Technologies, #4368814). 10µl of RNA sample was mixed with 10µl of 2X RT mix (2µl 10X RT buffer, 0.8µl 25X dNTP, 2µl 10X random RT primer, 1µl MultiScribe RT, 4.2µl RNase-free water). Reactions were incubated at 25^{o}C for 10min, 37^{o}C for 120min, and 85^{o}C for 5min. cDNA samples were stored at -20^{o}C until qPCR.

2.5.4 Relative quantitative PCR (qPCR)

Relative quantities of Fv1 cDNA were analysed by TaqMan real-time PCR assay (Life Technologies). Primers and probe (Sigma) used for the quantitation of Fv1 mRNA are listed in Table 2.10. Each 20µl PCR reaction contained 5µl of cDNA sample, 0.9µM forward Fv1 primer, 0.9µM reverse Fv1 primer, 0.25µM of Fv1 probe (5'-6FAM/3'-BHQ1), 1µl of Mouse GAPDH Endogenous Control mix (VIC/MGB probe, primer limited, Life Technologies, #E4352339E) and 10µl of 2X TaqMan Fast Universal PCR Master Mix (Life Technologies, #4366072). qPCR was carried out using the 7500 Fast Real-Time PCR System (Life Technologies) and the supplied software, with default cycling parameters for TagMan assays. Relative quantities of Fv1 and GAPDH in each sample were interpolated from standard curves of Fv1 and GAPDH derived from serial dilutions of cDNA of one particular sample in water. The relative quantities of Fv1 cDNA were normalised against the relative quantities of GAPDH cDNA. The mean and error values of relative Fv1 mRNA expression were calculated from results of 2 qPCR repeats from each of 2 biological samples.

Oligonucleotides	**Sequence**
Forward primer	TGTGAGGTTAGCTGATGTGCAA
Reverse primer	TCACCTTATCTGCAGACATTTCC
Probe	6[FAM]CCCAGGTCATGTGTCAGCCTGCC[BHQ1]

Table 2.10 Primers and probe used for TaqMan qPCR analysis of Fv1 mRNA

2.6 Luciferase assay

2.6.1 Screening of rtTA3 SCCs by luciferase assay

rtTA3 SCCs was transduced with TREPuro-Luc vector virus at a MOI less than 0.1, and selected with puromycin for 10 days. Cells were then reseeded in 24-well plates, and treated with or without 1µg/ml doxycycline for 24h. Luciferase assay was carried out using the Luciferase Assay System (Promega). Cells were lysed with 100µl of 1X the supplied Cell Culture Lysis Buffer, and cell debris was removed by centrifugation at 450 x g for 10min. For the analysis of samples without doxycycline treatment, 20µl of lysate was added to a white 96-well plate (Corning). Samples treated with 1µg/ml doxycycline were diluted 100-fold before analysis using 20µl of diluted lysate. Light emitted from the bioluminescent reaction catalysed by firefly luciferase was measured (sensitivity level of 150, 10s measurement) using the Synergy 2 plate reader and the Gen5 software. 100µl Luciferase Assay Reagent was dispensed 2s before measurement. Cells from duplicate wells in 24-well plate were counted, and relative luminescence signal was normalised to the cell count to obtain normalised relative luciferase activity. In later experiments with induction at multiple doxycycline concentrations, cells transduced with the TREPuro-Luc vector and selected with puromycin were directly seeded to white 96-well plate and treated with various concentration of doxycycline. Cells were either resuspended in trypsin and counted, or lysed with 20µl of lysis buffer for luciferase assay under optimised conditions (sensitivity level of 70, 2s delay, 1s measurement time, 100µl Luciferase Assay Reagent).

2.7 Flow cytometry

2.7.1 Standard flow cytometry (FACS) analyses

Confluent cells in 12-well plates were resuspended in 1ml trypsin and fixed by mixing with 3ml of 2% formaldehyde-PBS in 5ml round bottom tubes (Corning, #352008). Cells were pelleted by 400 x g centrifugation for 5min, and resuspended in 300µl PBS. Samples were filtered through 35µm nylon mesh (Corning, #352235) before analysis. Flow cytometry (FACS) analyses were carried out using FACSVerse, LSR II or LSRFortessa flow cytometers (BD Biosciences), and the FACSDiva and FACSuite software (BD Biosciences). In two colour analyses, filters optimised for simultaneous detection of GFP and YFP signals were used. Due to the overlapping in the emission spectra of EGFP and EYFP, there are significant spillover of GFP signal to the YFP detection channel, and vice versa. Therefore, GFP and YFP signals were compensated for spillover using a compensation matrix. Further optimisation of compensation values and data analyses were carried out using the FlowJo software (Tree Star). The 2-colour FACS analysis allows determination of the percentages of GFP^- YFP^-, GFP^- YFP^+, GFP^+ YFP^- and GFP^+ YFP^+ populations among the analysed cells.

2.7.2 High throughput FACS analyses

A high throughput procedure was used for analyses of large number of samples. Confluent cells in 24-well plates were resuspended in 0.5ml trypsin and fixed by mixing with 1.5ml of 2% formaldehyde-PBS in 2ml deep-well plate (Eppendorf, #0030501.306). Cells were pelleted by 400 x g centrifugation for 5min, and resuspended in 150µl PBS. Samples were filtered through a 40µm MultiScreen-MESH Filter Plate (Merck Millipore, #MANMN4010) to a round-bottom 96-well collection plate (Corning), and analysed using FACSVerse with microplate sample loader.

2.7.3 Screening of SSC with inducible Fv1 expression

To screen SCCs derived from R18 cells transduced with TGx-Fv1 or TGIx-Fv1 vectors, 2.5x10^4 SCC cells were seeded in 24-well plate and induced with 1µg/ml doxycycline for 72h before FACS analysis. SCCs each consisted of a single GFP$^+$ population were chosen for later studies.

2.7.4 Restriction assay in cells with non-inducible Fv1 expression

MLV restriction assays in cells with non-inducible Fv1 expression using LxIG-Fv1 vectors had been described before (Bock et al., 2000). YFP tester viruses were prepared using plasmids for expression of the VSV-g envelope (pVSVg), MLV gag-pol (pCIGN for N-MLV, pCIGB for B-MLV and pHIT60 for NB-MLV) and vector genome for EYFP expression (pCFG-YFP). The MOI of transduction is linked to the fraction of cells expressing the fluorescent marker (f_p) using the following equation:

$$MOI = -2ln(1 - f_p)$$

R18 cells were transduced with LxIG-Fv1 vector at MOI of 0.7 (~30% GFP$^+$), and 2.5x10^4 transduced cells were seeded per well in 24-well plate. 24h later, the transduced cells were infected with YFP tester viruses with N, B or NB-tropic capsid at MOI of 0.7. At 72hpi, cells were studied by FACS analyses to determine the percentages of cells expressing GFP, YFP or both. Restriction ratio was calculated as follow:

$$Restriction\ ratio = \frac{GFP^+YFP^+}{GFP^+} \div \frac{GFP^-YFP^+}{GFP^-}$$

2.7.5 Restriction assay in cells with non-inducible T5 expression

MLV restriction assays with in MDTF cells with non-inducible T5 expression using LxIY-T5 vectors had been described before (Yap et al., 2004). Since the transduction vectors expressed EYFP, GFP tester viruses were prepared using the vector plasmid pLNCG. Restriction assay was carried out as described for Fv1, but restriction ratio was calculated using a modified equation:

$$Restriction\ ratio = \frac{YFP^{+}GFP^{+}}{YFP^{+}} \div \frac{YFP^{-}GFP^{+}}{YFP^{-}}$$

2.7.6 Restriction assay in cells with inducible Fv1 expression

MLV restriction in R18 cells transduced with TGIx-Fv1 or TGx-Fv1 vectors at MOI of 0.7 were studied using a modified protocol. Transduced cells were seeded at $2.5x10^4$/well in 24-well plate in medium containing 0 to 1000ng/ml doxycycline. 24h later, cells were infected with YFP tester viruses at MOI of 0.7. At 24hpi, a high dose of doxycycline was added to the medium to a final concentration of 10µg/ml. At 72hpi, cells were studied by FACS analysis as described before. Restriction studies in SCC cells with inducible Fv1 expression was carried out as described, except that $1.25x10^4$ SCC cells were seeded along with $1.25x10^4$ untransduced R18 cells.

2.7.7 Restriction assay in cells with superexpression of Fv1

MDTF cells seeded at 2.5x10^4/well in a 24-well plate were transduced with different volume of LxIG-Fv1 vector viruses, or with the NB-MLV GFP tester virus as a control. After 72h, cells from a transduced well were mixed with cells from an untransduced well, and reseeded at 2.5x10^4/well in a 24-well plate. 24h later, cells were infected with YFP tested viruses. FACS analyses were carried out at 72hpi. The MOI of transduction was calculated as follow:

$$MOI = \left(\frac{-2ln0.7}{V_{30}}\right) \times V$$

MOI The MOI of transduction

V_{30} The volume of vector virus needed for transduction to obtain a 30% GFP$^+$ population (before mixing), interpolated from the plot of percentage of GFP$^+$ cells (before mixing) against volume of transducing virus

V Volume of vector virus used for transduction

2.7.8 Abrogation assay

Abrogation of endogenous Fv1^b in B-3T3 cells and endogenous HuT5 in TE671 cells had been described before (Dodding et al., 2005). Abrogating particles were prepared with plasmids expressing envelope (pVSVg), wt or mutant MLV gag-pol (pCIGN for N-MLV, pCIGB for B-MLV), and vector for LacZ expression (pHIT111). Cells were seeded at 5x10^4/well in 12-well plate for TE671 (or 2.5x10^4/well in 24-well plate for B-3T3). On the next day, cells were incubated with various volumes of freshly prepared abrogating particles for 2h, before infection with N-MLV GFP tester virus at a MOI of 0.7 (based on previous titration on MDTF cells). The percentage of GFP$^+$ cell population was determined by FACS analysis at 72hpi.

2.8 Binding assay

2.8.1 Generation of lipid nanotubes

Lipids used for generation of nanotubes are listed in Table 2.5. Typically, 70µl of 2.5mg/ml GalCer, 30µl of 2.5mg/ml DGS-NTA(Ni) and 50µl of 25µg/ml BioPEG PE were mixed in glass vial using a Hamilton Syringe. Bio PE and BioCap PE were also used in initial optimisation experiments. Chloroform and methanol were slowly evaporated under a gentle stream of nitrogen gas. Dried lipids were resuspended in 500µl of nanotube buffer (10mM Tris-HCl pH 8.0, 10mM KCl, 100mM NaCl) using a sonication bath and a vortex.

2.8.2 Screening of nanotube immobilisation conditions

Initial optimisation of nanotube immobilisation conditions were carried out using High Bind 96-well plate (Corning, #3590) coated with neutravidin (Thermo Fisher, #31000, cheaper alternative to Streptavidin) and blocked with 5% BSA (Sigma) in house. In these early trials, 100µg/ml of naked or coated nanotubes were incubated for 4 to 16h, and coated with CA for 1h. Capsids were eluted in 1X SDS-Loading buffer, and analysed by SDS-PAGE followed by gel staining.

2.8.3 Preparation of fresh lysate

Confluent cells expressing Fv1 or T5HA on a 10cm dish were scraped off in 10ml PBS and pelleted by centrifugation at 300 x g for 5min. Cells were resuspended in 500µl ice-cold hypotonic buffer (10mM Tris-HCl pH 8.0, 10mM KCl) and incubated on ice for 10min. Cells were lysed by centrifugation through a QIAShredder column (Qiagen, #79654) at 13k x g for 2min at 4^{o}C. Supernatant was centrifuged again at 13k x g for 10min to remove cell debris. The salt concentration was adjusted by adding 1/10 volume of 10X salt buffer (10X: 10mM Tris-HCl pH 8.0, 10mM KCl, 3M NaCl, and 100mM imidazole). The total protein concentration of cell lysate was measured by Bradford assay and standardised to 0.5mg/ml. In some experiments, standardised lysate expressing Fv1 was diluted with standardised blank lysate from untransduced MDTF cells.

2.8.4 Generation of frozen lysate library

MDTF cells were seeded at $5x10^4$/ml in 12-well plate and transduced with LxIG-Fv1 vectors at different MOIs, and allowed to grow to confluency in a T175 flask. Cells were resuspended in 5ml trypsin, mixed with 30ml medium and pelleted at 300 x g for 5min. Cells were washed with 30ml PBS, pelleted, and resuspended in 1.5ml ice-cold hypotonic buffer. Lysate was prepared as described above, and dispensed into PCR tubes as 160µl aliquots. Trays of PCR tubes were immersed into liquid nitrogen for 10s, and stored at -80^oC immediately. An aliquot of each sample in the lysate library was thawed for analysis of total protein by Bradford assay and for analysis of Fv1 concentration by quantitative LI-COR western blot. Diluted Fv1 lysate with specified Fv1 concentration and 0.5mg/ml total protein concentration was prepared by mixing appropriate amount of thawed Fv1 lysate, blank lysate from untransduced MDTF cells and binding buffer (10mM Tris-HCl pH 8.0, 10mM KCl, 300mM NaCl, and 10mM imidazole).

2.8.5 Optimised microplate pull down assay

A Reacti-Bind Streptavidin High Binding Capacity Coated 96-well plate (Thermo Fisher, #15501) was washed 3 times with nanotube buffer, followed by addition of 100µl/well of 10µg/ml lipid nanotube. The plate was incubated at 25^{o}C for 1h with shaking, and washed 3 times with nanotube buffer. 100µl of 15µM MLV CA-His or HIV-1 CA-p2-His (confirmed by absorbance at 280nm) was added to each well, and the plate was incubated at 25^{o}C for 1h with shaking. After 3 washes with nanotube buffer, 100µl of 0.5mg/ml lysate was added to each well. The plate was incubated at 25^{o}C for 1h with shaking, and then washed 10 times with wash buffer (10mM Tris-HCl pH 8.0, 10mM KCl and 300mM NaCl). 1M imidazole was added to wash buffer in some control experiments. To elute proteins, 100µl of elution buffer (10mM Tris-HCl pH 8.0, 10mM KCl, 300mM NaCl, 2% SDS, 0.5M imidazole) pre-heated to 37^{o}C was added to each well, and the plate was incubated at 37^{o}C for 20min with shaking. 80µl of eluted sample was mixed with 20µl of 5X SDS-free loading buffer (5X: 250mM Tris-HCl pH 6.8, 10% SDS, 0.1% w/v bromophenol blue, 50% glycerol) in PCR tubes, and boiled at 98^{o}C for 5min. Eluted samples were analysed along with input samples by chemiluminescent or LI-COR western blot.

2.9 Software

Analyses of DNA and protein sequences were performed using Lasergene 10 (DNASTAR) and Serial Cloner (SerialBasics). Flow cytometry data were analysed with FlowJo (Tree Star). Quantitative western blot analyses were achieved using ImageStudio (LI-COR). Curve fitting and correlation analysis were carried out using Prism 5 (GraphPad). Images of capsid structures were produced using PyMOL (Schrödinger).

Chapter 3

Study of the relationship between Fv1 expression level and restriction specificity

One of the key questions in this thesis is what controls the Fv1 restriction specificity. In addition to sequence determinants in Fv1 alleles, there was some evidence that the concentration of Fv1 may also affect the apparent restriction specificity (Felton, 2012). This chapter describes a number of experiments to study the relationship between Fv1 expression level and restriction specificity.

The two Fv1 alleles which control N and B tropism, $Fv1^n$ and $Fv1^b$, differ at three variable sites: position 358, position 399 and the C-terminal tail (Best et al., 1996). In order to study the determinants controlling the different restriction specificities of $Fv1^n$ and $Fv1^b$, "mix-and-match" mutants expressing chimeric Fv1 proteins harbouring different combinations of sequences at the 3 variable sites have been studied along with C-terminal tail deletion mutants (Table 1.1) (Bishop et al., 2001; Bock et al., 2000). When over-expressed using the LxIG-Fv1 vector, these mutants have diverse restriction phenotypes against N-MLV, B-MLV and NB-MLV. In section 3.1, I wanted to test the hypothesis that at the over-expression level, these residues at the 3 variable sites affect restriction specificity mainly through changes in apparent binding affinity to CA. Since $Fv1^b$ has been hypothesised to gain inhibition of NB-MLV and B-MLV at the over-expression level, it is possible that some restriction phenotypes of the variable site mutants can be explained by the differences in the Fv1 protein levels when over-expressed using the LxIG-Fv1 vector. For example, $Fv1^b$ and its two tail mutants, Fv1bbn and Fv1bb_, all restrict N-MLV and NB-MLV. However, while over-expressed $Fv1^b$ only weakly inhibits B-MLV, over-expressed Fv1bb_ and Fv1bbn showed partial and full restriction, respectively. It is possible that the mutation or deletion at the C-terminus increase the Fv1 protein level expressed using the LxIG-Fv1 vector, thereby allowing the restriction of B-MLV without affecting the apparent binding affinity to B-MLV CA. Therefore I wanted to

compare the Fv1 protein levels of the mix-and-match mutants and the C-terminal deletion mutants. This will allow the identification of sequence which leads to higher Fv1 protein level despite being expressed using the same vector, and to test if the restriction of B-MLV by $Fv1^b$, Fv1bbn and Fv1bb_ can be correlated with the Fv1 concentration in cells.

$Fv1^b$ expressed at endogenous levels in BALB/c mice and B-3T3 cells restricts N-MLV, but neither B-MLV nor NB-MLV (Hartley et al., 1970). However, $Fv1^b$ expressed by retroviral vector in MDTF cells appears to restrict N-MLV by 20-fold, restrict NB-MLV by 5-fold, and inhibit B-MLB by 30% (Bock et al., 2000). The observations of high $Fv1^b$ restriction specificity at the endogenous level of B-3T3, and a low $Fv1^b$ restriction at the over-expression level in transduced MDTF strongly suggested a link between Fv1 concentration and restriction specificity. However, since these observations were made in different cell lines, it is possible that some other cell type specific factors unrelated to Fv1 could influence the restriction specificity. To exclude such possibility, it would be desirable to develop a system which allow the inducible expression of recombinant Fv1 in the Fv1 MDTF cell line, and allow the study of Fv1 restriction from the endogenous level to an over-expression level using the FACS-based restriction assay. In section 3.2, I wanted to test the hypothesis that the over-expression of $Fv1^b$ leads to an increase in restriction specificity, using a novel inducible expression system which allow the expression of Fv1 from the endogenous level to an over-expression level.

$Fv1^n$ expressed at endogenous levels in NIH/Swiss mice and N-3T3 cells restricts B-MLV, but neither N-MLV nor NB-MLV (Hartley et al., 1970). In contrast to $Fv1^b$, which appears to inhibit all MLV strains at the over-expression level, $Fv1^n$ does not appear to inhibit N-MLV and NB-MLV even when over-expressed (Bock et al., 2000). In section 3.3, I asked the question whether $Fv1^n$ can inhibit N-MLV and NB-MLV at a very high “super-expression” level.

3.1 Study of Fv1 expression using a quantitative assay

3.1.1 The vector-mediated $Fv1^b$ protein expression was 26-fold higher than the endogenous level

In order to test the hypothesis that residues at the 3 variable sites affect restriction specificity solely through changes in apparent binding affinity to CA, I compared the Fv1 protein levels of $Fv1^n$, $Fv1^b$, 6 mix-and-match mutants and 2 C-terminal tail deletion mutants (Table 1.1). I started by developing an Fv1 quantitation assay by optimising the LI-COR quantitative western blot procedure. The LI-COR system uses a high resolution scanner to detect infrared fluorescent signals from secondary antibody conjugated to an infrared dye (IRDye). This system is advantageous over traditional chemiluminescent detection using HRP-conjugated antibodies by having a wider sensitivity range and much better linearity between signal and protein quantity. The high resolution of western blot image also allows easy quantitation of protein bands. Absolute quantitation of the target protein can also be carried out by relating the fluorescent signals from samples to that from purified protein standards of known concentration.

Figure 3.1 shows an example of quantitative western blot analysis for Fv1. In this assay, the absolute quantities of Fv1 were measured from cell lines that express Fv1 endogenously (N-3T3 and B-3T3) and from MDTF cells transduced with LxIG-Fv1 vectors expressing various Fv1 alleles and mutants. Cells were lysed in RIPA buffer, and the total protein concentration of cell lysates were measured by BCA protein assay and standardised to 1mg/ml. 25µg of cell lysate were analysed by western blot along with purified Fv1-NTD standards of various known quantities. While there has been no reported success in the purification of full length Fv1, the amino-terminal domain comprising residues 20-200 of Fv1 (Fv1-NTD) is highly stable and could be purified as standard (Bishop et al., 2006). Because the much smaller size of Fv1-NTD (22kDa) compared to full length Fv1 (about 50kDa), the samples and standards could be loaded to the same lane to maximise the number of lysates that can be compared on the same blot. Fv1 was detected using an anti-Fv1 rabbit serum

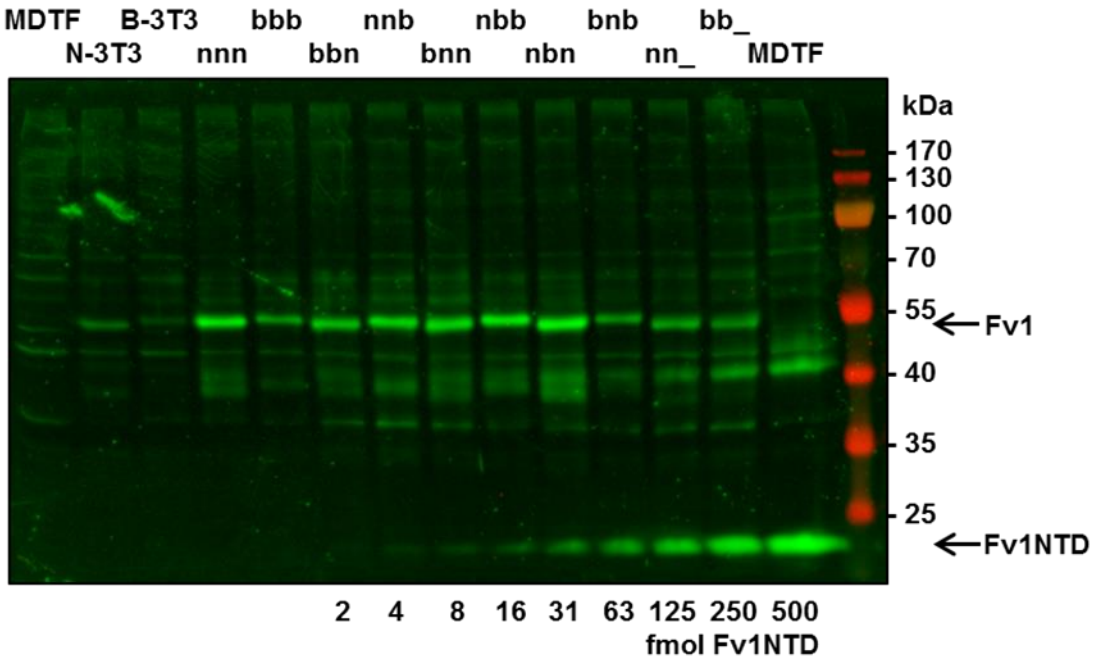

(#6689) which was raised against Fv1-NTD as the primary antibody, and an IRDye-800 conjugated secondary antibody.

Figure 3.1 Quantitation of Fv1 in cell lysate by LI-COR western blot

Cells of MDTF, N-3T3, B-3T3, and MDTF transduced with LxIG-Fv1 vectors (~30% GFP^+) expressing wild type or mutant Fv1 were lysed in RIPA buffer. The 3-letter code for each mutant indicated the source of sequence at position 358, position 399 and C-terminus, respectively. Cell lysates were analysed by SDS-PAGE along with purified Fv1-NTD standards of known concentration. Fv1 was detected by LI-COR quantitative western blot using anti-Fv1 primary antibody and IRDye-800 labelled secondary antibody. Signals detected from the 800nm channel were shown in green. Quantification data from this western blot is shown in Figure 3.3.

The infrared fluorescent signal at 800nm of each band was measured using the LI-COR Odyssey scanner. Using the GraphPad Prism software, the quantity of Fv1 from each sample band was interpolated from a standard curve fitted to data from Fv1-NTD (Figure 3.2). To relate the quantity of Fv1 in cell lysate to the expression level in cells, I determined that on average each lysed cell results in 120pg of proteins using my lysis protocol. This was determined by lysing $2x10^6$ MDTF cells in 100µl lysis buffer, measuring the total protein concentration by BCA assay, and finally dividing the total protein yield by the number of cells lysed. This allowed the calculation of the average number of Fv1 molecules per cell. For the transduced MDTF samples, the percentage of $Fv1^+/GFP^+$ cells was determined by FACS analysis. In the restriction assay as well as this Fv1 quantitation assay, MDTF cells were transduced at a MOI of 1 or below, typically at 0.7. Based on the Poisson distribution, it is calculated that after transduction at a MOI of 0.7, 50% of cells will be transduced, of which 69% would contain 1 copy of provirus. However, since each integration event occurs in one copy of the diploid genome, it will only be inherited by one of the daughter cells. After cell division, 30% of cells will contain provirus, of which the majority of cells (84%) will have a single copy of provirus. The number of Fv1 molecules in the transduced population was calculated by dividing the average number of Fv1 molecules per cell by the percentage of GFP^+ cells.

The results from the Fv1 quantitation assay are illustrated in Figure 3.2. In agreement with earlier studies, the Fv1 protein level in transduced MDTF was found to be significantly higher than the endogenous level for both $Fv1^n$ and $Fv1^b$. The exogenous $Fv1^n$ level is 37-fold higher than the endogenous level, while the exogenous $Fv1^b$ level is 26-fold higher than the endogenous level. The high Fv1 protein levels in transduced cells are consistent with the hypothesis that the additional inhibition activities in cells expressing $Fv1^b$ exogenously are due to overexpression of Fv1. It is surprising that although a 26-fold increase in $Fv1^b$ expression appears to cause significant increase in restriction activities, a 37-fold increase of $Fv1^n$ still does not allow inhibition of N-MLV and NB-MLV.

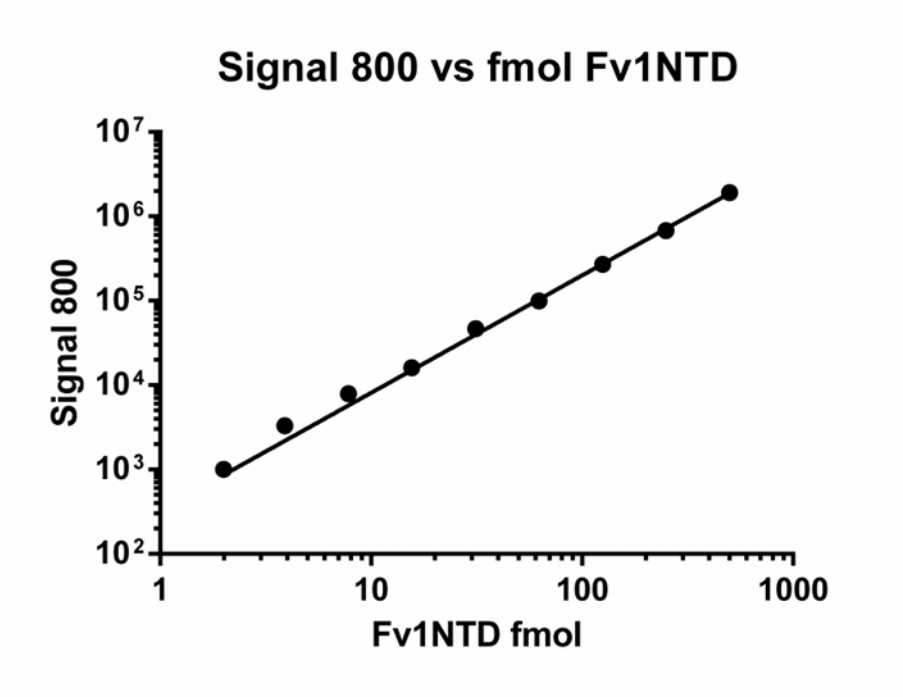

Figure 3.2 A typical standard curve for Fv1 quantitation

Signals of bands from different known quantities of Fv1-NTD in Figure 3.1 were fitted to a standard curve using the GraphPad Prism software.

3.1.2 Sequences at position 358 and the C-terminus of Fv1 strongly influence the vector-mediated Fv1 expression level

Since $Fv1^n$ and $Fv1^b$ differ from each other at positions 358, 399 and the C-terminus, Fv1 quantification was carried out on MDTF cells transduced with LxIG-Fv1 vectors expressing 6 mix-and-match Fv1 mutants (bbn, nnb, bnn, nbb, nbn and bnb) and two C-terminal tail-truncation Fv1 mutants (nn_ and bb_) previously made to study determinants of MLV restriction (Bishop et al., 2001; Bock et al., 2000). Study of Fv1 protein levels of these mutants in MDTF cells would be very useful to understand the contributions of the 3 positions to protein expression level, and may also help to explain some of the restriction phenotypes of these mutants.

In MDTF cells transduced with LxIG-Fv1 vectors, the $Fv1^n$ protein level was 4-fold higher than the $Fv1^b$ level (Figure 3.3). Previously, equal mRNA level was found in MDTF cells transduced with $Fv1^n$ and $Fv1^b$ vectors. The fact that both alleles were expressed using the same promoter, vector and cell line suggested that the difference in exogenous protein levels was due to differences during or after translation. An analysis on how mutations at each position influenced the Fv1 protein level is summarised in Table 3.1. The presence of the $Fv1^n$-specific Lys residue instead of the $Fv1^b$-specific Glu residue at position 358 consistently led to higher Fv1 protein level in all cases. The presence of the $Fv1^n$-specific Val residue instead of the $Fv1^b$-specific Arg residue at position 399 did not show consistent change in protein level, with increase in two cases and decrease in two cases. The short C-terminal tail of $Fv1^n$ (TKL) was associated with higher Fv1 protein level. In all cases, mutation from the $Fv1^n$ tail to the $Fv1^b$ tail led to decrease in Fv1 protein level. This result could be explained either by an enhancing effect of the short $Fv1^n$ tail, or by an inhibitory effect of the long $Fv1^b$ tail. The observations that the truncation of the short tail from $Fv1^n$ led to a 70% drop in protein level while the deletion of the long tail $Fv1^b$ did not significantly increase protein level support the first possibility. Taken together, the presence of K358 and TKL tail from $Fv1^n$ strongly enhances the expression of Fv1 in MDTF cells.

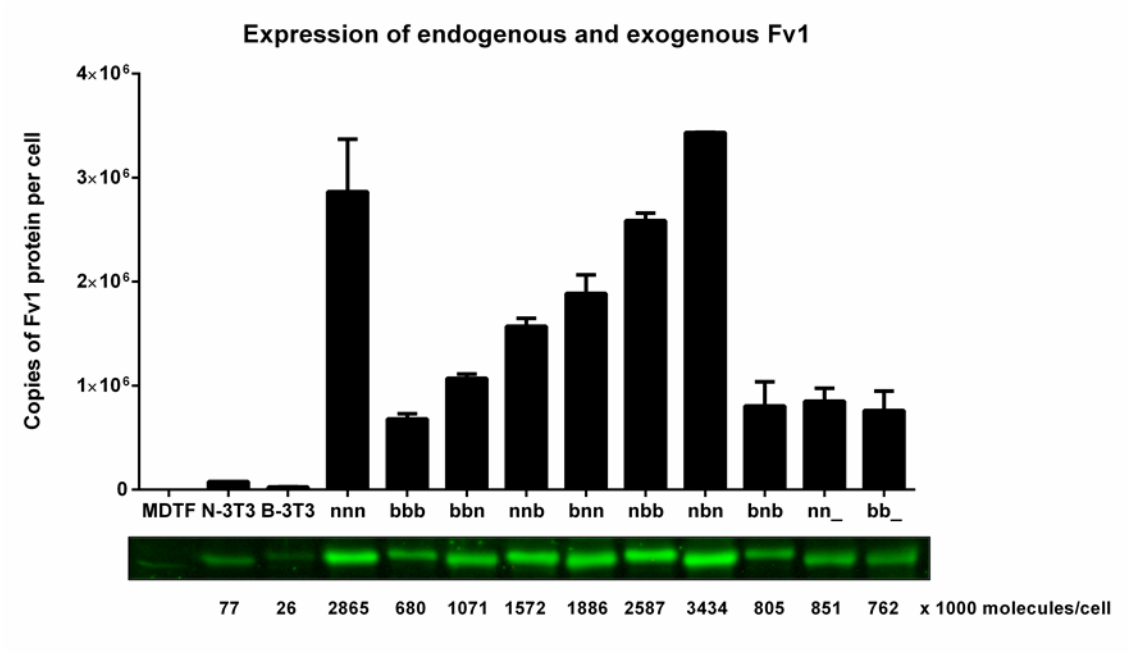

Figure 3.3 Quantification of endogenous and exogenous Fv1 protein levels

The amount of Fv1 in each band was quantified by interpolating from the standard curve shown in Figure 3.1. The number of Fv1 molecules per cell was calculated using the Fv1 and total protein concentration of lysate, the percentage of GFP^+ cells expressing Fv1, and the amount of protein per lysed cell (120pg/cell). The graph showed mean and mean deviation from two independent experiments.

nxx	>	bxx	Difference	% Difference
nnn	>	bnn	-979	-34%
nnb	>	bnb	-767	-49%
nbb	>	bbb	-1907	-74%
nbn	>	bbn	-2363	-69%

xnx	>	xbx	Difference	% Difference
nnn	>	nbn	569	20%
bnb	>	bbb	-125	-16%
nnb	>	nbb	1015	65%
bnn	>	bbn	-815	-43%

xxn	>	xxb	Difference	% Difference
nnn	>	nnb	-1293	-45%
bbn	>	bbb	-391	-37%
bnn	>	bnb	-1081	-57%
nbn	>	nbb	-847	-25%

xxx	>	xx_	Difference	% Difference
nnn	>	nn_	-2014	-70%
bbb	>	bb_	82	12%

Table 3.1 The influence of mutations on the exogenous protein level of Fv1

A summary of the data from Figure 3.2 showing the differences in protein expression level (as 1000 Fv1 molecules/cell) caused by each mutation.

A comparison of the protein levels of $Fv1^b$, Fv1bbn and Fv1bb_ showed that Fv1bbn is expressed at the highest level, followed by Fv1bb_ then $Fv1^b$. Interestingly, the restriction activities towards B-MLV follows the same order, with the strongest effect from Fv1bbn, followed by Fv1bb_ then $Fv1^b$ (Bishop et al., 2001; Bock et al., 2000). However, the difference in protein levels among these Fv1 alleles is low (less than 2-fold), and is unlikely to have significant effect on restriction. A comparison of Fv1 protein levels in N-3T3 and B-3T3 cells showed that the endogenous protein level of $Fv1^n$ was 3-fold higher than that of $Fv1^b$. Since a higher Fv1 mRNA level in N-3T3 cell than in B-3T3 has been reported (Felton, 2012), it is not certain whether the difference in endogenous protein levels is mainly due to differences during or after translation, or due to the different transcription levels.

3.1.3 The lower vector-mediated $Fv1^b$ protein expression compared to $Fv1^n$ was not due to higher rate of degradation by proteasome

A fusion protein containing the Fv1-NTD and a CypA domain (Fv1Cyp) was previously shown to have a long half-life in cells with no detectable reduction in protein level 8h after blocking of protein synthesis with cycloheximide (Schaller et al., 2007). It is possible the lower expression of $Fv1^b$ in MDTF cells was due to a higher rate of degradation by proteasomes leading to a more rapid turnover. To test this hypothesis, the effect of proteasome inhibitor MG132 on Fv1 protein expression in transduced cells was studied using the Fv1 quantitation assay (Figure 3.4). MDTF cells transduced with either LxIG-$Fv1^n$ or LxIG-$Fv1^b$ vectors were treated with or without 10μM MG132 for 24h. In addition to cell lysis with RIPA buffer, lysate was also prepared using a detergent-free hypotonic buffer and mechanical sheering of cells through QiaShredder columns. Cell lysates were standardised by total protein concentration using the BCA assay. The detergent-free method was used in preparing lysate for binding assays described in later chapters, and the amount of Fv1 in lysate prepared using either method was highly similar. If the lower protein level of $Fv1^b$ was due to higher rate of degradation by proteasome, similar expression levels of $Fv1^n$ and $Fv1^b$ would be expected in cells treated with MG132. Instead, the $Fv1^b$ level was lower than the $Fv1^n$ level in in both MG132-treated and non-treated

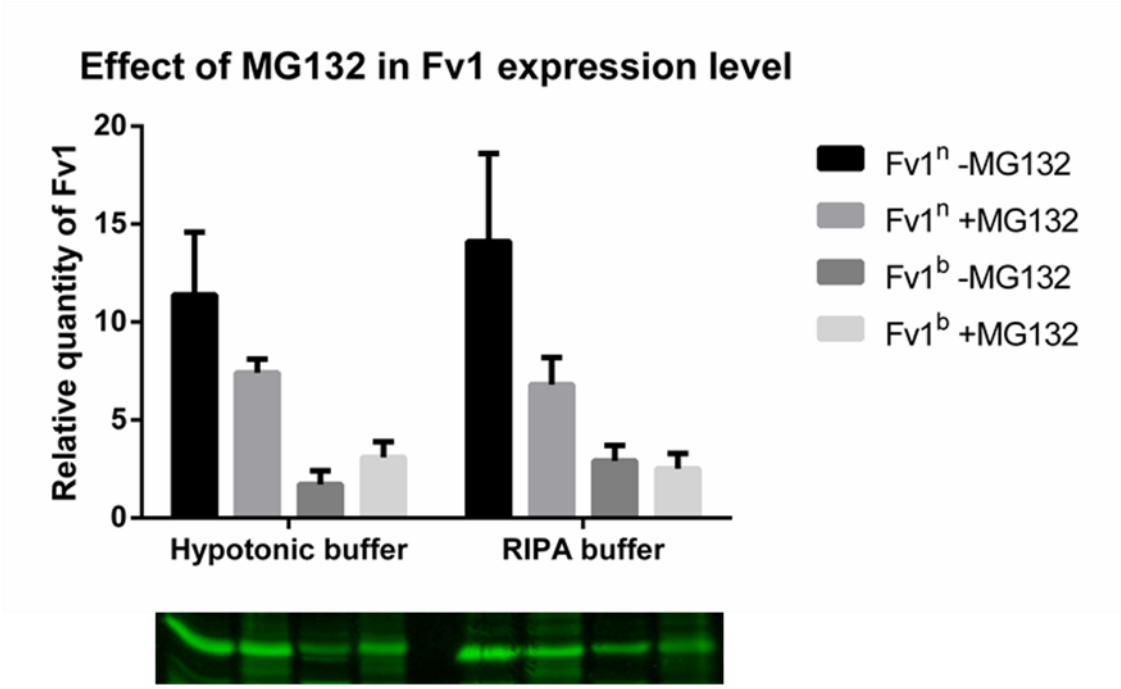

cells. The protein level of both $Fv1^n$ and $Fv1^b$ were lower in cells treated with

Figure 3.4 Effect of protease inhibitor on Fv1 expression level

MDTF cells transduced with either LxIG-$Fv1^n$ or LxIG-$Fv1^b$ vectors at about 30% GFP^+, and treated with or without 10μM MG132 for 24h before cell lysis. Cells were lysed either by spinning through QiaShredder in hypotonic buffer, or by 30min incubation in RIPA buffer. Lysate samples were standardised by protein concentration before SDS-PAGE and western blot analysis. The graph showed mean and mean deviation from two quantitative western blot analyses of the same lysate sample.

MG132. Because MG132 treatment causes cell cycle arrest (Mellgren, 1997) and accumulation of proteins in cytoplasm, it may lead to an increase in total protein quantity per cell. As a result, cell lysate that was standardised to total protein concentration would be from fewer cells in samples treated with MG132, causing underestimation of Fv1 expression level. From this assay I could conclude that degradation by proteasome did not play a major role in the different protein expression levels of $Fv1^n$ and $Fv1^b$ in MDTF cells.

3.2 Study of the dose dependency of Fv1 restriction using an optimised inducible expression system and a 2-colour FACS assay

3.2.1 Previous attempts to study restriction of recombinant Fv1 expressed from natural Fv1 promoter

The observations of high $Fv1^b$ restriction specificity at the endogenous level of B-3T3, and a low $Fv1^b$ restriction at the over-expression level in transduced MDTF strongly suggested a link between Fv1 concentration and restriction specificity. However, since these observations were made in different cell lines, it is possible that some other cell type specific factors unrelated to Fv1 could influence the restriction specificity. Several attempts were made to develop new retroviral vectors that would allow the expression of Fv1 under its natural promoter in MDTF (Felton, 2012), so that the restriction specificity can be compared to the LxIG vector using the same FACS-based restriction assay (Bock et al., 2000). These vectors were made by introducing the Fv1 promoter into self-inactivating (SIN) vectors which contain large deletion in the U3 promoter of 3'LTR, resulting in the loss of LTR promoter functions after the integration of vector into host genome (Yu et al., 1986). Transcripts from these vectors contain the Fv1 ORF at the 5' end, followed by an IRES and a reporter gene such as EYFP. However, due to the weak promoter activity the natural Fv1 promoter, there was insufficient expression of the reporter gene for the separation of transduced cells from untransduced cells by FACS. A dual

promoter SIN vector with the arrangement of P_{Fv1}-Fv1-P_{CMV}-EYFP did provide sufficient YFP separation for 2-colour restriction assay (Felton, 2012). Interestingly, results from the study of $Fv1^b$ using this vector showed restriction of N-MLV and no inhibition of B-MLV, a phenotype which resembles that of endogenous $Fv1^b$. However, it was uncertain how the protein level of Fv1 expressed using this vector compared with the endogenous level in B-3T3. The possibility of that the neighbouring CMV promoter could have negatively influenced the activity of the Fv1 promoter activity could not be ruled out (Curtin et al., 2008). The results from the dual promoter SIN vector showed that at a expression level sufficient to restrict N-MLV, $Fv1^b$ does not restrict B-MLV. However, there was still no direct evidence proving that the inhibition of B-MLV and NB-MLV by $Fv1^b$ in cells transduced with the LxIG-Fv1 vector was due to overexpression of $Fv1^b$ above its endogenous level. It was decided that restriction studies in cells with inducible expression of Fv1 would be best suited to address this question.

3.2.2 Tet-On inducible expression systems

The Tet-On inducible expression system was developed for controlling the transcription of transgenes in mammalian cells (Gossen et al., 1995). The system consists of two basic components (Figure 3.5): a constitutively expressed reverse tetracycline-controlled transactivator (rtTA) protein and a tetracycline-controlled inducible promoter containing copies of the *tet* operator sequence (*tet*O). The rtTA protein specifically binds to *tet*O sequences only in the presence of doxycycline, activating transcription from the inducible promoter. As a result, the transcriptional level from the inducible promoter is dependent on the concentration of doxycycline added.

The first rtTA protein was constructed through the fusion of a modified version of Tet repressor (rTetR) protein (Gossen et al., 1995) and transcriptional activating domain of herpes simplex virus (HSV) VP16 protein (Triezenberg et al., 1988). Since then, the system had been improved in order to minimise the basal transcription activity in the absence of doxycycline (leakiness) and to maximise the activation in transcription activity in the presence of doxycycline.

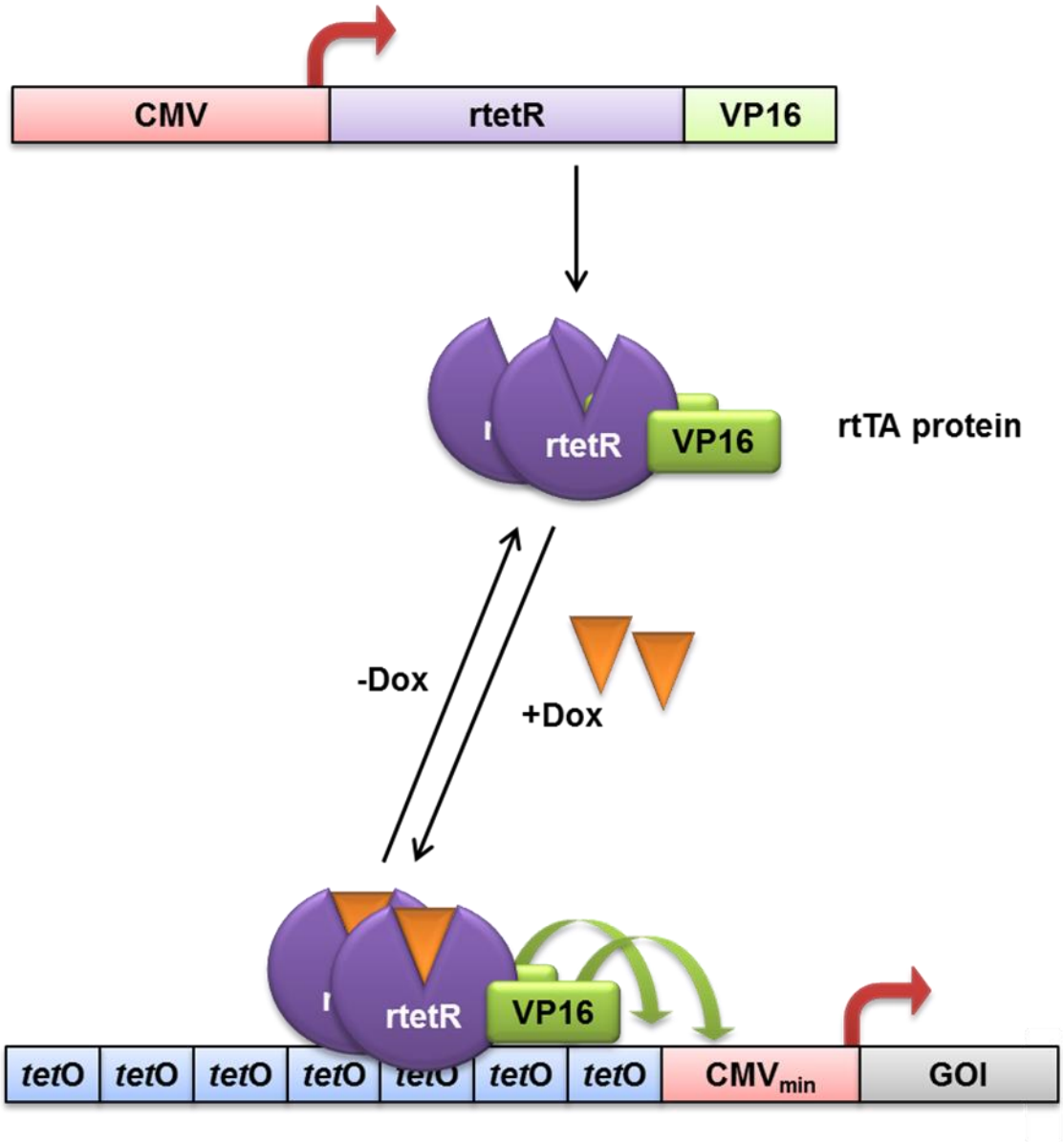

Figure 3.5 Components of the Tet-On inducible expression system

The tet-on system requires a cell line that constitutively expresses the tetracycline-responsive transactivator protein, rtTA. The protein was a fusion product between the rtetR and transactivating sequence from HSV VP16. The rtTA protein forms a dimer, and specifically binds to *tet*O sequence only in the presence of doxycycline through the rtetR domain, and the VP16 domain activates transcription of the gene of interest by the minimal CMV promoter.

The rtTA2 using in the second generation Tet-On Advanced system (Urlinger et al., 2000) and contains 3 copies of minimal transactivating sequence from VP16 to maximise induction (Triezenberg et al., 1988), human codon optimised sequence, and a number of mutations to reduce non-specific binding to *tet*O in the absence of doxycycline for lower leakiness.

The first generation of inducible promoter consists of a tetracycline-responsive element (TRE), which contains 7 repeats of *tet*O sequence upstream of a minimal CMV promoter (P_{CMVmin}) (Gossen et al., 1995). The P_{tight} promoter used in the Tet-On Advanced system contains deletions of endogenous mammalian transcription factor binding sites in P_{CMVmin} leading to reduced leakiness (Pluta et al., 2005). In the P_{TRE3G} promoter used in the Tet-On 3G system, 5' UTR region of P_{CMVmin} was replaced with inert sequence from turnip yellow mosaic virus (TYMV), resulting in even lower basal transcription activity (Loew et al., 2010).

3.2.3 A previous attempt to study dose dependency of $Fv1^b$ restriction using an inducible system

The Tet-On Advanced inducible system was previously implemented for developing cell lines with inducible Fv1 expression (Felton, 2012). The goal was to develop cells with inducible expression of Fv1 from an endogenous level to an overexpressed level, so the change in restriction could be correlated with the Fv1 protein level. First, a MDTF cell line expressing the rtTA2 protein was constructed. MTDF cells transduced with a retroviral vector expressing both rtTA2 and the neomycin resistance gene, followed by selection with G418. Picked single cell clones (SCCs) were transfected with the P_{tight}-luciferase PCR product, and screened for luciferase activity with or without pre-treatment with doxycycline. Cell lines with inducible Fv1 expression was then constructed by stable transfection of the rtTA2 cell line with a plasmid with the P_{tight} promoter controlling the transcription of Fv1-IRES-EYFP mRNA, along with a plasmid with the hygromycin resistance marker. After selection with hygromycin selection, picked SCCs were tested for inducibility of Fv1 expression by comparing the shift in YFP signal in FACS analysis after doxycycline treatment.

Figure 3.6 shows the restriction data from this previous study (Felton, 2012), the infectivity of MLV in $Fv1^n$ and $Fv1^b$ SCCs induced with different amount of doxycycline were compared to that in parental rtTA2 cell line. In SCC expressing $Fv1^b$, N-MLV is fully restricted in the absence of doxycycline. A 50% inhibition of NB-MLV was observed even in the absence of doxycycline, but the infectivity is further reduced to about 20% at higher induction level. Despite high variation in the infectivity of B-MLV in these cells, at above 250 ng/ml doxycycline a mild decrease in infectivity to about 70% could be observed. In SCC expressing $Fv1^n$ cells, the infectivity of all MLV appeared to be inhibited by 30% even in the absence of doxycycline. However, further reduction in infectivity was only observed for B-MLV at higher doxycycline concentration. Since $Fv1^n$ was not found to inhibit N-MLV and NB-MLV even when overexpressed by using LxIG-Fv1 vector, the 30% inhibition was likely due to clone-specific factors unrelated to the expression of Fv1. From this study it could be concluded that increasing Fv1 expression level led to increasing inhibition.

The strong inhibition of NB-MLV in SCC expressing $Fv1^b$ in the absence of doxycycline suggested that the expression of $Fv1^b$ is leaky. The high leakiness of Fv1 expression using this system prevented the study of whether NB-MLV and B-MLV were inhibited by $Fv1^b$ at the endogenous level. Further improvement in the minimisation of leakiness would be required to study restriction of MLV restriction at an endogenous $Fv1^b$ level. The lower infectivity of all MLV in $Fv1^n$ SCC also highlighted the difficulties in determining inhibition of Fv1 by comparing MLV infectivity between clonal and parental cell lines. The infectivity in SCC could be different from the parental cell line for many reasons unrelated to Fv1. This potential difference in infectivity also prevented the conclusion on whether B-MLV was inhibited by $Fv1^b$ at the uninduced level. Minor differences could develop after many passage even in stable clones expressing a transgene when compared to its parental cell line. For example, since MLV intasome could only reach the chromosomes during mitosis when the nuclear membrane is dissolved (Roe et al., 1993b), any difference in mitotic rate between two cell lines could potentially lead to a difference in infectivity. It is difficult to conclude with confidence that small difference in infectivity between

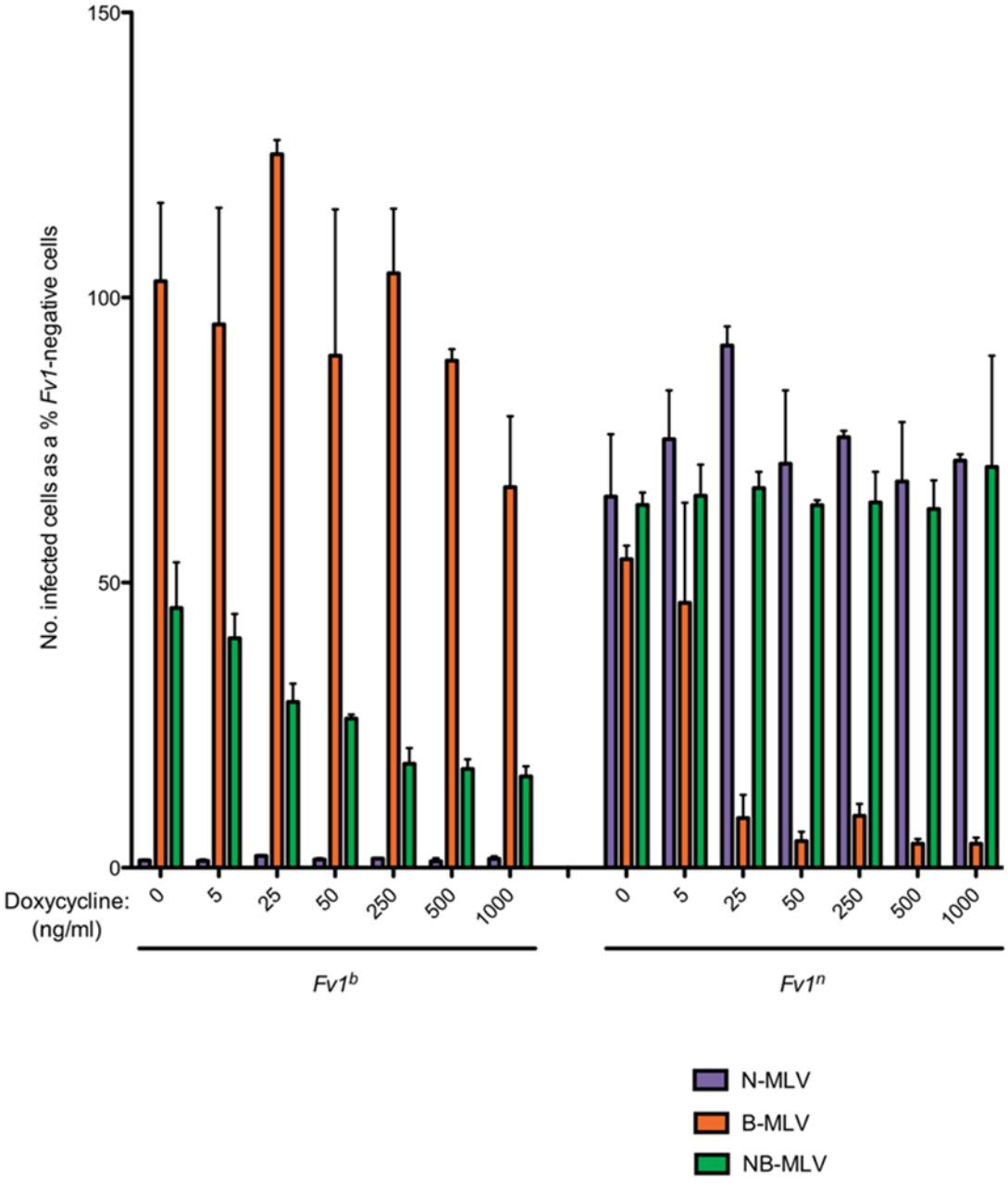

Figure 3.6 A previous analysis of MLV restriction in Fv1 inducible cell lines

Reprinted from the thesis of Victoria Felton (Felton, 2012). Inducible $Fv1^n$ or $Fv1^b$ cell lines were incubated with 0 to 1µg/ml doxycycline for 72h before infection with N-MLV, B-MLV or NB-MLV GFP-expressing tester virus. The percentage of GFP^+ cells was determined by FACS analysis. The results were shown as a percentage of that in permissive MDTF cells infected in parallel.

two cell lines was due to the presence of Fv1 or other cell line specific properties. The use of a transient assay is advantageous over the comparison of infectivity between cell lines because the use of an internal untransduced control (Bock et al., 2000). The 2-colour assay allowed comparison of infectivity between $Fv1^+$ and $Fv1^-$ populations from the same passage in the same well, with the integration of Fv1-expressing vector being the only difference between the two populations. Therefore, an optimised inducible system with lower leakiness and the use of a transient 2-colour restriction assay would be needed to answer these questions.

3.2.4. Development of a Dox-inducible system for expression of Fv1 from sub-endogenous levels

In order to reduce the background expression level of Fv1 to a minimum, I sought to minimise the transcriptional leakiness by using the Tet-on 3G system, and to reduce the translational efficiency by expressing Fv1 using an IRES or inserting extra sequences. The third generation Tet-On 3G system uses the rtTA3 protein which has higher sensitivity to doxycycline compared to rtTA2 used by Tet-On Advanced (Zhou et al., 2006). The Tet-On 3G system also uses the P_{TRE3G} promoter, which has a lower basal transcription level compared to the P_{tight} used by Tet-On Advanced (Loew et al., 2010). To develop a system compatible with the transient restriction assay, a MDTF cell line constitutively expressing rtTA3 was generated, and SIN retroviral vectors with P_{TRE3G} driven transcription were constructed (Figure 3.7). A cloning site for the Gateway system (Thermo Fisher) was introduced to allow efficient enzyme-free cloning of Fv1 alleles (Figure 2.1), mutants and potentially other restriction factors from our library of pENTR vectors. The expression cassette was also redesigned for minimal Fv1 expression and maximal EGFP expression. The approach was taken to avoid both the high leakiness observed in previous inducible vectors, and the insufficient expression of fluorescent reporter protein for separation of $Fv1^+$ from $Fv1^-$ populations by FACS assay seen in vectors with endogenous Fv1 promoter.

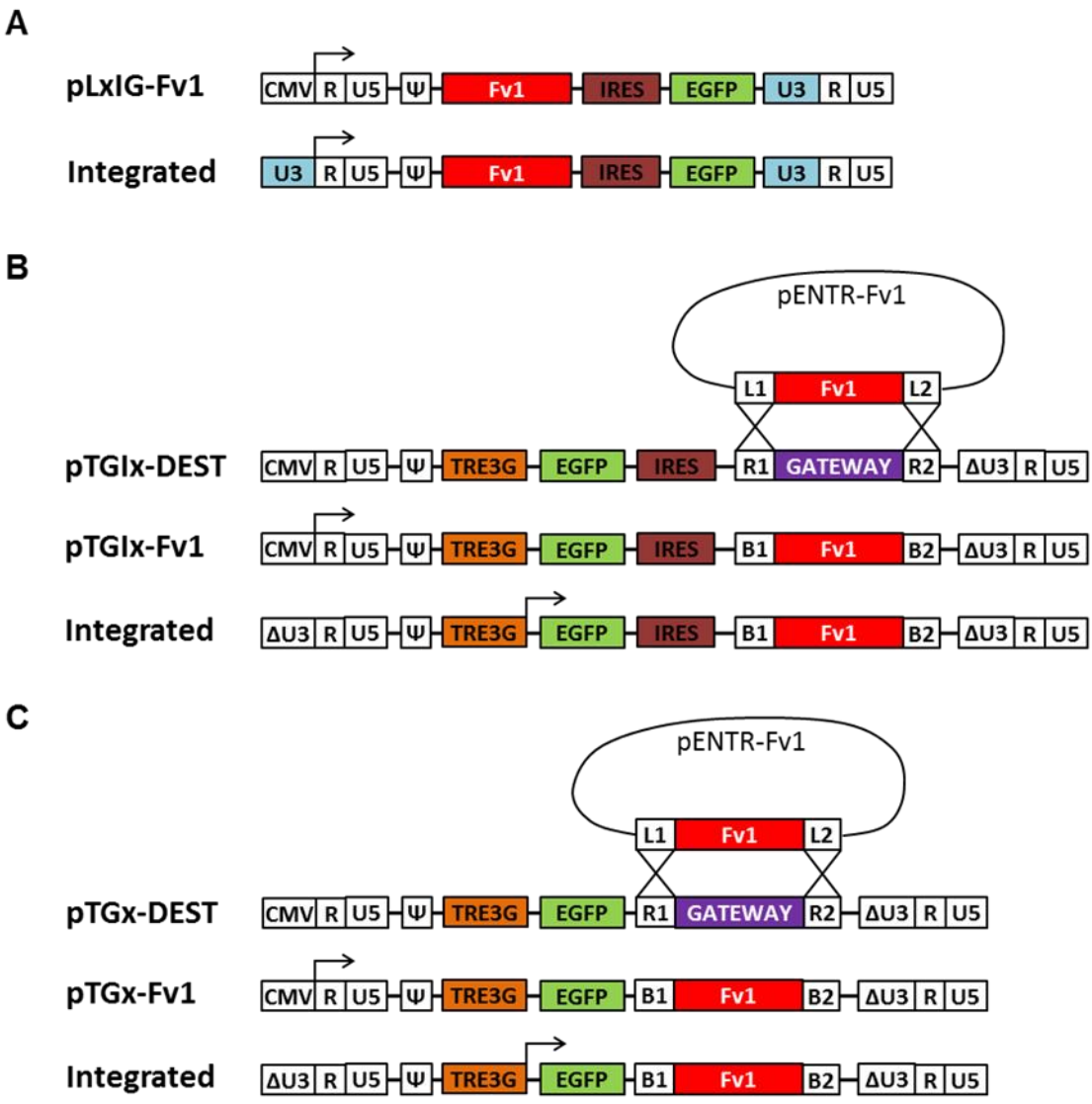

Figure 3.7 New gateway-compatible retroviral vectors for inducible expression of Fv1 with minimal leakiness

(A) Non-inducible retroviral vector used by Bock *et al* for studying Fv1 restriction using a transient FACS assay. After integration, transcription of Fv1 mRNA was driven by the strong U3 promoter of MLV LTR. (B and C) In the new TGIx SIN vector, the U3 promoter was inactive and transcription of Fv1 mRNA was driven only by the TRE3G promoter. Maximal EGFP protein level was achieved by cap-dependent translation. A Gateway site was inserted to allow enzyme-free cloning of Fv1 alleles and mutants from pENTR vectors. Attenuated translation of Fv1 was achieved either (B) by an IRES-dependent machanism in TGIx vectors, or (C) by expressing Fv1 in a downstream ORF through leaky ribosome scanning.

3.2.5 Implementation of the Tet-On 3G system

The first step in the implementation of the Tet-On 3G system for study of Fv1 was the generation of a clonal MDTF cell line expressing the rtTA3 protein. Figure 3.8 shows the procedure used in the generation and screening of the rtTA3 cell line. MDTF cells were transduced with a lentiviral vector expressing rtTA3 and the blasticidin resistance gene. Transduced cells were selected with blasticidin, and SCCs were picked from the selected population. These rtTA3 SCCs were then screened by luciferase induction assay. In this assay, SCC cells were transduced with a SIN lentiviral vector with expression of luciferase gene under the P_{TRE3G} promoter, and expression of puromycin resistance gene under a separate promoter. After selection with puromycin, cells were treated with or without 1µg/ml doxycycline for 72h, before analysis by luciferase assay. The relative luciferase activity was normalised to cell count. Transduction of lentiviral vector at low MOI was used for delivering the luciferase gene instead of transfection because it removed the bias from differences in transfection efficiency among different SCCs. Together with normalisation by cell count, this allowed more accurate measurement of the basal transcription activity of P_{TRE3G} in these cells. Figure 3.9 shows the results from the screening of rtTA3 clones. Among the four clones which gave the highest activation per cell (SCC 9, 18, 26, 44), SCC 18 had the lowest activity in the absence of doxycycline. The dose dependency of P_{TRE3G} induction in this cell line (named R18) was analysed in a separate experiment (Figure 3.10). Induction with up to 1µg/ml doxycycline led over 4000-fold activation in signal, with the highest increase in signal observed within the range of 1-10ng/ml doxycycline.

3.2.6 New gateway-compatible SIN vectors for inducible expression of Fv1

Two new vectors were introduced for inducible expression of Fv1. The original retroviral vector used by Bock et al used a non-SIN retroviral vector (Figure 3.7 A). After reverse transcription and integration of vector sequence, transcription of Fv1 mRNA was controlled by promoter activity in the U3 region

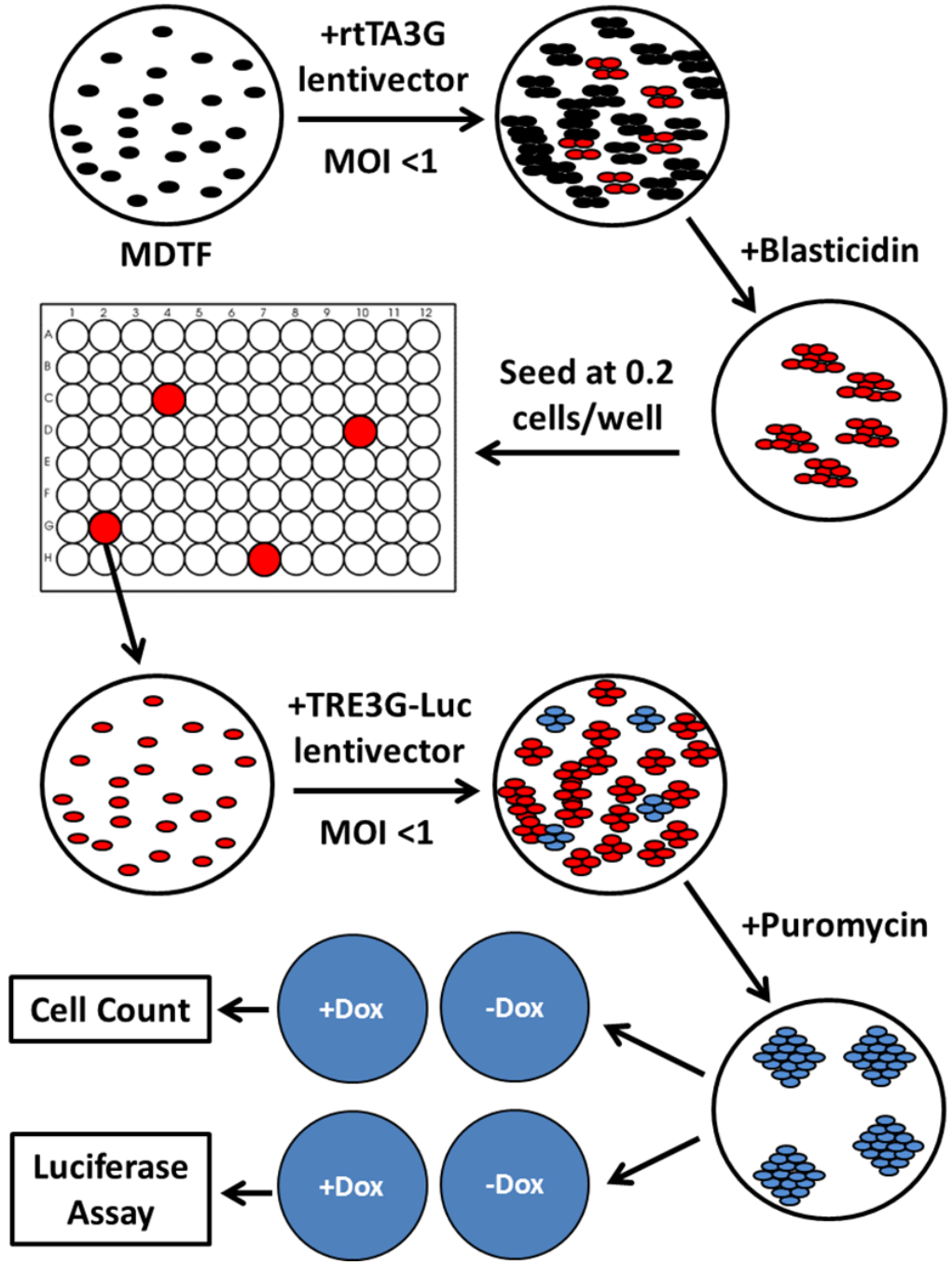

Figure 3.8 Generation of MDTF cell lines expressing rtTA3

MDTF cells were transduced with lentivector expressing rtTA3 and the blasticidin resistance gene at low MOI. Cells expressing rtTA3 was selected with blasticidin, the plated at limiting dilution to obtain SCCs. For screening of SCCs, cells were transduced at low MOI with lentivector expressing luciferase gene under the TRE3G promoter and the puromycin resistance gene, selected with puromycin, and analysed by luciferase assay normalised to cell count.

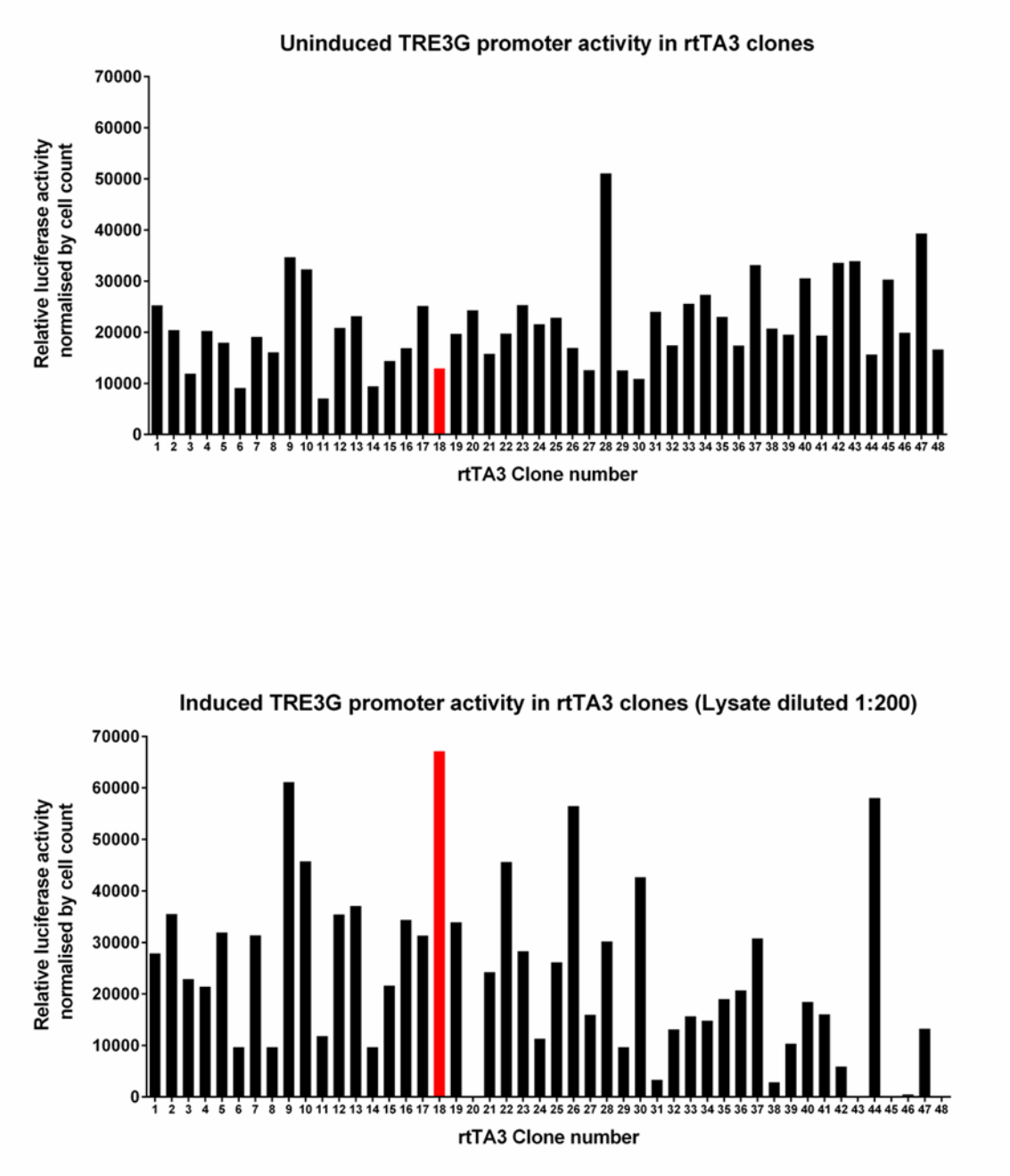

Figure 3.9 Screening of MDTF SCC expressing rtTA3

48 SCCs were screened by luciferase assay with or without 1µg/ml Dox. Luciferase activities were normalised by cell count. In the assay with Dox, lysate was diluted 200-fold to ensure the signals within the range of sensitivity. The clone, R18 (highlighted in red), was selected for its low uninduced and high induced activities. Clone 48 represents a negative control from MDTF cells not transduced with the rtTA3 vector virus.

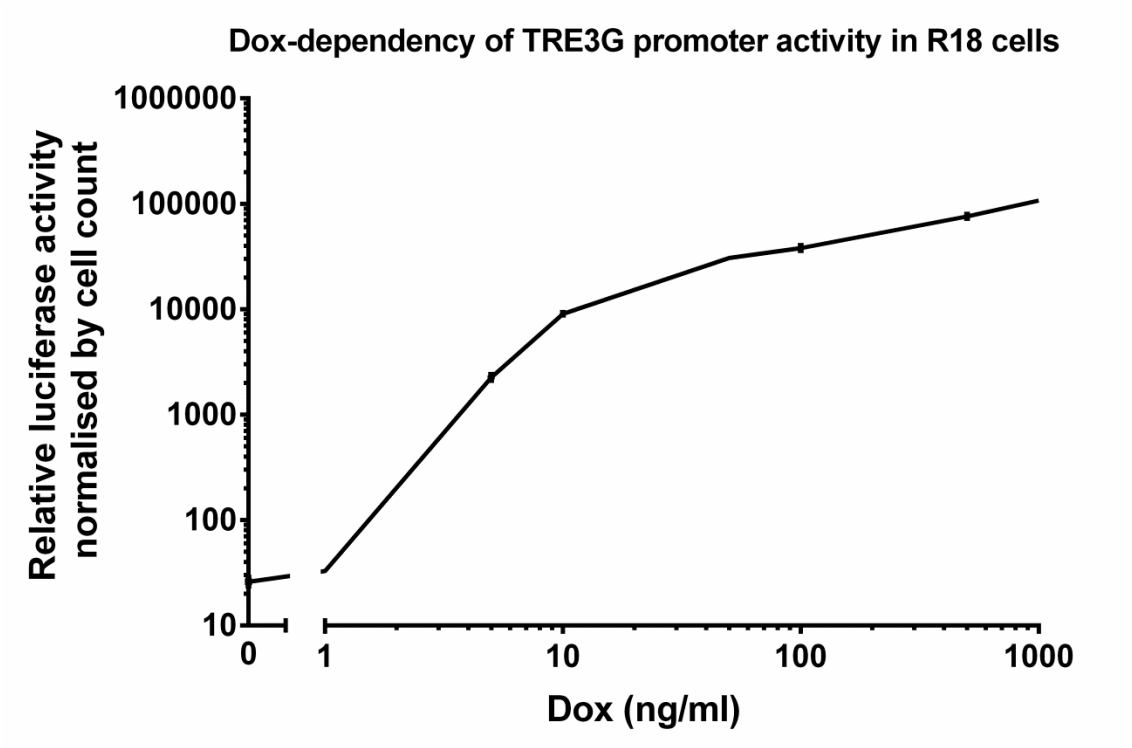

Figure 3.10 Dose dependency of P_{TRE3G} promoter to Dox in R18 cells

R18 cells were induced at different concentration of Dox before analysis by luciferase assay. The graph showed mean and absolute deviation values from duplicate samples in the same experiment.

of MLV LTR. The new vectors were constructed using the backbone from a SIN vector (Figure 3.10 B and C), deletions in U3 region prevented potential promoter interference with the inducible P_{TRE3G} promoter.

Before the first vector was designed, I considered the relative translation activity of the two ORFs in a bicistronic mRNA containing an IRES. A previous study had identified two major determinants in the level of CAP-independent translation activity mediated by the EMCV IRES (Bochkov and Palmenberg, 2006). First, the EMCV IRES found in our vectors have attenuated translation efficiency compared to the wt EMCV IRES. In the wt EMCV IRES, an A-rich loop structure termed bifurcation loop contains the A6 (AAAAAA) sequence. However, in our vectors an insertion of A into the bifurcation loop leads to the A7 (AAAAAAA) sequence. The presence of A7 sequence has been reported to cause a 40% drop in translational activity compared the wild type A6 sequence (Bochkov and Palmenberg, 2006). Secondly, it was found that the insertion of a long sequence between the minimal IRES sequence and the start codon of ORF could lead to further attenuation of the IRES activity. It was shown that translation from an A7 IRES with a 32nt attenuating sequence was 7.5 fold lower than that from the CAP-dependent translation. Therefore, the TGIx-Fv1 vector was designed to have the EGFP-IRES-Fv1 arrangement to maximise the expression of EGFP and minimise the expression of Fv1 (Figure 3.7 B). A strong Kozak sequence (GCCGCCATGG) (Kozak, 1986) was used in the EGFP start codon for optimal CAP-dependent translation. In order to construct the gateway compatible vector, the DEST cassette was inserted downstream of the IRES. The DEST cassette contains the suicide gene *ccdB* and the chloramphenicol resistance gene flanked by the attR1 and attR2 recombination sites. The LR reaction between the pTGIx-DEST and the pENTR-Fv1 vectors resulted in the pTGIx-Fv1 vector, which has an Fv1 ORF flanked by the attB1 and attB2 sites. The 71nt (mostly from attB1) sequence between the IRES and Fv1 ORF also serves as an IRES-attenuating sequence.

Given the very low natural level of $Fv1^b$ protein, it was anticipated that the 7.5 fold attenuation of translation may not be sufficient for reducing Fv1 expression to endogenous levels. I therefore studied other IRES-independent approaches for further attenuation of translation. There are many natural

examples in which the presence of an upstream ORF (uORF) could lead to inhibited translation of a downstream ORF in the absence of IRES element (Kozak, 2002). Most of these could be explained by a ribosome reinitiation mechanism, in which after the termination of translation in the uORF, the 40S ribosome subunit remains bound and continues scanning on the mRNA until reaching the start codon of the downstream ORF where translation is reinitiated. Since ribosome reinitiation is inefficient, the downstream ORF is often translated with suboptimal efficiency. Examples of such a mechanism include the 4 inhibitory uORFs found in the 5' UTR of the yeast GCN4 mRNA (Hinnebusch et al., 1988) and two uORFs in the long form of human MDM2 mRNA which caused 10-fold inhibition of MDM2 translation (Jin et al., 2003). In the absence of IRES, the efficiency of reinitiation of a downstream ORF in a bicistronic mRNA decreases with the length of uORF (Kozak, 2001) and increases with the intercistronic distance up to 79nt (Kozak, 1987). In one study it was reported that in IRES-free bicistronic mRNAs with two reporter ORFs, the expression of the downstream ORF could be between 100 and 1000 fold lower than the uORF, depending on the sequence of the uORF (Mizuguchi et al., 2000).

Taking advantage of the ribosome reinitiation mechanism, the IRES-free bicistronic vector TGx-Fv1 vector was designed (Figure 3.7 C). The EGFP ORF was given a strong Kozak sequence (GCCGCCATGG) (Kozak, 1986) and serves as the uORF for the attenuation of the downstream Fv1 ORF. The long 720nt EGFP ORF, together with a relatively short 54nt intercistronic distance should provide a strong inhibition in the translation of Fv1. However, further shortening of the intercistronic distance would not be possible due to the presence of the attB1 site. Similar to the TGIx-DEST vector, the TGx-DEST vector contains the DEST cassette for cloning by LR reaction (Figure 2.1) to obtain the TGx-Fv1 vector.

3.2.7 The new inducible vectors allowed study of restriction from very low Fv1 expression levels

Before using the vectors for restriction study, I first tested if the new vectors could support the production of sufficient EGFP for separation of $Fv1^+$ populations by FACS analysis. Figure 3.11 shows that in R18 cells transduced with TGx-$Fv1^b$ vector at an MOI of 1, clear separation required 24h incubation with doxycycline from a concentration of 100ng/ml. Figure 3.12 shows the protocol developed for a 2-colour FACS assay that can be used together with the inducible vectors. R18 cells were first transduced with either TGIx-Fv1 or TGx-Fv1 vector vectors. After induction at various concentration of doxycycline (0 to 1µg/ml), cells were infected with EYFP-expressing tester virus with gag-pol from N-MLV, B-MLV or NB-MLV. At 24hpi, a high dose of 10µg/ml doxycycline was added, and cells were analysed by FACS after another 48h. This high dose of doxycycline leads to full activation of the P_{TRE3G} promoter and maximal translation of EGFP in transduced cells. This final addition of doxycycline was included to ensure the expression of EGFP to allow separation by FACS analysis. It was assumed that at 24hpi, almost all infectious particles would have undergone integration, so the accompanied increase in Fv1 expression at this time point would not affect the percentage of GFP^+/YFP^+ cells.

Figure 3.13 shows the FACS data from a restriction assay with $Fv1^b$ from the inducible vectors TGx-$Fv1^b$ and TGIx-$Fv1^b$, and the non-inducible LxIG-$Fv1^b$ vector. The 4 populations (GFP^-/YFP^-, GFP^-/YFP^+, GFP^+/YFP^-, GFP^+/YFP^+) could be clearly separated in this assay. Comparing the percentage of YFP^+ subpopulations between the $GFP^+/Fv1^+$ and the $GFP^-/Fv1^-$ population allows the analysis of Fv1 mediated restriction. The second row of Table 3.2 shows the results from 3 repeats of such analysis, the restriction by Fv1 is expressed as a ratio of the percentage of YFP^+ subpopulations in the $GFP^+/Fv1^+$ relative to that in the $GFP^-/Fv1^-$ population. A lower restriction ratio indicates stronger inhibition by Fv1. In the absence of doxycycline, $Fv1^b$ expressed by the TGx-Fv1 vector shows not inhibition activity against any MLV. This suggested that the leakiness of Fv1 expression from the TGx-Fv1 vector is very low, insufficient for any

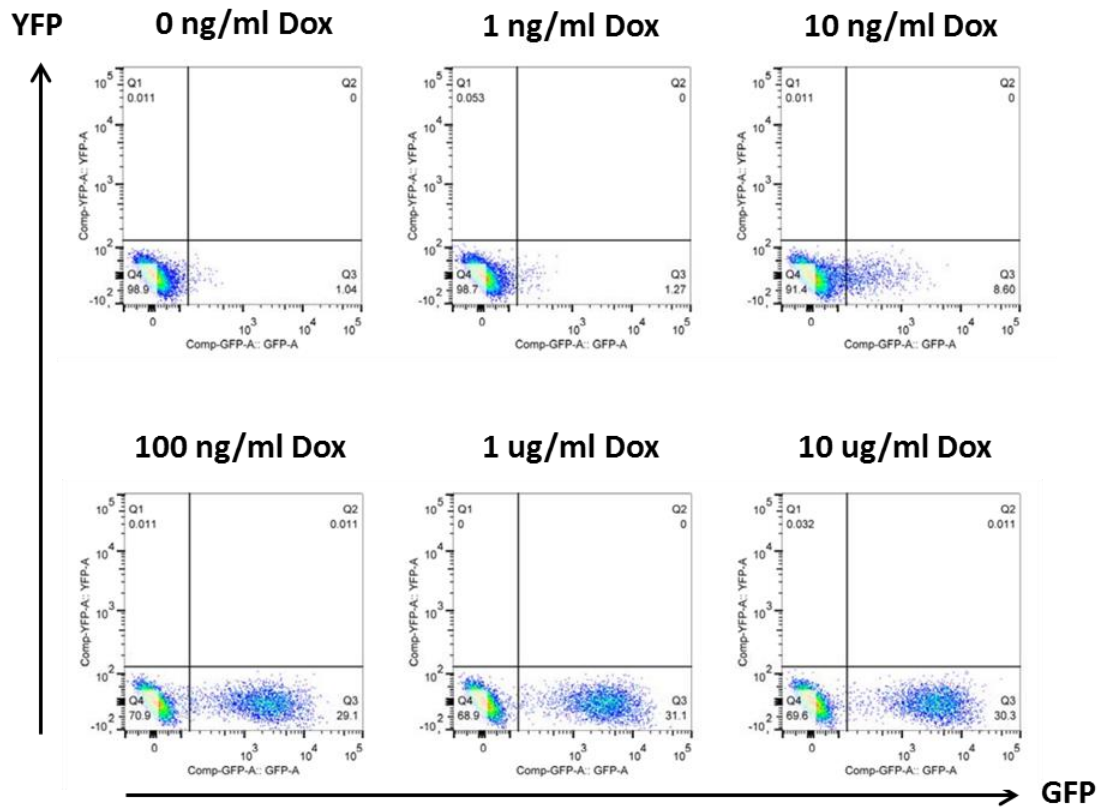

Figure 3.11 GFP separation of cells transduced with a TGx vector

R18 cells transduced with TGx-Fv1^{b} were induced with different concentration of Dox for 24h before analysis by FACS.

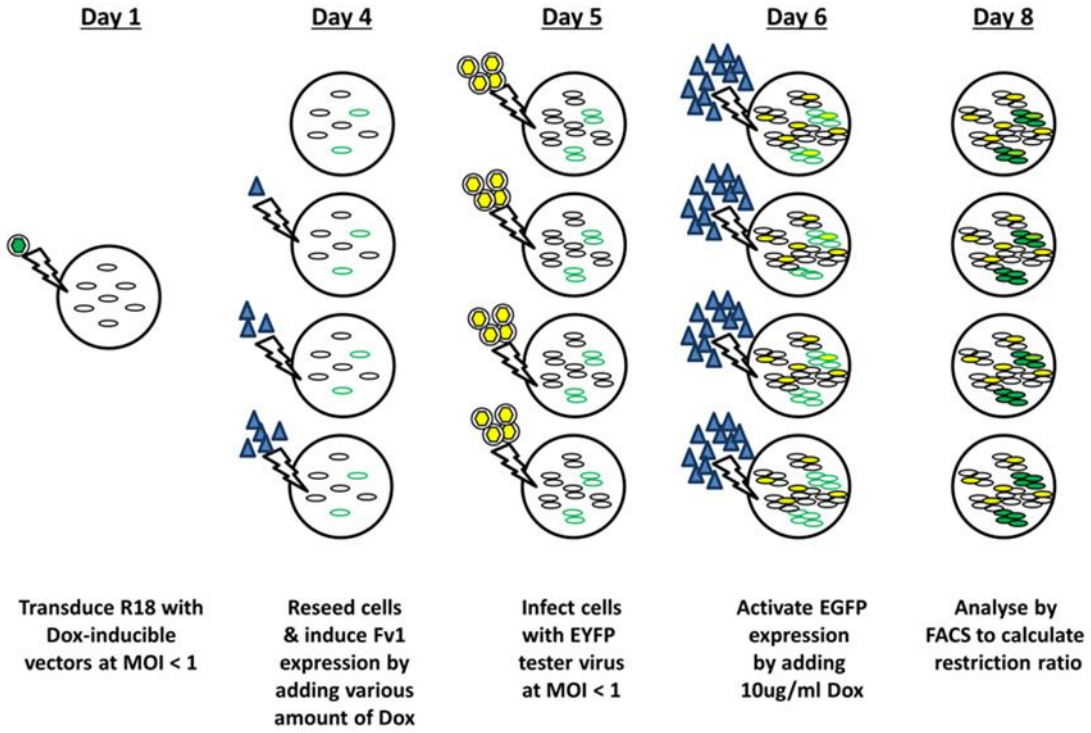

Figure 3.12 A transient assay to study the dose dependency of Fv1 restriction

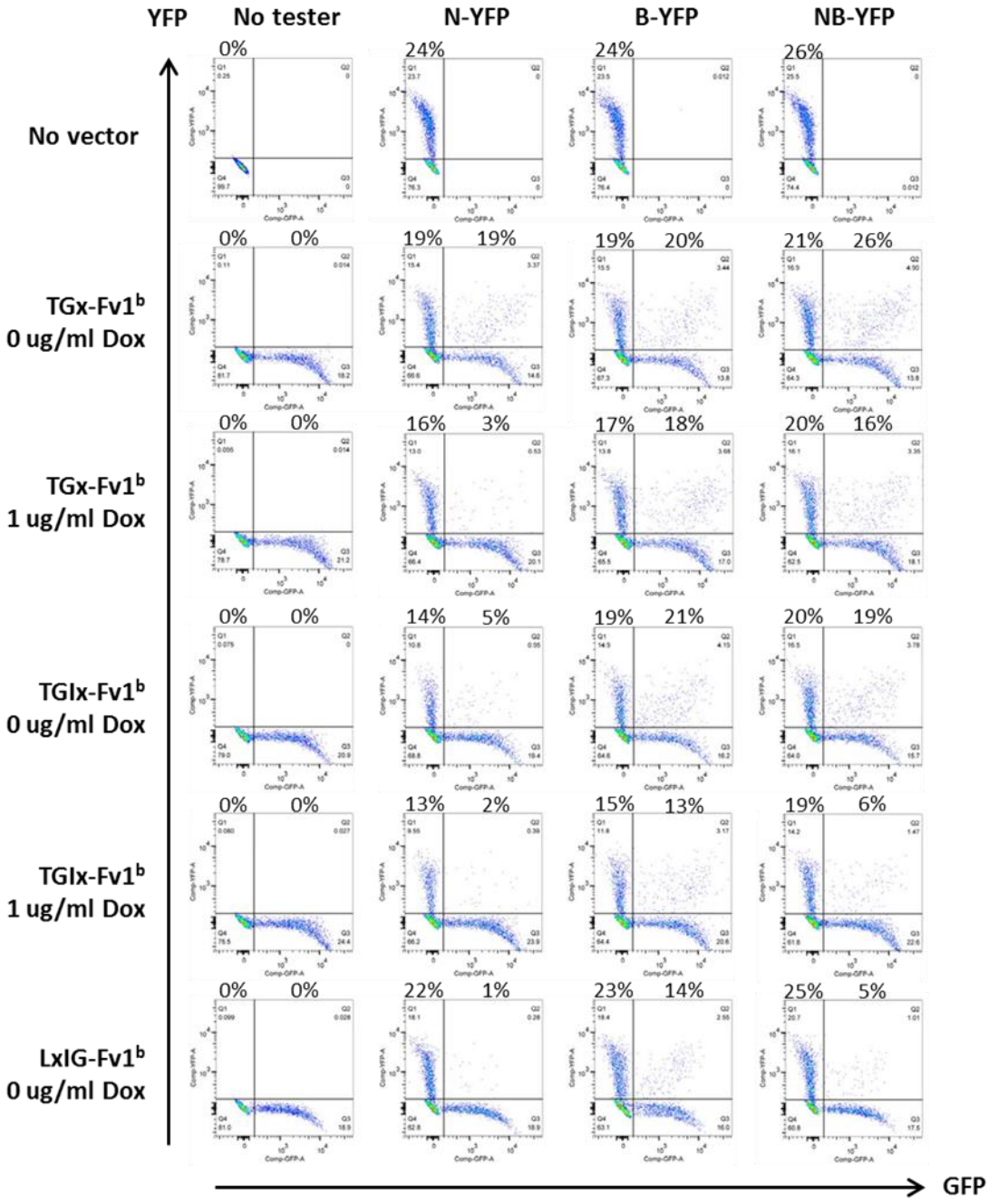

Figure 3.13 Restriction of MLV by Fv1^b expressed using different vectors

FACS dot plots from a restriction assay of R18 cells transduced with TGIx-Fv1^b, TGx-Fv1^b or LxIG-Fv1^b, with or without the addition of 1µg/ml Dox on day 4. The percentage of YFP$^+$ sub-population in GFP$^-$ and GFP$^+$ cells were indicated above each plot.

Fv1	MLV	TGx-Fv1		TGIx-Fv1		LxIG-Fv1	
		-DOX	+DOX	-DOX	+DOX	-DOX	+DOX
nnn	N	1.15 ± 0.07	1.16 ± 0.04	1.22 ± 0.11	1.13 ± 0.05	1.07 ± 0.03	
	B	1.15 ± 0.09	0.24 ± 0.04	0.56 ± 0.01	0.14 ± 0.02	0.06 ± 0.01	
	NB	1.17 ± 0.06	1.18 ± 0.04	1.21 ± 0.04	1.09 ± 0.06	1.08 ± 0.01	
bbb	N	1.02 ± 0.09	0.17 ± 0.01	0.45 ± 0.09	0.13 ± 0.01	0.07 ± 0.02	
	B	1.13 ± 0.07	1.10 ± 0.06	1.12 ± 0.02	0.87 ± 0.01	0.63 ± 0.02	
	NB	1.21 ± 0.04	0.79 ± 0.03	1.01 ± 0.07	0.35 ± 0.02	0.21 ± 0.03	
bbn	N	0.97 ± 0.02	0.17 ± 0.06	0.38 ± 0.04	0.11 ± 0.00	0.06 ± 0.01	
	B	1.10 ± 0.02	0.29 ± 0.06	0.58 ± 0.10	0.11 ± 0.02	0.07 ± 0.03	
	NB	0.96 ± 0.08	0.19 ± 0.04	0.33 ± 0.07	0.08 ± 0.02	0.08 ± 0.02	
nnb	N	1.18 ± 0.06	1.07 ± 0.07	1.09 ± 0.07	0.72 ± 0.10	0.58 ± 0.04	
	B	1.13 ± 0.09	0.52 ± 0.03	0.76 ± 0.03	0.14 ± 0.03	0.09 ± 0.02	
	NB	1.15 ± 0.10	1.07 ± 0.10	1.16 ± 0.06	1.07 ± 0.13	1.07 ± 0.05	
bnn	N	1.14 ± 0.07	0.18 ± 0.07	0.46 ± 0.01	0.12 ± 0.02	0.09 ± 0.06	
	B	1.20 ± 0.01	0.93 ± 0.05	1.04 ± 0.04	0.33 ± 0.03	0.12 ± 0.03	
	NB	1.21 ± 0.12	1.12 ± 0.06	1.09 ± 0.10	1.02 ± 0.03	0.98 ± 0.05	
nbb	N	1.17 ± 0.04	1.05 ± 0.07	1.17 ± 0.02	1.01 ± 0.03	0.93 ± 0.07	
	B	1.18 ± 0.04	0.66 ± 0.03	0.81 ± 0.08	0.12 ± 0.05	0.07 ± 0.02	
	NB	1.15 ± 0.06	1.12 ± 0.11	1.09 ± 0.05	1.17 ± 0.07	1.10 ± 0.07	
nbn	N	1.20 ± 0.05	1.12 ± 0.09	1.10 ± 0.03	1.03 ± 0.07	1.02 ± 0.11	
	B	1.12 ± 0.07	0.23 ± 0.01	0.50 ± 0.04	0.09 ± 0.02	0.08 ± 0.03	
	NB	1.11 ± 0.02	0.33 ± 0.05	0.62 ± 0.11	0.12 ± 0.03	0.09 ± 0.02	
bnb	N	1.05 ± 0.08	0.22 ± 0.03	0.56 ± 0.06	0.10 ± 0.02	0.06 ± 0.01	
	B	1.09 ± 0.05	1.08 ± 0.08	1.13 ± 0.02	1.12 ± 0.10	1.11 ± 0.04	
	NB	1.13 ± 0.07	1.08 ± 0.11	1.09 ± 0.09	1.09 ± 0.05	1.12 ± 0.08	
nn_	N	1.17 ± 0.04	1.09 ± 0.07	1.15 ± 0.04	1.18 ± 0.05	1.10 ± 0.06	
	B	1.12 ± 0.11	1.07 ± 0.02	1.11 ± 0.04	0.37 ± 0.05	0.09 ± 0.02	
	NB	1.12 ± 0.10	1.12 ± 0.13	1.11 ± 0.05	1.05 ± 0.06	1.11 ± 0.05	
bb_	N	1.07 ± 0.17	1.07 ± 0.04	1.04 ± 0.05	0.15 ± 0.04	0.06 ± 0.02	
	B	1.14 ± 0.04	1.09 ± 0.11	1.15 ± 0.05	0.77 ± 0.04	0.22 ± 0.01	
	NB	1.13 ± 0.03	1.07 ± 0.10	1.04 ± 0.06	0.20 ± 0.01	0.05 ± 0.02	

Table 3.2 Restriction of MLV by Fv1^n, Fv1^b and mutants expressed using TGx, TGIx and LxIG vectors

A summary of results from transient restriction assays for Fv1^n, Fv1^b, mix-and match mutants, and C-terminus tail truncation mutants. The 3-letter code for each mutant indicated the source of sequence at position 358, position 399 and C-terminus, respectively. Underscore indicated deletion. Black shading indicated restriction (ratio < 0.3), while grey shading indicated partial restriction (ratio between 0.3 and 0.7). 1µg/ml Dox was used for induction (+DOX). Mean and standard deviation values from 3 independent experiments were shown in the table.

inhibition of any MLV by Fv1^{b}. After induction with 1µg/ml doxycycline, a 5-fold restriction of N-MLV and a 20% inhibition of NB-MLV could be observed in cells transduced with TGx-Fv1^{b}.

In the absence of doxycycline, Fv1^{b} expressed by the TGx-Fv1 vector causes a 2-fold inhibition of N-MLV but there is no effect on B-MLV or NB-MLV. Compared with the previously described inducible system (Figure 3.6), which shows full restriction of N-MLV and 2-fold inhibition of NB-MLV by Fv1^{b} in the absence of doxycycline, the TGx-Fv1 vector still appears to have a much lower leakiness in Fv1 expression. After induction with 1µg/ml doxycycline, an 8-fold restriction of N-MLV and 3-fold inhibition of NB-MLV could be observed in cells transduced with the TGx-Fv1^{b}. The restriction activities of TGIx-Fv1^{b} vector were stronger than those of TGx-Fv1^{b}, but weaker than those of the non-inducible LxIG-Fv1^{b} vector. Taken together, it appeared that the TGx-Fv1 vector has a lower but overlapping Fv1 expression range than the TGIx-Fv1 vector, and both TGx-Fv1 and TGIx-Fv1 appeared to have lower expression level than the non-inducible LxIG-Fv1 vector.

3.2.8 Restriction phenotype of Fv1^{n}, Fv1^{b} and mutants at low expression level

Because of the encouraging results from the study of Fv1^{b}, the assay was extended to include Fv1^{n}, the mix-and-match mutants and the C-terminus truncation mutant shown in Table 1.1. Since the inducible vector appeared to have overlapping Fv1 expression range, both were used in this study. Table 3.2 showed the summary of data from 3 restriction experiments with all constructs. The restriction phenotype of R18 cells transduced with the LxIG-Fv1 vectors was in good agreement with previous data (Bishop et al., 2001; Bock et al., 2000). Interestingly, no inhibition activities were observed with all TGx-Fv1 constructs in the absent of doxycycline, suggesting that Fv1 mutants were expressed below its functional concentration. It was also worth noting that the average infectivity ratio in these non-inhibiting phenotypes was 1.14, indicating that the transduction with vector may have caused a 13% increase in the infectivity of MLV in these cells. Fv1^{n} only inhibited B-MLV in both TGx-Fv1 and TGIx-Fv1 vectors; this is expected as the LxIG-Fv1, which has a higher

expression of Fv1, does not restrict B-MLV or NB-MLV. $Fv1^b$ showed a consistent preference of MLV inhibition in the order of N > NB > B. Interestingly, none of the conditions tested showed exclusive restriction of N-MLV by $Fv1^b$ without any inhibition of NB-MLV.

With some mutants, the restriction appeared to be more specific in an induction level when compared to the overexpressed level using LxIG-Fv1 vector. For example, both N-MLV and B-MLV were equally restricted by Fv1bnn using the LxIG-Fv1 vector, but only N-MLV restriction could be observed when using the TGx-Fv1 vector. Similarly, Fv1bb_ appeared to restrict all MLVs with only slight preference to N-MLV and NB-MLV using the LxIG-Fv1 vector. Such preference became very obvious when the TGIx-Fv1 vector was used. Some other mutants showed consistent but weak preferences to certain MLVs. For example, Fv1nbn consistently showed a 10% stronger inhibition of N-MLV than NB-MLV using both inducible vectors, while Fv1bbn consistently showed a 10% weaker inhibition of B-MLV than N-MLV and NB-MLV. The fact that these small differences were observed reproducibly using two different vectors suggested that these were genuine properties of these mutants. From the data in this study, it could be concluded that the restriction spectrum of $Fv1^b$ and many other mutants became more specific at lower induction level.

3.2.9 An attempt to improve the induction range of inducible vectors

Although together both inducible vectors had provided a wide induction range from no detectable MLV inhibition to phenotypes close to that in the non-inducible vector, it would be ideal to have a single vector covering the same range. An attempt was made to modify the TGIx-Fv1 vector to further reduce the basal expression level without changing the maximal expression level. Similar to approach used in TGx-$Fv1^b$ vector, a short uORF with 3 codons was inserted 4nt upstream of the start codon of Fv1. The extremely short intercistronic distance would result in very inefficient reinitiation (Kozak, 1987), instead leaky scanning would be the main mechanism in the expression of the downstream ORF (Ferreira et al., 2013). In such a context, scanning 40S ribosomes that did not initiate translation at the start codon of the uORF would continue scanning on the mRNA and initiate translation at the downstream ORF

(Kozak, 2002). The expression from the downstream ORF dependent on the relative strength of Kozak sequences between the two ORFs. The short uORF tested here with equally strong ACC sequences before both ORFs had been reported to cause a 85% inhibition of translation (Ferreira et al., 2013). Figure 3.14 shows the comparison in restriction activity of $Fv1^b$ of this new TGIx-uORF-$Fv1^b$ vector with the two previously described inducible vector. The results showed that although this vector showed a decrease in the inhibition of N-MLV in the absence of doxycycline when compared to TGIx-$Fv1^b$, it also led to a reduction in NB-MLV inhibition in the presence of doxycycline. These results suggested that it was not possible to reduce the basal translation level of the TGIx-$Fv1^b$ vector without also affecting its maximal expression level.

3.2.10 Inhibition associated with the TGx-Fv1 vector was not due to the synthesis of fusion protein

One of the criticisms of the use of the TGx-Fv1 vector was that since the EGFP ORF was placed in frame upstream of the Fv1 ORF, there is a possibility that the observed restriction could be due to the expression of an EGFP-Fv1 fusion protein from the read-through of the EGFP stop codon. In order to address this question, the start codon of the $Fv1^b$ ORF was mutated to a non-start AGG codon resulting in TGx-AGG-$Fv1^b$ (Figure 3.15 A). It was anticipated that such mutation would abolish the translation of authentic Fv1 but not EGFP-Fv1 fusion protein, so the restriction activities should also be abolished unless they were caused by the putative fusion protein. Alternatively, in the TGx-TAATAA-$Fv1^b$ mutant the EGFP ORF was given an additional stop codon, which should definitely eliminate the production of any fusion protein. Figure 3.15 C confirmed that the AGG mutation did abolish the translation of authentic Fv1. The restriction data showed that while the AGG mutation abolished all restriction, the double-stop mutation had no effect. These data strongly supported the hypothesis that the restriction phenotypes in cells transduced with TGx-Fv1 vectors were not due to the synthesis of fusion protein.

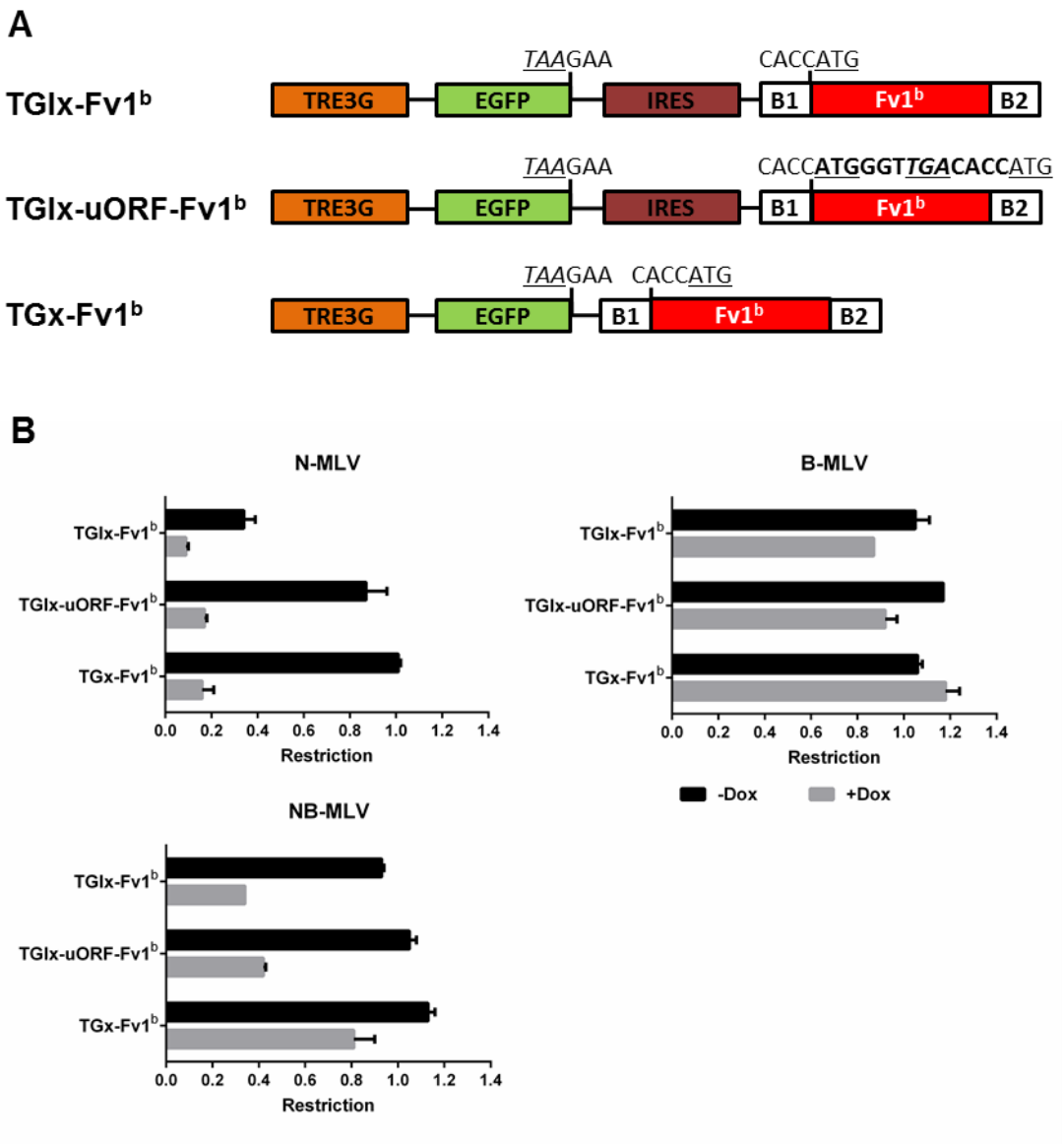

Figure 3.14 Restriction of MLV by Fv1^b expressed from different translation attenuating inducible vectors

(A) The TGIx-uORF-Fv1^b vector was generated by inserting a short (2aa) out-of-frame ORF at 4nt upstream of the start codon of Fv1 ORF. (B) Restriction of MLV by all 3 vectors with or without Dox induction (160ng/ml). Mean and mean deviation values from two independent experiments were shown in the bar chart.

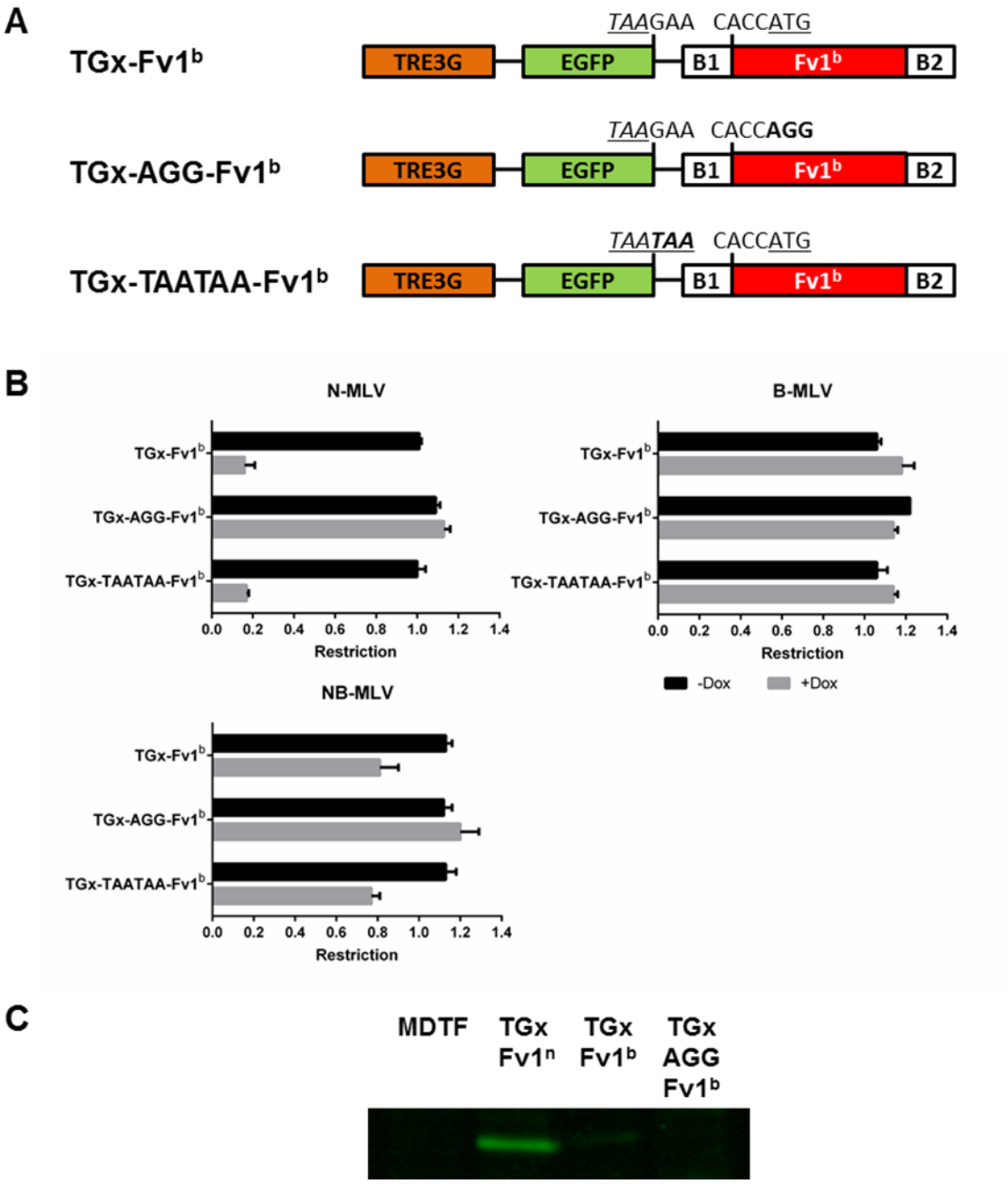

Figure 3.15 Restriction of MLV by Fv1^b expressed by mutant TGx-Fv1 vectors

(A) The TGx-AGG-Fv1^b mutant has non-start codon (AGG) instead of the start codon of Fv1 ORF, while the TGx-TAATAA-Fv1^b mutant has a double stop codon at the EGFP ORF. (B) Restriction of MLV by different TGx vectors with or without Dox induction (160ng/ml). Mean and mean deviation values from two independent experiments were shown in the bar chart. (C) Western blot analysis of R18 cells transduced with TGx-Fv1 vectors at a high MOI and induced with 1µg/ml Dox.

3.2.11 Addition of high dose of doxycycline at 24hpi did not affect restriction

It was assumed that the Fv1 sensitive steps of infection by the EYFP-expressing tester virus should be complete at 24hpi, so increase of Fv1 expression by doxycycline induction at this time should have no effect on the restriction phenotype. To test this hypothesis, N-MLV restriction assay in cells transduced with TGx-Fv1^{b} vector was repeated with the final high dose of doxycycline added at time points between 0 and 24hpi (Figure 3.16). The results showed no further changes in the apparent restriction value when the final dose of doxycycline was added after 20hpi, supporting the idea that by 24hpi no interaction between Fv1 and tested virus will occur.

3.2.12 Correlation between Fv1 protein level and MLV restriction activity in transduced R18 cells

The ultimate goal of using the inducible system was to correlate the expression level of Fv1 to its restriction activity, and to identify the restriction phenotype of Fv1 at the endogenous level. A more detailed analysis of protein expression level and restriction activity was carried out with both TGx-Fv1 and TGIx-Fv1 vectors for both Fv1^{n} and Fv1^{b}. In a pilot experiment, it was shown that there was no significant change in the restriction activities of Fv1^{b} between 100 and 1000ng/ml doxycycline (data not shown); therefore a 2-fold dilution series in the range of 1 to 160ng/ml doxycycline was used in this analysis. In addition to Fv1^{n} and Fv1^{b}, two other mutants Fv1bbn and Fv1bb_ were also analysed. In the restriction data described earlier (Table 3.2), Fv1bbn restricts all MLV when expressed using the TGx-Fv1 vector at 1000ng/ml doxycycline, although with the restriction activities to N-MLV and NB-MLV appear to be stronger than that to B-MLV. Similarly, Fv1bb_ showed stronger restriction towards N-MLV and NB-MLV when expressed using the TGIx-Fv1 vector at 1000ng/ml doxycycline. I wanted to test whether Fv1^{b}, Fv1bbn and Fv1bb_ are able to demonstrate high specificity towards different MLV at lower expression levels. When over-expressed using the LxIG-Fv1 vector, the protein levels of Fv1^{b}, Fv1bbn and Fv1bb_ appear to correlate with their restriction activities against B-MLV (Figure 3.3, discussed in section 3.1.2). I also wanted to further investigate whether the

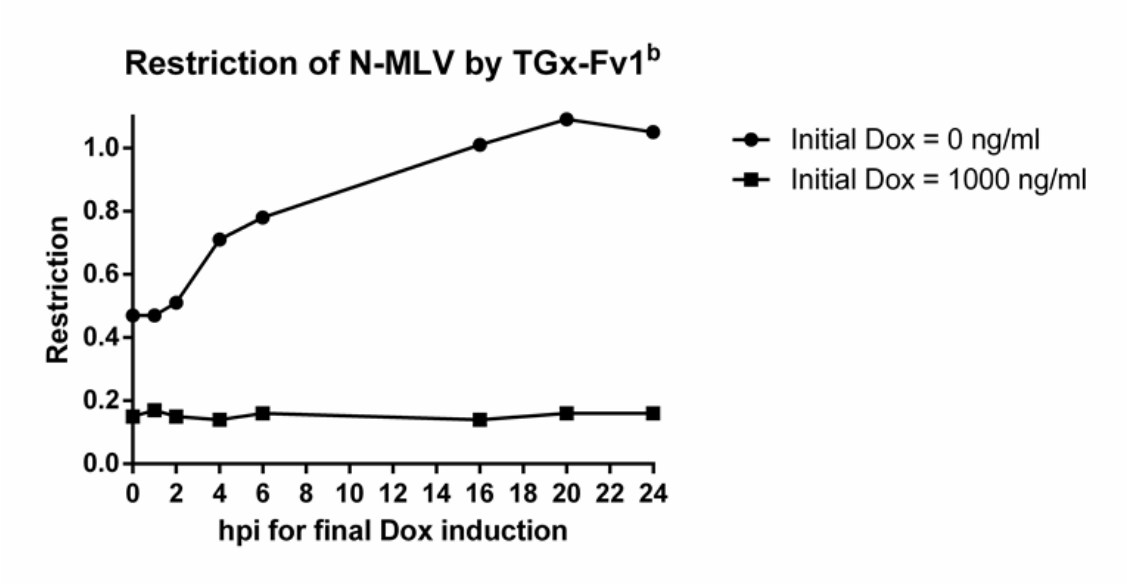

Figure 3.16 Effect of changing the timing of final Dox induction on the observed restriction of N-MLV by TGx-Fv1^b

Transient restriction assay was carried out as described before except that 10µg/ml Dox was added at various time points after the infection with YFP tester virus, instead of 24hpi normally.

C-terminal tail modifications in Fv1bbn and Fv1bb_ enhances the restriction of B-MLV by increasing apparent binding affinity, by comparing the amount of $Fv1^b$, Fv1bbn and Fv1bb_ required to inhibit B-MLV to the same level.

Figure 3.17 shows the data from the quantitative western blot analysis of transduced R18 cells at a range of doxycycline concentration. In all constructs, the increase in doxycycline leads to an increase in Fv1 protein level. As expected, the TGIx-Fv1 vector leads to a higher expression of $Fv1^n$ and $Fv1^b$ than the TGx-Fv1 vector. The expression levels of $Fv1^n$, $Fv1^b$ and Fv1bb_ by the TGIx-Fv1 vector at all doxycycline concentrations are sufficient for Fv1 quantitation. Similar to western blot data from the earlier inducible system (Felton, 2012), $Fv1^n$ was expressed at higher protein level than $Fv1^b$ at all doxycycline concentrations using the TGIx-Fv1 vector. From 0 to 40ng/ml doxycycline, expression of Fv1bb_ by TGIx-Fv1 vector was lower than that of $Fv1^b$. However, similar expression levels of $Fv1^b$ and Fv1bb_ were observed above 40ng/ml. Unfortunately, the expression of $Fv1^n$, $Fv1^b$ and Fv1bbn by the TGx-Fv1 vector was too low for quantitation.

The restriction and Fv1 quantitation data from the same doxycycline titration experiment is shown in Figure 3.18. In cells expressing $Fv1^n$ using the TGIx-$Fv1^n$ vector, no inhibition of N-MLV or B-MLV could be observed. B-MLV is inhibited by more than 40% in the absence of doxycycline, and this was increased to a 10-fold inhibition from 20ng/ml doxycycline, with no further increase in inhibition at higher doxycycline concentrations. In cells expressing $Fv1^n$ using the TGIx-$Fv1^b$ vector, N-MLV is inhibited by more than 60% in the absence of doxycycline, and this was increased to a 10-fold inhibition from 10ng/ml doxycycline, with no further increase in inhibition at higher doxycycline concentrations. A 10% inhibition of NB-MLV was observed in the absence of doxycycline, and this was increased to about 65% at 40ng/ml doxycycline, with no further inhibition at higher doxycycline concentrations. No inhibition of B-MLV was observed in the absence of doxycycline, but a weak inhibition of less than 20% was observed from 10ng/ml doxycycline. All the inhibition activities of $Fv1^n$ and $Fv1^b$ are increased at higher Fv1 protein levels, therefore confirming the dependency of Fv1 restriction on Fv1 concentration. A full 10-fold restriction of B-MLV of $Fv1^n$ was observed from 20ng/ml doxycycline concentration, while full

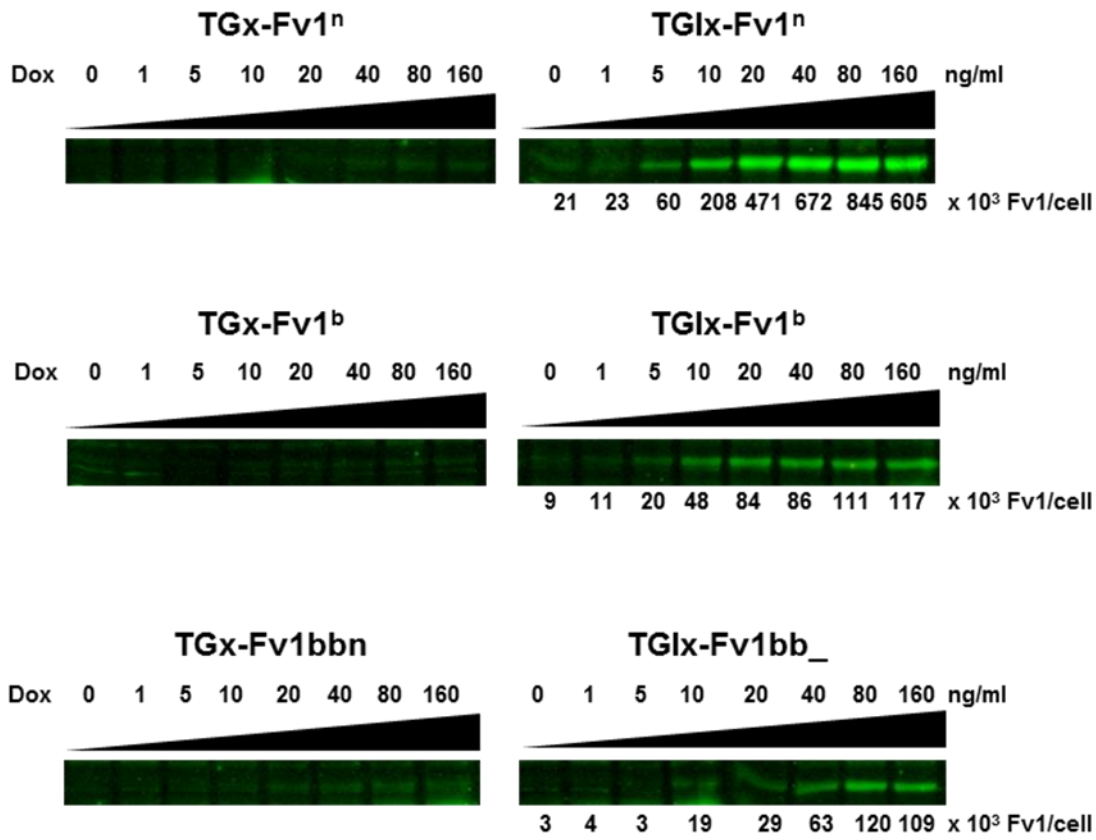

Figure 3.17 Quantitative western blot analysis of Fv1 protein levels at different Dox concentrations in transiently transduced cells

R18 cells transduced with TGIx-Fv1 or TGx-Fv1 vectors were reseeded and treated with various concentration of Dox for 24h before lysing for quantitative western blot analysis. The intensities of bands from TGx-Fv1 samples were insufficient for quantification.

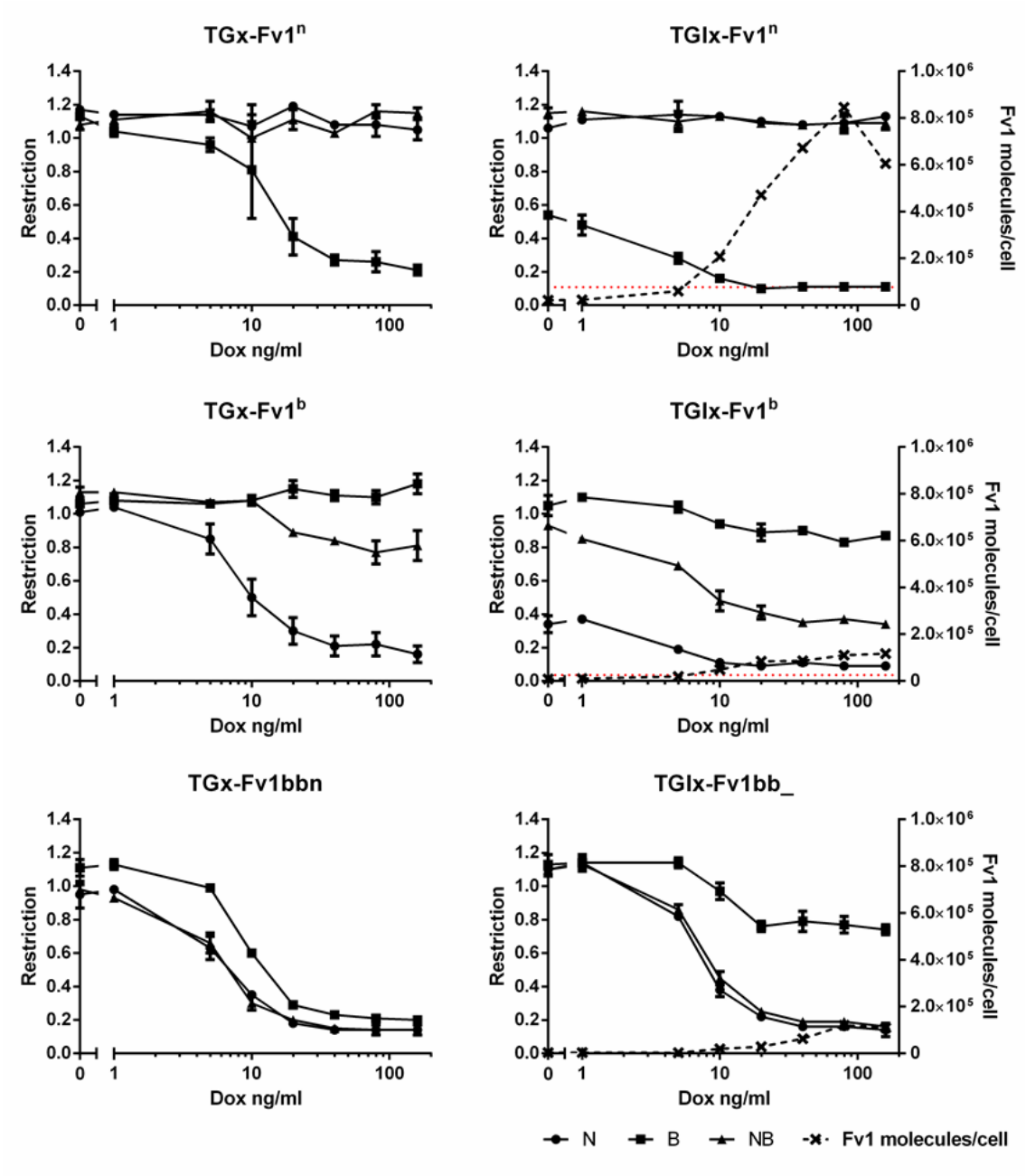

Figure 3.18 MLV restriction by Fv1^n, Fv1^b, Fv1bbn and Fv1bb_ at different Dox concentrations in transiently transduced cells

R18 cells transduced with TGIx-Fv1 or TGx-Fv1 vectors were reseeded and treated with various concentration of Dox for 24h before infecting with YFP tester virus for restriction assay. Mean and mean deviation values from two independent restriction experiments were plotted in the graphs. Quantity of Fv1 for TGIx-Fv1 samples were represented by black dotted lines. Endogenous protein levels of Fv1^n and Fv1^b were illustrated by the red horizontal dotted lines.

restriction of N-MLV by $Fv1^b$ was observed from 10ng/ml doxycycline. Interestingly, at these conditions the protein level of $Fv1^n$ was almost 10-fold higher than that of $Fv1^b$; therefore these data suggested that $Fv1^b$ was more potent in restriction than $Fv1^n$.

In cells expressing $Fv1^n$ using the TGx-$Fv1^n$ vector, no inhibitions of N-MLV and NB-MLV are observed in any doxycycline concentration; B-MLV is not inhibited in the absence of doxycycline, but inhibition of B-MLV become apparent from 10ng/ml doxycycline, and a 5-fold can be observed from 40ng/ml doxycycline. In cells expressing $Fv1^b$ using the TGx-$Fv1^b$ vector, no inhibition of any MLV is observed in the absence of doxycycline; the inhibition of N-MLV becomes apparent from 5ng/ml doxycycline, and a 5-fold inhibition of N-MLV can be observed from 40ng/ml doxycycline; the inhibition of NB-MLV becomes apparent from 20ng/ml doxycycline, and a 20% inhibition of NB-MLV can be observed from 80ng/ml doxycycline; no inhibition of B-MLV can be observed even with 160ng/ml doxycycline.

While $Fv1^n$ only restricts B-MLV, $Fv1^b$ appears to display different restriction specificities at 3 different phases of $Fv1^b$ concentrations: phase I involves partial restriction of N-MLV only (TGx-$Fv1^b$, 10ng/ml doxycycline); phase II involves a 5-fold restriction of N-MLV and mild inhibition of NB-MLV (TGx-$Fv1^b$, 40ng/ml doxycycline; TGIx-$Fv1^b$, 5ng/ml doxycycline); and phase III involves a 10-fold full restriction of N-MLV, partial restriction of NB-MLV and mild inhibition of B-MLV (TGIx-$Fv1^b$, 20ng/ml dox; LxIG-$Fv1^b$). Importantly, at no point full restriction of N-MLV alone was observed without inhibition of NB-MLV. The expression levels of Fv1 by TGIx-Fv1 were also compared to that of endogenous Fv1 determined earlier (Figure 3.2) in order to predict the endogenous restriction phenotype. At 5ng/ml doxycycline concentration, the Fv1 expression level by TGIx-Fv1 vector was closest to the endogenous level for both $Fv1^n$ and $Fv1^b$. At this induction level, $Fv1^n$ inhibits only B-MLV by 70%; while $Fv1^b$ restricts N-MLV by 80% and inhibits NB-MLV by 30%. This suggested that the endogenous phenotype of $Fv1^b$ belongs to the second phase, with a mild inhibition of NB-MLV. The switch from phase II to phase III requires a 4-fold increase in the protein level of $Fv1^b$ (from 20k to 84k Fv1 per cell), suggesting that a 4-fold increase in the endogenous protein level of $Fv1^b$

was sufficient to achieve partial restriction of NB-MLV and inhibition of B-MLV. In cells expressing Fv1^b using the non-inducible LxIG-Fv1 vector, which has a 26-fold higher expression of Fv1^b than the endogenous level (Figure 3.3), NB-MLV is fully restricted by 5-fold and B-MLV is partially restricted by about 40%. Therefore, the transition from phase III to this final phenotype would another 6-fold increase in Fv1^b protein level. Together these analyses of Fv1^b restriction and quantity suggested that Fv1^b restricts N-MLV and slightly inhibits NB-MLV at the endogenous level, and the overexpression of Fv1^b can lead to at least 5-fold restriction of N-MLV and NB-MLV, and a 40% inhibition of B-MLV.

By comparing the restriction phenotypes of TGx-Fv1^b, TGx-Fv1bbn and TGIx-Fv1bb_ at various doxycycline concentrations, it appears that in contrast to Fv1^b, Fv1bbn and Fv1bb_ inhibits N-MLV and NB-MLV equally at all concentrations. This suggested that the C-terminal tail mutations have increased the ability of Fv1bbn and Fv1bb_ to restriction NB-MLV, most likely by increasing the apparent binding affinity to NB-MLV CA. The amount of Fv1^b, Fv1bbn and Fv1bb_ required to inhibit B-MLV to the same level were compared. Fv1bbn clearly has the strongest ability to restrict B-MLV, since it is able to restrict B-MLV by 5-fold at a concentration that is too low for quantitation analysis. At the highest doxycycline concentration of 160ng/ml, while similar levels of Fv1^b and Fv1bb_ were expressed using the TGIx-Fv1 vector, Fv1bb_ shows a stronger inhibition of B-MLV than Fv1^b. Therefore, at the same Fv1 concentration, the ability for B-MLV restriction is in the order of Fv1bbn > Fv1bb_ > Fv1^b, and this probably reflects the relative apparent affinities of Fv1 towards B-MLV CA. The very low concentration of Fv1bbn required for B-MLV restriction also suggested that the observed stronger restriction against B-MLV by Fv1bbn than Fv1^b at over-expression level was due to an increase in binding apparent affinity rather than small increase in protein level identified in section 3.1.2).

3.2.13 Relationship between Fv1 protein level and MLV restriction activity in SCCs

A shortcoming of the above study was that Fv1 expressed using the TGx-Fv1 vector was insufficient for quantitation. Since the transduction of R18 cells at a MOI of 0.7 would only result in about 30% of $Fv1^+$ cells, the sensitivity of Fv1 quantitation by western blot was limited. It was hoped that the study of a 100% $Fv1^+$ population, such as SCC, would allow higher sensitivity and detection of Fv1 expressed from TGx-Fv1 vector. This would allow the confirmation that the increase in restriction activities in TGx-Fv1 expressing cells at higher doxycycline concentrations is due to a higher Fv1 protein level. By analysing the Fv1 RNA and protein levels in the SCCs, it would also allow the confirmation that the TGx-Fv1 vector causes a lower Fv1 protein level than TGIx-Fv1 due to a stronger inhibition in translation.

One SCC was picked from each transduced R18 population from the previous study in section 3.2.12. Transduced R18 cells were seeded at limiting cell dilution in 96-well plates, from which individual clones were picked for screening. $Fv1^+$ clones were screened by the expression of GFP by FACS analysis. Figure 3.19 shows the quantitation of Fv1 from one SCC of each construct compared to the endogenous and overexpressed levels. The detection and quantitation of Fv1 expressed by TGx-Fv1 vectors were possible at 100ng/ml doxycycline. At this doxycycline concentration, $Fv1^n$ protein level in the TGIx-$Fv1^n$ SCC is 17-fold higher than in TGx-$Fv1^n$ SCC, while $Fv1^b$ protein level in the TGIx-$Fv1^b$ SCC is 5-fold higher than in TGx-$Fv1^n$ SCCs. However, comparison between Fv1 protein levels revealed a number of differences between quantitation results from experiments using SCC (Figure 3.19) and from experiments using transduced cells (Figure 3.17). First, despite the higher expression level of TGIx-$Fv1^n$ than TGIx-$Fv1^b$ across all doxycycline concentrations in transduced cells (Figure 3.17), expression of $Fv1^n$ was similar to that of $Fv1^b$ in TGIx-Fv1 SCCs (Figure 3.19). Secondly, the expression level of the TGx-$Fv1^b$ SCC appeared to be higher than that of the TGx-$Fv1^n$ SCC, although transduced cells $Fv1^n$ is always expressed at higher protein level than $Fv1^b$ with both inducible and non-inducible vectors. These differences in the

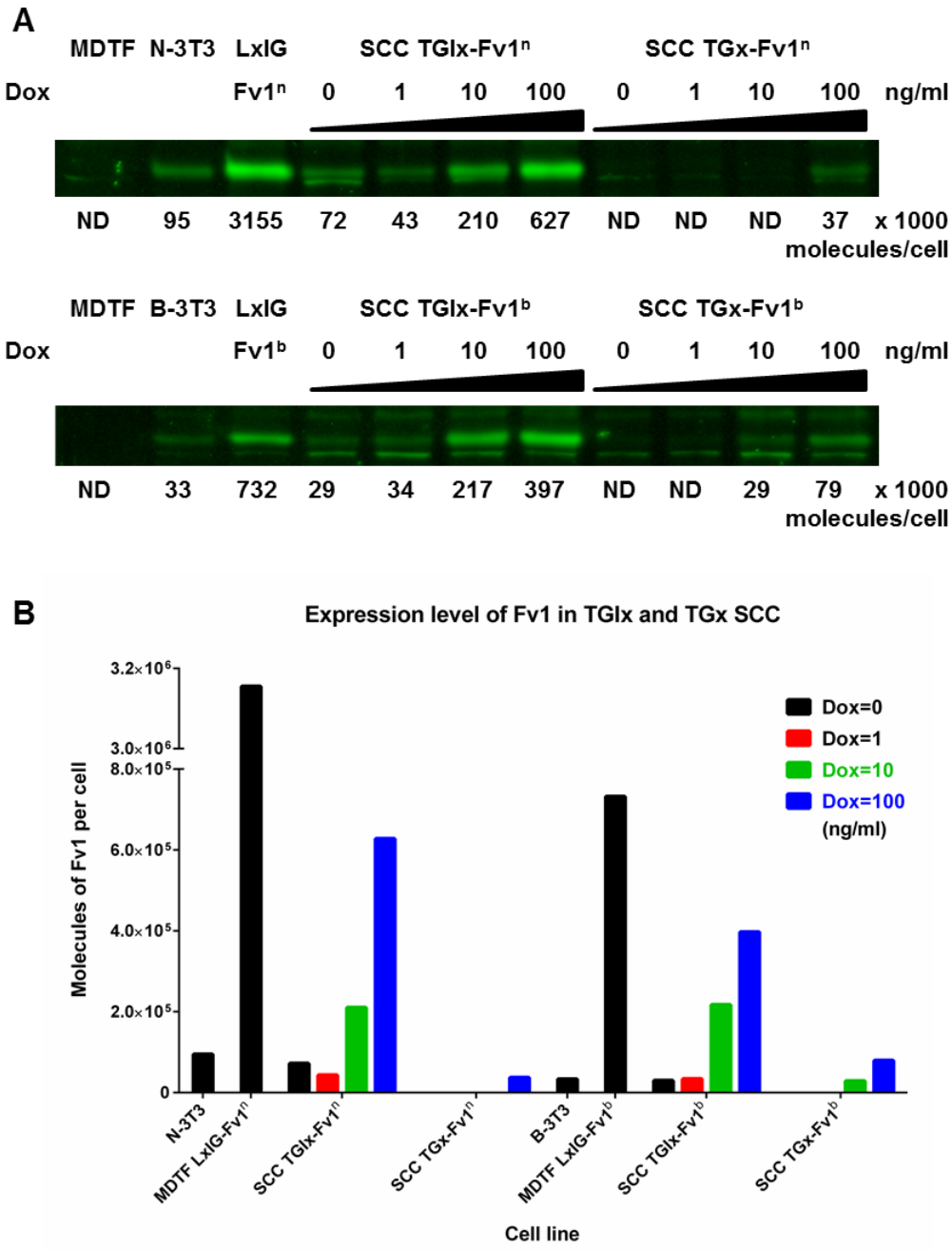

Figure 3.19 Quantitative western blot analysis of Fv1 protein levels in TGIx-Fv1 and TGx-Fv1 SCCs

(A) SCCs were isolated from R18 cells transduced with TGx-Fv1 or TGIx-Fv1 vectors by plating to 96-well plate at limiting cell dilution. GFP^+ clones were screened by inducing at 1µg/ml doxycycline followed by FACS analysis. One clone of each construct was selected. SCCs were induced at 0-100 ng/ml Dox for 24h before quantitative western blot analysis. (B) The quantification data from the western blots were illustrated in the bar chart.

relative protein levels of $Fv1^n$ to $Fv1^b$ between transduced cells and SCCs are most likely results of clone-to-clone variations in Fv1 expression. In transduced R18 cells, each individual cell would express Fv1 at different levels depending on the integration site used by the vector virus. Although on average a high $Fv1^n$ to $Fv1^b$ expression ratio can be observed, the expression levels in individual clones would vary around the mean expression level following the Poisson distribution. Therefore, the comparison of Fv1 levels between any SCCs would not be informative unless a large number of clones were used. However, these SCC would still allow the correlation between Fv1 protein level and restriction activities, as well as Fv1 protein and RNA levels. To confirm that the lower expression level of TGx-Fv1 vector relative to TGIx-Fv1 vector is due to a stronger inhibition in translation, the relative expression levels of Fv1 mRNA in SCCs were studied by quantitative PCR (qPCR) (Figure 3.20). At all doxycycline induction levels, the relative quantities of Fv1 mRNA expressed using both vectors were very similar, while the expression from TGIx-Fv1 constructs are higher than TGx-Fv1 constructs. This suggested like the TGIx-Fv1 vector, the IRES-free TGx-Fv1 vector allowed doxycycline-dependent protein expression of Fv1 at a more attenuated translational level.

To confirm that the increase in restriction activities in TGx-Fv1 cells at higher doxycycline concentrations is due to a higher Fv1 protein level, the restriction of MLV in the inducible SCCs was studied using a modified 2-colour FACS assay (Figure 3.21). To provide an internal $Fv1^-$ control, SCC and R18 cells were seeded in the same well at a 1:1 ratio before doxycycline induction. The basal infectivity of MLV in SCCs varies significantly from experiment to experiment, probably due to slightly different mitotic rate of the SCC at different passages. Therefore, results for $Fv1^n$ was normalised to the infectivity ratio of N-MLV in the absence of doxycycline, while the results for $Fv1^b$ was normalised to the infectivity ratio of B-MLV in the absence of doxycycline. This would be appropriate because restriction data from transient transduction (Table 3.2) showed no inhibition of N-MLV by $Fv1^n$ and B-MLV by $Fv1^b$ in the absence of doxycycline using both TGIx-Fv1 and TGx-Fv1 vectors. The normalised restriction results are shown in Figure 3.22. In TGx-$Fv1^n$ SCC, the increase in B-MLV inhibition coincides with the increase in $Fv1^n$ protein level, from 10 to 100ng/ml doxycycline concentrations. Similarly in TGx-$Fv1^b$ SCC, the increase

in the inhibitions of N-MLV, NB-MLV and B-MLV coincides with the increase in $Fv1^b$ protein level, from 1 to 100ng/ml doxycycline. Therefore these data confirm that in cells transduced with TGx-Fv1 vectors, the increase in Fv1 protein levels lead to the increase in restriction activities against MLVs.

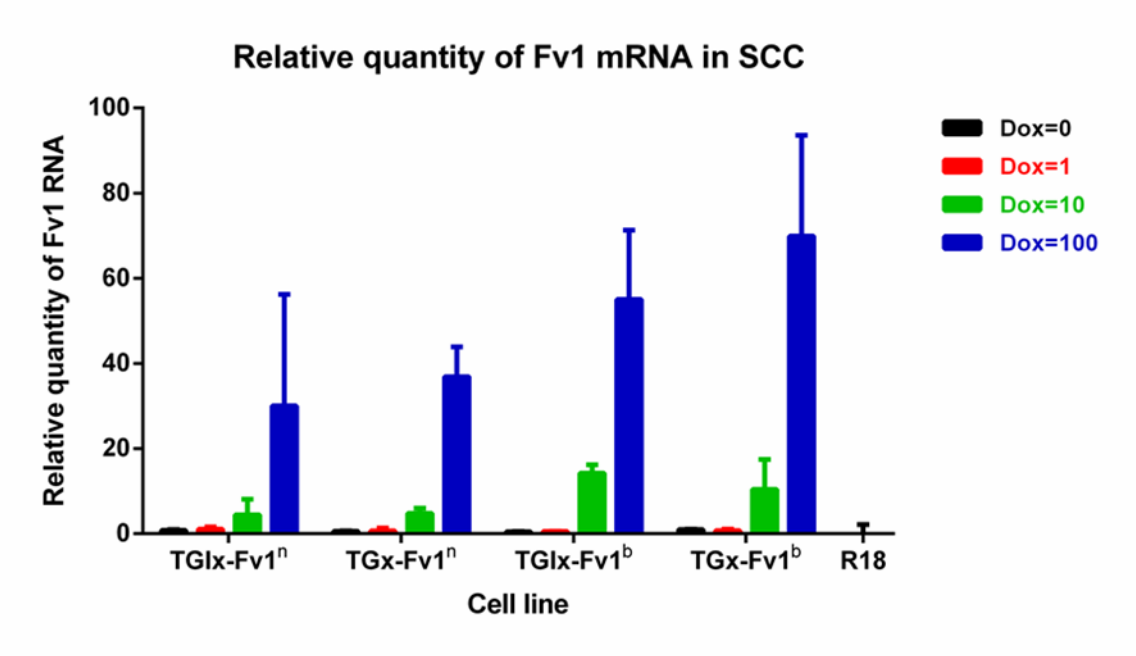

Figure 3.20 Quantitative RT-PCR of Fv1 mRNA levels TGIx-Fv1 and TGx-Fv1 SCCs

SCCs were induced at 0-100 ng/ml Dox for 24h before lysed for quantitative RT-PCR analysis. Relative quantity of Fv1 mRNA was normalised to the relative quantity of GAPDH. Mean and mean deviation values of 4 repeats (2 biological repeats, each with 2 technical repeats) were plotted in the bar chart.

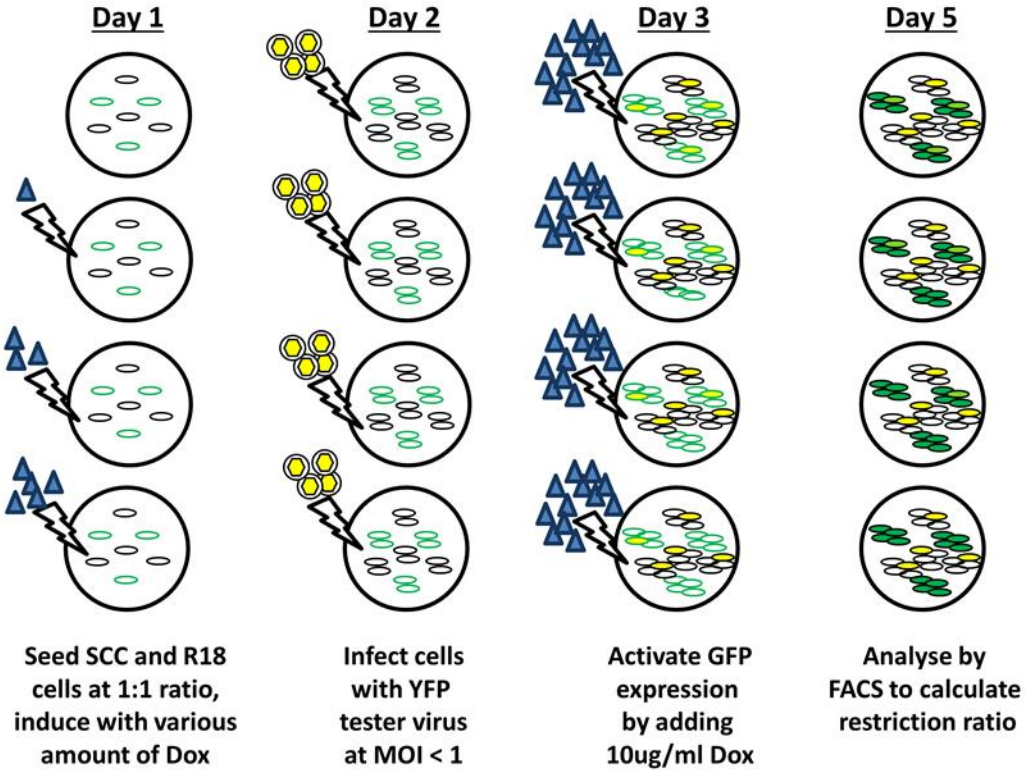

Figure 3.21 Study of MLV restriction in SCC with inducible expression of Fv1

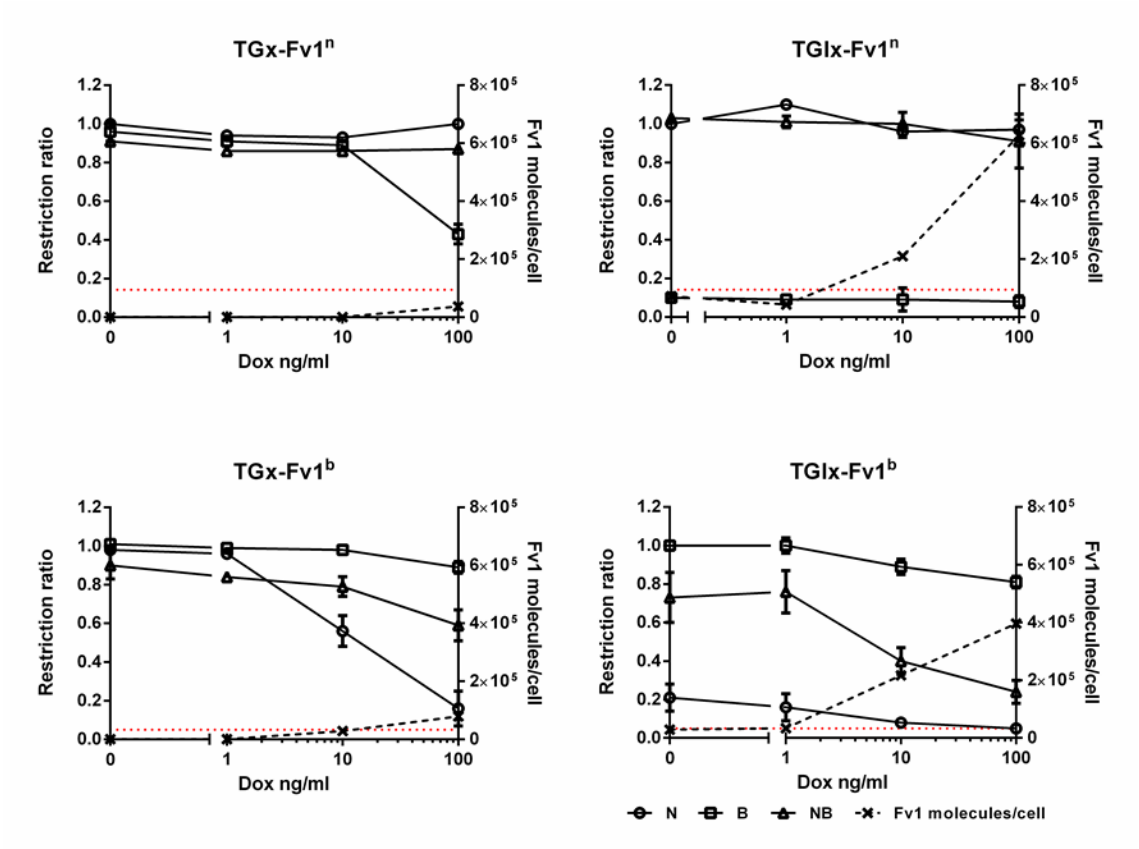

Figure 3.22 MLV restriction by Fv1^n and Fv1^b at different Dox concentrations in TGx-Fv1 and TGIx-Fv1 SCCs

TGIx-Fv1 or TGx-Fv1 SCCs were mixed 1:1 with R18 cells, and treated with various concentration of Dox for 24h before infecting with YFP tester virus for restriction assay. Fv1^n restriction values were normalised to the restriction value against B-MLV in the absence of Dox, while Fv1^b restriction values were normalised to the value against N-MLV in the absence of Dox. Mean and mean deviation values from two independent restriction experiments were plotted in the graphs. Quantities of Fv1 were represented by the dotted line.

3.3 Study of MLV restriction by Fv1 superexpression

The previous data showed that a 26-fold overexpression of $Fv1^b$ above its endogenous level could cause restriction of NB-MLV and inhibition of B-MLV, but 37-fold overexpression of $Fv1^n$ above its already higher endogenous level did not allow gain of NB-MLV or N-MLV inhibition. Therefore, I wanted to test if further increase in $Fv1^n$ expression from the overexpression level, or "superexpression", would lead to inhibition of N-MLV and NB-MLV.

3.3.1 A transient assay to study the restriction of MLV by Fv1 "super-expression"

The procedure for an assay to study restriction during superexpression of Fv1 is shown in Figure 3.23. MDTF cells were transduced with different amount of LxIG-Fv1 or control vectors up to a MOI of 60 in order to achieve a very high expression level of Fv1. A vector expressing EGFP through a CMV promoter was used as the negative control. After transduction at a high MOI, almost all cells would be GFP^+. In order to provide an $Fv1^-$ internal control, the transduced cells were mixed with untransduced MDTF before reseeding for infection with YFP tester virus at an MOI of less than 1. Infected cells were analysed using a 2-colour FACS assay. Figure 3.24 shows the results for $Fv1^n$ and $Fv1^b$. It was obvious from the negative control data that high MOI transduction led to an Fv1-independent inhibition of MLV infectivity. This inhibition became prominent from an MOI of 4, and was likely due to a combination of the effects of provirus disrupting the genome of transduced cells, as well as the overexpression of EGFP. However, the reduction in relative infectivity for $Fv1^n$ against N-MLV and NB-MLV did not appear to be greater than that of the negative control. Instead, the reduction in relative infectivity was greater with the negative control. This could be due to a higher expression of EGFP in cells transduced with the control vector than in the LxIG-Fv1 vector. EGFP is expressed using a highly efficient CMV promoter and CAP-dependent translation in the control vector, while EGFP is expressed using the U3 promoter of MLV LTR and IRES-dependent translation in the LxIG-Fv1 vector. The assay could be improved by using an alternative control vector such as an LxIG-Fv1 vector expressing Fv1-NTD and EGFP. Nevertheless, the data suggest that even at the highest Fv1

protein level that can be supported by MDTF cells, $Fv1^n$ still does not inhibit N-MLV and NB-MLV.

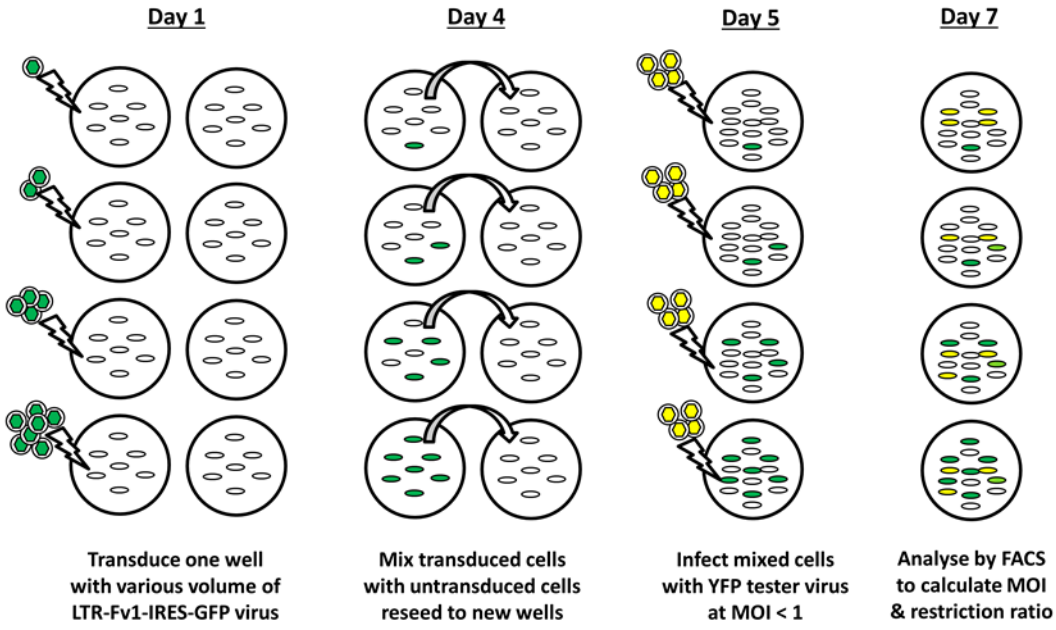

Figure 3.23 A transient assay to study the restriction of MLV during Fv1 "super-expression"

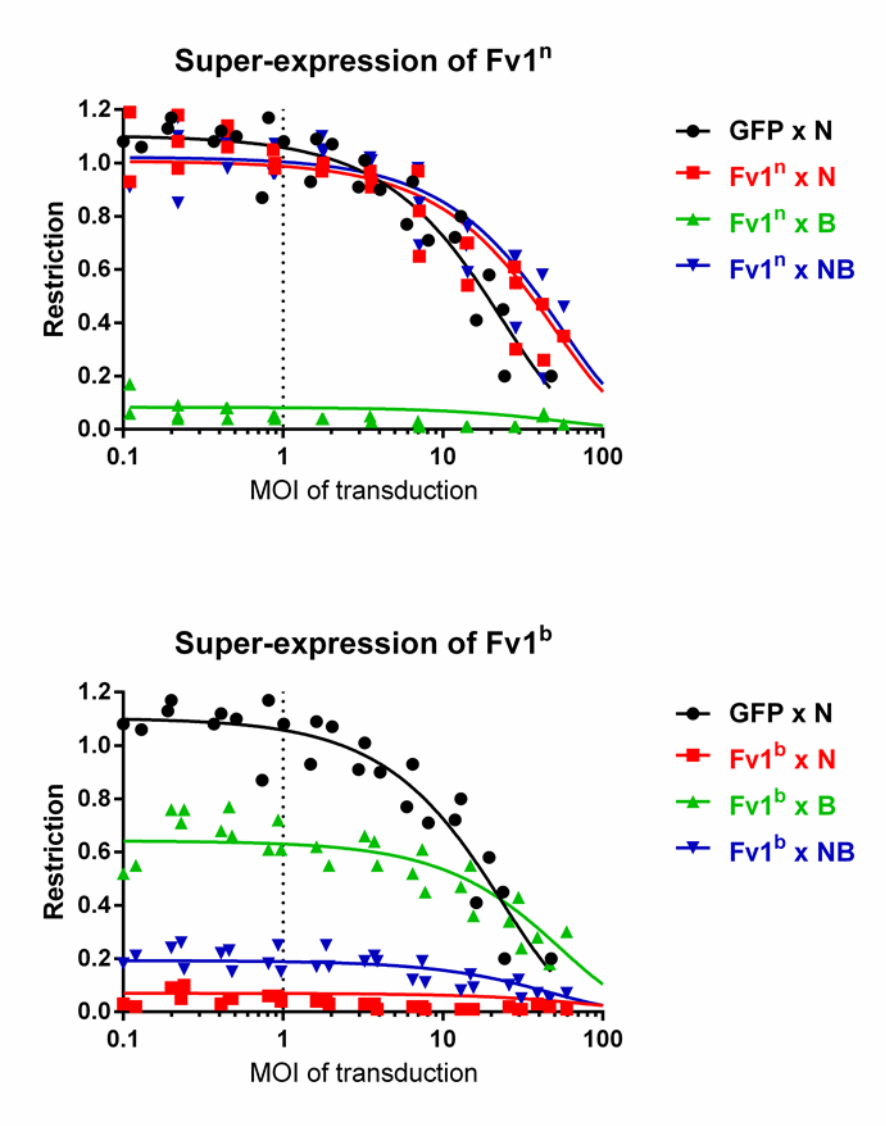

Figure 3.24 Restriction of MLV in MDTF cells transduced with LxIG-Fv1 vectors at very high MOI

A vector expressing EGFP under a CMV promoter was used as an $Fv1^-$ control (GFP, black line). Data points from 3 independent experiments were plotted and used for curve fitting.

3.4 Discussion

Through quantitative analyses of the expression level and restriction of Fv1, data presented in this chapter highlighted how the overexpression of Fv1 can lead to additional inhibition activities. Analysis of the over-expression levels of 10 different Fv1 variants revealed that sequence at residue 358 and the C-terminus have strong influence on the relative protein levels of $Fv1^n$ and $Fv1^b$. Using a novel inducible expression system with minimal leaky expression, I studied how expression level of $Fv1^b$ can alter its restriction specificity. $Fv1^b$ appears to restrict N-MLV and weakly inhibit NB-MLV at the endogenous level, and an increase in $Fv1^b$ concentration allows restriction of both N-MLV and NB-MLV, as well as inhibition of B-MLV. In contrast, $Fv1^n$ only restricts B-MLV and shows no inhibition against N-MLV and NB-MLV. This high specificity remains the same from the endogenous level to a "super-expression" level. The difference in B-MLV inhibition of $Fv1^b$, Fv1bb_ and Fv1bbn observed in previous studies (Bishop et al., 2001; Bock et al., 2000) cannot be explained by the difference in their over-expression levels alone. Instead, it is likely that these Fv1 variants possess different apparent affinities against B-MLV.

Previous studies of Fv1 protein level in cells transduced with LxIG-Fv1 vector had revealed effects of the sequence of Fv1 on the overexpression level (Bishop et al., 2001; Bock et al., 2000). Presumably through effects on protein stability, this led to a 4-fold difference in the overexpression levels of $Fv1^n$ and $Fv1^b$. A similar difference between $Fv1^n$ and $Fv1^b$ protein levels were also observed using the TGIx-Fv1 vector (Figure 3.17). However, it remained unclear whether these effects contributed the 3-fold difference between the endogenous protein levels in N-3T3 and B-3T3. It would be expected that a 23-fold higher mRNA level (Felton, 2012) and a 4-fold difference in protein stability would lead to a much bigger difference in expression than 3-fold.

By relating the restriction activity to the protein level of Fv1 under doxycycline induced expression, it was concluded that the endogenous restriction phenotype of $Fv1^b$ would include a mild inhibition of NB-MLV. Interestingly, a previous observation from B-3T3 cells overexpressing $Fv1^n$ supported this conclusion (Bock et al., 2000). It was found that overexpression of an Fv1 allele in cells endogenously expressing a different Fv1 allele leads to restriction phenotype of the overexpressed Fv1, and loss of the endogenous phenotype. For example, while the transduction of N-3T3 by LxIG-$Fv1^b$ reduced infectivity of N-MLV and NB-MLV by 15-fold and 3.5-fold, respectively, the infectivity of B-MLV was increased by 5.3-fold. The mechanism for the loss of endogenous phenotype was not known, but it had been hypothesised that the overexpressed Fv1 outcompete the endogenous Fv1 for either localisation site or capsid binding. Transduction of B-3T3 by LxIG-$Fv1^n$ reduced B-MLV infectivity by 8.7-fold and increased the infectivity of N-MLV by 10-fold. Surprisingly, a reproducible increase in NB-MLV infectivity from 27% to 34% was also observed. This result suggested an endogenous $Fv1^b$ phenotype of 90% restriction of N-MLV and 20% inhibition of NB-MLV.

Weak or moderate retroviral inhibition activities could be found in other natural alleles of Fv1. A previous study in our lab analysed the retroviral restriction activities of 16 different natural Fv1 alleles from wild mice (Yap et al., 2014). While some alleles exhibited restriction activities against N-MLV, B-MLV and NB-MLV, others also displayed restriction activities against non-gammaretroviruses. Two alleles, Fv1SPR1 and Fv1MAC, demonstrated restriction activity against N-MLV and the lentivirus EIAV. On the other hand, Fv1CAR1 showed restriction against the spumavirus FFV. However, since Fv1 was overexpressed using the LxIY-Fv1 vector (an EYFP-expressing version of LxIG-Fv1), there was concern whether these activities would be present at the endogenous level. Recent work by Melvyn Yap in our lab studied the restriction activities of these Fv1 alleles using the new inducible expression system described earlier (Figure 3.25). I constructed an EYFP-expression version of the TGIx-DEST vector, named TYIx-DEST, which was used to generate TYIx-Fv1 vectors for inducible expression of wild mice Fv1 alleles. At a doxycycline induction level (10ng/ml) where $Fv1^b$ was expressed at endogenous level, the

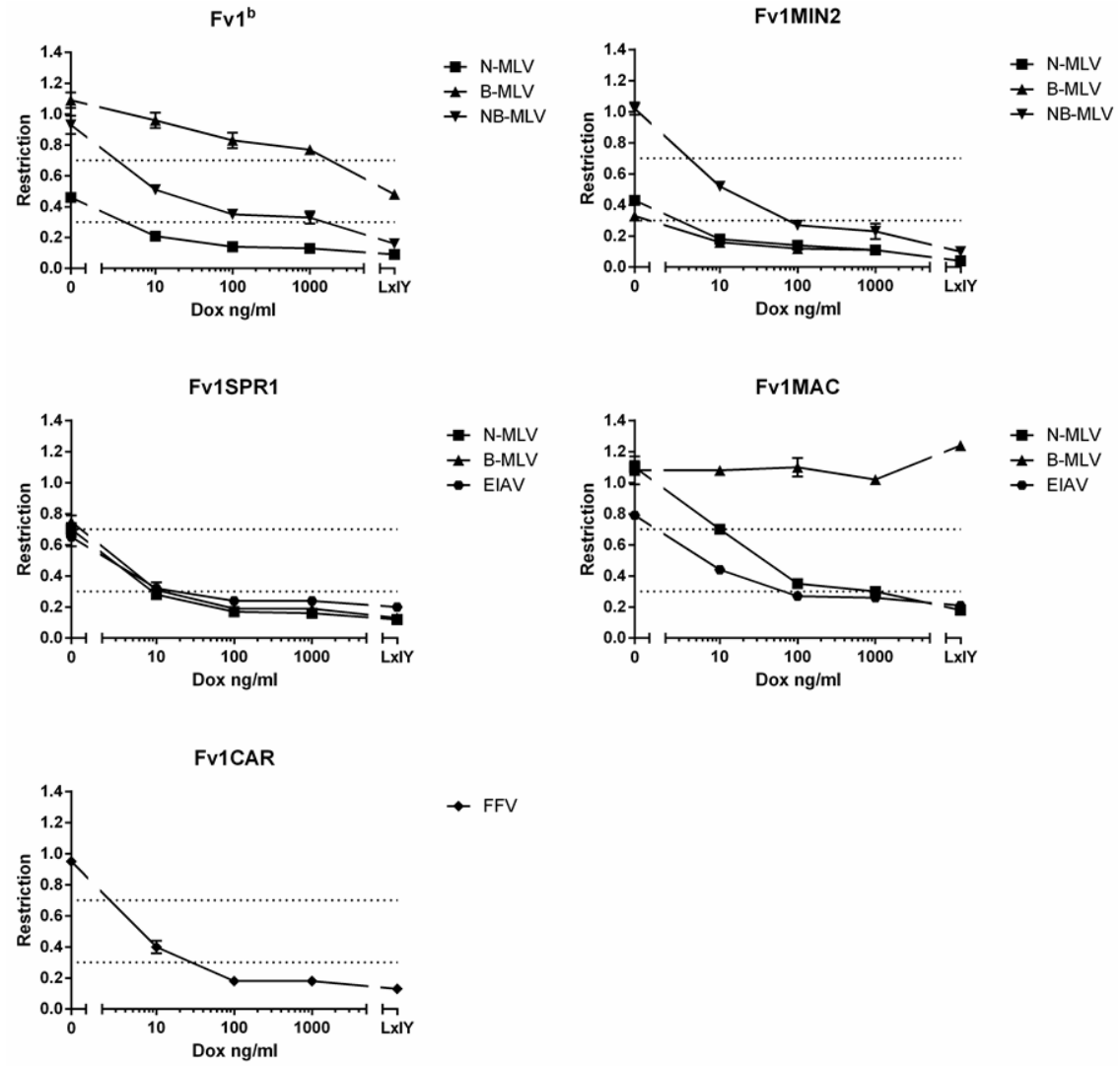

wild mice Fv1 alleles still

Figure 3.25 Dose-dependency of retrovial restriction by wild mice Fv1

This restriction study was carried out by Melvyn Yap. R18 cells transduced with TYIx-Fv1 vectors were reseeded and treated with various concentration of Dox for 24h before infecting with GFP tester virus for restriction assay. Mean and mean deviation values from 4 independent restriction experiments were plotted in the graphs. Results for LxIY were published previously (Yap et al., 2014). The two dotted lines represent the restriction ratios of 0.7 and 0.3. A restriction ratio of less than 0.3 indicates as full restriction, while a restriction ratio of between 0.3 and 0.7 indicates as partial restriction**.**

inhibited EIAV and FFV by more than 2-fold. The question remains whether these moderate inhibition activities could affect outcome of natural retroviral infection of wild mice, which could be very different from single-cycle infection with pseudotyped viruses on mouse cell line. Given the higher expression of Fv1 in N-3T3 than B-3T3, it is also possible that the endogenous level of Fv1 in wild mice is very different from that in $Fv1^b$, and may vary among different cell types.

The finding that many of the gained restriction activities of Fv1 mutants such as Fv1bbn could be observed using a vector with very low expression level (TGx-Fv1) suggested that they were not merely caused by overexpression of Fv1 (Table 3.2). The gain of restriction activity was most likely due to higher apparent binding affinity towards MLV CA, although it is possible that some mutations affect binding to other cofactor proteins. Detailed study of binding of Fv1, which will be described in chapter 4, would allow the building of a better picture of the relationships between CA binding, expression level and restriction activities.

Chapter 4

Study of the relationship between Fv1 binding and restriction specificity

As discussed in Chapter 3, while $Fv1^n$ only restricts B-MLV, $Fv1^b$ displayed strong restriction against N-MLV, moderate inhibition against NB-MLV, and weak inhibition against B-MLV. If the apparent binding affinity to capsid was the major determinant in restriction specificity, a similar binding specificity towards MLV capsid would be expected. However, data from a previous binding study in our lab showed that while $Fv1^n$ appeared to bind B-MLV only, $Fv1^b$ appeared to bind MLV of all tropisms (Figure 4.1) (Hilditch et al., 2011). Since the overexpression of $Fv1^b$ could lead to additional inhibition of NB-MLV and B-MLV, it is possible that a high concentration of $Fv1^b$ in cell lysate could have led to binding of all MLVs. In parallel to the restriction study in Chapter 3, the first goal of the work in this chapter was to test whether $Fv1^b$ shows higher binding specificity at a lower concentration. I also wanted to understand how the restriction specificity was influenced by the sequence at the 3 variable sites of $Fv1^n$ and $Fv1^b$, namely position 358, position 399 and the C-terminus. In particular, I wanted to test whether the diverse restriction specificities of the Fv1 mix-and-match mutants and C-terminus deletion mutants (Table 1.1) can be completely explained by the difference in apparent binding affinity towards MLVs of different tropisms (Bishop et al., 2001; Bock et al., 2000). To do this I attempted to correlate Fv1 binding and restriction phenotypes of these mutants.

4.1 Development and validation of a microplate assay to study Fv1 binding to MLV capsid assembly

The initial aim was to test if the binding of $Fv1^b$ could become more specific at a lower Fv1 concentration. This would require the comparison of MLV binding specificity at multiple Fv1 concentrations in parallel pull down experiments.

Unfortunately, the number of samples that can be analysed using the pull down assay developed by Hilditch et al was rather limited. This assay requires the separation of capsid-coated nanotubes from unbound Fv1 by ultracentrifugation through a sucrose cushion (Figure 4.2), hence restricting the number of samples that can be analysed to 6 per rotor. Therefore, the study of both Fv1 alleles at multiple concentrations in the same experiment would require the development of a new medium- or high-throughput pull down assay. Such assay may also allow the comparison of binding of different Fv1 mutants to different MLV capsids, and might eventually be extended to compare the binding between Fv1 and T5 to MLV capsid.

4.1.1 Immobilisation of capsid-coated nanotube to microplate

The most obvious way of increasing the sample throughput of the existing pull down assay was to eliminate the need of ultracentrifugation. Instead, similar to an enzyme-linked immunosorbent assay (ELISA), capsid-coated nanotubes could be immobilised on a microplate. In this case, lysate containing Fv1 could be incubated with the immobilised nanotubes, and unbound Fv1 could be removed by multiple washes with buffer. Bound Fv1 could then either be eluted from the well, or assayed directly inside the well. Such approach had been used for the development of an assay to study interactions between the membrane-binding protein kinase Cα (PKCα) protein and lipids present on liposomes (Losey et al., 2009). In the PKCα binding assay, a very small amount of a lipid with biotin-functionalised anchor was added to the composition of liposomes, allowing the immobilisation of liposomes to streptavidin-coated microplates. Similarly, biotin-functionalised lipid could be added to the composition of lipid nanotube, allowing the immobilisation to streptavidin microplates. Figure 4.3A shows the structure of three commercially available lipids with biotin-functionalised head groups. The length of the linker between the biotin group and the nitrogen in the phosphatidylethanolamine (PE) group varies among the three lipids. The lipid with a long PEG-2000 linker offered the highest efficiency of nanotube immobilisation, and was selected for subsequent experiments (Figure 4.3B).

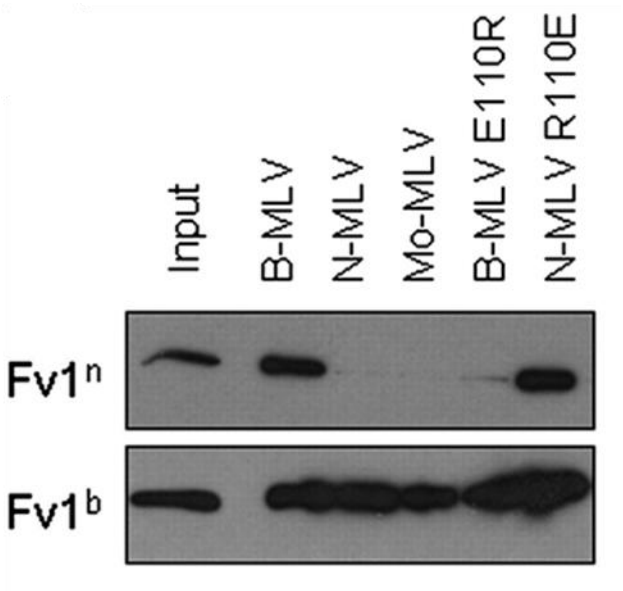

Figure 4.1 Binding data from the original MLV capsid pull down assay

Western blot showing $Fv1^n$ and $Fv1^b$ binding to various MLV CA nanotubes. Mo-MLV, Moloney MLV, known as NB-MLV in this thesis. Reproduced with permission from *Proceedings of the National Academy of Sciences USA* (Hilditch et al., 2011).

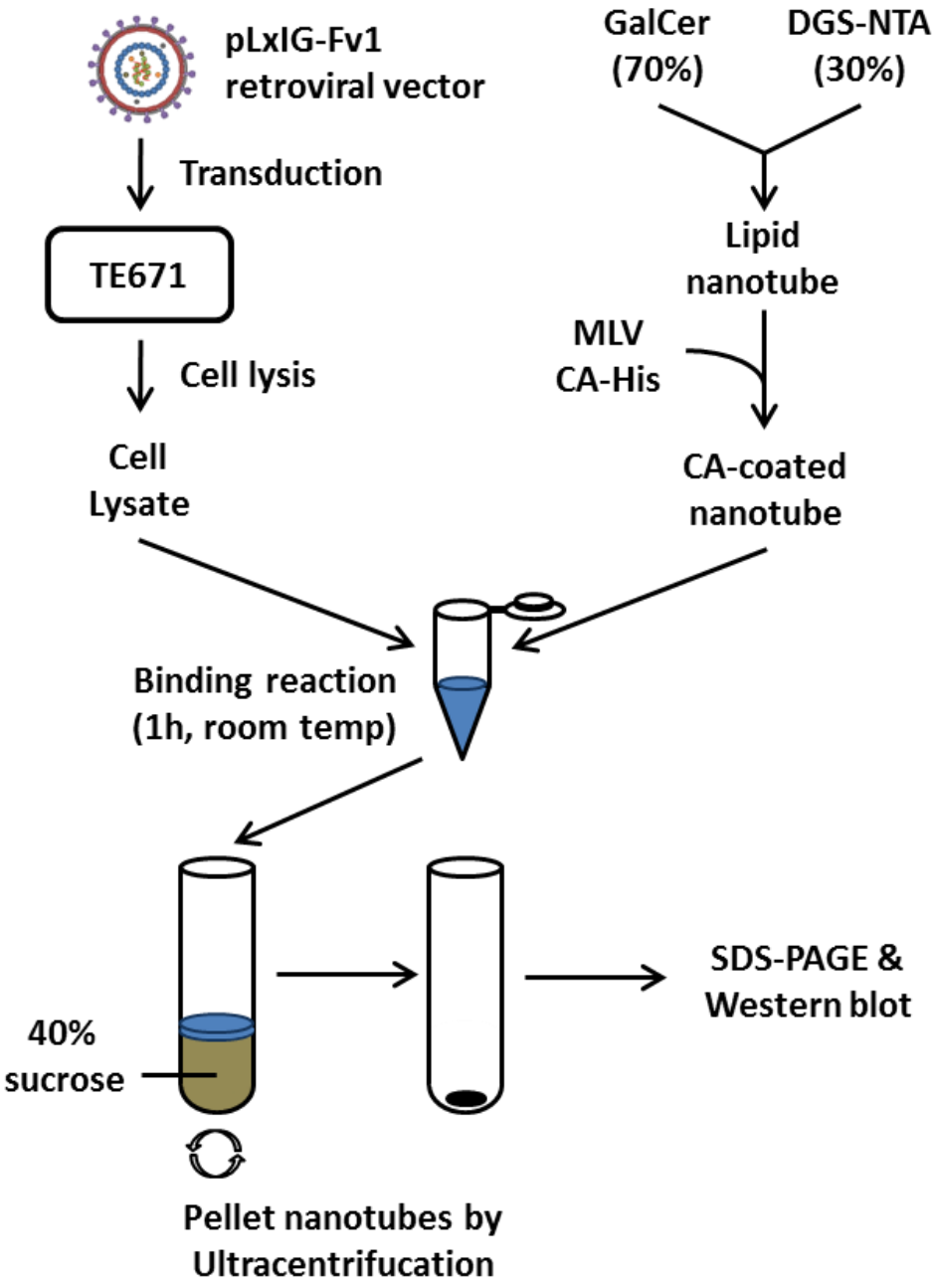

Figure 4.2 The original MLV capsid pull down assay

This pull down assay was developed by Laura Hilditch, a previous student in our lab (Hilditch et al., 2011). Lipid nanotubes were generated by mixing the curvature-forming lipid GalCer with the His-tag binding DGS-NTA(Ni) lipid in a 7:3 ratio, followed by drying with nitrogen gas and resuspension in buffer. The nanotubes were coated with a regular array of capsid by incubating with purified MLV CA-His protein. The coated nanotubes were then incubated with lysate extracted from cells expressing Fv1 following transduction with a LxIG-Fv1 retroviral vector. Nanotubes together with bound Fv1 were separated from lysate and unbound Fv1 by pelleting through a 40% sucrose cushion using ultracentrifugation. The amount of bound Fv1 in the pellet was analysed by western blotting using an anti-Fv1 antibody.

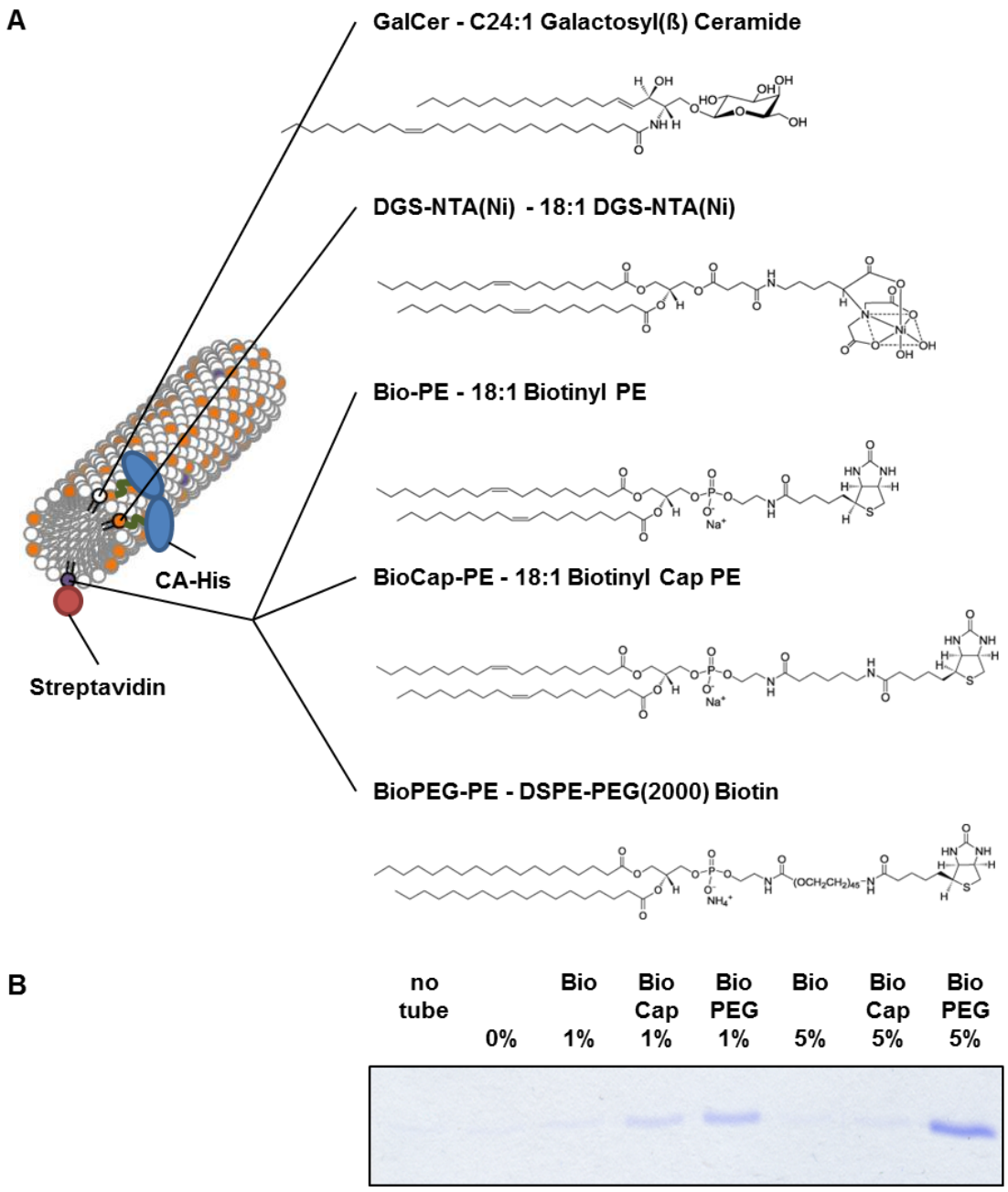

Figure 4.3 Immobilisation of capsid-coated nanotubes to streptavidin-coated microplates by biotin-functionalised lipids

(A) Composition of biotinyl lipid nanotube. In addition to GalCer and DGS-NTA(Ni) lipids used in the original pull down assay, one of the biotin-functionalised lipids was also included. The three biotinyl lipids have linkers of different lengths between the biotin group and the nitrogen atom of PE. (B) Lipid nanotubes with 0, 1 or 5% (mole/mole) of biotinyl lipid was coated with N-MLV CA-His. 5µg of capsid-coated nanotube was incubated in well in neutravidin-coated plate for 4h. Immobilised capsid was eluted by boiling in SDS-PAGE-loading buffer, and visualised after SDS-PAGE by coomassie blue staining.

Two alternative procedures for immobilising capsid-coated nanotubes were tested (Figure 4.4). In method A, lipid nanotubes were first coated with CA-His before addition to the microplate. However, this method led to stronger immobilisation of N-like capsids (N-MLV wt and B-MLV E110R) than B-like capsids (B-MLV wt and N-MLV R110E). This could pose a problem in the interpretation of binding data when comparing Fv1 binding to different capsids. In method B, naked lipid nanotubes were first attached to microplate, before coating with CA-His. Using method B, the amount of capsid detected was similar for both N-like and B-like capsid-coated nanotubes, and therefore allows the comparison of Fv1 binding to same amount of different capsid. Using this method, some of the CA-His could be non-specifically bound to the plastic or protein content of the microplate. However, such non-specific binding of capsid should have very minimal effect on the detected bound signal because of the lack of Fv1 binding to monomeric capsid (Dodding et al., 2005), and the fact that the amount of polymerised capsid was determined by the fixed quantity of lipid nanotubes in each well. During the development of the binding assay, microtitre plates were individually coated with neutravidin and then blocked with BSA. Due to high variability in the amount of capsid immobilised between experiments, this was subsequently changed to commercially available microplates pre-coated with streptavidin.

4.1.2 Optimisation of Fv1 lysate production from transduced MTDF cells

In the original capsid pull down assay, TE671 cells transduced with LxIG-Fv1 vectors at high MOI was used as the source of cell lysate (Hilditch et al., 2011). Since all previous Fv1 restriction experiments were carried out in the $Fv1^{o}$ MDTF cell lines, it would be preferable to carry out binding studies using the same cell line. Figure 4.5A shows that the expression of Fv1 in transduced MDTF cells were comparable to that in transduced TE671 cells. Due to the use of lipid nanotubes, lysate was prepared in a hypotonic detergent-free lysis buffer. The inefficient procedure of preparing cell lysates by Dounce homogenisation also limited the number of lysates that could be assayed. The yield of lysate prepared by mechanical sheering through QIAShredder spin

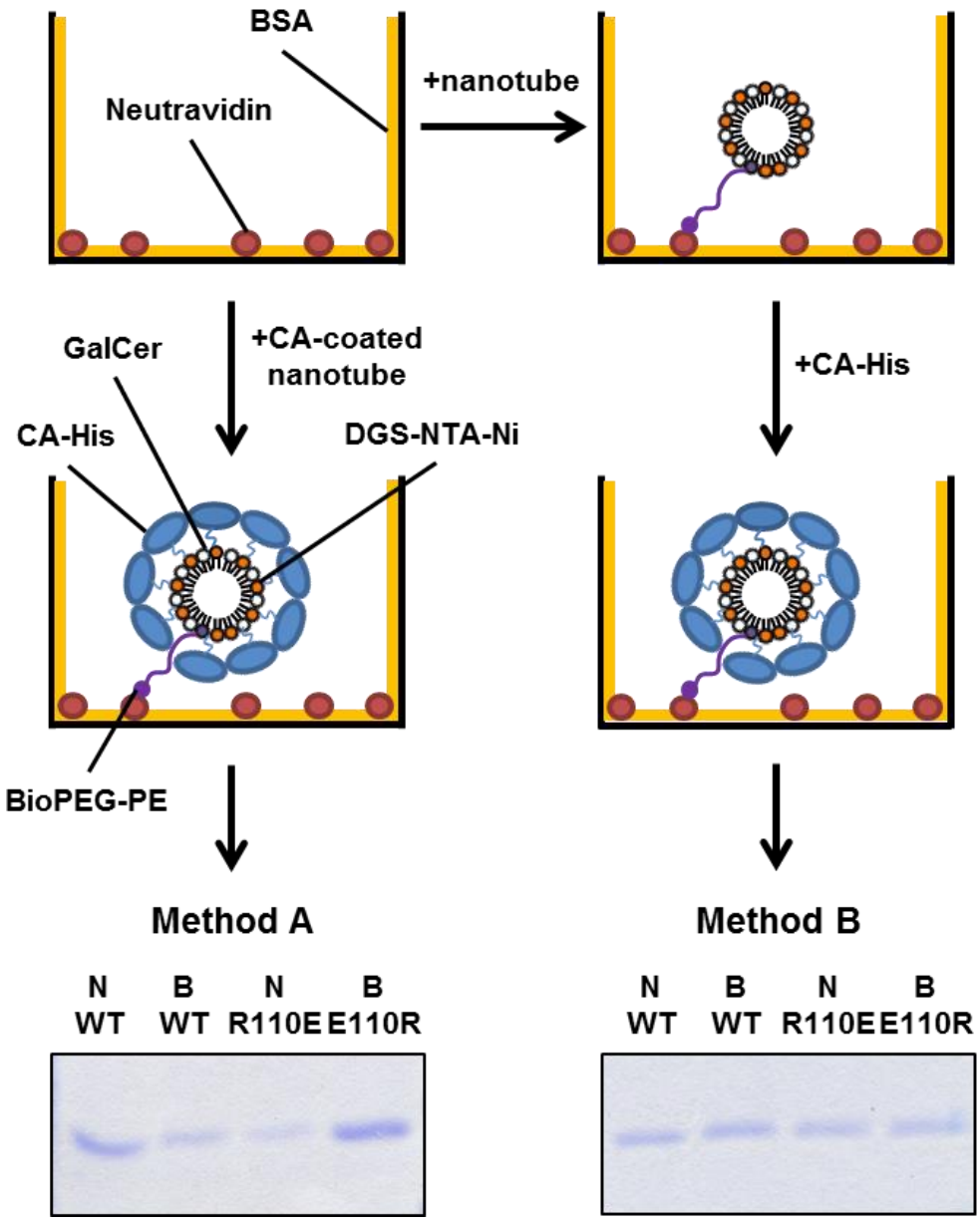

Figure 4.4 Two alternative methods for capsid-coated nanotube immobilisation

Lipid nanotubes could be coated with CA-His either before (Method A) or after (Method B) anchoring to neutravidin-coated microplates. Using method A, nanotubes pre-coated with N-like capsids (N-MLV wt and B-MLV E110R) were immobilised more efficiently than those pre-coated with B-like capsids (B-MLV wt and N-MLV R110E). In contrast, using method B, coating with CA-His after attaching of lipid nanotube to microplate led to even immobilisation of all MLV capsids.

columns was compared to Dounce homogenisation in Figure 4.5. Higher yields were obtained using the spin columns, and it allowed preparation of a large number of lysate samples in parallel. The protein level of $Fv1^n$ is higher than that of $Fv1^b$ in these lysates, consistent with previous finding that the overexpression level of $Fv1^n$ is higher than that of $Fv1^b$.

4.1.3 Demonstration of specific binding of $Fv1^n$ to B-MLV using a microplate pull down assay

The optimisations described earlier led to the development of a microtitre capsid pull down assay, as illustrated in Figure 4.6. In this assay, lipid nanotubes containing 0.5% (v/v) of the BioPEG-PE lipid were first immobilised to streptavidin-coated plate, then coated with MLV CA-His, followed by incubation with Fv1 lysate. MDTF cells transduced with LxIG-Fv1 vector at a high MOI was used as a source of cell lysate to test if the binding phenotype described by Hilditch et al could be demonstrated using this microplate assay. As discussed in Chapter 3, the overexpression level of $Fv1^n$ was higher than that of $Fv1^b$; therefore the $Fv1^n$ lysate was diluted by 4 to 8 fold with blank lysate from untransduced MDTF cells to the same level as $Fv1^b$. However, from these early attempts, even $Fv1^n$ appeared to bind non-specifically to all capsids. It was hypothesised that the lack of specificity could be due to high level of non-specific binding to microplate surface, requiring further optimisation on the stringency of the washing and binding buffers. In a typical ELISA assay, the wash and binding buffer is often supplemented with a detergent such as tween-20 to allow efficient removal of unbound proteins. However, due to the use of lipid nanotube, detergent was omitted from the wash buffer which could lead to a lower stringency of the washing steps. It was noted that in purification of His-tagged protein using Nickel-chelating columns, a buffer with high ionic strength (300mM NaCl) is often used in the binding and washing step to reduce non-specific binding.

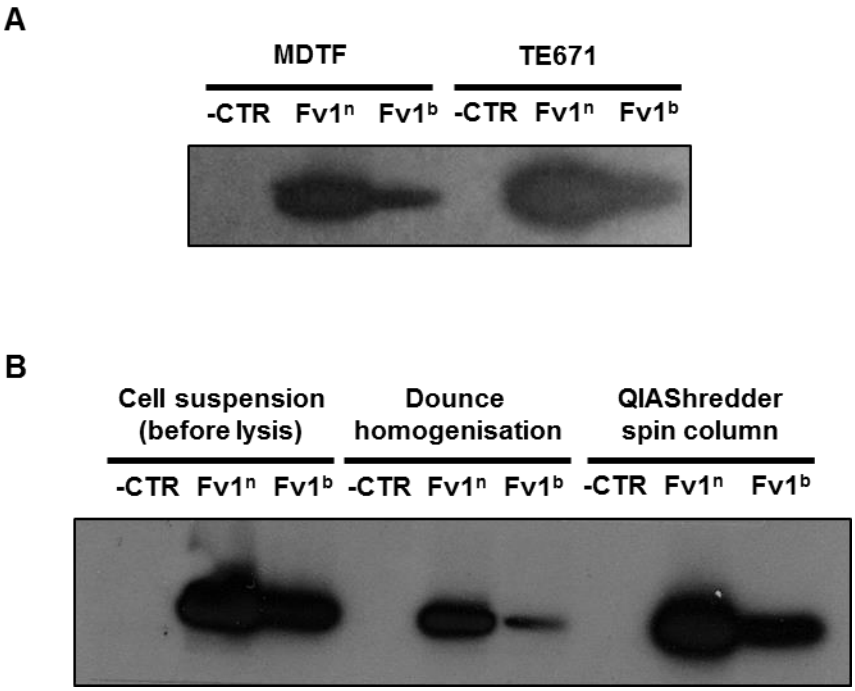

Figure 4.5 Generation of cell lysates from transduced MDTF cells

(A) Western blot analysis of Fv1 in lysate prepared from transduced MDTF and TE671. Lysate from cells transduced with 500µl of LxIG-Fv1 vector was compared to lysate from untransduced cells (-CTR). Equal amounts of protein was loaded to each well. Western blot was carried out with anti-Fv1 (#6689) antibody and HRP-conjugated secondary antibody. (B) Western blot analysis of Fv1 in lysate prepared by Dounce homogenisation and centrifugation through QIAShredder spin columns. Cells were suspended in hypotonic buffer, and subjected to either Dounce homogenisation or a 2min centrifugation through a QIAShredder column. Equal amount of protein was loaded to each lane for SDS-PAGE. Western blot was carried out with anti-Fv1 (#6689) antibody.

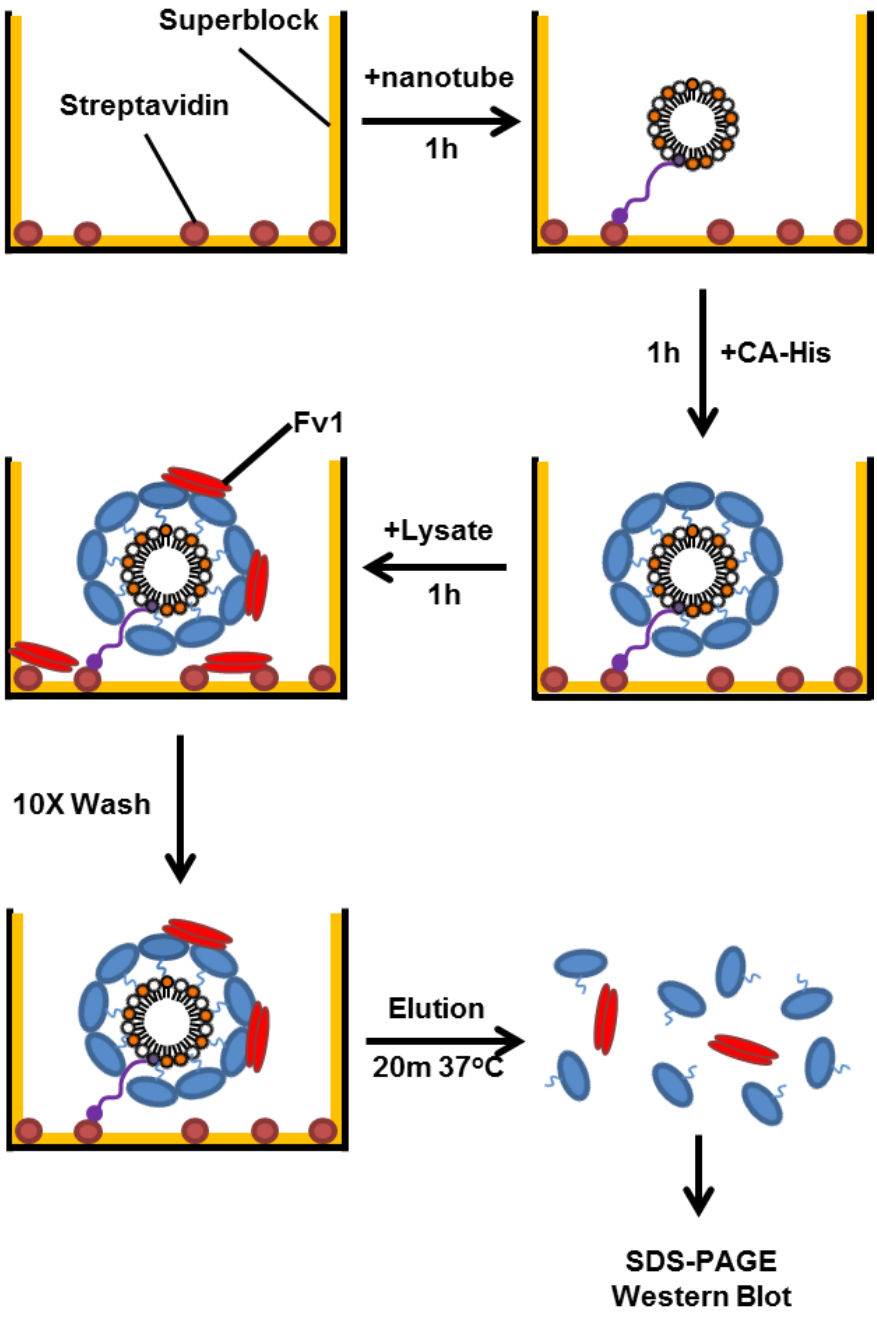

Figure 4.6 Procedure of the microplate capsid pull down assay

10µg/ml lipid nanotubes containing 0.5% (v/v) BioPEG-PE lipid was incubated in Streptavidin-coated microplate for 1h at room temperature. After 3 washes, 500µg/ml of CA-His was added and incubated at room temperature for 1h. After 3 washes, 500µg/ml lysate was added and incubated at room temperature for 1h. After 10 washes, bound Fv1 and capsid were eluted using a buffer containing 2% SDS and 500mM imidazole at 37^{o}C for 20min. Eluted samples were analysed along with input Fv1 samples by western blot analysis.

The use of high salt buffer (300mM NaCl) allowed the detection of specific binding of $Fv1^n$ to B-MLV and N-MLV R110E mutant (Figure 4.7). The binding of $Fv1^b$ resembles that from the study by Hilditch et al, with similar amount of bound Fv1 to all capsids. In order to provide a source of Fv1 lysate with consistent Fv1 concentration, SCCs of MDTF cells with "superexpression" of $Fv1^n$ and $Fv1^b$ were selected for subsequent optimisation and validation experiments. The effect of the ionic strength of binding buffer was further studied by combining the binding assay with semi-quantitative western blot analysis (Figure 4.8). Using the LI-COR western blot system, Fv1 and CA were detected simultaneously at the 800nm and 700nm channels, respectively. It appeared that using a binding buffer with 150mM NaCl, a high level of non-specific binding of Fv1 could be detected even in the absence of CA or nanotubes. This non-specific binding was almost completely eliminated by the use of a binding buffer with 300mM NaCl. Further increase in salt concentration to 500mM NaCl completely removed all the bound Fv1 signals (data not shown). Together, the data suggested that specific binding of $Fv1^n$ could be demonstrated using a microplate pull down assay with high stringency buffer, and the detected binding phenotype of $Fv1^b$ was the same in as the previous study.

4.1.4 Detection of Fv1 binding signal required assembled CA lattice

In order to validate that bound Fv1 signal detected using the microplate assay was due to the presence of assembled capsid lattice on nanotubes rather than non-specific binding, the binding of $Fv1^n$ and $Fv1^b$ to MLV capsids with P1G and D54A mutations were tested. A salt bridge between P1 and D54 stabilised the N-terminal β-hairpin structure in MLV CA (Mortuza et al., 2004), and such disruption had been shown to cause deformation of the regular CA lattice on capsid-coated nanotubes by electron microscopy (Hilditch et al., 2011). In agreement to the previous study, these mutations significantly reduced $Fv1^n$ binding (Figure 4.9), confirming that the majority of eluted $Fv1^n$ signal was bound to assembled capsid lattice. A similar effect was observed with $Fv1^b$, although the effect of D54A mutation to the binding of $Fv1^b$ to N-MLV was consistently weaker. Using a separate approach to validate the CA dependency

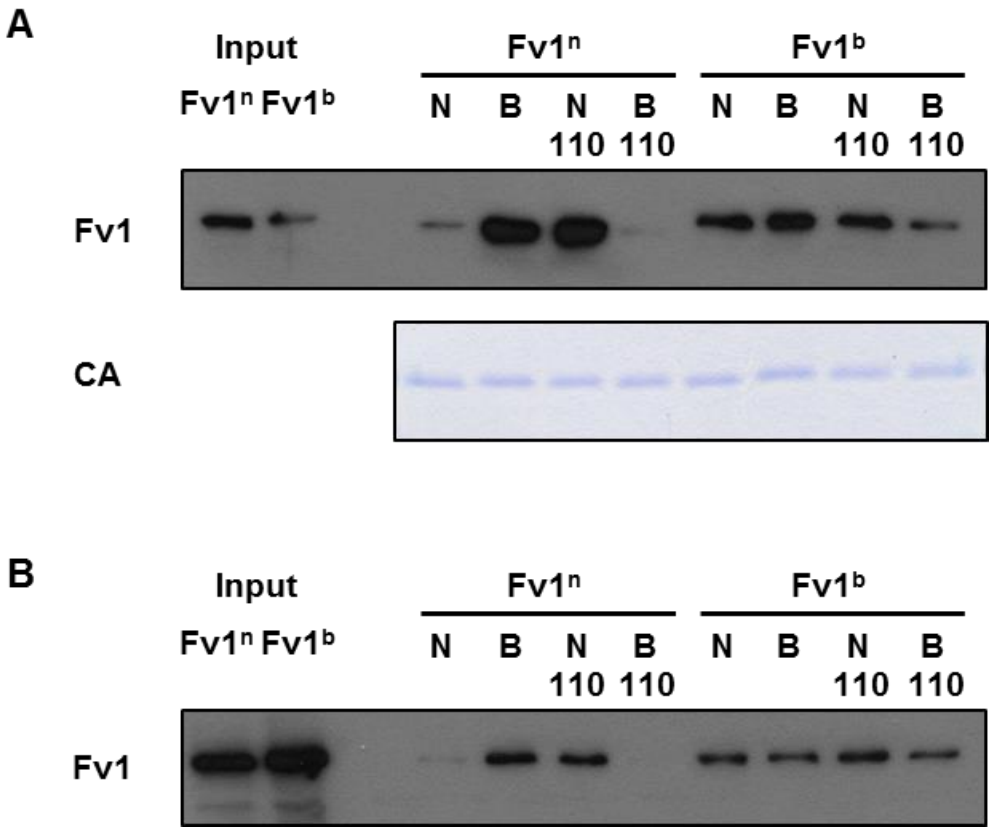

Figure 4.7 Binding of Fv1^n and Fv1^b to MLV capsids

(A) Lysate from MDTF cells transduced at high MOI was tested for binding using the procedure described in Figure 4.6 and a buffer with high ionic strength in the washing and binding steps. Fv1 was detected by western blot using an anti-Fv1 (#6689) antibody and HRP-conjugated secondary antibody. CA was visualised from SDS-PAGE gel by Coomassie blue staining. (B) Result of Fv1 binding from another independent experiment.

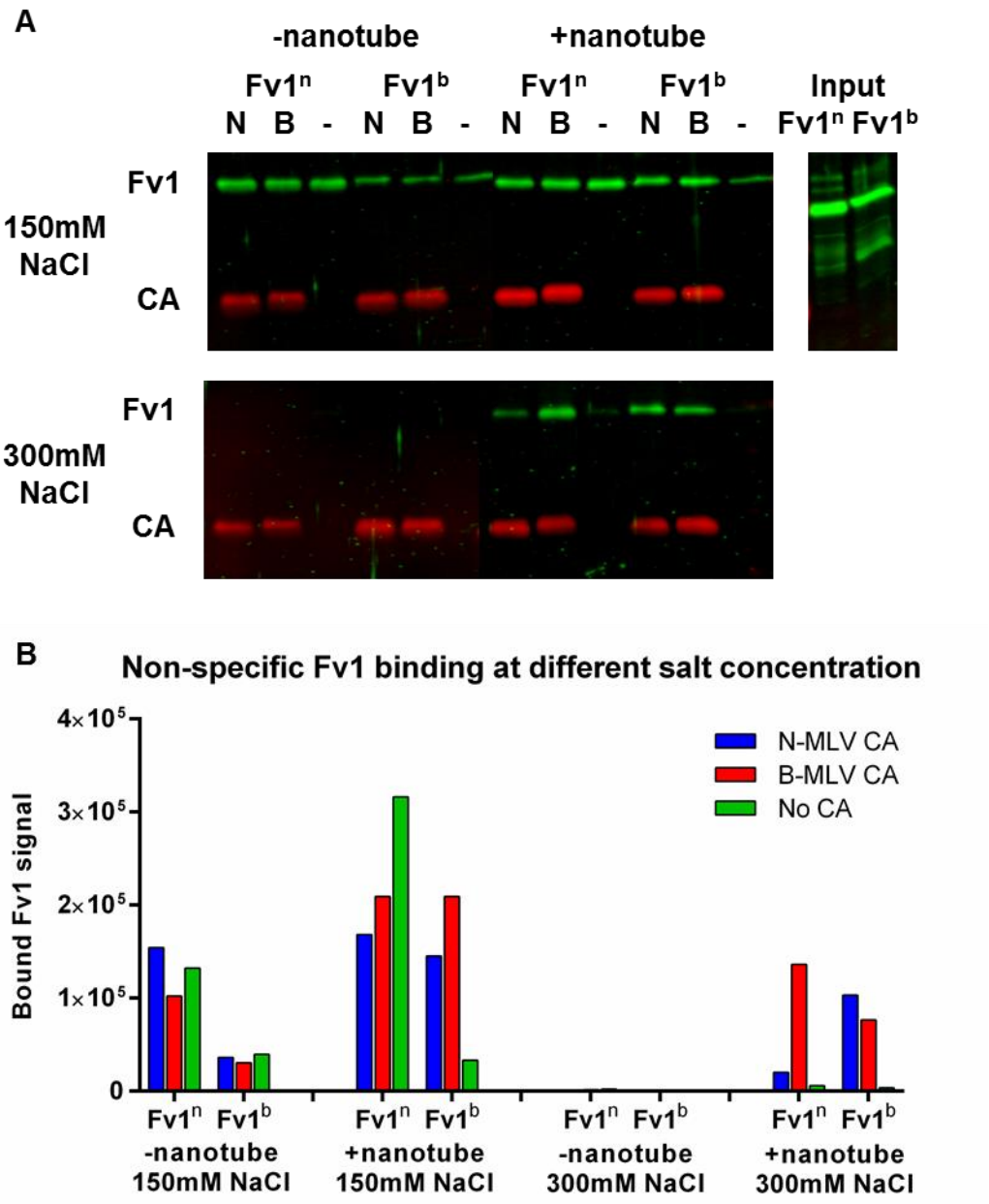

Figure 4.8 Semi-quantitative analysis of non-specific binding at different ionic strength

Lysate from SCCs expressing of $Fv1^n$ and $Fv1^b$ were used for binding assay as described in Figure 4.5. In this experiment, while a wash buffer of 150mM NaCl was used, the binding buffer contained either 150mM or 300mM NaCl. (A) Eluted proteins were analysed by LI-COR western blot. Fv1 was detected at the 800nm channel (green) using an anti-Fv1 (#6689) primary antibody and an IRDye-800 conjugated secondary antibody. CA was detected at the 700nm channel (red) using a monoclonal anti-5His primary antibody and an IRDye-680 conjugated secondary antibody. (B) Bound Fv1 signals from the blot above were illustrated using a bar chart.

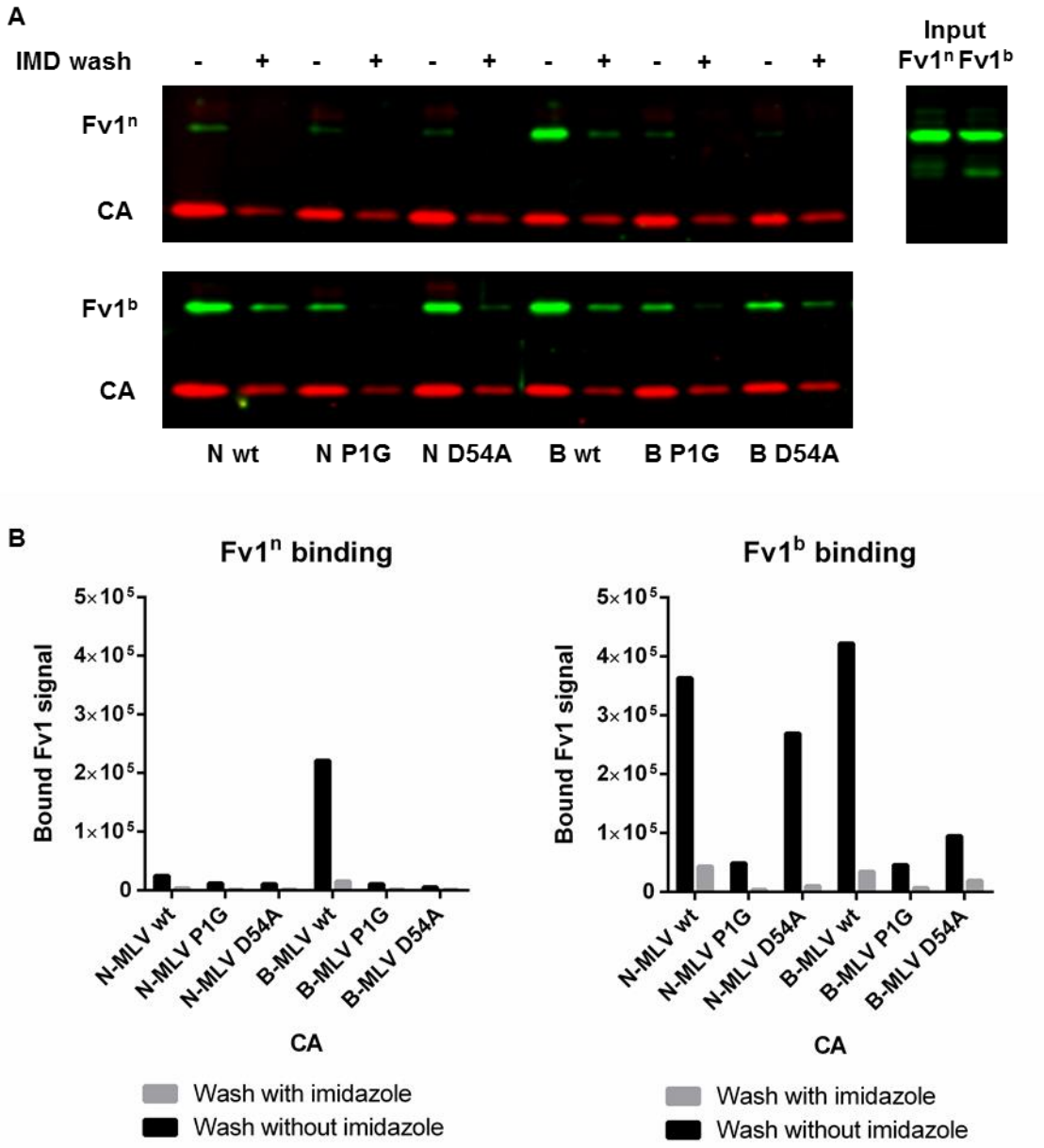

Figure 4.9 Detection of Fv1 binding signal requires assembled CA lattice

Binding of Fv1 to wt CA or lattice-destabilising CA mutants was analysed using lysate from SCCs. A binding experiment with 500mM imidazole included in the wash buffer was carried out in parallel. (A) Fv1 (green) and CA (red) signals were detected using LI-COR western blot analysis as described in Figure 4.8. (B) Bound Fv1 signals from the blot above were illustrated using a bar chart.

of bound Fv1 signal, 500mM imidazole was included in the wash buffer in a parallel binding experiment. The imidazole wash should release all CA-His together with all CA-bound Fv1, leaving only non-specifically bound Fv1. In all cases, the presence of imidazole in wash buffer caused significant reduction in both CA and bound Fv1 signals, confirming that the detected Fv1 signals reflected binding to assembled CA.

4.1.5 The use of frozen lysate did not significantly alter binding results

Fresh lysate prepared immediately before binding experiment had been used in all previous Fv1 binding studies. The use of frozen aliquots of lysate for binding experiments could be beneficial in several ways. First, the separation of the lysate preparation step would allow the comparison of more lysate samples in the same experiment. Secondly, as the expression level of Fv1 in SCCs varied between passages, the use of frozen lysate allowed repeat of binding experiments at the exact same Fv1 concentration. Lastly, the use of frozen aliquots allowed the determination of Fv1 concentration in lysate prior to binding assay, therefore allowing the study of binding activity of different Fv1 mutants at the same concentration. In Figure 4.10, the bound Fv1 signals from a binding experiment using fresh lysate was compared to a repeated experiment a day later using frozen lysate. A single freeze-thaw cycle did not appear to significantly alter the binding results. However, it was also found that after 3 months storage at -20^{o}C, the majority of proteins in aliquots of frozen lysate were precipitated. Storage of lysate at -80^{o}C after snap freezing in liquid nitrogen may be better for long term storage of Fv1 lysate.

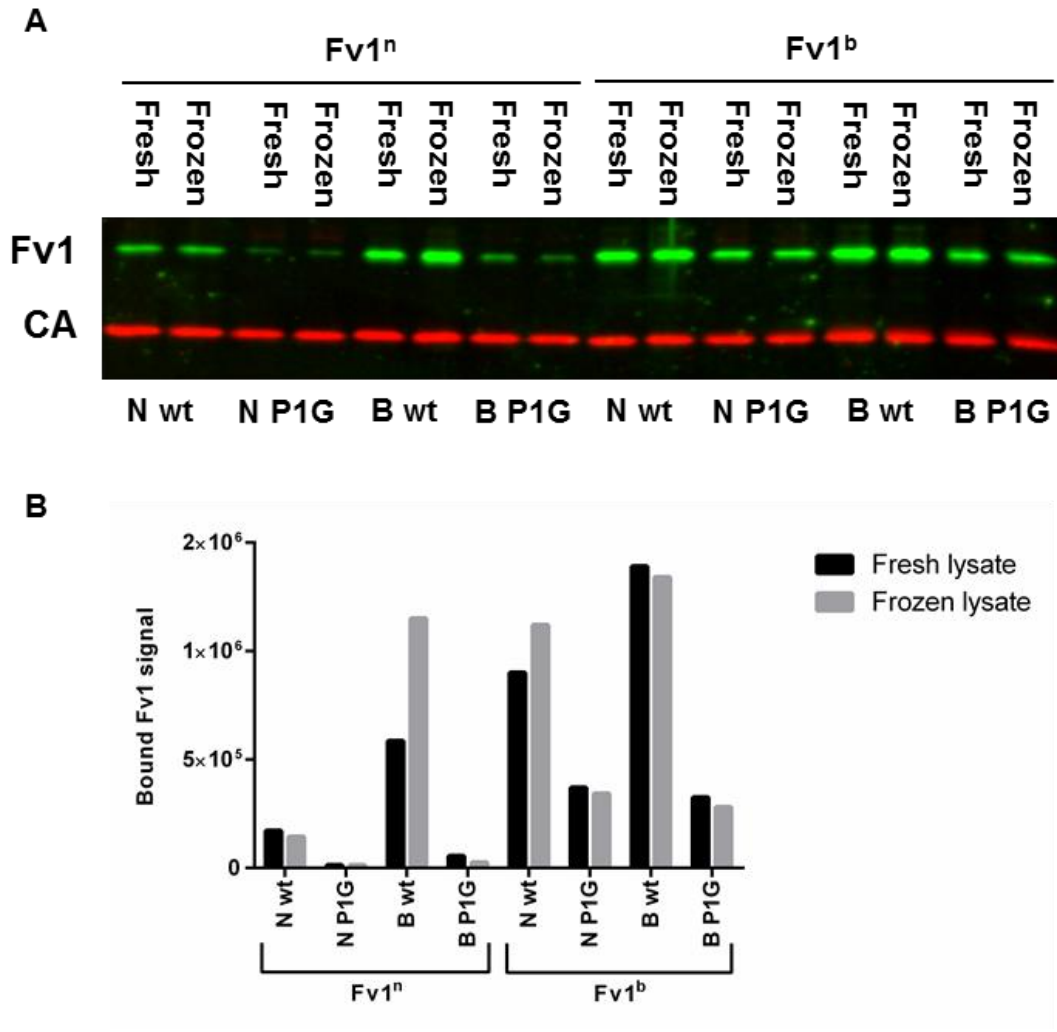

Figure 4.10 Freezing cell lysate did not significantly affect binding results

Lysates prepared from SCCs expressing $Fv1^n$ and $Fv1^b$ were used in binding assay, and the remaining lysate was frozen as aliquots of above 1mg/ml concentration at -20^{o}C overnight. The binding assay was repeated on the next day with thawed lysate. (A) Western blot analysis of bound Fv1 (Green) and CA (red) signals. (B) A bar chart illustrating the bound Fv1 signal from the western blot analysis.

4.2 Study of Fv1 binding using a microplate pull down assay

4.2.1 Specific binding of Fv1^b could not be detected

The first aim of using this novel microplate pull down assay was to compare the CA binding at multiple Fv1^b concentrations, in an attempt to detect specific binding of Fv1^b to N-MLV. Lysates containing different concentrations of Fv1 can be generated in two ways. First, a lysate sample from MDTF cells transduced with the LxIG-Fv1 vector at a very high MOI can be serially diluted with a blank lysate from untransduced MDTF cells. However, there was a concern on whether this method would results in lysates with predominantly aggregated Fv1. Since T5 has been shown to form aggregation (Langelier et al., 2008), Fv1 may also aggregate at high concentrations. It is possible that the specific binding of Fv1^b requires a less aggregated form of Fv1 which is maintained at a lower concentration. The formation of Fv1 aggregation at high concentration could potentially be irreversible, so diluting of such sample with blank lysate may only result in a lower concentration of aggregated Fv1 rather than increasing amount of dimeric Fv1. A second way is to generate lysate from MDTF cells transduced with LxIG-Fv1 vectors at different MOIs. Using this method, the lysate samples with lower total Fv1 concentration have not been exposed to the "super-expression" level of Fv1, therefore minimising the chances of Fv1 aggregation.

Figure 4.11 shows a comparison of CA nanotube binding by Fv1^n and Fv1^b using lysates with different Fv1 concentrations. At the lowest concentrations of Fv1^n, only binding to B-MLV could be detected. At high concentrations of Fv1^n, strong non-specific binding could be detected in binding reactions even without CA. In contrast, Fv1^b appears to bind all MLV CA equally even at the lowest concentration where binding could be detected. The data suggested that within the sensitivity limits of this microplate pull down assay, no specific binding of Fv1^b could be detected.

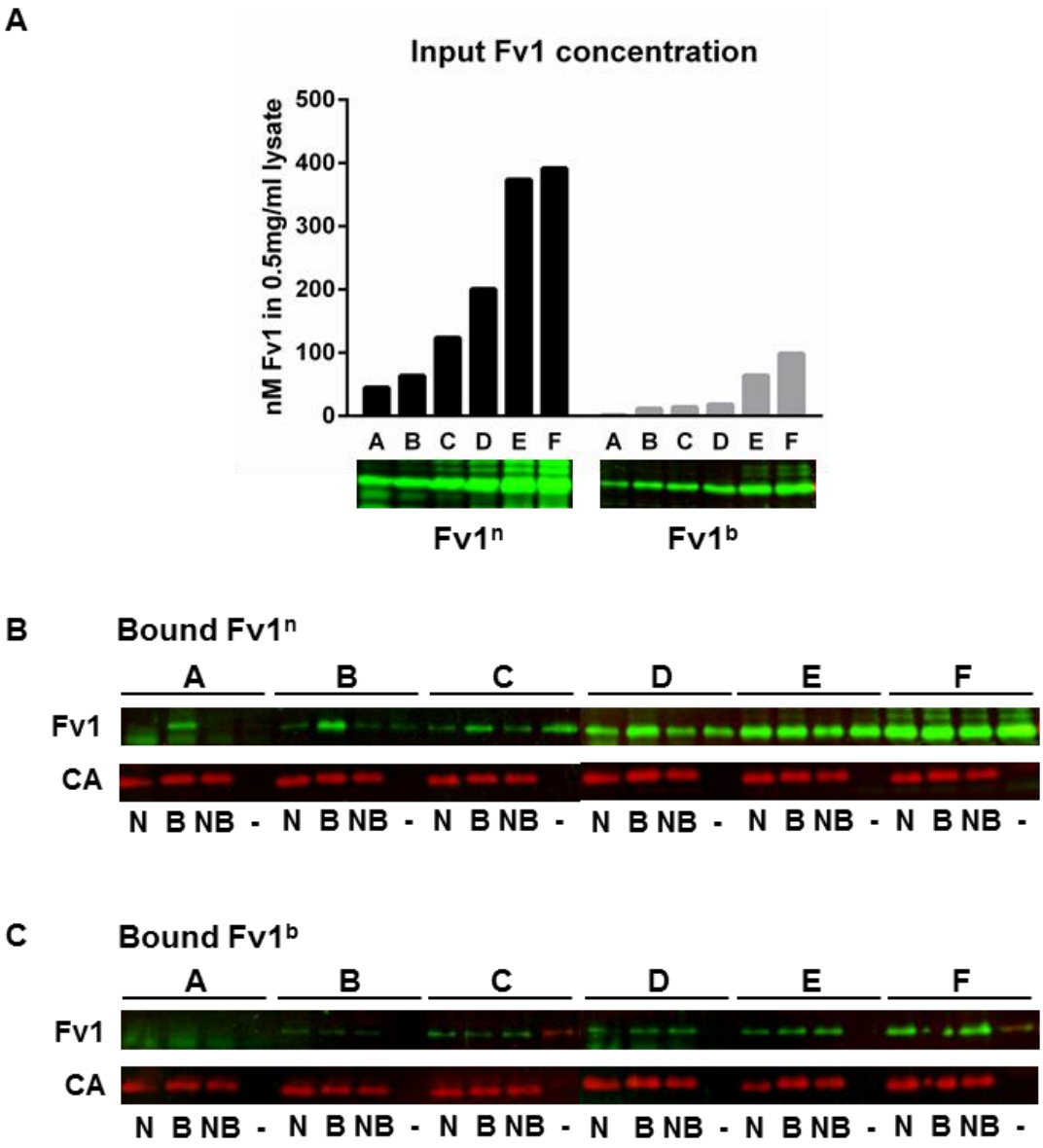

Figure 4.11 Binding studies at low concentrations of Fv1^{n} and Fv1^{b}

(A) Quantities of Fv1 in cell lysates prepared from MDTF cells transduced with LxIG-Fv1 vectors at different MOI were analysed by quantitative western blot using purified Fv1NTD standards as described in Chapter 3. The quantity of Fv1 from the western blot was illustrated in the bar chart. (B) Western blot analysis of bound Fv1^{n} (green) and CA (red) signals using lysate shown in (A).

4.2.2 Study of correlation between binding and restriction by Fv1

As discussed in Chapter 3, $Fv1^n$, $Fv1^b$, the mix-and-match mutants and the tail mutants all display different restriction phenotypes. The variety in restriction phenotypes made them ideal targets for studying the correlation between restriction and binding. The aim of this study was to compare the binding of all 10 Fv1 variants to MLV capsids in the same experiment at very similar Fv1 concentrations, using N-MLV P1G as a control for non-specific binding. Similar to the study in 4.2.1, MDTF cells were transduced with LxIG-Fv1 vectors expressing one of the 10 Fv1 variants at 7 different MOIs to generate a library of Fv1 lysates. After growing of transduced cells to large quantity, stock lysates was prepared and stored as aliquots at -80^{o}C after snap freezing with liquid nitrogen. An aliquot of each sample in the lysate library was thawed for analysis of total protein and Fv1 concentrations. By mixing Fv1 lysate, blank lysate and buffer, diluted Fv1 lysates with specific total protein and Fv1 concentrations could be generated. Nevertheless, as illustrated in Figure 4.12A, despite the best attempts to standardise the Fv1 concentrations between Fv1 variants tested in the same experiment, there was still a two-fold difference between the samples with highest and lowest Fv1 concentration.

The results for the binding study are illustrated in Figure 4.12B and C. The binding phenotype of $Fv1^n$ and $Fv1^b$ were similar to previous binding studies, supporting the idea that the use of frozen lysate did not affect binding results. In some binding reactions with NB-MLV CA, the normalised percentage of bound Fv1 was negative indicating that the binding to NB-MLV was lower than to the N-MLV P1G control. However, in most of these cases the values were close to zero. Table 4.1 compares the sequence, restriction, binding and overexpression protein levels of all 10 variants. Among all the sequence determinants, the influence of E358 on restriction, binding and expression was most obvious. The previous studies have reported that E358 from $Fv1^b$ strongly correlates with the restriction of N-MLV (Bishop et al., 2001; Bock et al., 2000), although Fv1nnb is able to inhibit N-MLV despite having K358. The presence of E358 is also associated with lower Fv1 protein level. Interestingly, the 6 Fv1

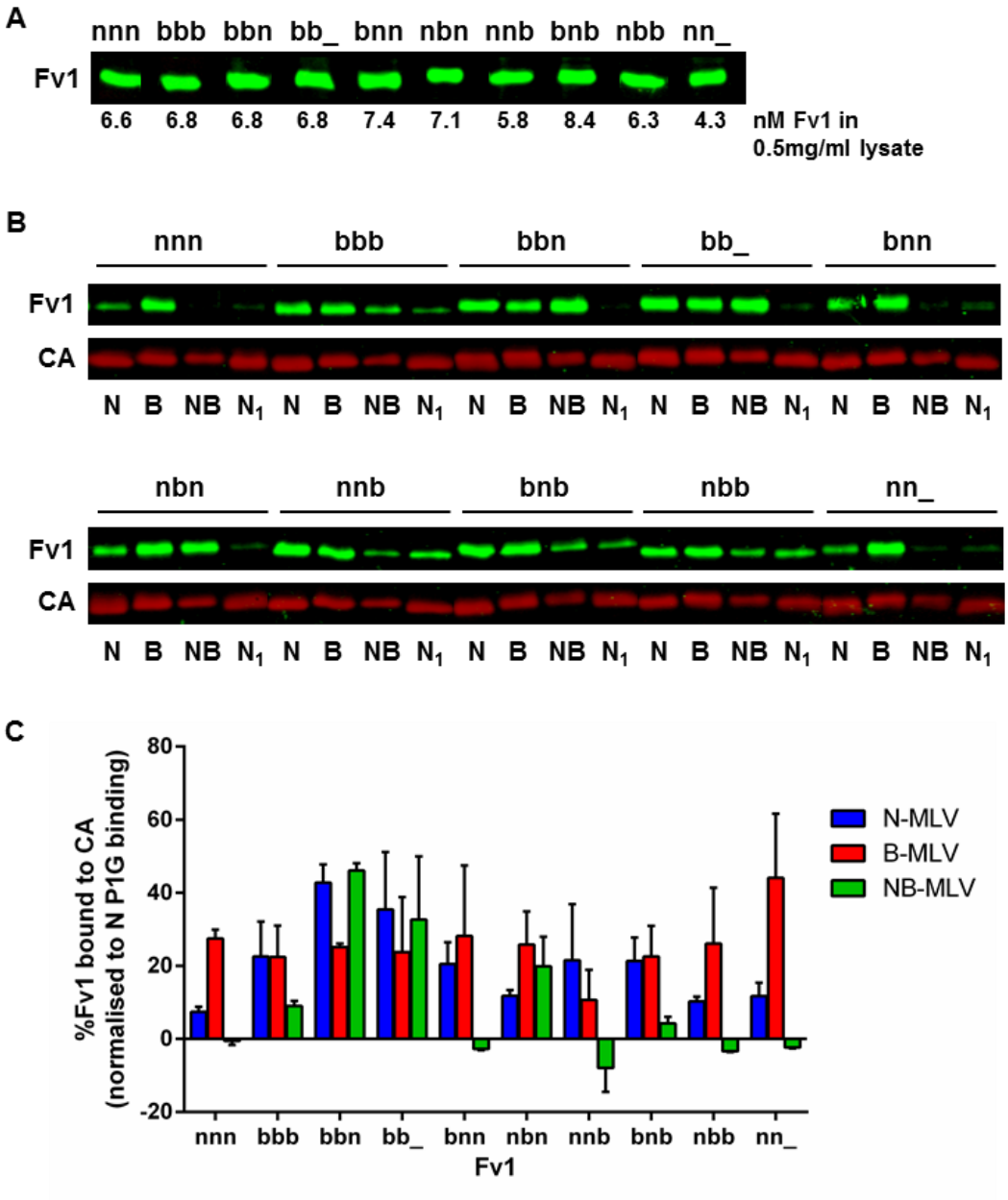

Figure 4.12 Binding data from Fv1^{n}, Fv1^{b} and mutants

(A) Western blot analysis of input Fv1 in each lysate sample used in a binding study. The amount of Fv1 in each diluted lysate was analysed by quantitative western blot using purified Fv1NTD standards. (B) Western blot analysis of the amount of bound Fv1 of all 10 Fv1 variants. N_1 indicates samples with N-MLV P1G control. (C) A bar chart showing binding data of all 10 Fv1 variants. Quantity of bound Fv1 was expressed as a percentage of quantity of input Fv1, with non-specific binding to N-MLV P1G subtracted. The height of each bar represents the mean value from two binding experiments, while the error bars show values of mean deviation.

N-MLV

Fv1	358	399	Tail	TGx	LxIG	Fv1/cell	Binding
bbn	E	R	TKL	0.17	0.06	1071	42.7%
bbb	E	R	GLTSVGSVGVLSLSPWKHQSNS	0.17	0.07	680	22.6%
bnn	E	V	TKL	0.18	0.09	1886	20.5%
bnb	E	V	GLTSVGSVGVLSLSPWKHQSNS	0.22	0.06	805	21.3%
bb_	E	R		1.07	0.06	762	35.4%
nnb	K	V	GLTSVGSVGVLSLSPWKHQSNS	1.07	0.58	1572	21.5%
nbb	K	R	GLTSVGSVGVLSLSPWKHQSNS	1.05	0.93	2587	10.3%
nbn	K	R	TKL	1.12	1.02	3434	11.7%
nn_	K	V		1.09	1.10	851	11.7%
nnn	K	V	TKL	1.16	1.07	2865	7.4%

B-MLV

Fv1	358	399	Tail	TGx	LxIG	Fv1/cell	Binding
nbn	K	R	TKL	0.23	0.08	3434	25.8%
nnn	K	V	TKL	0.24	0.06	2865	27.5%
bbn	E	R	TKL	0.29	0.07	1071	25.2%
nnb	K	V	GLTSVGSVGVLSLSPWKHQSNS	0.52	0.09	1572	10.7%
nbb	K	R	GLTSVGSVGVLSLSPWKHQSNS	0.66	0.07	2587	26.1%
bnn	E	V	TKL	0.93	0.12	1886	28.2%
nn_	K	V		1.07	0.09	851	44.1%
bb_	E	R		1.09	0.22	762	23.8%
bbb	E	R	GLTSVGSVGVLSLSPWKHQSNS	1.10	0.63	680	22.4%
bnb	E	V	GLTSVGSVGVLSLSPWKHQSNS	1.08	1.11	805	22.6%

NB-MLV

Fv1	358	399	Tail	TGx	LxIG	Fv1/cell	Binding
bbn	E	R	TKL	0.19	0.08	1071	46.1%
nbn	K	R	TKL	0.33	0.09	3434	19.9%
bbb	E	R	GLTSVGSVGVLSLSPWKHQSNS	0.79	0.21	680	9.0%
bb_	E	R		1.07	0.05	762	32.7%
bnn	E	V	TKL	1.12	0.98	1886	-2.7%
nnb	K	V	GLTSVGSVGVLSLSPWKHQSNS	1.07	1.07	1572	-7.9%
bnb	E	V	GLTSVGSVGVLSLSPWKHQSNS	1.08	1.12	805	4.2%
nbb	K	R	GLTSVGSVGVLSLSPWKHQSNS	1.12	1.10	2587	-3.4%
nn_	K	V		1.12	1.11	851	-2.3%
nnn	K	V	TKL	1.18	1.08	2865	-0.5%

Table 4.1 Summary of sequence, restriction activity, binding activity and overexpression level of all 10 Fv1 variants

The table was arranged in the order of decreasing restriction activities at the endogenous (TGx) and at the overexpression (LxIG) Fv1 levels. Positively charged amino acids were highlighted in red, while negatively charges amino acids were highlighted in blue. The red bars indicate mean restriction values from 3 experiments using the TGx-Fv1 vector in the presence of 1µg/ml doxycycline, these values are derived from Table 3.2. The green bars indicate mean restriction values from 3 experiments using the LxIG-Fv1 vector in MDTF-R18 cells, these values are derived Table 3.2. The blue bars show the mean Fv1 expression level (unit: 10^3 molecules per cell) from 2 experiments in MDTF cells transduced with LxIG-Fv1 at MOI of 1, these values are derived from Figure 3.3). In comparison, the endogenous levels of $Fv1^n$ and $Fv1^b$ are 77 x 10^3/cell and 26 x 10^3/cell, respectively. The yellow bars show mean percentage Fv1 binding from 2 experiments, as shown earlier in Figure 4.12.

variants which show strong inhibition or restriction of N-MLV at the over-expression level (bbn, bbb, bnn, bnb, bb_ and nnb) also show stronger binding to N-MLV CA nanotubes. Similarly, the 4 Fv1 variants which restrict NB-MLV at the over-expression level (bbn, nbn, bbb, bb_) all show stronger binding to NB-MLV CA nanotubes. 9 out of 10 Fv1 variants restrict or inhibit B-MLV at the over-expression level, with Fv1bnb as the exception. However, the binding of Fv1bnb to B-MLV CA nanotubes is not significantly lower than other mutants. Since all Fv1 mutants were derived from $Fv1^n$ and $Fv1^b$, both of which inhibits B-MLV, it is likely that they all possess at least a weak apparent binding affinity towards B-MLV CA.

To test whether CA nanotube binding is correlated with MLV restriction by Fv1, binding and restriction data from all 10 variants were subjected to two-tailed correlation analysis (Figure 4.13). Interestingly, strong correlations were identified for N-MLV and NB-MLV between binding and restriction at overexpression level (LxIG-Fv1). In the case of N-MLV, all 6 Fv1 variants that conferred full or partial restriction of N-MLV when overexpressed also showed strong binding to N-MLV capsid exceeding 20% of input Fv1. A two-tailed test confirmed the significant correlation between N-MLV binding and restriction at overexpression, with a Pearson correlation coefficient of 0.0053. In the case of NB-MLV, all 4 variants that showed restriction of NB-MLV at overexpression level also demonstrated strong binding of at least 9%. The two-tailed test confirmed the significance of the correlation between NB-MLV binding and restriction at overexpression, with a Pearson correlation coefficient of 0.0014. In contrast, no correlation could be found between B-MLV binding and restriction. When overexpressed, 8 out of 10 Fv1 variants conferred full restriction of B-MLV. The two exceptions were $Fv1^b$, which conferred partial restriction of B-MLV, and Fv1bnb, which did not show any inhibition towards B-MLV. All Fv1 variants except Fv1bnb display some inhibition against B-MLV, and therefore must have some interaction with B-MLV core. Since the binding of the non-restrictive Fv1bnb appears to be similar to other restrictive variants, the data suggested that all 10 Fv1 variants were capable of binding to B-MLV CA.

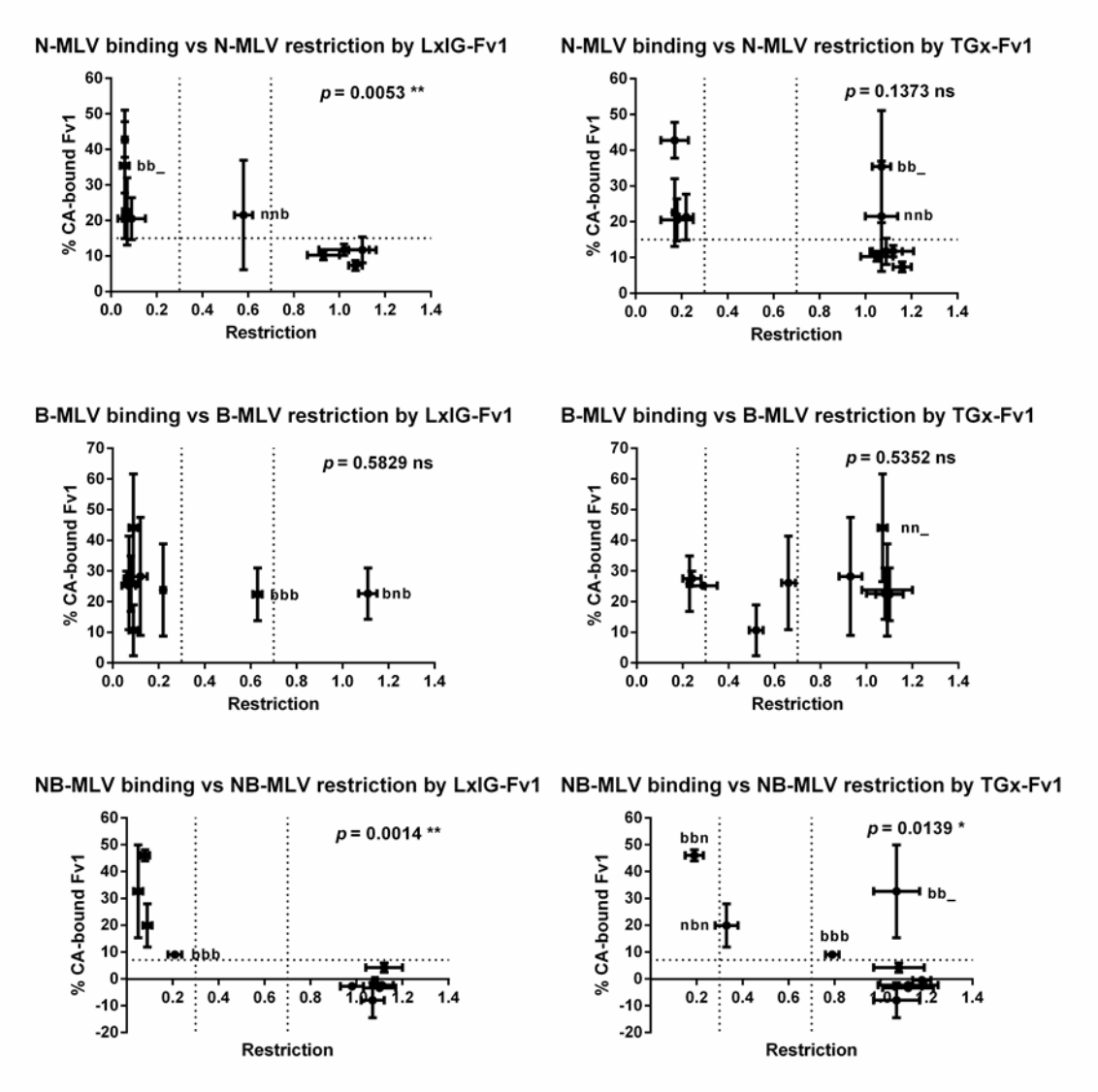

Figure 4.13 Correlation analyses between Fv1 binding and restriction

Binding data from 2 experiments and restriction data (either LxIG-Fv1 or TGx-Fv1 with 1µg/ml Dox) from 2 experiments were subjected to two-tailed correlation test. *P* value shows the Pearson correlation coefficient. Vertical dotted lines indicate restriction values of 0.3 and 0.7. Horizontal dotted lines show potential separation of capsid-binding and non-binding phenotypes.

In contrast to the strong correlation between N-MLV binding and restriction at overexpression level, no significant correlation was found between N-MLV binding and restriction at endogenous level (TGx-Fv1 +Dox). This was mainly due to the lack of restriction at endogenous level by two variants which strongly bind N-MLV, Fv1bb_ and Fv1nnb. Similarly, the lack of NB-MLV restriction by Fv1bb_ at endogenous level led to a weak correlation between NB-MLV binding and restriction at endogenous level. Together, these data suggested that the binding of Fv1 to CA nanotubes indicates an apparent binding affinity which is sufficient to cause MLV inhibition at an over-expression level, but may be insufficient to cause inhibition at the endogenous level.

4.3 Discussion

In this chapter, the development of a microplate pull down assay designed to allow the study of the relationship between MLV binding and Fv1 concentration, and between MLV binding and restriction by Fv1 is described. By studying the binding of $Fv1^n$ and $Fv1^b$ to MLV CA nanotubes at different Fv1 concentrations, it was observed that while $Fv1^n$ specifically binds B-MLV CA nanotubes, $Fv1^b$ binds N-MLV, B-MLV and NB-MLV CA nanotubes equally. In contrast, $Fv1^b$ is abrogated by N-MLV but not B-MLV (Boone et al., 1990), suggesting a measurable difference in the apparent binding affinity of $Fv1^b$ towards MLV of different tropisms. So what causes the difference in the apparent binding specificities of $Fv1^b$ to MLV cores and CA nanotubes?

The apparent lack of binding specificity of $Fv1^b$ to CA nanotubes could be due to the high concentration of CA and/or Fv1 required for the detection of bound Fv1 in the assay. At the binding equilibrium, the concentration of bound Fv1:CA complex is dependent on concentrations of both Fv1 and CA. Data from the restriction studies in Chapter 3 suggested that the strong inhibitions of NB-MLV and B-MLV is observed only at high $Fv1^b$ concentration, but not at the low endogenous $Fv1^b$ concentration. Although $Fv1^b$ appeared to bind MLVs of all tropisms equally even at the lowest $Fv1^b$ concentration which allowed detection

of bound $Fv1^b$, it remains possible that this low Fv1 concentration is already sufficient to overcome the weaker apparent binding affinity of $Fv1^b$ to NB-MLV and B-MLV. However, the concentration of Fv1 used in the binding assay is actually relatively low compared with the concentration of CA. Among the proteins eluted from binding reactions, a band corresponding to MLV CA is clearly visible on SDS gel by Coomassie blue staining (Figure 4.7), while Fv1 can only be detected by western blot. It is more likely that the high concentration of CA in the binding reaction overcomes the weak apparent binding affinity of $Fv1^b$ to NB-MLV and B-MLV, leading to the equal binding to MLV CA of all tropisms. At a low concentration, the $Fv1^n$ appears to bind CA nanotubes of B-MLV only, this suggested that the apparent affinity of $Fv1^n$ to CA of N-MLV and NB-MLV are much lower than to B-MLV, and cannot be overcome by the high CA concentration. It is possible that at a higher $Fv1^n$ concentration, $Fv1^n$ binds to CA of all MLV tropisms equally. However, the high background non-specific binding of $Fv1^n$ to the microplate well does not allow one to confidently distinguish the bound $Fv1^n$ signal from background signal. Instead of studying Fv1 binding with lysates containing different Fv1 concentrations, it may be possible to detect stronger binding of $Fv1^b$ to N-MLV than to NB-MLV and B-MLV by using a fixed amount of Fv1 and different amount of CA nanotubes. The quantitation of both Fv1 and CA in such binding assay may allow one to distinguish small differences in apparent binding affinities of $Fv1^b$ against MLV CA of different tropisms. However, it is anticipated that the study of Fv1 binding at lower CA nanotube concentrations may be difficult for several reasons. First, the limited sensitivity of the Fv1 western blot may not be sufficient to detect the lower amount of bound Fv1 at lower CA concentrations. Secondly, even if $Fv1^b$ binds exclusively to N-MLV CA nanotubes at a low CA concentration, it would be difficult to distinguish such weak binding from background signals resulted from the non-specific binding of Fv1 to the microplate well.

The differences between the CA lattice on lipid nanotubes and the CA lattice on mature MLV core could also mean that the binding apparent affinity of Fv1 to nanotubes and core may be different. First, the curved CA array on lipid nanotube may not mimic those found in mature core. The CA array is formed on the curved surface of lipid nanotubes imposed by the lipid GalCer, forming

tubes with a diameter of 50nm (Hilditch et al., 2011). In contrast, the mature core of MLV was described as polygonal and roughly spherical, with variable diameter within a particle of 120nm (Yeager et al., 1998). Secondly, the C-terminus of CA is attached to DGS-NTA lipid via a His-tag (Hilditch et al., 2011), while in MLV mature core both N- and C-termini of CA are not tethered. Importantly, these differences may lead to the difference in the spacing between CA hexamers, which may influence the recognition of CA by Fv1. The inter-hexamer spacing is known to be different between immature and mature CA lattice. In HIV-1 core, the inter-hexamer spacing changes from 80Å in immature core to 96Å in mature core (Briggs et al., 2004). In MLV, the inter-hexameric spacing immature-like lattice of MLV CA tethered in one or both ends are about 80Å (Barklis et al., 1997; Yeager et al., 1998; Zuber et al., 2000), but crystal structure of processed MLV CA showed an inter-hexameric spacing of 99Å (Burns, 2009; Mortuza et al., 2008). The crystal structure of mature MLV CA showed that the CA-CTD forms CTD-CTD inter-hexameric interactions, and the conformational changes in CA-CTD may be contributing to this increase in inter-hexamer spacing (Burns, 2009). In MLV CA nanotubes, the inter-hexamer spacing was found to be about 70Å (Hilditch et al., 2011), which resembles that of an immature CA lattice. Although the processed N-terminus allows the stabilisation of β-hairpin, the tethering of the C-terminus of CA may still prevent some structural changes in the CA-CTD required the formation of a mature-like lattice. How the presence of an immature-like lattice on the CA nanotube could affect binding is not known. N-MLV with the processing of gag at the CA/NC junction abolished by protease site mutation failed to abrogate $Fv1^b$ (Dodding et al., 2005), however an electron microscopy study also showed defect in core formation of this mutant (Oshima et al., 2004), therefore it is difficult to conclude whether a CA lattice with processing at the N-terminus but not the C-terminus can be recognised by Fv1. Since the inter-hexamer spacing of an immature-like CA lattice is lower than that of a mature CA lattice, the density of CA hexamers in an immature-like lattice would be higher than in a mature CA lattice. The higher density of binding sites for Fv1 may potentially enhance the apparent binding affinity of Fv1 to CA, which may overcome the weak apparent affinities of $Fv1^b$ against CA of NB-MLV and B-MLV. Testing whether the C-terminal processing of CA is required for Fv1 binding *in vitro* would require the comparison between the binding of Fv1 to an immature-like CA lattice such as

those on lipid nanotubes, and binding of Fv1 to a mature CA lattice on an *in vitro* assembly. Currently there is no *in vitro* assembly with a mature MLV CA lattice, since purified MLV CA does not polymerised into *in vitro* assemblies. Identification of an alternative method for polymerizing CA, insensitive to detergent washing, might provide a possible approach to this problem.

The studies of binding and restriction of 10 different Fv1 variants revealed a strong correlation between the observed binding to CA nanotube and the restriction phenotype at over-expression level of Fv1 for both N-MLV and NB-MLV. All Fv1 variants except Fv1bnb show at least some inhibition towards B-MLV at over-expression level of Fv1. Since the binding of the non-restrictive Fv1bnb to B-MLV CA nanotubes appears to be similar to other restrictive Fv1 variants, it is likely that all 10 Fv1 variants were capable of binding to B-MLV CA. The correlations between CA nanotube binding and restriction at an over-expression level are in agreement with the hypothesis that the apparent lack of binding specificity to CA nanotubes may be due to the high concentrations of CA and/or Fv1 present in the binding reaction. Therefore, strong binding of Fv1 to MLV CA nanotubes may indicate that the Fv1 possess an apparent affinity to cores that is sufficient for MLV inhibition when Fv1 is over-expressed, but such interaction may be too weak for any measurable inhibition as a lower concentration close to the endogenous level. As for the Fv1bnb mutant, it is likely Fv1bnb has some very weak apparent affinity against B-MLV CA, which is insufficient to cause inhibition of B-MLV even at a high concentration Fv1.

Chapter 5

Attempts to study binding of T5 to MLV CA

RhT5, but not HuT5, restricts HIV-1 (Stremlau et al., 2004). The interaction between rhesus T5 to *in vitro* capsid assemblies of purified HIV-1 CA-NC proteins (Gross et al., 1997) could be demonstrated using a pull down assay (Stremlau et al., 2006), which involved pelleting of tubular CA-NC complexes through a 70% sucrose cushion by ultracentrifugation. This assay had since been used in numerous studies mainly from the Sodroski lab to study the binding of T5 to HIV capsids (Kar et al., 2008; Kim et al., 2011; Langelier et al., 2008; Li et al., 2006b; Li et al., 2006c; Liberatore and Bieniasz, 2011; Lienlaf et al., 2011; Yang et al., 2014).

Similar to the endogenous restriction specificity of $Fv1^b$, both HuT5 and RhT5 also restrict N-MLV but not B-MLV (Hatziioannou et al., 2004; Perron et al., 2004; Yap et al., 2004). Since N-MLV capsid is the target of both T5 and Fv1 restriction, there has been strong interest in our lab to develop an assay that would allow comparison of the binding of these two restriction factors to MLV capsid. Previously, the specific binding of T5 to N-MLV capsid using a CA-pulled down assay had been described by the Luban lab (Sebastian and Luban, 2005). This assay involved pull-down of CA by GST-tagged T5 from core particles prepared by stripping the membrane envelope of MLV virions with detergent, and was used in a subsequent study in their lab (Sebastian et al., 2009). However, despite many attempts in our lab, the specific binding of T5 to MLV could not be demonstrated using this assay (Sadayuki Ohkura, unpublished data). In the previous study by Laura Hilditch, the original MLV CA-coated nanotube pull down assay that had been used to demonstrate Fv1 binding was applied to study T5 (Hilditch, 2010). However, pull down of HA-tagged RhT5 (RhT5HA) or HA-tagged HuT5 (HuT5HA) by MLV CA-coated nanotubes could not be demonstrated. Data in this chapter describes further attempts to show specific binding of T5 to MLV capsid *in vitro*.

5.1 Binding of T5 to MLV capsid-coated nanotube

Since the microplate pull down assay described in chapter 4 allowed detection of specific $Fv1^n$ to B-MLV reproducibly, it might be thought that this assay could be used to study T5 binding to MLV capsids. Compared to the original nanotube pull down assay (Figure 4.1), the microplate assay could eliminate the potential bias in binding results due to aggregation of restriction factor at high concentration. T5 had been known to localise to cytoplasmic bodies (Reymond et al., 2001) related to aggresomes (Diaz-Griffero et al., 2006). Since aggresomes contain aggregated cytoplasmic proteins (Johnston et al., 1998), this suggested T5 may have aggregation properties. Aggregated T5 in cell lysate might then be pelleted through sucrose cushion even in the absence of capsid, causing a high background of binding signal.

5.1.1 Human T5HA showed stronger binding to B-MLV than N-MLV

In the previous study, Laura Hilditch suggested that the failure to detect binding of HA-tagged T5 (T5HA) to MLV capsid using the original pull down assay could be largely due to the low concentration of T5HA in cell lysate (Hilditch, 2010). Therefore, SCCs of MDTF cells transduced with LxIY-T5HA vectors at very high MOI were picked and screened for high T5HA expression by LI-COR western blot (Figure 5.1). Since antibody with good sensitivity against both HuT5 and RhT5 was not available, constructs with C-terminal HA-tag was once again used in this study. It had been shown previously that the presence of a C-terminal HA-tag did not have any significant effect on HIV-1 restriction by T5 (Stremlau et al., 2004). Some of the clones that expressed high level of Hu T5HA had much slower cell division, and would not serve as a reliable source of cell lysate for binding assays. A clone was selected each for HuT5HA and RhT5HA, and both clones have similar T5HA expression to eliminate the need for diluting T5HA lysate with blank lysate.

Parallel binding experiments using the microplate assay described in chapter 4 was carried out with lysates from SCCs expressing $Fv1^n$, $Fv1^b$, HuT5HA and RhT5HA (Figure 5.2). As expected, binding of $Fv1^n$ to B-MLV

only and binding of $Fv1^b$ to both capsids were observed. Surprisingly, a much stronger binding of HuT5HA to B-MLV than to N-MLV was observed. This observed binding specificity is inconsistent with the specific restriction of N-MLV by HuT5HA. At the same concentration, binding of RhT5HA to neither N-MLV nor B-MLV capsids could be observed. Results from repeated experiments were consistent. Since the signal from HuT5HA bound to B-MLV was weak compared to the input, there was a possibility that the concentration of T5HA was too low for detectable specific binding, and the observed binding signal was difference in non-specific binding. It is also impossible to compare the amount of input Fv1 and T5 used in these binding experiments because the detection of Fv1 and T5 were carried out using different antibodies.

In order to increase the specific binding of T5HA to polymerised CA, the assay was repeated with increasing amount of lipid nanotubes (Figure 5.3). Since binding of RhT5HA to MLV capsids could not be observed earlier, binding to nanotubes coated with HIV-1 CA-p2 was also tested. A regular array had been found on lipid nanotubes coated with HIV-1 CA-p2 by electron microscopy (Goldstone et al., 2014; Hilditch, 2010), and this construct had been used to form capsid array to study binding of Fv1Cyp (Goldstone et al., 2014). In agreement to previous restriction data, binding of RhT5HA but not HuT5HA to HIV-1 CA-p2 was detected at all nanotube concentrations. At all nanotube concentrations, the signal of B-MLV binding was significantly higher than that of N-MLV or no CA control. As the amount of nanotube increases, the detected signal of HuT5HA bound to B-MLV also increases. At 40ng/ml nanotube concentration, more than 50% of input HuT5HA is bound to B-MLV CA. The binding of HuT5HA to N-MLV was not significantly higher than to the CA-negative control. The restriction phenotypes of HuT5HA and RhT5HA were confirmed by two colour restriction assay (Table 5.1). Both T5HA alleles restrict N-MLV but not B-MLV, although for HuT5 and HuT5HA a weak inhibition of B-MLV could be observed. The fact that T5 restriction can be abrogated by N-MLV but not B-MLV (Towers et al., 2002) strongly suggested that T5 specifically recognises N-MLV cores but not B-MLV cores. Therefore, the observed stronger binding of HuT5HA to B-MLV than N-MLV is unlikely to reflect the specific binding of HuT5HA to MLV cores.

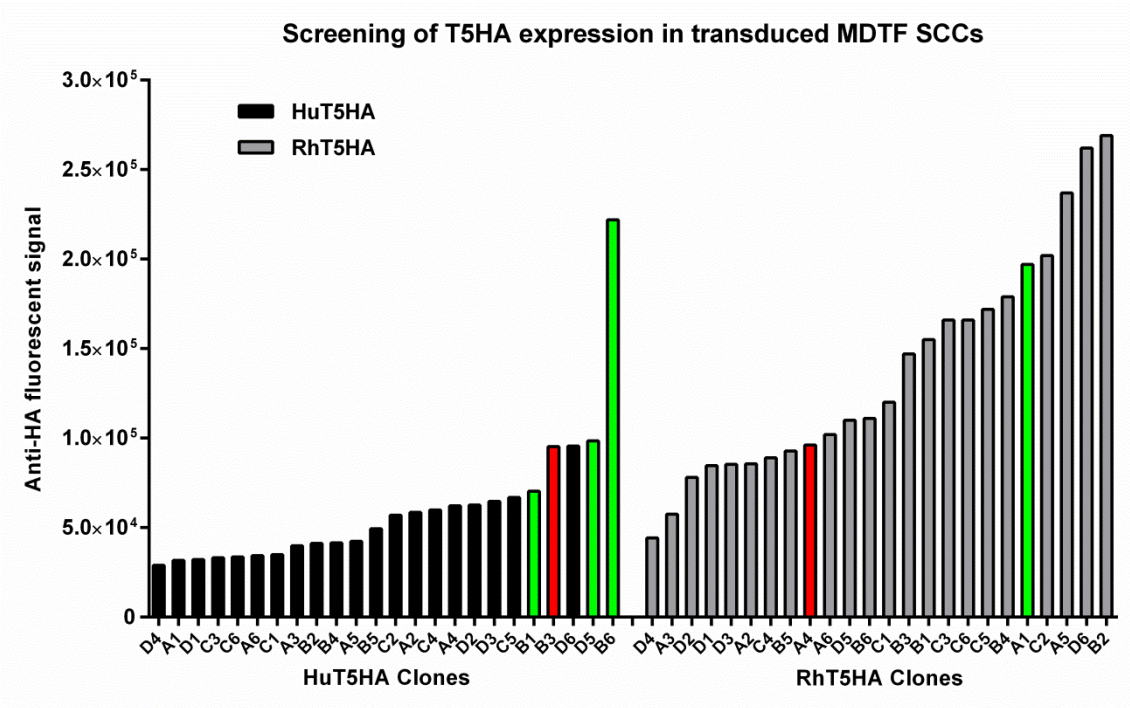

Figure 5.1 Screening of MDTF SCCs expressing human and rhesus T5HA

MDTF cells were transduced with LxIY vectors (EYFP-expressing version of LxIG) expressing either human or rhesus T5HA at high MOI (500µl per 12 well plate). SCCs were picked at limiting cell dilution. A lysate sample was prepared from each SCC and normalised by total protein concentration. The relative expression level of T5HA was analysed by LI-COR western blot using a monoclonal anti-HA primary antibody, and IRDye-800 conjugated secondary antibody. Signals at 800nm from T5HA bands were illustrated in the bar chart. SCCs with slow cell division are indicated by the green bars. The selected SCCs expressing HuT5HA and RhT5HA were indicated by the red bars.

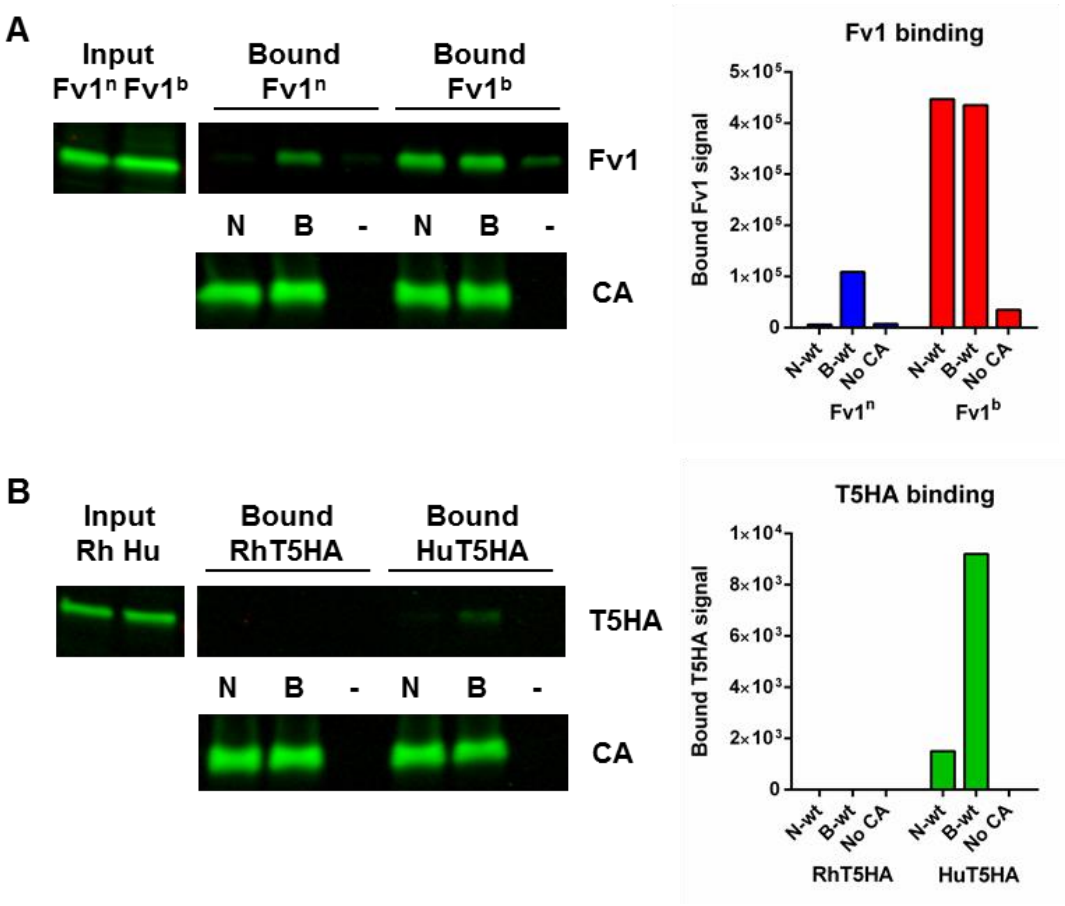

Figure 5.2 Binding of Fv1 and T5HA to MLV capsids

Cell lysate from SCCs expressing (A) Fv1 or (B) T5HA were used to binding assay against N-MLV and B-MLV using the microplate assay described in chapter 4 with 10µg/ml nanotubes. As a negative control, binding reactions were also carried out in the absence of CA. Fv1 was detected using an anti-Fv1 (#6689) antibody, T5HA was detected using an anti-HA antibody, and CA was detected using an anti-His antibody. An IRDye800-conjugated secondary antibody was used in all blots.

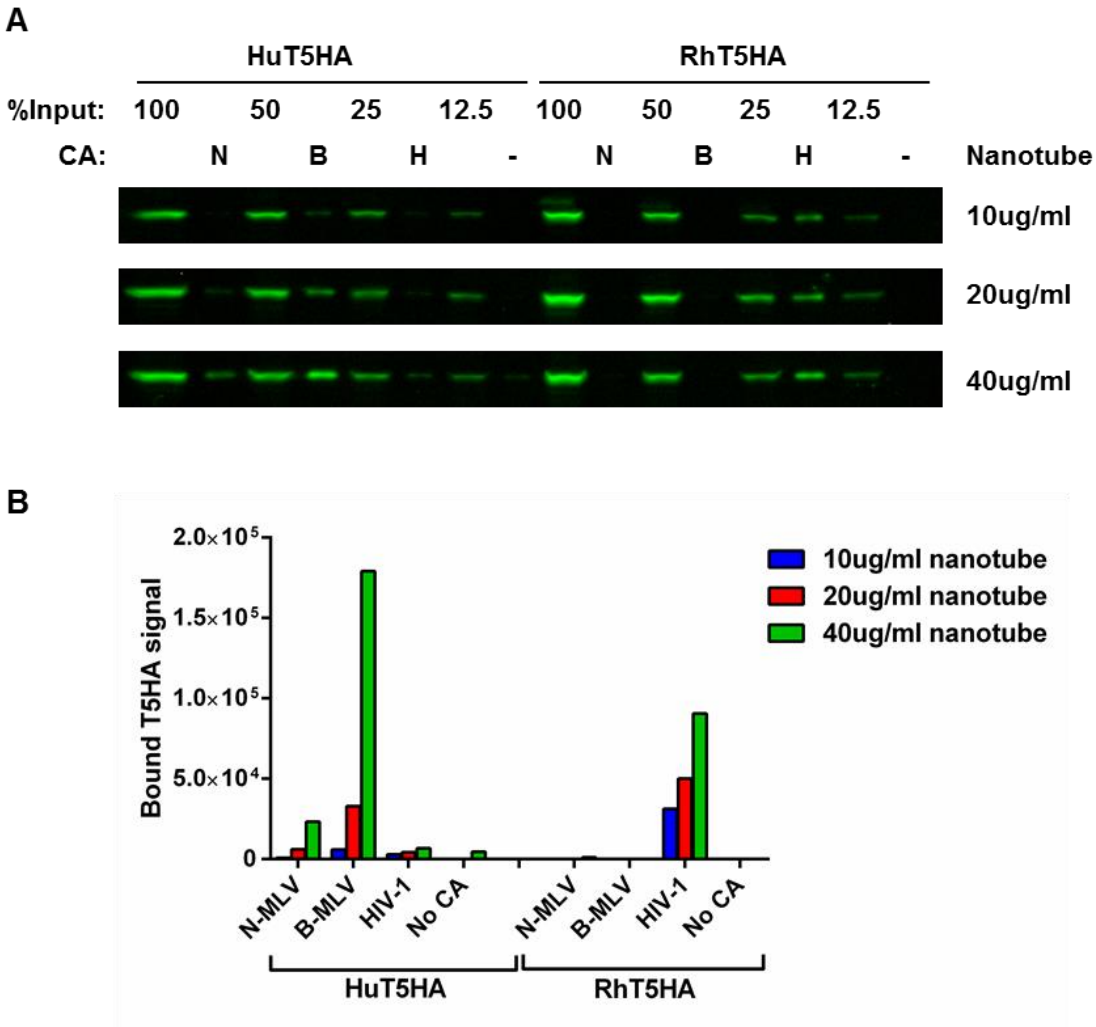

Figure 5.3 Binding of T5HA to MLV and HIV-1 capsids

(A) Lysate from SCCs expressing human or rhesus T5HA were tested for binding to nanotubes coated with N-MLV CA, B-MLV CA, HIV-1 CA-p2 or no capsids using the microplate assay. T5HA was detected by LI-COR western blot with anti-HA antibody. (B) The bound T5HA signals were illustrated in the bar chart.

A

Trim5α	N	B
HuT5	0.1 ± 0.05	0.9 ± 0.04
RhT5	0.3 ± 0.08	1.1 ± 0.01

Yap et al, 2005

B

Trim5α	N	B	NB
HuT5	0.07	0.57	1.22
RhT5	0.10	1.09	1.08
HuT5HA	0.10	0.84	1.11
RhT5HA	0.22	1.15	1.17

Table 5.1 Restriction phenotypes of T5 and T5HA

(A) Restriction data of HuT5 and RhT5 from a previous study (Yap et al., 2005). (B) Restriction data of HuT5, RhT5, HuT5HA and RhT5HA from this study. Restriction ratio of less than 0.3 is highlighted in black.

5.2 An attempt to generate hyperstable MLV cores for binding studies of T5 and Fv1

Since the binding of RhT5HA and HuT5HA to MLV CA nanotubes do not appear to reflect their interaction with MLV cores, it may be possible that T5 recognises some structures of N-MLV that is not present in capsid lattice formed on the lipid nanotubes *in vitro*, and the detection of specific binding of T5 to MLV may require purified cores. Unfortunately, successful purification of intact mature MLV cores has not been demonstrated. Although membrane envelope can be stripped from virions by incubation with mild detergents such as X-100, the use of such treatment followed by separation through equilibrium density gradient did not allow recovery of intact mature cores (Andersen, 2013; Fassati and Goff, 1999). Purification of HIV-1 cores had been achieved by ultracentrifugation of virion through a layer of detergent overlaid on a density gradient (Forshey and Aiken, 2003), but a previous attempt in our lab to use this method for extraction of intact MLV cores was unsuccessful (Dodding, 2006). The lack of previous success could be due to a low stability of MLV cores in the absence of the membrane envelope. One way to circumvent this difficulty could be by introducing mutations that enhance stability of MLV cores.

Based on the hexamer structure of HIV-1 CA, a previous study screened for pairs of cysteine mutations which could lead to crosslinking between purified CA monomers through introduction of disulphide bonds (Pornillos et al., 2010). Pairs of cysteine mutations were introduced at residues in close proximity with each other between helix 1 (H1), helix 2 (H2) and helix 3 (H3). Two particular mutants, A14C/E45C and A42C/T54C, showed strong stabilisation of capsid hexamer (Figure 5.4). The introduction of additional mutations W184A/M185A to destabilise CTD-CTD interaction allowed the purification of soluble hexamers, from which crystal structures had been determined (Pornillos et al., 2010). Enrichment of capsid hexamers could also be observed in HIV-1 vector virions harbouring A14C/E45C mutations (Meng et al., 2012). Therefore, we hypothesised that similar double cysteine mutations might stabilise the mature MLV core, allowing purification on equilibrium density gradients. The

work described in this section was carried out in collaboration with Ophélie Cosnefroy (Kate Bishop's lab, Division of Virology, NIMR), and her contributions to this work are clearly stated in the figure legend.

5.2.1 Design of N-MLV double cysteine mutants

Figure 5.5 shows an alignment between capsid sequence of N-MLV and HIV-1. The first approach of selecting residues for cysteine mutations would be to identify the equivalent positions of the HIV-1 A14C/E45C and A42C/T54C mutations on the MLV CA structure. Unfortunately, the equivalent of A14 in N-MLV CA would be P14, and the mutation of a proline is not desirable as it often leads to changes in protein structure (Ian Taylor, personal communication). The equivalent for the A42C/T54C mutations in N-MLV would be S43C/Q57C. Cysteine mutations were introduced to pairs of residues among H1, H2 and H3 with less than 6Å distance between beta-carbons (Cβ) in the screening of HIV-1 crosslinking mutants, and this Cβ-Cβ distance was suggested as the optimal spacing for the formation of disulphide bonds between cysteine residues (Pornillos et al., 2010). Table 5.2 summarises the mutants tested and the distance between mutated residues. Apart from S43/Q57, four other pairs of residues including S17/D19, S17/N22, Y21/N26 and T46/D53 were also within the 6Å distance and were included in the screen. It was anticipated that some double mutants could have defects in virus production or proteolytic processing, and therefore not suitable for generation of hyperstable cores for studying restriction factor binding. To maximize the chance of success, additional mutants were picked by selecting the next closest residues to Q57 and D53, leading to the selection of V44/Q57, T47/Q57 and T46/D53. Finally, two pairs of distant residues with Cβ-Cβ distance over 10Å, Y21/N27 and H48/Q57, were selected as negative controls. The locations of these 10 double mutations were shown in Figure 5.6 and Figure 5.7. While 4 mutants were selected for H1-H1 crosslinking, 6 mutants were selected for H2-H3 crosslinking.

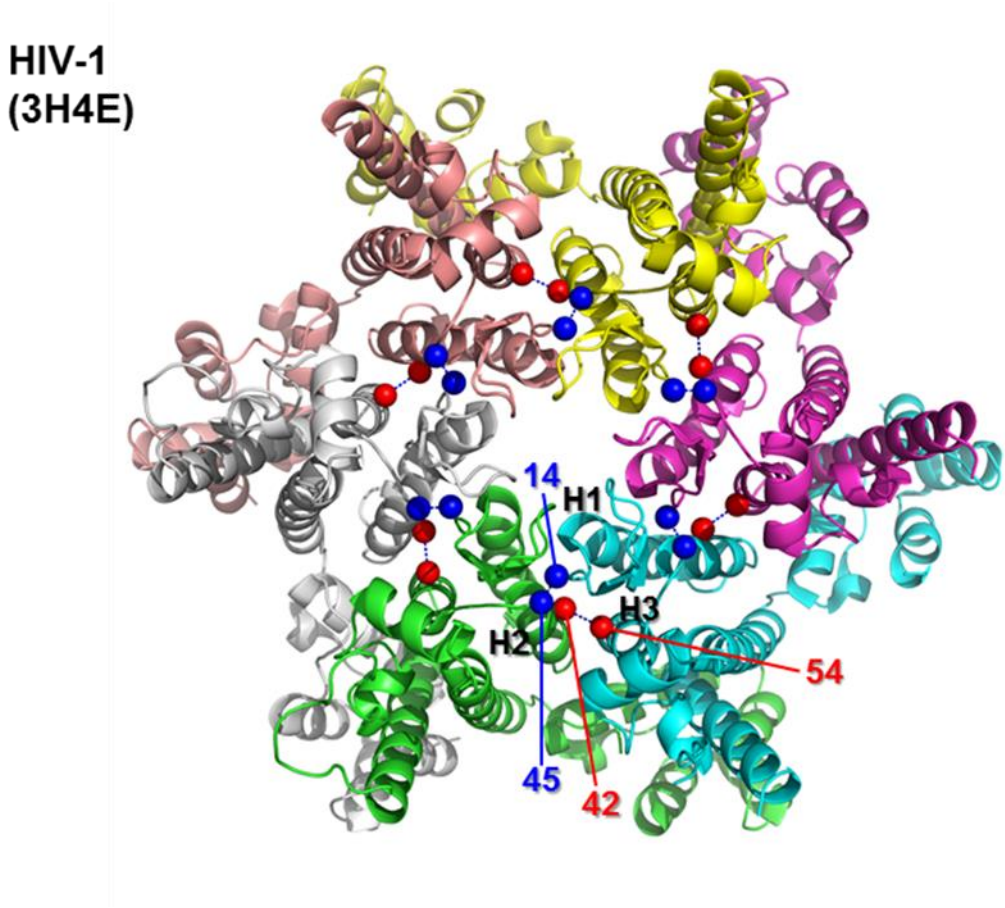

Figure 5.4 Double-cysteine mutations of HIV-1 CA

The two pairs of double-cysteine mutations that had been previously described to stabilise the capsid hexamer of HIV-1 *in vitro* (Pornillos et al., 2010) were illustrated on the hexamer structure of HIV-1 capsid (PDB: 3H4E) (Pornillos et al., 2009). The positions of A14C/E45C mutations were labelled with blue spheres, while the positions of A42C/T54C mutations were labelled with red spheres.

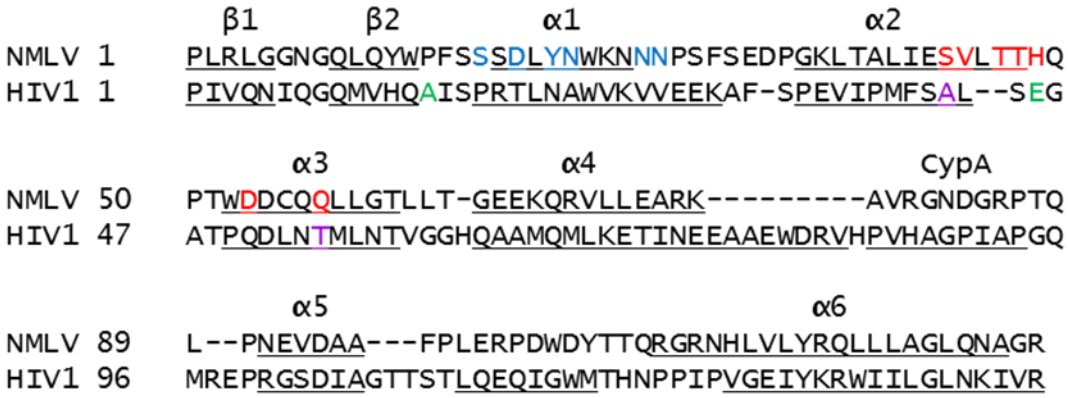

Figure 5.5 Alignment of N-MLV and HIV-1 CA sequence

Amino acid sequences of N-terminal domains of N-MLV and HIV-1 CA were aligned based on the secondary structure, modified from Mortuza et al, 2004. Positions of alpha helices, beta-sheet and cyclophilin-binding loop (labelled as CypA) were indicated by underlined residues. Mutated residues in the HIV-1 A14C/E45C and A42C/T54C capsid mutants (Pornillos et al., 2010) were coloured in green and purple, respectively. Residues mutated in this study for H1-H1 crosslinking were coloured in blue. Residues mutated for H2-H3 crosslinking of N-MLV CA were labelled in red.

Helices	Mutations		Cβ-Cβ distance	Higher Order complex
H1-H1	S17C	D19C	4.6Å	+
H1-H1	S17C	N22C	4.2Å	+
H1-H1	Y21C	N26C	6.0Å	-
H1-H1	Y21C	N27C	10.9Å	-
H2-H3	S43C	Q57C	5.5Å	Not tested
H2-H3	V44C	Q57C	8.6Å	(+)
H2-H3	T47C	Q57C	6.8Å	+
H2-H3	H48C	Q57C	10.6Å	-
H2-H3	S43C	D53C	6.4Å	Not tested
H2-H3	T46C	D53C	4.9Å	Low yield

Table 5.2 Summary of N-MLV double cysteine mutations

Site-directed mutagenesis of pCIG-N for production of N-MLV vectors with double cysteine mutations were carried out jointly with Ophélie Cosnefroy. All mutants which included the Q57C mutation were constructed by Ophélie Cosnefroy, while other mutants were constructed by me. Distances between Cβ were measured using the published crystal structure of N-MLV hexamer (PDB: 1U7K) (Mortuza et al., 2004).

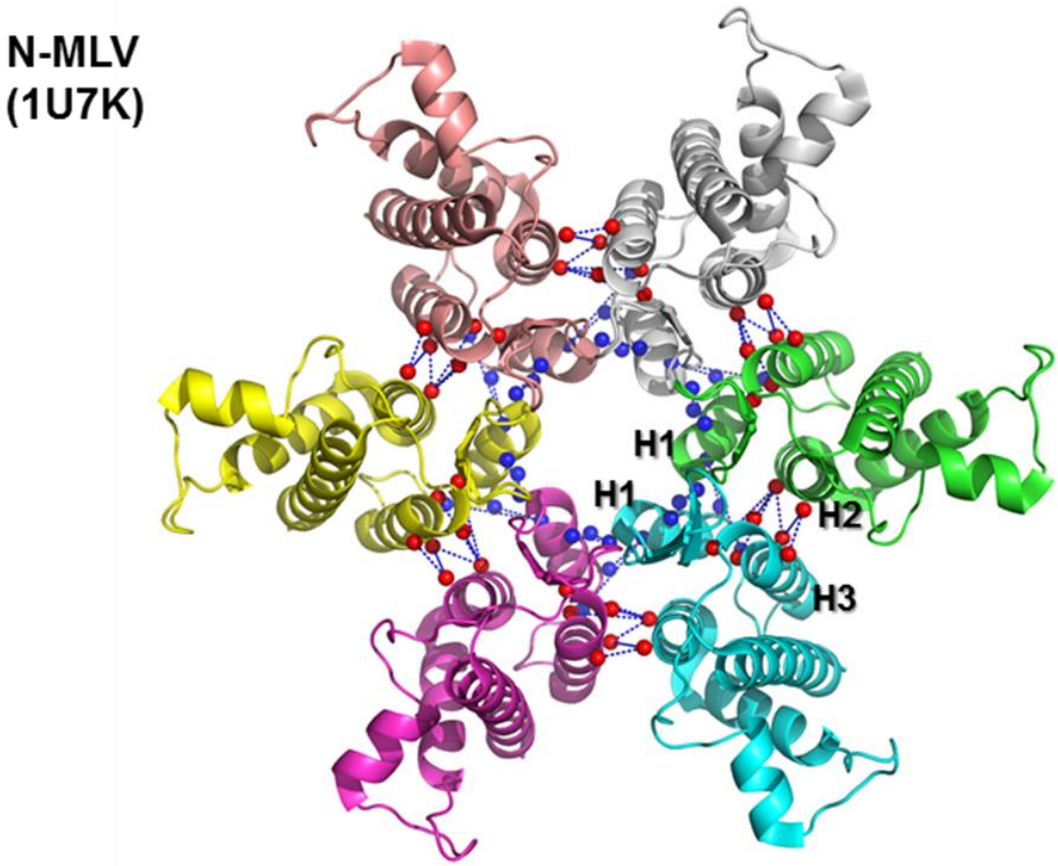

Figure 5.6 Positions of double cysteine mutations on N-MLV CA hexamer

Double cysteine mutations listed in table 5.2 were illustrated on the crystal structure of N-MLV CA hexamer (PDB: 1U7K) (Mortuza et al., 2004). Mutations for H1-H1 crosslinking were represented by blue spheres and dotted lines. Mutations for H2-H3 crosslinking were shown by red spheres and dotted lines.

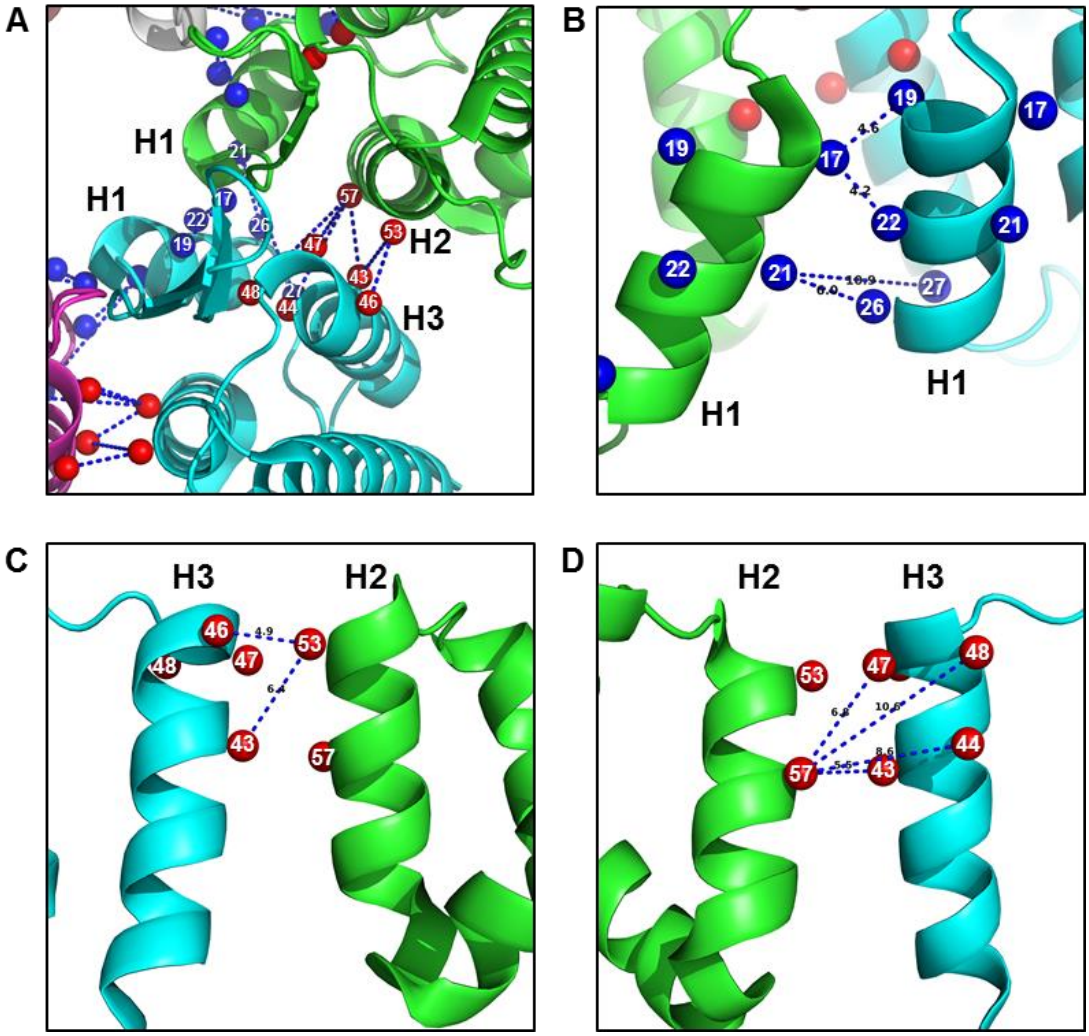

Figure 5.7 Magnified view of N-MLV double cysteine mutations

(A) A magnified view of the structure in Figure 5.6 of showing pairs of residues mutated for crosslinking. (B) A magnified view of mutations selected for H1-H1 crosslinking. (C-D) Magnified views of mutations selected for H2-H3 crosslinking.

5.2.2 Screening of N-MLV double cysteine mutants for CA crosslinking in virions

Before the screening of N-MLV double cysteine mutants, I first tested whether crosslinking of HIV-1 A14C/E45C mutant could be detected by non-reducing western blot analysis (Figure 5.8). A slow migration band with size expected from a CA hexamer (180kDa) was observed with the A14C/E45C mutant but not wt HIV-1 in non-reduced samples. Based on the fluorescent signals from CA bands, about 50% of CA was crosslinked as hexamers. Only CA monomers were detected in presence of reducing agent. Therefore, this method appeared to be effective in screening crosslinking within virions.

Site-directed mutagenesis was first performed to generate single and double mutants with the S43C/Q57C mutations. Surprisingly, western blot analysis of CA in wt and mutant virions under reducing condition showed that a band with high molecular weight was found in all mutants with the S43C mutation (Figure 5.9). Since all disulphide bonds between crosslinked CA multimers would be reduced by the presence of β-mercaptoethanol, the band with high molecular weight would most likely be unprocessed p65-gag polyprotein. This suggested that the S43C mutation could have led to a defect in proteolytic processing of gag (Figure 5.9). We therefore excluded S43C/Q57C and S43C/D53C from later studies.

I then analysed CA from MLV virions of other mutants by western blot under reducing or non-reducing conditions (Figure 5.10). From the analysis of non-reduced samples, S17C/D19C, S17C/N22C, T47C/Q57C, and to less extent V44C/Q57C mutants showed bands at high molecular weight exceeding 180kDa. For S17C/D19C, T47C/Q57C and V44C/Q57C mutants, CA signals could be detected even above 300kDa. A 60kDa band was detected for four single mutants S17C, N22C, Y21C and N26C, most likely reflecting the formation of CA dimer. A band with molecular weight just below 70kDa could be observed in both reducing and non-reducing samples of S17C/D19C, Y21C and V44C/Q57C. Similar to the earlier observation with the S43C mutant, this band would most likely represent unprocessed p65gag polyprotein. Despite two

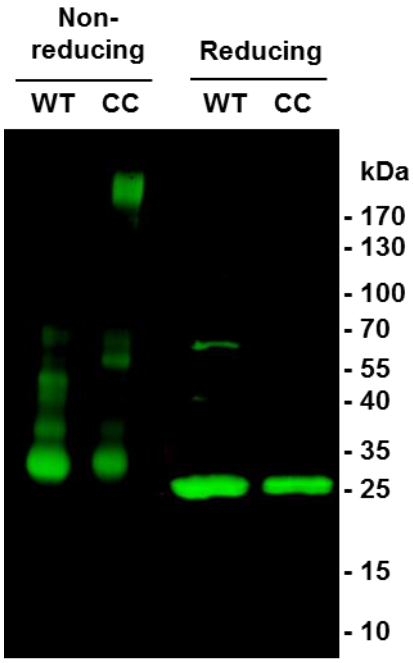

Figure 5.8 Western blot analysis of HIV-1 virion with A14C/E45C mutations

HIV-1 virions of WT and A14C/E45C (CC) mutant were generated by transient transfection in 293T cells. Virions were pelleted by ultracentrifugation, and analysed by SDS-PAGE with or without 2% β-mercaptoethanol in loading buffer. The western blot was carried out with a monoclonal anti-p24 primary antibody and an IRDye800-conjugated secondary antibody.

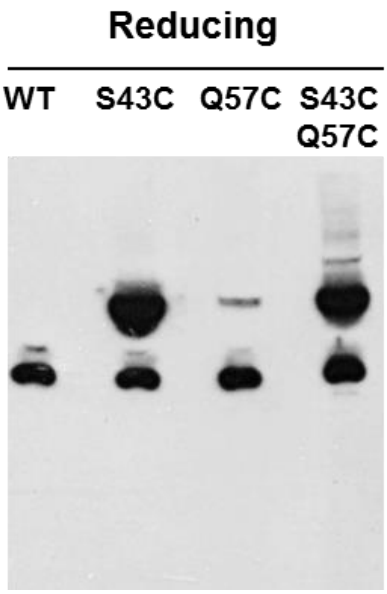

Figure 5.9 Reducing western blot analysis of N-MLV S43C/Q57C mutant

Ophélie Cosnefroy carried out both mutagenesis and reducing western blot analysis shown in this figure. N-MLV virions produced by transient transfection of 293T cells were pelleted and analysed by western blot under reducing conditions. CA western blot was performed using a monoclonal anti-CA antibody.

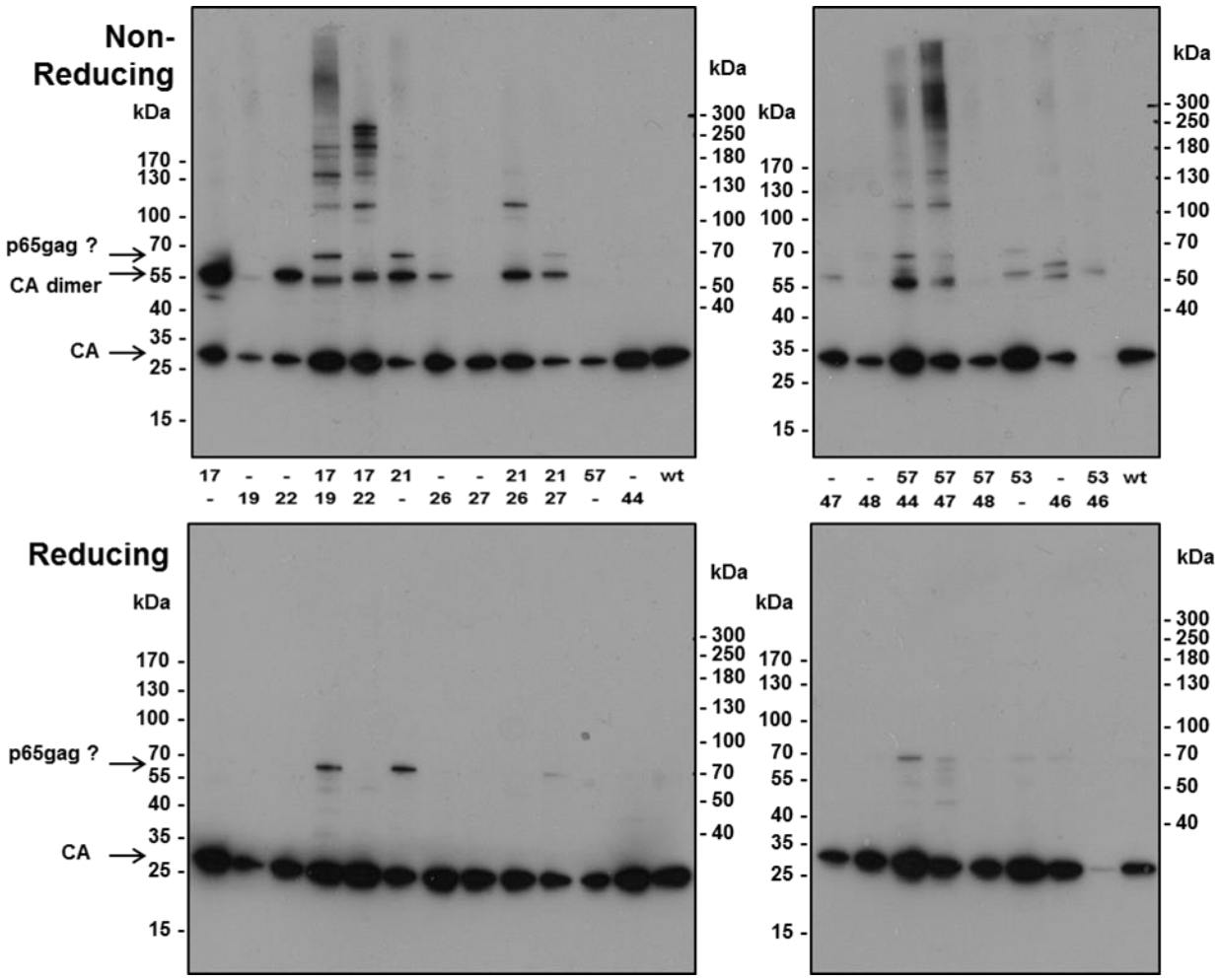

Figure 5.10 Screening of N-MLV double cysteine mutations

I carried out screening of CA crosslinking in virions using mutants constructed by me and Ophélie Cosnefroy. Virions were produced by transient transfection of 293T cells and pellet by centrifugation. Samples were analysed by SDS-PAGE with or without 2% β-mercaptoethanol in loading buffer. Western blots were carried out with a monoclonal anti-p30 primary antibody and an HRP-conjugated secondary antibody.

attempts, very low amount of CA could be detected from virion samples of T46C/D53C. From this screen, S17C/N22C and T47C/Q57C mutants (illustrated in Figure 5.11) appeared to allow formation of large crosslinked CA complex without noticeable defect in gag processing. These mutants were characterised in detail in later studies.

5.2.3 MLV mutants with crosslinked cores were non-infectious and defective in reverse transcription

The infectivity and reverse transcription of the two selected double cysteine mutants were studied in detail by Ophélie Cosnefroy. Figure 5.12 shows the infectivity data. The S17C/N22C double mutant was found to be non-infectious, and so were the single mutants S17C and N22C. The T47C/Q57C appeared to have very low infectivity, while single mutants T47C and Q57C had infectivity comparable to wt N-MLV. Figure 5.13 shows the quantification of early (strong stop) and late (second strand) RT products. Compared to wt N-MLV, both S17C/N22C and T47C/Q57C showed 3-log decreases in quantity of both strong stop and second strand DNA, suggesting strong impairment before reverse transcription of both mutants.

5.2.4 Crosslinked MLV cores failed to abrogate T5 and Fv1 restriction

Since the goal of this project was to compare binding of Fv1 and T5 to the same hyperstable MLV core, it was important that cores with the selected double cysteine mutations could be recognised by Fv1 and T5. The recognition of capsid core by a restriction factor could be tested using an abrogation assay (Duran-Troise et al., 1977). In a typical assay, cells are first treated with abrogating virus at a high MOI, followed by the infection of a second tester virus that is normally restricted by the restriction factor. If the abrogating virus is recognised by the restriction factor, it leads to saturation of restriction factor in the cell and therefore allows infection of the tested virus. If the abrogating virus is not recognised by the restriction factor, the tester virus will be restricted. I compared the ability of wt B-MLV, wt N-MLV, S17C/N22C N-MLV and T47C/Q57C N-MLV to abrogate restriction of endogenous HuT5 in TE671 cells

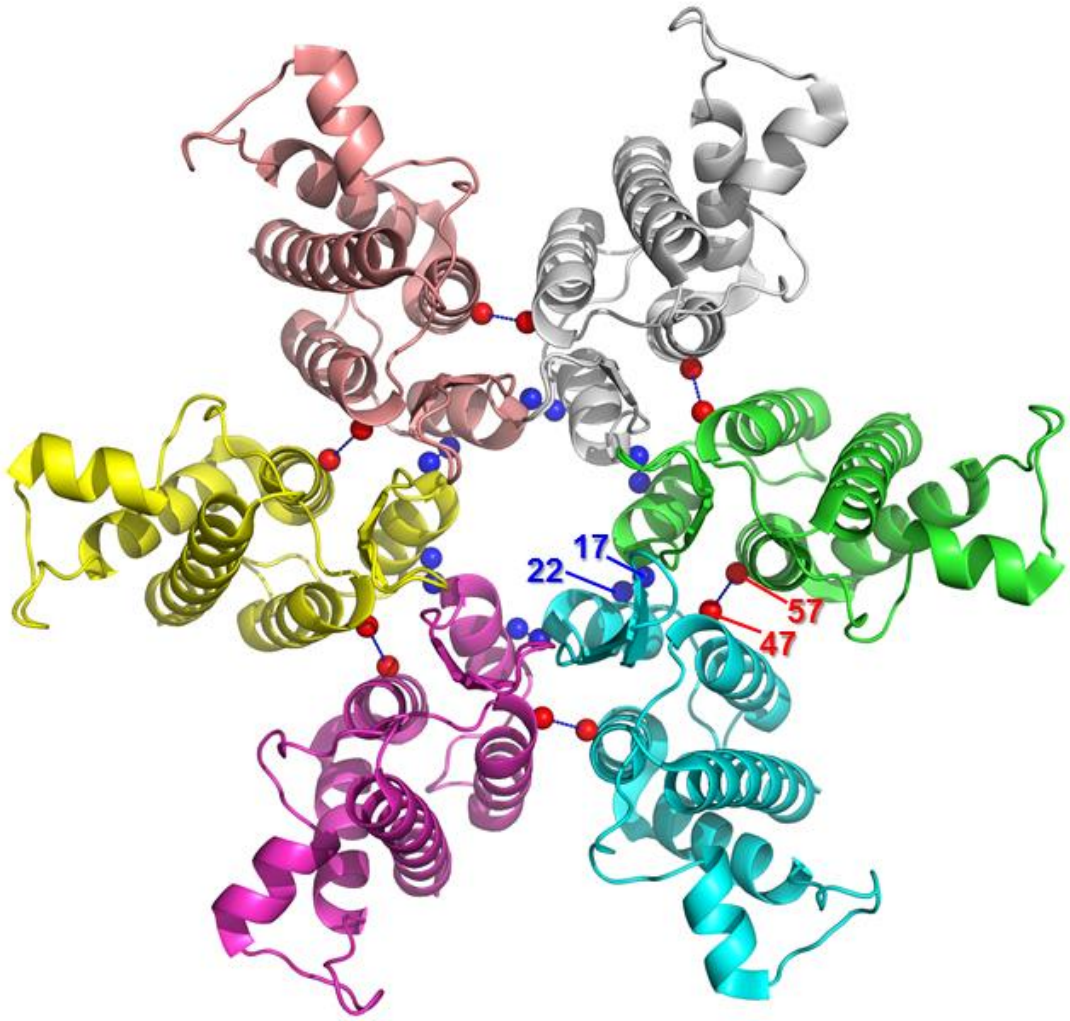

Figure 5.11 Locations of S17C/N22C and T47C/Q57C on N-MLV CA hexamer

The two selected double cysteine mutants, S17C/N22C (blue) and T47C/Q57C (red), were labelled on the hexamer CA structure of N-MLV.

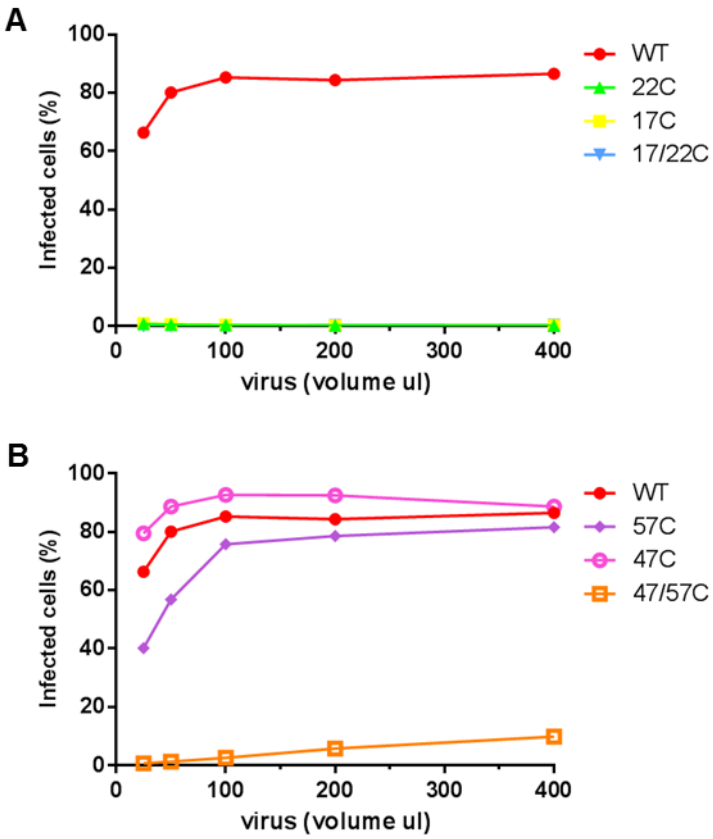

Figure 5.12 Infectivity of N-MLV mutants S17C/N22C and T47C/Q57C

The infectivity assay was carried out by Ophélie Cosnefroy. D17 cells were infected with different volume of GFP-expressing tested virus with wt, or mutant N-MLV capsid sequence. The percentages of GFP^+ cells were measured by FACS analysis.

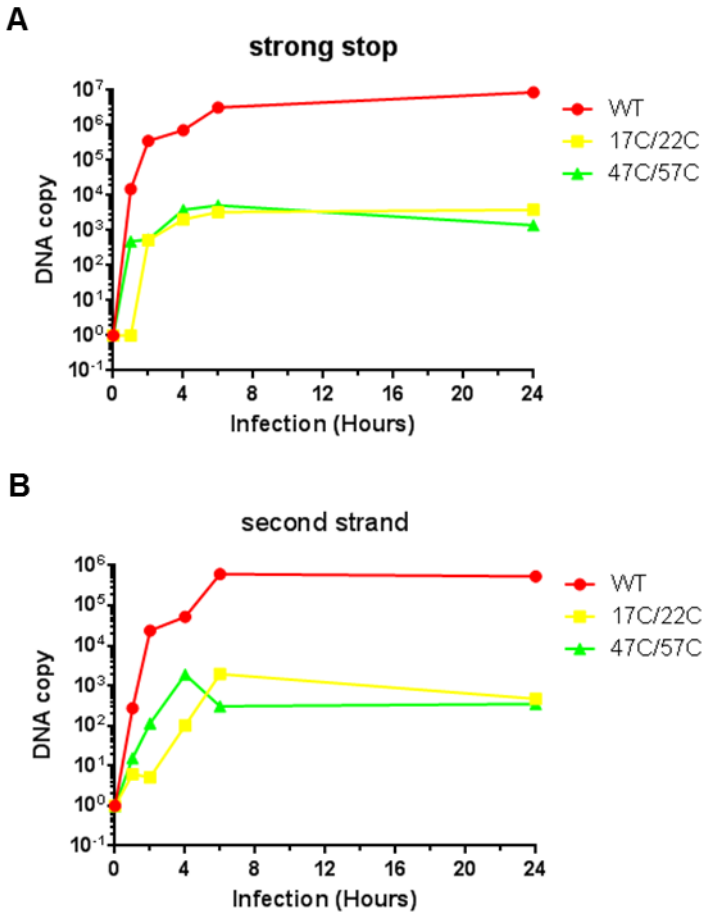

Figure 5.13 Reverse transcription by N-MLV mutants S17C/N22C and T47C/Q57C

The quantification of early and late reverse transcription products was carried out by Ophélie Cosnefroy. D17 cells were infected with different volume of GFP-expressing tested virus with wt, or mutant N-MLV capsid sequence. The strong stop and second strand viral DNA products were detected using quantitative PCR.

and of endogenous $Fv1^b$ in B-3T3 cells (Figure 5.14). Similar to B-MLV, neither of the double cysteine N-MLV mutants was capable of abrogating restriction by HuT5 or $Fv1^b$. The abrogation of $Fv1^b$ appeared to be more difficult than of T5, restriction was relieved by just 3% even with the highest amount of N-MLV abrogating virus. These results suggested that the S17C/N22C N-MLV and T47C/Q57C crosslinking mutants were not recognised by Fv1 and T5, and would not be suitable for studying binding of these restriction factors to MLV cores.

5.3 Discussion

This chapter described attempts to study binding of T5 to MLV capsid through two different approached. Unfortunately, while the binding of T5 to MLV CA nanotubes does not appear to reflect the binding specificity of T5 to MLV core detected from abrogation assays, crosslinked MLV cores with double cysteine mutations were recognised by neither Fv1 nor T5.

Using the microplate binding assay, HuT5 appeared to bind more strongly to the non-restrictive B-MLV than to the restrictive N-MLV, and this result is reproducible. This result resembles the finding that Fv1bnb binds to B-MLV nanotubes but does not restrict B-MLV even when over-expressed. Abrogation studies showed that HuT5 restriction is abrogated by N-MLV but not B-MLV (Towers et al., 2002), suggesting that at the endogenous level T5 recognises N-MLV but not B-MLV. Therefore, the recognition of CA nanotubes by HuT5HA under the conditions of the binding assay may be different from the recognition of the capsid shell on the mature MLV cores at an endogenous HuT5 concentration. However, HuT5HA and HuT5 may possess some weak apparent affinity towards B-MLV CA, since both HuT5HA and HuT5 appear to weakly inhibit B-MLV when over-expressed using the LxIY vector, a variant of LxIG vector which expresses EYFP instead of EGFP (Table 5.1). The high concentration of B-MLV CA used in the binding assay may allow the detection of this weak binding.

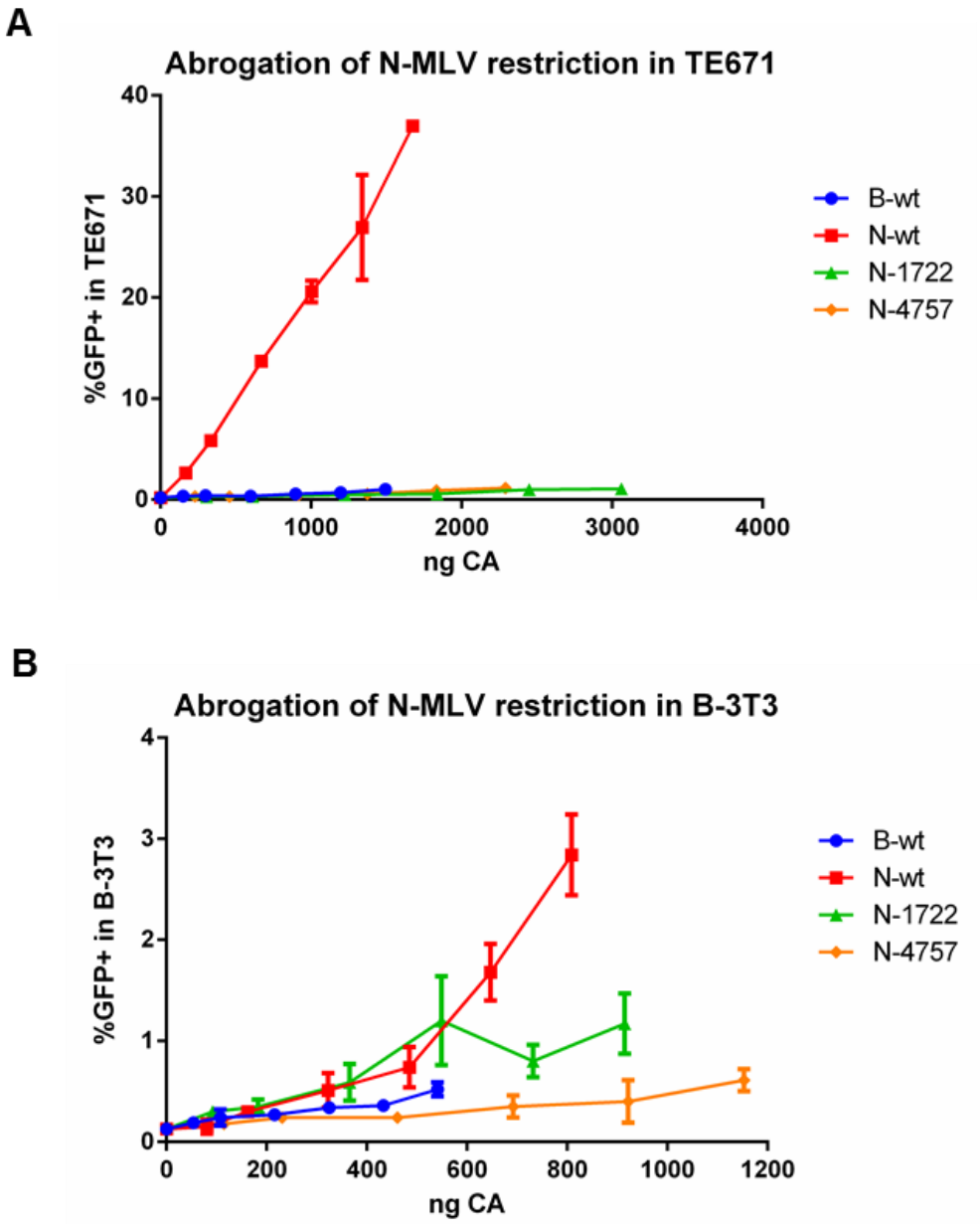

Figure 5.14 Abrogation of Fv1 and Trim5α restriction by double cysteine mutants of N-MLV

(A) Abrogation of human Trim5α restriction in TE671 cells. TE671 cells in 12 well plates were incubated with various amount of abrogating particles with LacZ-expressing genome and capsid sequence from B-MLV, N-MLV, N-MLV S17C/N22C mutant or N-MLV T47C/Q57C mutant. After 3h incubation, cells were infected with N-MLV tester virus containing a GFP-expressing genome. The percentage of GFP^+ cells in each sample was determined at 72hpi by FACS analysis. The amount of CA in each sample of abrogating particle was determined by quantitative western blot using a monoclonal anti-p30 primary antibody, an IRDye800-conjugated secondary antibody, and purified CA standards of known concentrations. Data from triplicate samples from the same experiment is shown. (B) Abrogation of $Fv1^b$ restriction in B-3T3 cells. The abrogation assay was carried out in the same way as (A) except it was performed on 24 well plates.

It was also surprising that despite the fact HuT5 restriction is abrogated by N-MLV but not B-MLV (Dodding et al., 2005; Towers et al., 2002), the HuT5HA appeared to show stronger binding to B-MLV than N-MLV CA nanotubes. First, it is possible that the high concentration of restrictive N-MLV capsid in the binding reaction could have triggered proteasomal degradation of HuT5HA *in vitro*. A previous study had demonstrated that infection of cells expressing HuT5 with N-MLV but not B-MLV at high MOI could induce proteasomal degradation of HuT5 (Rold and Aiken, 2008). However, since the proteasomal degradation of RhT5 by HIV-1 infection at high MOI had also been reported in the study, it is hard to comprehend how this effect could only affect binding of HuT5 to N-MLV but not RhT5 to HIV-1. Future binding experiments carried out in the presence of proteasome inhibitors could test whether N-MLV causes T5 degradation. Secondly, it is also possible that the presence of RhT5 and HuT5 leads to disruption of the N-MLV CA lattice on lipid nanotubes, which in turns disrupt the binding of T5 to the CA lattice. The disruption to HIV-1 CA-NC tubes by lysate containing RhT5 has been demonstrated *in vitro* (Black and Aiken, 2010; Zhao et al., 2011), and similar disruption to N-MLV CA nanotube could occur. However, it is important to point out that despite this reported CA disruption activity, binding of RhT5 to HIV-1 CA-NC tubes has been observed in many studies (Kar et al., 2008; Kim et al., 2011; Langelier et al., 2008; Li et al., 2006b; Li et al., 2006c; Liberatore and Bieniasz, 2011; Lienlaf et al., 2011; Stremlau et al., 2006; Yang et al., 2014), suggesting that the disruption to the CA-lattice by RhT5 does not prevent the detection of RhT5 binding. Therefore, the potential disruptions to N-MLV CA nanotubes by RhT5HA is unlikely to prevent the detection of RhT5HA binding to N-MLV CA nanotubes. Lastly, it is possible that the binding of T5HA to N-MLV cores require a structure that is not present on the N-MLV CA lattice of lipid nanotubes. For example, the inter-hexameric spacing of the CA lattice found on nanotubes is different from that of mature cores. As a result, the binding specificity of T5HA to CA nanotubes may not reflect the binding specificity of T5HA to MLV cores.

Two pairs of double cysteine mutations, S17C/N22C and T47C/Q57C, were able to form crosslinked CA complexes when introduced to virions of N-MLV. The crosslink patterns of the two double mutants appeared to be different. The S17C/N22C mutant showed a ladder pattern of distinct bands up to 250kD, which resembles the phenotypes of many HIV-1 mutants with double cysteine mutations designed for the crosslinking between H1 of adjacent monomers (Meng et al., 2012; Pornillos et al., 2010). The T47C/Q57C mutant showed a "smeared" pattern at high molecular weight above 250kD rather than distinct bands. This suggested that the T47C/Q57C mutant could form large aggregates with crosslinking between multiple hexamers. 6 major bands could be observed for the S17C/N22C mutant, which could represent multimers of CA formed with 1 to 6 monomers. Since H1 is present close to the central point of the CA hexamer, these mutations would not be expected to form inter-hexamer crosslinking. Formation of crosslinked dimer had been observed for many single cysteine mutations in H1, but not in H2 or H3. This is within expectations because in the hexameric CA structure, the same residues on H1 from adjacent monomers are in close proximity near the central pore to allow formation of disulphide bond. In contrast, same residues on H2 or H3 from adjacent monomers are well separated. Nevertheless, the formation of crosslinked dimer is sufficient to completely abolish the infectivity in single mutants. The formation of large irregular CA aggregates could explain why T47C/Q57C mutant was not recognised by Fv1 and T5. However, the crosslinked CA complexes observed for the S17C/N22C mutant appeared to be more regular, yet this mutant is unable to abrogate Fv1 and T5. It is possible that the introduction of disulphide bonds between monomers of CA-NTD leads to unpredictable structural changes, turning the core unrecognisable by restriction factors. Ongoing work carried out by Neil Ball (Ian Taylor's lab, Division of Molecular Structure, NIMR) will attempt to express and purify recombinant N-MLV CA protein with S17C/N22C and T47C/Q57C mutations for *in vitro* crosslinking and further structural work.

The HIV-1 A14C/E45C mutant forms hexamers exclusively as in purified CA protein, and in virion this mutant shows ladder pattern but with enrichment of a band corresponding to CA hexamer (Meng et al., 2012; Pornillos et al., 2010). Interestingly, in contrast to the N-MLV double cysteine mutants, this HIV-1 A14C/E45C mutant can abrogate RhT5 in Vero cells (Ophélie Cosnefroy, unpublished data). The equivalent mutation in N-MLV would be P14C/H48C, although as mentioned earlier that mutating a Pro residue may alter the structure of CA, future experiments should test if such mutations would generate particles recognisable by Fv1 and T5.

Chapter 6

Discussion

6.1 Over-expression of Fv1^b leads to restriction of NB-MLV and inhibition of B-MLV

An early study of N, B, and NB tropism showed some apparent differences in the restriction specificity of Fv1^b between cells endogenously expressing Fv1^b and cells transiently expressing Fv1^b delivered using a retrovirus vector (Bock et al., 2000). Restriction of N-MLV only was observed in cells expressing endogenous Fv1^b, while restriction of NB-MLV and inhibition of B-MLV was also observed in cells with vector mediated Fv1^b expression. A later study revealed that the vector-mediated expression level of Fv1 is higher than that in cells endogenously expressing Fv1 (Yap and Stoye, 2003). This led to the hypothesis that the gain of NB-MLV and B-MLV inhibition could be linked to a higher expression level of Fv1^b. This was followed up by a study which showed that at the low expression level mediated by the endogenous Fv1 promoter, Fv1^b appeared to restrict N-MLV only; while at the high vector-mediated expression level, Fv1^b also appeared to restrict NB-MLV and inhibit B-MLV (Felton, 2012). It also showed that further increase in Fv1^b expression from an over-expression level leads to reduced NB-MLV and B-MLV infectivity, supporting a role of Fv1^b expression level in the inhibition of NB-MLV and B-MLV (Felton, 2012).

Chapter 3 in this thesis described the development of an assay to quantify the amount of Fv1 expressed in cells, and a novel inducible expression system which allow the study of Fv1 restriction from a very low level to an over-expression level. By correlating Fv1 protein level with restriction phenotype, it provided solid evidence that over-expression of Fv1^b leads to the restriction of NB-MLV and inhibition of B-MLV. It also confirmed an early observation that at

the endogenous level, the restriction of N-MLV is accompanied by a weak inhibition of NB-MLV (Bock et al., 2000). In contrast, no restriction of N-MLV and NB-MLV could be observed even at very high “super-expression” levels of $Fv1^n$. This suggested that while $Fv1^b$ is capable of recognising the cores of all three MLV strains, though with different apparent binding affinities, $Fv1^n$ does not recognise cores of N-MLV and NB-MLV at all.

6.2 Novel assays to compare the apparent binding affinities of restriction factors to retroviral cores

The combination of a novel inducible expression system with minimal leakiness and a two colour FACS assay described in Chapter 3 allows the study of the relationship between restriction and Fv1 expression level. The data presented in Chapter 3 on $Fv1^b$ and on wild mice Fv1 illustrated how this assay can be used to compare the relative binding affinity of Fv1 to different retroviral cores. The ability of expressing Fv1 or T5 at a low, saturable concentration may also allow the development of a new abrogation assay to binding of recombinant restriction factors to retroviral cores. Previously, all abrogation assays were carried out in cells endogenously expressing a restriction factor. Although recombinant restriction factors can be transiently expressed using the LxIG or LxIY vectors, the restriction factor is over-expressed in transduced cells and would require very high concentration of abrogating virus in order to achieve detectable saturation. By transducing MDTF cells with one of the new inducible vectors such as TYIx, recombinant restriction factors can be expressed at a low, saturable level. Pre-treatment of these cells with abrogating particles before infection with GFP tester virus, followed by incubation with a high dose of doxycycline would allow the detection of the loss of restriction in cells expressing the recombinant restriction factor. The YFP^- cells, which do not express the recombinant restriction factor, can also serve as an internal control showing what the infectivity of the GFP tester virus would be with a complete saturation of restriction factors. Such system would be particularly useful to study determinants of Fv1 and T5 which affect their binding to retroviral cores, by comparing the ability of viral cores to abrogate wt and mutant restriction factors.

6.3 Strong binding of CA may be necessary but not sufficient for Fv1 restriction

Many early attempts failed to demonstrate direct binding of Fv1 to monomeric CA (Dodding et al., 2005). This led to the hypothesis that Fv1 interacts with a polymeric form of CA, such as the CA lattice found on the capsid shell of mature MLV core. This was supported by evidence that abrogation of Fv1 restriction requires processing at both N-terminus and C-terminus of CA (Dodding et al., 2005). Subsequently, a binding assay was developed for studying the binding of Fv1 from cell lysate to regular array of MLV CA presented on the surface of functionalised lipid nanotubes (Hilditch et al., 2011). $Fv1^{n}$ binds to B-MLV CA nanotubes, but neither N-MLV nor NB-MLV CA nanotubes. The binding requires some structures present on the mature lattice such as a stable β-hairpin, which only forms after the processing at the N-terminus of CA (Kyere et al., 2008; Mortuza et al., 2004). The binding specificities of $Fv1^{n}$ and $Fv1^{nr}$ to MLV CA nanotubes appeared to correlate with their restriction specificities, concluded from binding experiments using many CA mutants. However, $Fv1^{b}$ appears to bind strongly to CA of N-MLV, B-MLV and NB-MLV presented on lipid nanotubes. Since $Fv1^{b}$ appears to display higher specificity at lower expression level, as discussed in the previous section, it was hypothesised that specificity of $Fv1^{b}$ binding to CA nanotubes may be observable only at low concentrations of Fv1.

Chapter 4 described the development of a medium-throughput binding assay which allows the comparison of the specificity of Fv1 binding to CA nanotubes using a range of Fv1 concentrations. However, in agreement to the previous study (Hilditch et al., 2011), $Fv1^{b}$ appears to bind to all MLV CA presented on lipid nanotubes even at the lowest concentration where bound $Fv1^{b}$ could be detected. Since endogenous $Fv1^{b}$ in B-3T3 cells could be abrogated by genome-deficient particles of N-MLV but not B-MLV (Boone et al., 1990), it is unlikely that this non-differential binding to CA nanotubes reflect the binding specificity towards MLV cores. However, the lack of $Fv1^{n}$ binding to N-MLV and NB-MLV CA nanotubes did correlate with the lack of N-MLV and NB-MLV restrictions even at very high $Fv1^{n}$ expression level. It is possible that presence of high concentration of CA and/or Fv1 in the binding reaction could

overcome some weak interactions such as $Fv1^b$ against B-MLV, but not very weak interactions such as $Fv1^n$ against N-MLV. Further binding studies of 10 Fv1 variants with various restriction phenotypes suggested a strong correlation between binding to CA nanotube and with the ability to restrict N-MLV and NB-MLV when over-expressed. However, Fv1bnb appears to bind B-MLV CA nanotubes but does not restrict B-MLV. These data suggested that *in vitro* binding to CA nanotube may represent an interaction that is required but insufficient for the binding to MLV core.

A model can be proposed to explain the findings in Chapter 3 and 4 regarding the binding and restriction specificities of $Fv1^n$ and $Fv1^b$, illustrated in Figure 6.1. $Fv1^n$ has a strong apparent affinity towards B-MLV CA, but very weak apparent affinities towards N-MLV and NB-MLV CA. At the endogenous concentration, $Fv1^n$ only binds and restricts B-MLV cores. $Fv1^b$ has a strong apparent affinity towards N-MLV CA, a moderate apparent affinity towards NB-MLV CA, and a weak apparent affinity towards B-MLV CA. At the endogenous concentration, $Fv1^b$ binds N-MLV cores strongly and binds NB-MLV moderately, leading to the restriction of N-MLV and the inhibition of NB-MLV. Even at over-expression level, $Fv1^n$ still only binds and restricts B-MLV cores. The high concentration of $Fv1^b$ overcomes the weaker apparent affinities of $Fv1^b$ to NB-MLV and B-MLV, allowing the restriction of NB-MLV and the inhibition of B-MLV. In the *in vitro* binding assay, the high concentrations of CA and/or Fv1 overcome the weaker apparent affinities of $Fv1^b$ to NB-MLV and B-MLV, allowing the detection of similar binding of $Fv1^b$ to CA nanotubes of all tropisms. However, the apparent affinities of $Fv1^n$ to N-MLV and NB-MLV are much weaker than those of $Fv1^b$ to NB-MLV and B-MLV, and cannot be overcome by the high CA and/or Fv1 concentrations used in the binding reaction.

6.4 The role of restriction factor multimerisation in CA binding

The ability to multimerise has been clearly demonstrated for T5 and TCyp. Like Fv1, the coiled-coil within the RBCC domain mediates the formation of an antiparallel T5 dimer (Goldstone et al., 2014). T5 dimers also form higher order

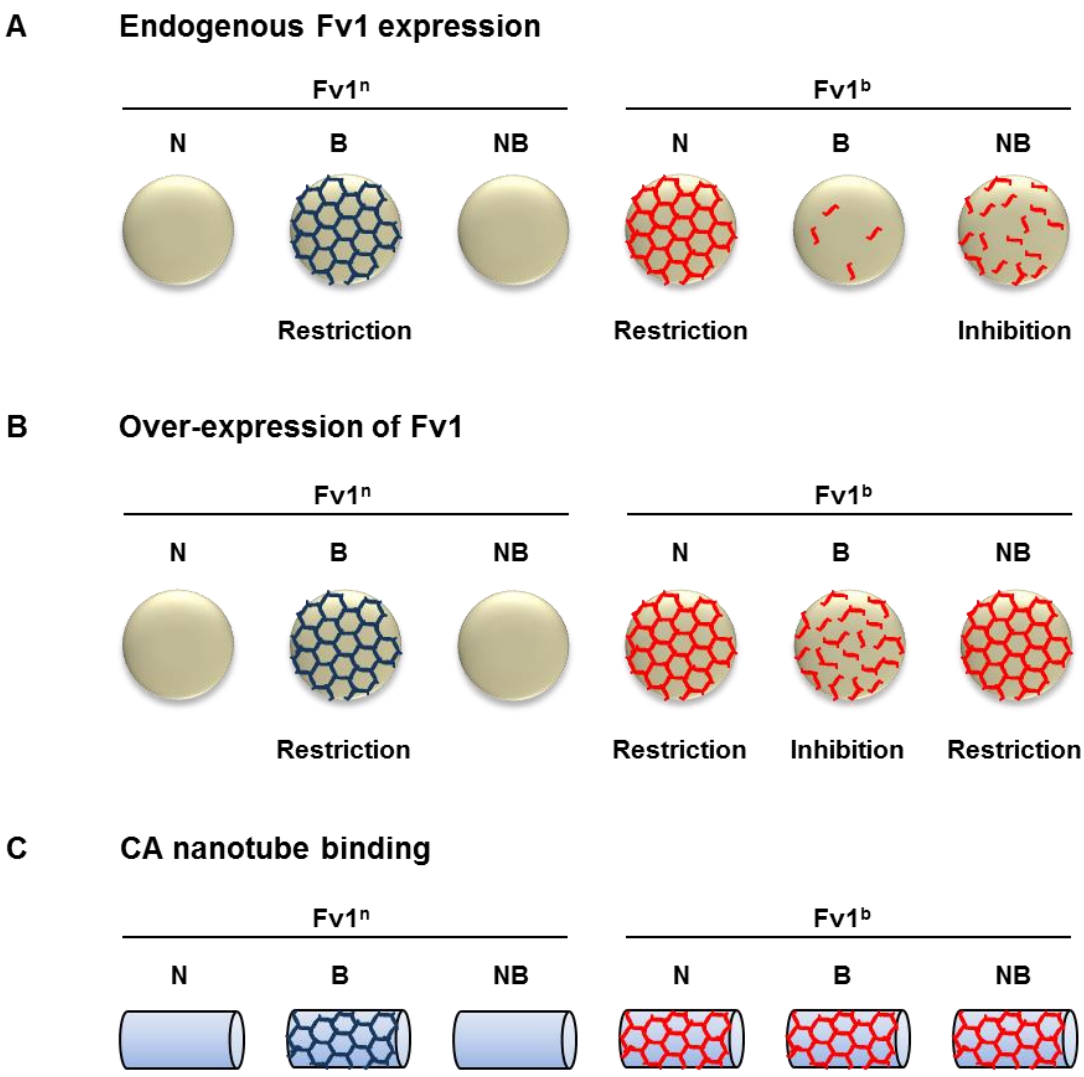

Figure 6.1 A model for Fv1 concentration, binding and restriction

(A) Binding and restriction by endogenously expressed Fv1. $Fv1^n$ has a strong apparent affinity towards B-MLV CA, but very weak apparent affinity towards N-MLV and NB-MLV CA. At the endogenous concentration, $Fv1^n$ only binds and restricts B-MLV cores. $Fv1^b$ has a strong apparent affinity towards N-MLV CA, a moderate apparent affinity towards NB-MLV CA, and a weak apparent affinity towards B-MLV CA. At the endogenous concentration, $Fv1^b$ binds N-MLV cores strongly and binds NB-MLV moderately, leading to the restriction of N-MLV and the inhibition of NB-MLV. (B) Binding and restriction by over-expressed Fv1. Even at over-expression level, $Fv1^n$ still only binds and restricts B-MLV cores. The high concentration of $Fv1^b$ overcomes the weaker apparent affinities of $Fv1^b$ to NB-MLV and B-MLV, allowing the restriction of NB-MLV and the inhibition of B-MLV. (C) Binding of Fv1 to CA nanotubes. The high concentrations of CA and/or Fv1 overcome the weaker apparent affinities of $Fv1^b$ to NB-MLV and B-MLV, allowing the detection of similar binding of $Fv1^b$ to CA nanotubes of all tropisms. However, the apparent affinities of $Fv1^n$ to N-MLV and NB-MLV are much weaker than those of $Fv1^b$ to NB-MLV and B-MLV, and cannot be overcome by the high CA and/or Fv1 concentrations used in the binding reaction.

assemblies, and studies of chemically crosslinked T5 mutants suggested that this requires the RING domain, the B-Box2 domain, the L2 region but not the B30.2 domain (Diaz-Griffero et al., 2009; Li and Sodroski, 2008; Liberatore and Bieniasz, 2011). The formation of higher order assembly correlates with stronger binding to HIV-1 CA-NC assemblies *in vitro* (Diaz-Griffero et al., 2009; Li and Sodroski, 2008; Liberatore and Bieniasz, 2011). The recombinant T5-21R protein with a Trim21 RING domain and a mutated B-Box2 domain which was found to self-assemble into a hexagonal super-lattice *in vitro*, has provided to the structural basis of T5 higher order self-association (Ganser-Pornillos et al., 2011). This T5 lattice has an inter-hexameric spacing of about 350Å, and would link across multiple CA hexamers on a CA lattice which has an inter-hexameric distance of less than 100Å (Ganser-Pornillos et al., 2011). The crystal structures of a soluble fragment of RhT5 comprising B-Box2, coiled coil and L2 (BCCL2) has been solved recently (Goldstone et al., 2014). BCCL2 forms an antiparallel dimer with the coiled-coil region forming a long rod, and one B-Box2 domain on each site of the rod. Since the B-Box and RING domain have been implicated in the higher order self-association of T5 (Diaz-Griffero et al., 2009; Li and Sodroski, 2008; Liberatore and Bieniasz, 2011), it is likely that each end of the rod interacts to link T5 dimers at the 3-fold symmetry axis of the T5 hexagonal lattice (Figure 6.2C) (Goldstone et al., 2014). Structural alignments between BCCL2 and the structure of RhT5 L2-B30.2 region suggested that the two B30.2 domains would be positioned at the centre of the T5 dimer (Goldstone et al., 2014; Yang et al., 2012). Therefore the B30.2 domains in the T5 super lattice would interact with a small number of CA monomers, and this was in agreement with the finding that TCyp only requires 25% of restriction-sensitive CA (Shi et al., 2013). The ability of T5 to form dimers and higher order assemblies suggest that the recognition of retroviral cores by T5 may involve avidity binding, where one T5 dimer binds across two CA hexamers, and the T5 hexagonal lattice binds to multiple sites on the CA lattice (Figure 6.2C). This avidity binding may involve positive cooperativity, for example binding of one B30.2 domain of a T5 dimer to CA lattice may make the binding of the second B30.2 domain to CA more favourable. The avidity binding of T5 is likely to enhance the observed apparent affinity of T5. The specific positioning of B30.2 domain on the T5 hexagonal lattice could also mean that

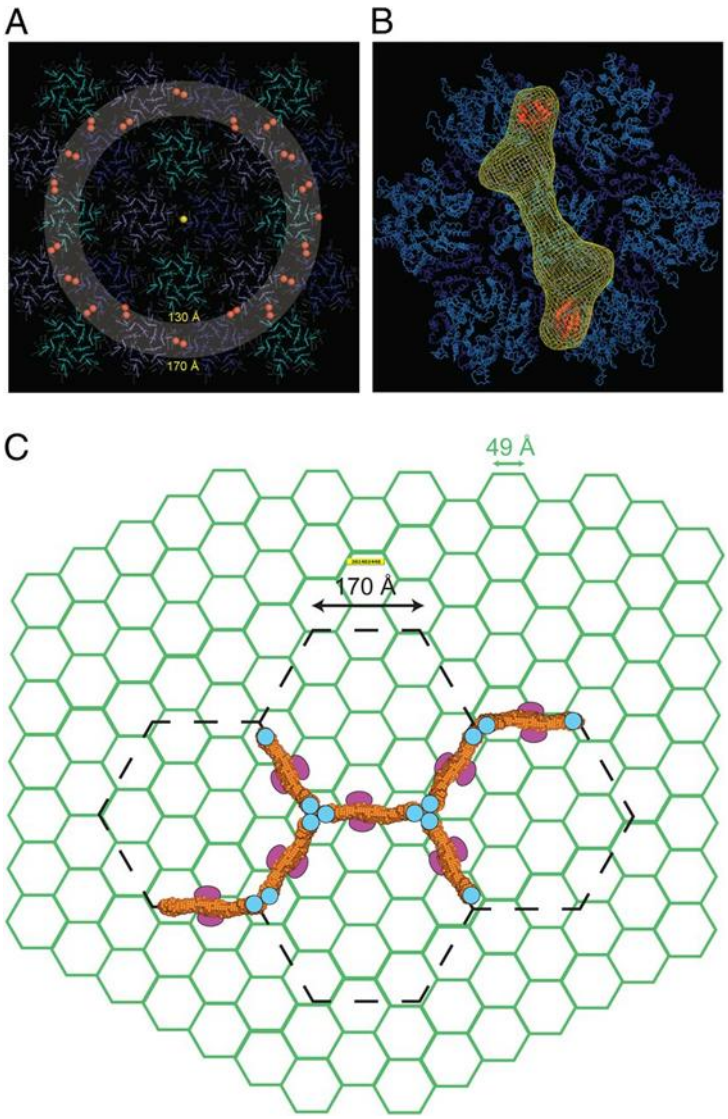

Figure 6.2 Interactions of Fv1Cyp and RhT5 to HIV-1 CA lattice

(A) A layer of HIV-1 CA lattice taken from PDB: 3J34. Red spheres mark the CypA binding loops and the gray region highlights those that are spaced at 130–170 Å from the central Cyp loop (yellow) and accessible to bind the second CypA of Fv1Cyp. (B) The SAXS envelope of Fv1Cyp dimer is positioned with one CypA domain located on the Cyp loop of a central hexamer and the second spaced between 140–150 Å located on the Cyp loop of an adjacent CA hexamer. (C) A schematic representation of the HIV-CA lattice (green) with the Trim5-21R lattice (Ganser-Pornillos et al., 2011) is overlaid as dashed lines (black). The SAXS model for the RhT5 (88–296) EK/RD dimer shown in orange surface representation has dimensions equating to the length of a single edge of the hexamer in the Trim5-21R lattice and sufficient to span adjacent hexamers in the CA lattice. The B-boxes are shown as cyan circles at the interface between Trim5α dimers and the B30.2 domains are represented by the magenta ovals toward the Trim5-21R twofold axis. Reproduced from the *Proceedings of the National Academy of Science* (Goldstone et al., 2014), with permission.

the CA lattice needs to be positioned in a certain way for avidity binding of T5 higher order assemblies, and the inter-hexameric distance between mature and immature lattice may affect this avidity binding.

Multimerisation of Fv1 has also been demonstrated before. Purified Fv1-NTD and the Fv1Cyp fusion protein are both found to be dimeric in solution (Bishop et al., 2006; Goldstone et al., 2014). The dimerisation of Fv1 is mediated by the coiled-coil region of the Fv1-NTD (Bishop et al., 2006). The fusion of CypA to Fv1-NTD, T5 RBCC, or other dimerisation domains such as the BAR domain, separated by a linker region, allows restriction of HIV-1 (Yap et al., 2007). This suggests that the dimerisation is essential for the recognition of retroviral core by Fv1 and T5. $Fv1^{n}$ but not $Fv1^{n}$-CTD binds to B-MLV CA nanotubes, suggesting that the dimerisation is necessary for Fv1 binding (Hilditch et al., 2011). The binding of Fv1Cyp and CypA to lipid nanotubes coated with C-terminally His-tagged CA-SP1 have been compared by surface plasmon resonance (SPR) analysis, and the apparent affinity of Fv1Cyp to HIV-1 CA lattice was found to be 18-fold higher than of CypA (Goldstone et al., 2014). This demonstrated how the avidity binding of Fv1 dimer to CA lattice can lead to a higher apparent affinity. Low resolution structures of Fv1-NTD and Fv1Cyp dimers have been recently determined by small-angle X-ray scattering (SAXS) (Goldstone et al., 2014). Fv1Cyp was found to contain two globular CypA domains 150Å apart, suggesting that the Fv1-NTD forms antiparallel dimer (Goldstone et al., 2014). Modelling of Fv1Cyp bound to the mature lattice of HIV-1 CA suggested that this interaction would involve binding of one Fv1Cyp to monomers of two CA hexamers (Figure 6.2 A-B) (Goldstone et al., 2014). A similar avidity binding interface would be expected between Fv1 dimer and MLV CA assay on the lipid nanotubes. Therefore, it is likely that the MLV CA lattice on lipid nanotubes allow binding of both Fv1-CTD on the same Fv1 dimer to CA, this may involve cooperative avidity binding in which binding of the first Fv1-CTD to CA lattice favours the binding of the second Fv1-CTD. In addition to dimerisation, crosslinking experiments in our lab have suggested a second multimerisation site within the Fv1-CTD which is sensitive to mutations at the MHR (Cécile Lemaître, unpublished data). The possession of two multimerisation sites could potentially allow the formation of higher order assemblies, similar to the hexagonal super-lattice observed for T5. Since in the

SAXS model Fv1Cyp, the capsid-targeting Fv1-CTD domain is placed on both ends of the dumb-bell shaped dimer (Goldstone et al., 2014), it may be possible for the Fv1-CTD of adjacent dimers to interact to form higher order assemblies. Therefore, like T5, the binding of Fv1 could involve avidity binding of dimers and higher order assemblies across multiple hexamers on the CA lattice.

Although the coiled-coil mediated dimerisation of Fv1 and T5 has been well characterised, future work should study the mechanism of Fv1 and T5 binding and should focus on the relationship between restriction factor multimerisation and the apparent binding affinity. In particular, it would be desirable to quantify and compare the contributions to the apparent binding affinity or restriction activity by the affinity between capsid-binding domain and CA monomer, the avidity due to dimerisation of restriction factor, and the avidity due to the formation of higher order assemblies. Using TCyp as a model system, one can compare the effects on restriction activity by mutations which modulate the binding affinity between CypA domain and CA such as D66N (Price et al., 2009), and by mutations which disrupt higher order assembly such as E120K/R121D in B-box2 (Diaz-Griffero et al., 2009) and deletion in the L2 linker region (Liberatore and Bieniasz, 2011). The use of new inducible vectors may allow better quantitation of the inhibitory effects of these mutations, while use of an abrogation assay with wt and mutant TCyp may allow the confirmation of the effects of mutations on the apparent binding affinity of TCyp. Similarly, the study of CypA D66N mutant of Fv1Cyp would also allow us to find out how much the affinity between the capsid-binding domain and CA contributed towards the interaction between a dimeric T5 protein and the CA lattice on viral core. Since the Fv1-CTD is probably involved in both CA binding and multimerisation, future work should also attempt to identify specific determinants in Fv1-CTD which affects multimerisation but not the affinity to CA.

6.5 Towards a common CA binding assay for Fv1 and T5

Since $Fv1^b$ and HuT5 both restrict N-MLV and show overlapping viral determinants for restriction (Bock et al., 2000; Ohkura et al., 2011; Ohkura and Stoye, 2013; Stevens et al., 2004), there has been strong interest in developing a system to compare the binding requirement for these two restriction factors to

N-MLV CA. Like Fv1, HuT5 can be abrogated by N-MLV (Towers et al., 2002), and abrogation requires the processing on both ends of MLV CA (Dodding et al., 2005). Binding of T5 to MLV CA nanotubes could not be detected in a previous study using the co-pelleting assay (Hilditch, 2010). Chapter 5 described another unsuccessful attempt to detect T5 to MLV CA nanotubes with the new microplate binding assay. It is possible that the avidity of T5 dimer to CA lattice on lipid nanotube is weak; the binding of T5 to core is more co-operative than Fv1 and is highly dependent on the correct inter-hexamer spacing of mature CA lattice. Since the low stability of MLV mature core prohibited the purification for binding study, the stabilisation of MLV core by introducing disulphide crosslinking was attempted. Two double cysteine mutants were found to form crosslinked CA without defects in gag processing. However, abrogation studies in cells endogenously expressing $Fv1^{b}$ and HuT5 suggested that the cores of these mutants do not form a structure that can be recognised by restriction factors. This is in contrast with the HIV-1 crosslink mutant A14C/E45C which abrogates RhT5 restriction (Ophélie Cosnefroy, unpublished data). The equivalent mutation in N-MLV would be P14C/H48C, although as mentioned earlier that mutating a Pro residue may alter the structure of CA, future experiments should test if such mutations would generate particles recognisable by Fv1 and T5. It is also possible that the crosslinking at the NTD-NTD interface within the MLV hexamer may disrupt some structure that is required for T5 and Fv1 recognition. Future experiments should also explore the crosslinking at the CTD-CTD inter-hexamer dimer interface. In addition to MLV, there are other retroviruses that can be recognised by both Fv1 and T5 alleles (Figure 6.3). The lentivirus EIAV is restricted by both HuT5 and RhT5 (Hatziioannou et al., 2004), and by two wild mice Fv1 alleles Fv1SPR1 and Fv1MAC (Yap et al., 2014). The binding of recombinant T5-21R to purified EIAV core has been reported (Langelier et al., 2008), and may provide an alternative binding substrate for the comparison between Fv1 and T5 recognition in future.

6.6 The significance of partial restriction activities

Using the novel inducible expression system described in chapter 3, it was found that many other wild mice Fv1 alleles also possess partial restriction activities against retroviruses at an expression level similar to endogenous $Fv1^b$, which turns into full restriction when at over-expression Fv1 level (Yap et al., 2014). However, without analysis of the Fv1 protein expression level from cells of wild mice, it is not known what the endogenous concentrations actually are. The difference between $Fv1^n$ in N-3T3 cells and $Fv1^b$ in B-3T3 cells suggested that Fv1 expression level may vary between mice species. There may also be variation in Fv1 expression level among different cell types, a higher expression level in the target cell type may be sufficient to control infection. Furthermore, the combined inhibition exerted by the partial restriction of these Fv1 alleles and other restriction factors such as murine APOBEC3 may be sufficient to confer protection (Rulli et al., 2008). A number of hypotheses can be suggested on how these partial restriction activities emerged. Some of these partial restriction activities could be once positively selected for due to the circulation of a retrovirus in the past, but as Fv1 evolves to recognise another new emerging virus, it accumulates mutations which lead to the decrease in restriction activity against the old virus. It is also possible that some of these Fv1 alleles are under selection from multiple retroviruses simultaneously, and Fv1 has been selected to inhibit all of these viruses, with the cost of weaker restriction against each of these viruses. It has been shown that forced passage of B-MLV in cells expressing $Fv1^n$ rapidly leads to the isolation of NB-MLV, while forced passage of N-MLV in $Fv1^b$ cells does not (Hopkins et al., 1977; Lilly and Pincus, 1973). The partial restriction activity against NB-MLV by $Fv1^b$ could have an important role in preventing the emergence of NB-tropic virus resulted from adaptation of B-MLV. It would also be interesting to see if similar concentration dependency of restriction can be found in T5 alleles, particular those which recognise multiple retroviruses (Figure 6.3). Future work should study the restriction by RhT5 against N-MLV, HIV-1 and EIAV at different expression levels of RhT5, similar to the analysis shown in Table 3.2. This would allow the comparison of the relative apparent affinities of RhT5 to different retroviral cores.

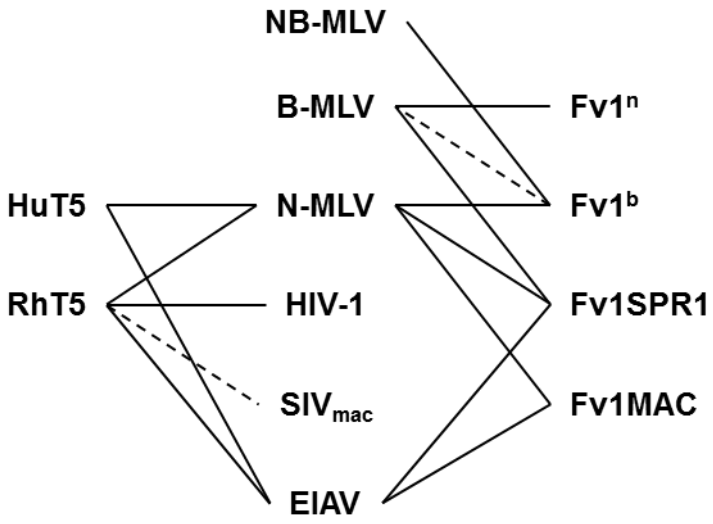

Figure 6.3 Restriction activities of selected Fv1 and T5

Solid lines represent full restriction activities, while dash lines represent partial restriction activities. Data from (Bock et al., 2000; Hatziioannou et al., 2004; Ohkura et al., 2006; Yap et al., 2014).

6.7 Evolution of the *Fv1* gene

In additional to *Fv1*^{n}, *Fv1*^{b} and *Fv1*^{nr} alleles isolated from inbred lab mice, previous studies have identified many *Fv1* alleles in wild mice (Yan et al., 2009; Yap et al., 2014) (Figure 6.4). Among different murine species, *Fv1* alleles could be amplified from *Mus mus*, *Mus nannomys* and *Mus pyromys* sub-genera, but not from the *Mus coelomys* sub-genus or the *Rattus* genus, suggesting that the *Fv1* gene was inserted about 5 million years ago roughly about the time when the *Mus* sub-genera diverged (Ellis, 2000; Qi et al., 1998b; Yap et al., 2014), probably as part of an endogenous retrovirus MERV-L (Benit et al., 1997; Best et al., 1996). Since then, these *Fv1* alleles diverged in their restriction specificities (Yap et al., 2014). Several *Mus nannomys Fv1* alleles, including *Fv1MIN1* and *Fv1MIN2* from *M. n. minutoides* and *Fv1SET* from *M. n. setulosus*, have evolved the ability to restrict multiple strains of MLV (Yan et al., 2009; Yap et al., 2014). Among the *Mus mus Fv1* alleles, restriction activities against non-MLV retroviruses have also been identified (Yap et al., 2014). These include *Fv1SPR1* from *M. m. spretus* and *Fv1MAC* from *M. m. macedonicus*, which not only restrict MLV but also the lentivirus EIAV; as well as *Fv1CAR1* from *M. m. caroli*, which restricts FFV (Yap et al., 2014). Data from chapter 3 showed that the restriction of EIAV and FFV by these alleles can be observed at relatively low expression levels (Figure 3.25), suggesting that these non-MLV restriction activities are most likely present when expressed at the endogenous level in cells of wild mice.

6 codons in the *Fv1* gene had been identified to show evidence of positive selections, including positions 261, 265, 270, 352, 399 and 401 (Yan et al., 2009). Interestingly, many residues that have been identified as key determinants for *Fv1* restriction activities overlap with the sites of positive selection (Yap et al., 2014). Key determinants of *Fv1* restriction include residues 352, 358 and 399 of *Fv1*^{n}, *Fv1*^{b} and *Fv1*^{nr} which are important for defining MLV restriction specificity (Bock et al., 2000; Stevens et al., 2004); residues 261, 268 and 270 of Fv1SPR1 which are important for its MLV and EIAV restriction activities (Yap et al., 2014); and residues 349 and 352 which are important for the FFV restriction activity of Fv1CAR1 (Yap et al., 2014).

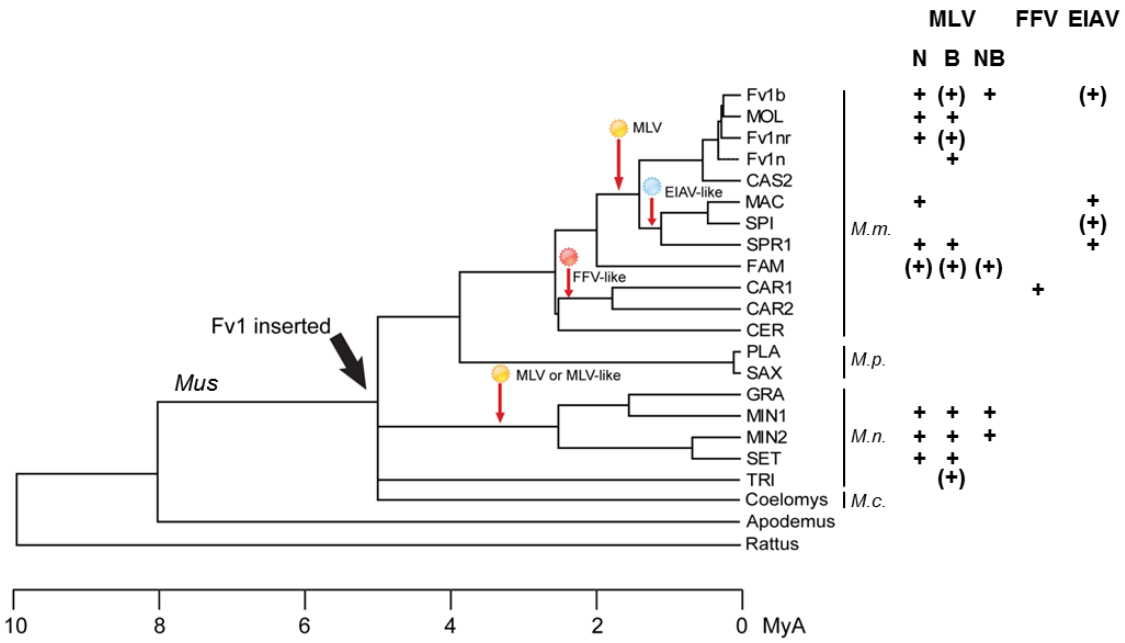

Figure 6.4. Restriction activities of Fv1 alleles from lab and wild mice

A phylogenetic tree showing the approximate times of Fv1 acquisition, retroviral restriction activities (using LxIY-Fv1 vector), and hypothetical virus infections leading to selection of new activities. +, restriction; (+) partial restriction. Sub-genera: *M.m., Mus mus; M.n., Mus nannomys; M.p., Mus pyromys; M.c., Mus coelomys.* Modified from (Yap et al., 2014), with permission under PLOS open-access license and the Creative Commons Attribution (CC BY) license.

In the case of the emergence of *Fv1*^{n} and *Fv1*^{b} alleles, genetic and function studies of *Fv1* alleles from lab and wild mice have provided insights on the events involved in the evolution of these genes (Ellis, 2000). In comparison to *Fv1*^{b}, *Fv1*^{n} contains different sequence at positions 358 and 399, as well as a 19aa shorter C-terminal tail resulted from a 1.3kb deletion in the genomic DNA (Best et al., 1996). Among the *Mus mus* sub-genus, all *Fv1* alleles have the *Fv1*^{n} sequence of K358 and V399, except for *Fv1*^{b} which has the sequence E358 and R399, and for Fv1MOL from *M. m. molossinus*, which has the sequence K358 and R399 (Ellis, 2000). This suggested that the progenitor of *Mus mus Fv1* alleles is likely to have the K358 and V399, with the V399R mutation acquired by the common progenitor of *Fv1MOL* and *Fv1*^{b}, followed by the K358E mutation acquired by *Fv1*^{b} after its divergence from *Fv1MOL*. At the C-terminus, most *Fv1* alleles possess an *Fv1*^{b}-like long tail. In contrast, *Fv1*^{n}, *Fv1*^{nr}, as well as *Fv1* from *M. m. domesticus* and *M. m. musculus* all have identical 3aa short C-terminal tail. 3 other *Fv1* alleles including *Fv1FAM* from *M. m. famulus*, *Fv1MIN1/2* from *M. n. minutoides*, and *Fv1PLA* from *M. p. platythrix* also possess shorter C-terminal tails (Ellis, 2000; Yap et al., 2014). However, the short C-terminal tails in these diverged *Fv1* alleles were caused by independent insertion events, all resulting in slightly different insertion of B1 repeat element, and are unrelated to the short tail in *Fv1*^{n}. The fact that most *Fv1* alleles possess the long *Fv1*^{b}-like tail suggested that the progenitor of *Fv1* would have a long C-terminal tail, and that the short C-terminal tail of Fv1^{n} has evolved after the divergence of *Fv1*^{n} and *Fv1*^{b} from *Fv1MOL* and *Fv1*^{b}. Together, these observations suggested that the common progenitor of *Fv1*^{n} and *Fv1*^{b} possess a sequence similar to the mutant Fv1nnb, with K358, V399, and a *Fv1*^{b}-like long C-terminal tail.

6.8 Selection pressure driving Fv1 evolution

The question remains on what drives the divergence of restriction specificities of different *Fv1* alleles after the insertion of the *Fv1* gene. The observed *Fv1* activities against EIAV and FFV could be the results of one of the two scenarios (Yap et al., 2014). First, *Fv1SPR1*, *Fv1MAC* and *Fv1CAR1* could be selected to recognise EIAV and FFV in additional to MLV, due to prior exposure to similar lentivirus and spumavirus. Alternatively, these *Fv1* alleles could be selected to

recognise MLV only, but the adaptations for MLV recognition also enables these *Fv1* alleles to interact with EIAV and FFV capsids. There are increasing lines of evidence against the second scenario. First, *Fv1SPR1* and *Fv1MAC* appeared to have evolved different mechanisms to restrict EIAV, while the restriction of both N-MLV and EIAV by *Fv1SPR1* require C268, *Fv1MAC* has the sequence R268 but still restrict N-MLV and EIAV (Yap et al., 2014). The convergent evolution of EIAV restriction activities using different mechanisms suggested that these *Fv1* alleles were likely to be under selection pressure from EIAV-like viruses. Secondly, although the C268R mutation can abolish both MLV and EIAV restriction activities of *Fv1SPR1*, there are mutations which can abolish EIAV but not MLV activities of *Fv1MAC* (Melvyn Yap, unpublished data). This suggested that the EIAV activity is unlikely to be simply the consequence of the selection against MLV, but most likely due to the exposure to an EIAV-like virus

Different *Fv1* alleles appear to display different restriction specificities towards MLV of different tropisms, suggesting that they may be under different selection pressure through exposure to different MLVs. Some Fv1 alleles have broad range activities against N-MLV, B-MLV and NB-MLV. For example, *Fv1MIN2* restricts all 3 MLVs when overexpressed, although at low concentration it has slightly weaker activity against NB-MLV (Figure 3.25). Similarly, $Fv1^{b}$ can restrict N-MLV and NB-MLV when overexpressed, but has slightly weaker activity against NB-MLV (Figure 3.25). On the other hand, some other Fv1 alleles show high restriction specificities. For example, $Fv1^{n}$ only restrict B-MLV even when overexpressed, while *Fv1MAC* only restrict N-MLV even when overexpressed. So what are the viruses which drove the selection of MLV restriction activities of *Fv1*, and the subsequent divergence of restriction specificity towards MLV of different tropisms? The identification of many endogenous MLVs present in mice genome has provided insight on what these viruses might be. Non-ecotropic (such as xenotropic and polytropic) endogenous MLVs have been found in the germline of *M. m. domesticus, M. m. musculus, M. m. molossinus, M. m. castaneous and M. m. spretus* (Ellis, 2000), and sequence analysis suggested that most of these viruses carry determinants for B-tropism (Stevens et al., 2004). Ecotropic endogenous MLVs have also been found in the genomes of many lab mice strains as well as in *M. m.*

molossinus (Inaguma et al., 1991; Kozak, 2014), most of which are N-tropic (Kozak, 2014). Although most of these endogenous MLVs contain fatal mutations which prevented the expression of infectious particles (Kozak, 2014), they are evidence that after the insertion of Fv1, mice in the *Mus mus* sub-genus had once been exposed to infectious N-tropic and B-tropic MLVs, which could create strong selection pressure against these viruses. Once these MLVs entered the germ line, there is additional selection pressure for Fv1 to evolve restriction activities against N-tropic and B-tropic viruses in order to control the endogenous MLVs. Since the mostly B-tropic non-ecotropic endogenous MLVs appeared to have entered the germ line earlier than the mostly N-tropic ecotropic endogenous MLVs in the *Mus mus* lineage (Ellis, 2000), it is likely that the progenitor of $Fv1^{n}$ and $Fv1^{b}$ alleles were first selected for restriction of B-MLV, and later also selected for restriction of N-MLV in some mice which gave rise to the $Fv1^{b}$ allele.

References

Aaronson, S.A., Hartley, J.W., Todaro, G.J., 1969. Mouse leukemia virus: "spontaneous" release by mouse embryo cells after long-term in vitro cultivation. Proceedings of the National Academy of Sciences of the United States of America 64, 87-94.

Abdurahman, S., Youssefi, M., Hoglund, S., Vahlne, A., 2007. Characterization of the invariable residue 51 mutations of human immunodeficiency virus type 1 capsid protein on in vitro CA assembly and infectivity. Retrovirology 4, 69.

Abrahamyan, L.G., Markosyan, R.M., Moore, J.P., Cohen, F.S., Melikyan, G.B., 2003. Human immunodeficiency virus type 1 Env with an intersubunit disulfide bond engages coreceptors but requires bond reduction after engagement to induce fusion. Journal of virology 77, 5829-5836.

Achong, B.G., Mansell, P.W., Epstein, M.A., Clifford, P., 1971. An unusual virus in cultures from a human nasopharyngeal carcinoma. Journal of the National Cancer Institute 46, 299-307.

Aiken, C., 1997. Pseudotyping human immunodeficiency virus type 1 (HIV-1) by the glycoprotein of vesicular stomatitis virus targets HIV-1 entry to an endocytic pathway and suppresses both the requirement for Nef and the sensitivity to cyclosporin A. Journal of virology 71, 5871-5877.

Albritton, L.M., Tseng, L., Scadden, D., Cunningham, J.M., 1989. A putative murine ecotropic retrovirus receptor gene encodes a multiple membrane-spanning protein and confers susceptibility to virus infection. Cell 57, 659-666.

Alcami, J., Lain de Lera, T., Folgueira, L., Pedraza, M.A., Jacque, J.M., Bachelerie, F., Noriega, A.R., Hay, R.T., Harrich, D., Gaynor, R.B., et al., 1995. Absolute dependence on kappa B responsive elements for initiation and Tat-mediated amplification of HIV transcription in blood CD4 T lymphocytes. The EMBO journal 14, 1552-1560.

Alfadhli, A., Barklis, E., 2014. The roles of lipids and nucleic acids in HIV-1 assembly. Frontiers in microbiology 5, 253.

Alfadhli, A., Barklis, R.L., Barklis, E., 2009a. HIV-1 matrix organizes as a hexamer of trimers on membranes containing phosphatidylinositol-(4,5)-bisphosphate. Virology 387, 466-472.

Alfadhli, A., Huseby, D., Kapit, E., Colman, D., Barklis, E., 2007. Human immunodeficiency virus type 1 matrix protein assembles on membranes as a hexamer. Journal of virology 81, 1472-1478.

Alfadhli, A., McNett, H., Tsagli, S., Bachinger, H.P., Peyton, D.H., Barklis, E., 2011. HIV-1 matrix protein binding to RNA. Journal of molecular biology 410, 653-666.

Alfadhli, A., Still, A., Barklis, E., 2009b. Analysis of human immunodeficiency virus type 1 matrix binding to membranes and nucleic acids. Journal of virology 83, 12196-12203.

Alkhatib, G., Combadiere, C., Broder, C.C., Feng, Y., Kennedy, P.E., Murphy, P.M., Berger, E.A., 1996. CC CKR5: a RANTES, MIP-1alpha, MIP-1beta receptor as a fusion cofactor for macrophage-tropic HIV-1. Science 272, 1955-1958.

Ambrose, Z., Aiken, C., 2014. HIV-1 uncoating: connection to nuclear entry and regulation by host proteins. Virology 454-455, 371-379.

Amorim, R., Costa, S.M., Cavaleiro, N.P., da Silva, E.E., da Costa, L.J., 2014. HIV-1 transcripts use IRES-initiation under conditions where Cap-dependent translation is restricted by poliovirus 2A protease. PloS one 9, e88619.

Andersen, K.B., 2013. The retrovirus MA and PreTM proteins follow immature MLV cores. Virus research 175, 134-142.

Anderson, J.L., Campbell, E.M., Wu, X., Vandegraaff, N., Engelman, A., Hope, T.J., 2006. Proteasome inhibition reveals that a functional preintegration complex intermediate can be generated during restriction by diverse TRIM5 proteins. Journal of virology 80, 9754-9760.

Arhel, N.J., Souquere-Besse, S., Munier, S., Souque, P., Guadagnini, S., Rutherford, S., Prevost, M.C., Allen, T.D., Charneau, P., 2007. HIV-1 DNA Flap formation promotes uncoating of the pre-integration complex at the nuclear pore. The EMBO journal 26, 3025-3037.

Armstrong, J.A., Porterfield, J.S., De Madrid, A.T., 1971. C-type virus particles in pig kidney cell lines. The Journal of general virology 10, 195-198.

Bailey, G.D., Hyun, J.K., Mitra, A.K., Kingston, R.L., 2012. A structural model for the generation of continuous curvature on the surface of a retroviral capsid. Journal of molecular biology 417, 212-223.

Bainbridge, J.W., Stephens, C., Parsley, K., Demaison, C., Halfyard, A., Thrasher, A.J., Ali, R.R., 2001. In vivo gene transfer to the mouse eye using an HIV-based lentiviral vector; efficient long-term transduction of corneal endothelium and retinal pigment epithelium. Gene therapy 8, 1665-1668.

Baltimore, D., 1970. RNA-dependent DNA polymerase in virions of RNA tumour viruses. Nature 226, 1209-1211.

Bannert, N., Fiebig, U., Hohn, O., 2010. Retroviral particles, proteins and genomes, in: Kurth, R., Bannert, N. (Eds.), Retroviruses: molecular biology, genomics and pathogenesis. Caister Academic Press, Norfolk, UK, pp. 71-106.

Barklis, E., McDermott, J., Wilkens, S., Fuller, S., Thompson, D., 1998. Organization of HIV-1 capsid proteins on a lipid monolayer. The Journal of biological chemistry 273, 7177-7180.

Barklis, E., McDermott, J., Wilkens, S., Schabtach, E., Schmid, M.F., Fuller, S., Karanjia, S., Love, Z., Jones, R., Rui, Y., Zhao, X., Thompson, D., 1997. Structural analysis of membrane-bound retrovirus capsid proteins. The EMBO journal 16, 1199-1213.

Barre-Sinoussi, F., Chermann, J.C., Rey, F., Nugeyre, M.T., Chamaret, S., Gruest, J., Dauguet, C., Axler-Blin, C., Vezinet-Brun, F., Rouzioux, C., Rozenbaum, W., Montagnier, L., 1983. Isolation of a T-lymphotropic retrovirus from a patient at risk for acquired immune deficiency syndrome (AIDS). Science 220, 868-871.

Basmaciogullari, S., Pizzato, M., 2014. The activity of Nef on HIV-1 infectivity. Frontiers in microbiology 5, 232.

Beemon, K., Keith, J., 1977. Localization of N6-methyladenosine in the Rous sarcoma virus genome. Journal of molecular biology 113, 165-179.

Benit, L., De Parseval, N., Casella, J.F., Callebaut, I., Cordonnier, A., Heidmann, T., 1997. Cloning of a new murine endogenous retrovirus, MuERV-L, with strong similarity to the human HERV-L element and with a gag coding sequence closely related to the Fv1 restriction gene. Journal of virology 71, 5652-5657.

Bentvelzen, P., Daams, J.H., 1969. Hereditary infections with mammary tumor viruses in mice. Journal of the National Cancer Institute 43, 1025-1035.

Bentvelzen, P., Daams, J.H., Hageman, P., Calafat, J., 1970. Genetic transmission of viruses that incite mammary tumor in mice. Proceedings of the National Academy of Sciences of the United States of America 67, 377-384.

Berlioz, C., Darlix, J.L., 1995. An internal ribosomal entry mechanism promotes translation of murine leukemia virus gag polyprotein precursors. Journal of virology 69, 2214-2222.

Bernstein, H.B., Compans, R.W., 1992. Sulfation of the human immunodeficiency virus envelope glycoprotein. Journal of virology 66, 6953-6959.

Bernstein, H.B., Tucker, S.P., Hunter, E., Schutzbach, J.S., Compans, R.W., 1994. Human immunodeficiency virus type 1 envelope glycoprotein is modified by O-linked oligosaccharides. Journal of virology 68, 463-468.

Besnier, C., Takeuchi, Y., Towers, G., 2002. Restriction of lentivirus in monkeys. Proceedings of the National Academy of Sciences of the United States of America 99, 11920-11925.

Best, S., Le Tissier, P., Towers, G., Stoye, J.P., 1996. Positional cloning of the mouse retrovirus restriction gene Fv1. Nature 382, 826-829.

Bharat, T.A., Castillo Menendez, L.R., Hagen, W.J., Lux, V., Igonet, S., Schorb, M., Schur, F.K., Krausslich, H.G., Briggs, J.A., 2014. Cryo-electron microscopy of tubular arrays of HIV-1 Gag resolves structures essential for immature virus assembly. Proceedings of the National Academy of Sciences of the United States of America 111, 8233-8238.

Bichel, K., Price, A.J., Schaller, T., Towers, G.J., Freund, S.M., James, L.C., 2013. HIV-1 capsid undergoes coupled binding and isomerization by the nuclear pore protein NUP358. Retrovirology 10, 81.

Biris, N., Yang, Y., Taylor, A.B., Tomashevski, A., Guo, M., Hart, P.J., Diaz-Griffero, F., Ivanov, D.N., 2012. Structure of the rhesus monkey TRIM5alpha PRYSPRY domain, the HIV capsid recognition module. Proceedings of the National Academy of Sciences of the United States of America 109, 13278-13283.

Bishop, K.N., Bock, M., Towers, G., Stoye, J.P., 2001. Identification of the regions of Fv1 necessary for murine leukemia virus restriction. Journal of virology 75, 5182-5188.

Bishop, K.N., Mortuza, G.B., Howell, S., Yap, M.W., Stoye, J.P., Taylor, I.A., 2006. Characterization of an amino-terminal dimerization domain from retroviral restriction factor Fv1. Journal of virology 80, 8225-8235.

Bishop, K.N., Verma, M., Kim, E.Y., Wolinsky, S.M., Malim, M.H., 2008. APOBEC3G inhibits elongation of HIV-1 reverse transcripts. PLoS pathogens 4, e1000231.

Bittner, J.J., 1936. Some Possible Effects of Nursing on the Mammary Gland Tumor Incidence in Mice. Science 84, 162.

Black, L.R., Aiken, C., 2010. TRIM5alpha disrupts the structure of assembled HIV-1 capsid complexes in vitro. Journal of virology 84, 6564-6569.

Blaise, S., de Parseval, N., Benit, L., Heidmann, T., 2003. Genomewide screening for fusogenic human endogenous retrovirus envelopes identifies syncytin 2, a gene conserved on primate evolution. Proceedings of the National Academy of Sciences of the United States of America 100, 13013-13018.

Blikstad, V., Benachenhou, F., Sperber, G.O., Blomberg, J., 2008. Evolution of human endogenous retroviral sequences: a conceptual account. Cellular and molecular life sciences : CMLS 65, 3348-3365.

Blond, J.L., Lavillette, D., Cheynet, V., Bouton, O., Oriol, G., Chapel-Fernandes, S., Mandrand, B., Mallet, F., Cosset, F.L., 2000. An envelope glycoprotein of the human endogenous retrovirus HERV-W is expressed in the human placenta and fuses cells expressing the type D mammalian retrovirus receptor. Journal of virology 74, 3321-3329.

Bobkova, M., Stitz, J., Engelstadter, M., Cichutek, K., Buchholz, C.J., 2002. Identification of R-peptides in envelope proteins of C-type retroviruses. The Journal of general virology 83, 2241-2246.

Bochkov, Y.A., Palmenberg, A.C., 2006. Translational efficiency of EMCV IRES in bicistronic vectors is dependent upon IRES sequence and gene location. BioTechniques 41, 283-284, 286, 288 passim.

Bock, M., Bishop, K.N., Towers, G., Stoye, J.P., 2000. Use of a transient assay for studying the genetic determinants of Fv1 restriction. Journal of virology 74, 7422-7430.

Boone, L.R., Innes, C.L., Heitman, C.K., 1990. Abrogation of Fv-1 restriction by genome-deficient virions produced by a retrovirus packaging cell line. Journal of virology 64, 3376-3381.

Bosco, D.A., Eisenmesser, E.Z., Pochapsky, S., Sundquist, W.I., Kern, D., 2002. Catalysis of cis/trans isomerization in native HIV-1 capsid by human cyclophilin A. Proceedings of the National Academy of Sciences of the United States of America 99, 5247-5252.

Boudinot, P., van der Aa, L.M., Jouneau, L., Du Pasquier, L., Pontarotti, P., Briolat, V., Benmansour, A., Levraud, J.P., 2011. Origin and evolution of TRIM proteins: new insights from the complete TRIM repertoire of zebrafish and pufferfish. PloS one 6, e22022.

Bowerman, B., Brown, P.O., Bishop, J.M., Varmus, H.E., 1989. A nucleoprotein complex mediates the integration of retroviral DNA. Genes & development 3, 469-478.

Brasey, A., Lopez-Lastra, M., Ohlmann, T., Beerens, N., Berkhout, B., Darlix, J.L., Sonenberg, N., 2003. The leader of human immunodeficiency virus type 1 genomic RNA harbors an internal ribosome entry segment that is active during the G2/M phase of the cell cycle. Journal of virology 77, 3939-3949.

Brass, A.L., Dykxhoorn, D.M., Benita, Y., Yan, N., Engelman, A., Xavier, R.J., Lieberman, J., Elledge, S.J., 2008. Identification of host proteins required for HIV infection through a functional genomic screen. Science 319, 921-926.

Brass, A.L., Huang, I.C., Benita, Y., John, S.P., Krishnan, M.N., Feeley, E.M., Ryan, B.J., Weyer, J.L., van der Weyden, L., Fikrig, E., Adams, D.J., Xavier, R.J., Farzan, M., Elledge, S.J., 2009. The IFITM proteins mediate cellular resistance to influenza A H1N1 virus, West Nile virus, and dengue virus. Cell 139, 1243-1254.

Brennan, G., Kozyrev, Y., Kodama, T., Hu, S.L., 2007. Novel TRIM5 isoforms expressed by Macaca nemestrina. Journal of virology 81, 12210-12217.

Briggs, J.A., Simon, M.N., Gross, I., Krausslich, H.G., Fuller, S.D., Vogt, V.M., Johnson, M.C., 2004. The stoichiometry of Gag protein in HIV-1. Nature structural & molecular biology 11, 672-675.

Briggs, J.A., Wilk, T., Welker, R., Krausslich, H.G., Fuller, S.D., 2003. Structural organization of authentic, mature HIV-1 virions and cores. The EMBO journal 22, 1707-1715.

Briones, M.S., Dobard, C.W., Chow, S.A., 2010. Role of human immunodeficiency virus type 1 integrase in uncoating of the viral core. Journal of virology 84, 5181-5190.

Brown, P., Nemo, G., Gajdusek, D.C., 1978. Human foamy virus: further characterization, seroepidemiology, and relationship to chimpanzee foamy viruses. The Journal of infectious diseases 137, 421-427.

Brown, P.O., Bowerman, B., Varmus, H.E., Bishop, J.M., 1989. Retroviral integration: structure of the initial covalent product and its precursor, and a role for the viral IN protein. Proceedings of the National Academy of Sciences of the United States of America 86, 2525-2529.

Bryant, M., Ratner, L., 1990. Myristoylation-dependent replication and assembly of human immunodeficiency virus 1. Proceedings of the National Academy of Sciences of the United States of America 87, 523-527.

Buck, C.B., Shen, X., Egan, M.A., Pierson, T.C., Walker, C.M., Siliciano, R.F., 2001. The human immunodeficiency virus type 1 gag gene encodes an internal ribosome entry site. Journal of virology 75, 181-191.

Bukrinsky, M.I., Sharova, N., McDonald, T.L., Pushkarskaya, T., Tarpley, W.G., Stevenson, M., 1993. Association of integrase, matrix, and reverse transcriptase antigens of human immunodeficiency virus type 1 with viral nucleic acids following acute infection. Proceedings of the National Academy of Sciences of the United States of America 90, 6125-6129.

Burns, A.E., 2009. Functional and structural studies of the Moloney murine leukemia virus capsid protein. Columbia University, New York.

Busnadiego, I., Kane, M., Rihn, S.J., Preugschas, H.F., Hughes, J., Blanco-Melo, D., Strouvelle, V.P., Zang, T.M., Willett, B.J., Boutell, C., Bieniasz, P.D., Wilson, S.J., 2014. Host and Viral Determinants of Mx2 Antiretroviral Activity. Journal of virology.

Byeon, I.J., Meng, X., Jung, J., Zhao, G., Yang, R., Ahn, J., Shi, J., Concel, J., Aiken, C., Zhang, P., Gronenborn, A.M., 2009. Structural convergence between Cryo-EM and NMR reveals intersubunit interactions critical for HIV-1 capsid function. Cell 139, 780-790.

Calattini, S., Chevalier, S.A., Duprez, R., Bassot, S., Froment, A., Mahieux, R., Gessain, A., 2005. Discovery of a new human T-cell lymphotropic virus (HTLV-3) in Central Africa. Retrovirology 2, 30.

Campbell, M., Eng, C., Luciw, P.A., 1996. The simian foamy virus type 1 transcriptional transactivator (Tas) binds and activates an enhancer element in the gag gene. Journal of virology 70, 6847-6855.

Campbell, S., Vogt, V.M., 1995. Self-assembly in vitro of purified CA-NC proteins from Rous sarcoma virus and human immunodeficiency virus type 1. Journal of virology 69, 6487-6497.

Carlson, L.A., Briggs, J.A., Glass, B., Riches, J.D., Simon, M.N., Johnson, M.C., Muller, B., Grunewald, K., Krausslich, H.G., 2008. Three-dimensional analysis of budding sites and released virus suggests a revised model for HIV-1 morphogenesis. Cell host & microbe 4, 592-599.

Carlson, L.A., de Marco, A., Oberwinkler, H., Habermann, A., Briggs, J.A., Krausslich, H.G., Grunewald, K., 2010. Cryo electron tomography of native HIV-1 budding sites. PLoS pathogens 6, e1001173.

Cen, S., Khorchid, A., Gabor, J., Rong, L., Wainberg, M.A., Kleiman, L., 2000. Roles of Pr55(gag) and NCp7 in tRNA(3)(Lys) genomic placement and the initiation step of reverse transcription in human immunodeficiency virus type 1. Journal of virology 74, 10796-10800.

Chan, R., Uchil, P.D., Jin, J., Shui, G., Ott, D.E., Mothes, W., Wenk, M.R., 2008. Retroviruses human immunodeficiency virus and murine leukemia virus are enriched in phosphoinositides. Journal of virology 82, 11228-11238.

Chang, Y.F., Wang, S.M., Huang, K.J., Wang, C.T., 2007. Mutations in capsid major homology region affect assembly and membrane affinity of HIV-1 Gag. Journal of molecular biology 370, 585-597.

Charneau, P., Clavel, F., 1991. A single-stranded gap in human immunodeficiency virus unintegrated linear DNA defined by a central copy of the polypurine tract. Journal of virology 65, 2415-2421.

Charneau, P., Mirambeau, G., Roux, P., Paulous, S., Buc, H., Clavel, F., 1994. HIV-1 reverse transcription. A termination step at the center of the genome. Journal of molecular biology 241, 651-662.

Chen, B., Vogan, E.M., Gong, H., Skehel, J.J., Wiley, D.C., Harrison, S.C., 2005. Structure of an unliganded simian immunodeficiency virus gp120 core. Nature 433, 834-841.

Chen, K., Huang, J., Zhang, C., Huang, S., Nunnari, G., Wang, F.X., Tong, X., Gao, L., Nikisher, K., Zhang, H., 2006. Alpha interferon potently enhances the anti-human immunodeficiency virus type 1 activity of APOBEC3G in resting primary CD4 T cells. Journal of virology 80, 7645-7657.

Cherepanov, P., Ambrosio, A.L., Rahman, S., Ellenberger, T., Engelman, A., 2005. Structural basis for the recognition between HIV-1 integrase and transcriptional coactivator p75. Proceedings of the National Academy of Sciences of the United States of America 102, 17308-17313.

Cheslock, S.R., Poon, D.T., Fu, W., Rhodes, T.D., Henderson, L.E., Nagashima, K., McGrath, C.F., Hu, W.S., 2003. Charged assembly helix motif in murine leukemia virus capsid: an important region for virus assembly and particle size determination. Journal of virology 77, 7058-7066.

Chook, Y.M., Suel, K.E., 2011. Nuclear import by karyopherin-betas: recognition and inhibition. Biochimica et biophysica acta 1813, 1593-1606.

Chukkapalli, V., Inlora, J., Todd, G.C., Ono, A., 2013. Evidence in support of RNA-mediated inhibition of phosphatidylserine-dependent HIV-1 Gag membrane binding in cells. Journal of virology 87, 7155-7159.

Chukkapalli, V., Oh, S.J., Ono, A., 2010. Opposing mechanisms involving RNA and lipids regulate HIV-1 Gag membrane binding through the highly basic region of the matrix domain. Proceedings of the National Academy of Sciences of the United States of America 107, 1600-1605.

Chun, R.F., Jeang, K.T., 1996. Requirements for RNA polymerase II carboxyl-terminal domain for activated transcription of human retroviruses human T-cell lymphotropic virus I and HIV-1. The Journal of biological chemistry 271, 27888-27894.

Ciuffi, A., Llano, M., Poeschla, E., Hoffmann, C., Leipzig, J., Shinn, P., Ecker, J.R., Bushman, F., 2005. A role for LEDGF/p75 in targeting HIV DNA integration. Nature medicine 11, 1287-1289.

Clavel, F., Guetard, D., Brun-Vezinet, F., Chamaret, S., Rey, M.A., Santos-Ferreira, M.O., Laurent, A.G., Dauguet, C., Katlama, C., Rouzioux, C., et al., 1986. Isolation of a new human retrovirus from West African patients with AIDS. Science 233, 343-346.

Clever, J.L., Wong, M.L., Parslow, T.G., 1996. Requirements for kissing-loop-mediated dimerization of human immunodeficiency virus RNA. Journal of virology 70, 5902-5908.

Cocka, L.J., Bates, P., 2012. Identification of alternatively translated Tetherin isoforms with differing antiviral and signaling activities. PLoS pathogens 8, e1002931.

Conte, M.R., Matthews, S., 1998. Retroviral matrix proteins: a structural perspective. Virology 246, 191-198.

Cordonnier, A., Casella, J.F., Heidmann, T., 1995. Isolation of novel human endogenous retrovirus-like elements with foamy virus-related pol sequence. Journal of virology 69, 5890-5897.

Cornilescu, C.C., Bouamr, F., Yao, X., Carter, C., Tjandra, N., 2001. Structural analysis of the N-terminal domain of the human T-cell leukemia virus capsid protein. Journal of molecular biology 306, 783-797.

Cortines, J.R., Monroe, E.B., Kang, S., Prevelige, P.E., Jr., 2011. A retroviral chimeric capsid protein reveals the role of the N-terminal beta-hairpin in mature core assembly. Journal of molecular biology 410, 641-652.

Cowan, S., Hatziioannou, T., Cunningham, T., Muesing, M.A., Gottlinger, H.G., Bieniasz, P.D., 2002. Cellular inhibitors with Fv1-like activity restrict human and simian immunodeficiency virus

tropism. Proceedings of the National Academy of Sciences of the United States of America 99, 11914-11919.

Craigie, R., Bushman, F.D., 2012. HIV DNA integration. Cold Spring Harbor perspectives in medicine 2, a006890.

Crawford, L.V., Crawford, E.M., 1961. The properties of Rous sarcoma virus purified by density gradient centrifugation. Virology 13, 227-232.

Crawford, S., Goff, S.P., 1985. A deletion mutation in the 5' part of the pol gene of Moloney murine leukemia virus blocks proteolytic processing of the gag and pol polyproteins. Journal of virology 53, 899-907.

Cui, J., Holmes, E.C., 2012. Endogenous lentiviruses in the ferret genome. Journal of virology 86, 3383-3385.

Cullen, B.R., 1991. Human immunodeficiency virus as a prototypic complex retrovirus. Journal of virology 65, 1053-1056.

Curtin, J.A., Dane, A.P., Swanson, A., Alexander, I.E., Ginn, S.L., 2008. Bidirectional promoter interference between two widely used internal heterologous promoters in a late-generation lentiviral construct. Gene therapy 15, 384-390.

D'Souza, V., Dey, A., Habib, D., Summers, M.F., 2004. NMR structure of the 101-nucleotide core encapsidation signal of the Moloney murine leukemia virus. Journal of molecular biology 337, 427-442.

D'Souza, V., Melamed, J., Habib, D., Pullen, K., Wallace, K., Summers, M.F., 2001. Identification of a high affinity nucleocapsid protein binding element within the Moloney murine leukemia virus Psi-RNA packaging signal: implications for genome recognition. Journal of molecular biology 314, 217-232.

D'Souza, V., Summers, M.F., 2004. Structural basis for packaging the dimeric genome of Moloney murine leukaemia virus. Nature 431, 586-590.

D'Souza, V., Summers, M.F., 2005. How retroviruses select their genomes. Nature reviews. Microbiology 3, 643-655.

Dang, T.X., Farah, S.J., Gast, A., Robertson, C., Carragher, B., Egelman, E., Wilson-Kubalek, E.M., 2005a. Helical crystallization on lipid nanotubes: streptavidin as a model protein. Journal of structural biology 150, 90-99.

Dang, T.X., Milligan, R.A., Tweten, R.K., Wilson-Kubalek, E.M., 2005b. Helical crystallization on nickel-lipid nanotubes: perfringolysin O as a model protein. Journal of structural biology 152, 129-139.

Daniel, M.D., Letvin, N.L., King, N.W., Kannagi, M., Sehgal, P.K., Hunt, R.D., Kanki, P.J., Essex, M., Desrosiers, R.C., 1985. Isolation of T-cell tropic HTLV-III-like retrovirus from macaques. Science 228, 1201-1204.

Dannull, J., Surovoy, A., Jung, G., Moelling, K., 1994. Specific binding of HIV-1 nucleocapsid protein to PSI RNA in vitro requires N-terminal zinc finger and flanking basic amino acid residues. The EMBO journal 13, 1525-1533.

Das, D., Georgiadis, M.M., 2004. The crystal structure of the monomeric reverse transcriptase from Moloney murine leukemia virus. Structure 12, 819-829.

Datta, S.A., Temeselew, L.G., Crist, R.M., Soheilian, F., Kamata, A., Mirro, J., Harvin, D., Nagashima, K., Cachau, R.E., Rein, A., 2011. On the role of the SP1 domain in HIV-1 particle assembly: a molecular switch? Journal of virology 85, 4111-4121.

Davis, T.L., Walker, J.R., Campagna-Slater, V., Finerty, P.J., Paramanathan, R., Bernstein, G., MacKenzie, F., Tempel, W., Ouyang, H., Lee, W.H., Eisenmesser, E.Z., Dhe-Paganon, S., 2010. Structural and biochemical characterization of the human cyclophilin family of peptidyl-prolyl isomerases. PLoS biology 8, e1000439.

De Guzman, R.N., Wu, Z.R., Stalling, C.C., Pappalardo, L., Borer, P.N., Summers, M.F., 1998. Structure of the HIV-1 nucleocapsid protein bound to the SL3 psi-RNA recognition element. Science 279, 384-388.

de Marco, A., Davey, N.E., Ulbrich, P., Phillips, J.M., Lux, V., Riches, J.D., Fuzik, T., Ruml, T., Krausslich, H.G., Vogt, V.M., Briggs, J.A., 2010a. Conserved and variable features of Gag structure and arrangement in immature retrovirus particles. Journal of virology 84, 11729-11736.

de Marco, A., Heuser, A.M., Glass, B., Krausslich, H.G., Muller, B., Briggs, J.A., 2012. Role of the SP2 domain and its proteolytic cleavage in HIV-1 structural maturation and infectivity. Journal of virology 86, 13708-13716.

de Marco, A., Muller, B., Glass, B., Riches, J.D., Krausslich, H.G., Briggs, J.A., 2010b. Structural analysis of HIV-1 maturation using cryo-electron tomography. PLoS pathogens 6, e1001215.

De Rijck, J., de Kogel, C., Demeulemeester, J., Vets, S., El Ashkar, S., Malani, N., Bushman, F.D., Landuyt, B., Husson, S.J., Busschots, K., Gijsbers, R., Debyser, Z., 2013. The BET family of proteins targets moloney murine leukemia virus integration near transcription start sites. Cell reports 5, 886-894.

Deffaud, C., Darlix, J.L., 2000. Characterization of an internal ribosomal entry segment in the 5' leader of murine leukemia virus env RNA. Journal of virology 74, 846-850.

Demirov, D.G., Orenstein, J.M., Freed, E.O., 2002. The late domain of human immunodeficiency virus type 1 p6 promotes virus release in a cell type-dependent manner. Journal of virology 76, 105-117.

Denner, J., 2010. Endogenous Retroviruses, in: Kurth, R., Bannert, N. (Eds.), Retroviruses: Molecular Biology, Genomics and Pathogenesis. Caister Academic Press, Norfolk, UK, pp. 35-70.

DesGroseillers, L., Jolicoeur, P., 1983. Physical mapping of the Fv-1 tropism host range determinant of BALB/c murine leukemia viruses. Journal of virology 48, 685-696.

Desimmie, B.A., Delviks-Frankenberrry, K.A., Burdick, R.C., Qi, D., Izumi, T., Pathak, V.K., 2014. Multiple APOBEC3 restriction factors for HIV-1 and one Vif to rule them all. Journal of molecular biology 426, 1220-1245.

Dey, A., York, D., Smalls-Mantey, A., Summers, M.F., 2005. Composition and sequence-dependent binding of RNA to the nucleocapsid protein of Moloney murine leukemia virus. Biochemistry 44, 3735-3744.

Diaz-Griffero, F., Li, X., Javanbakht, H., Song, B., Welikala, S., Stremlau, M., Sodroski, J., 2006. Rapid turnover and polyubiquitylation of the retroviral restriction factor TRIM5. Virology 349, 300-315.

Diaz-Griffero, F., Qin, X.R., Hayashi, F., Kigawa, T., Finzi, A., Sarnak, Z., Lienlaf, M., Yokoyama, S., Sodroski, J., 2009. A B-box 2 surface patch important for TRIM5alpha self-association, capsid binding avidity, and retrovirus restriction. Journal of virology 83, 10737-10751.

Dingwall, C., Ernberg, I., Gait, M.J., Green, S.M., Heaphy, S., Karn, J., Lowe, A.D., Singh, M., Skinner, M.A., 1990. HIV-1 tat protein stimulates transcription by binding to a U-rich bulge in the stem of the TAR RNA structure. The EMBO journal 9, 4145-4153.

Dingwall, C., Ernberg, I., Gait, M.J., Green, S.M., Heaphy, S., Karn, J., Lowe, A.D., Singh, M., Skinner, M.A., Valerio, R., 1989. Human immunodeficiency virus 1 tat protein binds trans-activation-responsive region (TAR) RNA in vitro. Proceedings of the National Academy of Sciences of the United States of America 86, 6925-6929.

Dodding, M.P., 2006. Interactions of retroviral capsid proteins with restriction factors. PhD Thesis, University of London, London.

Dodding, M.P., Bock, M., Yap, M.W., Stoye, J.P., 2005. Capsid processing requirements for abrogation of Fv1 and Ref1 restriction. Journal of virology 79, 10571-10577.

Dupressoir, A., Lavialle, C., Heidmann, T., 2012. From ancestral infectious retroviruses to bona fide cellular genes: role of the captured syncytins in placentation. Placenta 33, 663-671.

Duran-Troise, G., Bassin, R.H., Rein, A., Gerwin, B.I., 1977. Loss of Fv-1 restriction in Balb/3T3 cells following infection with a single N tropic murine leukemia virus particle. Cell 10, 479-488.

Ehrlich, L.S., Agresta, B.E., Carter, C.A., 1992. Assembly of recombinant human immunodeficiency virus type 1 capsid protein in vitro. Journal of virology 66, 4874-4883.

Elis, E., Ehrlich, M., Prizan-Ravid, A., Laham-Karam, N., Bacharach, E., 2012. p12 tethers the murine leukemia virus pre-integration complex to mitotic chromosomes. PLoS pathogens 8, e1003103.

Ellermann, V., Bang, O., 1908. Experimentelle Leukamie bei Huhnern. Zentralbl. Bakteriol. Parisitenkd. Infectionskr. Hyg. Abt. Orig. 46, 595-609.

Elliott, R.B., Escobar, L., Garkavenko, O., Croxson, M.C., Schroeder, B.A., McGregor, M., Ferguson, G., Beckman, N., Ferguson, S., 2000. No evidence of infection with porcine endogenous retrovirus in recipients of encapsulated porcine islet xenografts. Cell transplantation 9, 895-901.

Ellis, S., 2000. Evolutionary and functional studies of the mouse retrovirus restriction gene, *Fv1*. University of London.

Enarson, P., Enarson, M., Bastos, R., Burke, B., 1998. Amino-terminal sequences that direct nucleoporin nup153 to the inner surface of the nuclear envelope. Chromosoma 107, 228-236.

Enders, J.F., Peebles, T.C., 1954. Propagation in tissue cultures of cytopathogenic agents from patients with measles. Proceedings of the Society for Experimental Biology and Medicine. Society for Experimental Biology and Medicine 86, 277-286.

Erickson-Viitanen, S., Manfredi, J., Viitanen, P., Tribe, D.E., Tritch, R., Hutchison, C.A., 3rd, Loeb, D.D., Swanstrom, R., 1989. Cleavage of HIV-1 gag polyprotein synthesized in vitro: sequential cleavage by the viral protease. AIDS research and human retroviruses 5, 577-591.

Everitt, A.R., Clare, S., Pertel, T., John, S.P., Wash, R.S., Smith, S.E., Chin, C.R., Feeley, E.M., Sims, J.S., Adams, D.J., Wise, H.M., Kane, L., Goulding, D., Digard, P., Anttila, V., Baillie, J.K., Walsh, T.S., Hume, D.A., Palotie, A., Xue, Y., Colonna, V., Tyler-Smith, C., Dunning, J., Gordon, S.B., Gen, I.I., Investigators, M., Smyth, R.L., Openshaw, P.J., Dougan, G., Brass, A.L., Kellam, P., 2012. IFITM3 restricts the morbidity and mortality associated with influenza. Nature 484, 519-523.

Faller, D.V., Hopkins, N., 1977. RNase T1-resistant oligonucleotides of B-tropic murine leukemia virus from BALB/c and five of its NB-tropic derivatives. Journal of virology 23, 188-195.

Farnet, C.M., Haseltine, W.A., 1991. Determination of viral proteins present in the human immunodeficiency virus type 1 preintegration complex. Journal of virology 65, 1910-1915.

Fassati, A., 2012. Multiple roles of the capsid protein in the early steps of HIV-1 infection. Virus research 170, 15-24.

Fassati, A., Goff, S.P., 1999. Characterization of intracellular reverse transcription complexes of Moloney murine leukemia virus. J Virol 73, 8919-8925.

Fassati, A., Goff, S.P., 2001. Characterization of intracellular reverse transcription complexes of human immunodeficiency virus type 1. Journal of virology 75, 3626-3635.

Fay, J.C., Wu, C.I., 2000. Hitchhiking under positive Darwinian selection. Genetics 155, 1405-1413.

Feher, A., Boross, P., Sperka, T., Miklossy, G., Kadas, J., Bagossi, P., Oroszlan, S., Weber, I.T., Tozser, J., 2006. Characterization of the murine leukemia virus protease and its comparison with the human immunodeficiency virus type 1 protease. The Journal of general virology 87, 1321-1330.

Felber, B.K., Paskalis, H., Kleinman-Ewing, C., Wong-Staal, F., Pavlakis, G.N., 1985. The pX protein of HTLV-I is a transcriptional activator of its long terminal repeats. Science 229, 675-679.

Felton, V., 2012. Studies of the regulation of Fv1 expression: Implications for retroviral restriction. PhD Thesis, University College London, London.

Feng, S., Holland, E.C., 1988. HIV-1 tat trans-activation requires the loop sequence within tar. Nature 334, 165-167.

Feng, Y., Broder, C.C., Kennedy, P.E., Berger, E.A., 1996. HIV-1 entry cofactor: functional cDNA cloning of a seven-transmembrane, G protein-coupled receptor. Science 272, 872-877.

Ferreira, J.P., Overton, K.W., Wang, C.L., 2013. Tuning gene expression with synthetic upstream open reading frames. Proceedings of the National Academy of Sciences of the United States of America 110, 11284-11289.

Finkelshtein, D., Werman, A., Novick, D., Barak, S., Rubinstein, M., 2013. LDL receptor and its family members serve as the cellular receptors for vesicular stomatitis virus. Proceedings of the National Academy of Sciences of the United States of America 110, 7306-7311.

Forshey, B.M., Aiken, C., 2003. Disassembly of human immunodeficiency virus type 1 cores in vitro reveals association of Nef with the subviral ribonucleoprotein complex. J Virol 77, 4409-4414.

Forshey, B.M., Shi, J., Aiken, C., 2005. Structural requirements for recognition of the human immunodeficiency virus type 1 core during host restriction in owl monkey cells. Journal of virology 79, 869-875.

Forshey, B.M., von Schwedler, U., Sundquist, W.I., Aiken, C., 2002. Formation of a human immunodeficiency virus type 1 core of optimal stability is crucial for viral replication. Journal of virology 76, 5667-5677.

Fossen, T., Wray, V., Bruns, K., Rachmat, J., Henklein, P., Tessmer, U., Maczurek, A., Klinger, P., Schubert, U., 2005. Solution structure of the human immunodeficiency virus type 1 p6 protein. The Journal of biological chemistry 280, 42515-42527.

Fricke, T., Brandariz-Nunez, A., Wang, X., Smith, A.B., 3rd, Diaz-Griffero, F., 2013a. Human cytosolic extracts stabilize the HIV-1 core. Journal of virology 87, 10587-10597.

Fricke, T., Valle-Casuso, J.C., White, T.E., Brandariz-Nunez, A., Bosche, W.J., Reszka, N., Gorelick, R., Diaz-Griffero, F., 2013b. The ability of TNPO3-depleted cells to inhibit HIV-1 infection requires CPSF6. Retrovirology 10, 46.

Fricke, T., White, T.E., Schulte, B., de Souza Aranha Vieira, D.A., Dharan, A., Campbell, E.M., Brandariz-Nunez, A., Diaz-Griffero, F., 2014. MxB binds to the HIV-1 core and prevents the uncoating process of HIV-1. Retrovirology 11, 68.

Fujisawa, J., Seiki, M., Kiyokawa, T., Yoshida, M., 1985. Functional activation of the long terminal repeat of human T-cell leukemia virus type I by a trans-acting factor. Proceedings of the National Academy of Sciences of the United States of America 82, 2277-2281.

Fuller, S.D., Wilk, T., Gowen, B.E., Krausslich, H.G., Vogt, V.M., 1997. Cryo-electron microscopy reveals ordered domains in the immature HIV-1 particle. Current biology : CB 7, 729-738.

Gallay, P., Swingler, S., Song, J., Bushman, F., Trono, D., 1995. HIV nuclear import is governed by the phosphotyrosine-mediated binding of matrix to the core domain of integrase. Cell 83, 569-576.

Gamble, T.R., Vajdos, F.F., Yoo, S., Worthylake, D.K., Houseweart, M., Sundquist, W.I., Hill, C.P., 1996. Crystal structure of human cyclophilin A bound to the amino-terminal domain of HIV-1 capsid. Cell 87, 1285-1294.

Gamble, T.R., Yoo, S., Vajdos, F.F., von Schwedler, U.K., Worthylake, D.K., Wang, H., McCutcheon, J.P., Sundquist, W.I., Hill, C.P., 1997. Structure of the carboxyl-terminal dimerization domain of the HIV-1 capsid protein. Science 278, 849-853.

Ganser-Pornillos, B.K., Chandrasekaran, V., Pornillos, O., Sodroski, J.G., Sundquist, W.I., Yeager, M., 2011. Hexagonal assembly of a restricting TRIM5alpha protein. Proceedings of the National Academy of Sciences of the United States of America 108, 534-539.

Ganser-Pornillos, B.K., Cheng, A., Yeager, M., 2007. Structure of full-length HIV-1 CA: a model for the mature capsid lattice. Cell 131, 70-79.

Ganser-Pornillos, B.K., von Schwedler, U.K., Stray, K.M., Aiken, C., Sundquist, W.I., 2004. Assembly properties of the human immunodeficiency virus type 1 CA protein. Journal of virology 78, 2545-2552.

Ganser, B.K., Cheng, A., Sundquist, W.I., Yeager, M., 2003. Three-dimensional structure of the M-MuLV CA protein on a lipid monolayer: a general model for retroviral capsid assembly. The EMBO journal 22, 2886-2892.

Ganser, B.K., Li, S., Klishko, V.Y., Finch, J.T., Sundquist, W.I., 1999. Assembly and analysis of conical models for the HIV-1 core. Science 283, 80-83.

Gao, D., Wu, J., Wu, Y.T., Du, F., Aroh, C., Yan, N., Sun, L., Chen, Z.J., 2013. Cyclic GMP-AMP synthase is an innate immune sensor of HIV and other retroviruses. Science 341, 903-906.

Garrus, J.E., von Schwedler, U.K., Pornillos, O.W., Morham, S.G., Zavitz, K.H., Wang, H.E., Wettstein, D.A., Stray, K.M., Cote, M., Rich, R.L., Myszka, D.G., Sundquist, W.I., 2001. Tsg101 and the vacuolar protein sorting pathway are essential for HIV-1 budding. Cell 107, 55-65.

Gendron, K., Ferbeyre, G., Heveker, N., Brakier-Gingras, L., 2011. The activity of the HIV-1 IRES is stimulated by oxidative stress and controlled by a negative regulatory element. Nucleic acids research 39, 902-912.

Gifford, R.J., Katzourakis, A., Tristem, M., Pybus, O.G., Winters, M., Shafer, R.W., 2008. A transitional endogenous lentivirus from the genome of a basal primate and implications for lentivirus evolution. Proceedings of the National Academy of Sciences of the United States of America 105, 20362-20367.

Gilbert, C., Maxfield, D.G., Goodman, S.M., Feschotte, C., 2009. Parallel germline infiltration of a lentivirus in two Malagasy lemurs. PLoS genetics 5, e1000425.

Girard, P.M., Bonnet-Mathoniere, B., Muriaux, D., Paoletti, J., 1995. A short autocomplementary sequence in the 5' leader region is responsible for dimerization of MoMuLV genomic RNA. Biochemistry 34, 9785-9794.

Gitti, R.K., Lee, B.M., Walker, J., Summers, M.F., Yoo, S., Sundquist, W.I., 1996. Structure of the amino-terminal core domain of the HIV-1 capsid protein. Science 273, 231-235.

Goldstone, D.C., Ennis-Adeniran, V., Hedden, J.J., Groom, H.C., Rice, G.I., Christodoulou, E., Walker, P.A., Kelly, G., Haire, L.F., Yap, M.W., de Carvalho, L.P., Stoye, J.P., Crow, Y.J., Taylor, I.A., Webb, M., 2011. HIV-1 restriction factor SAMHD1 is a deoxynucleoside triphosphate triphosphohydrolase. Nature 480, 379-382.

Goldstone, D.C., Walker, P.A., Calder, L.J., Coombs, P.J., Kirkpatrick, J., Ball, N.J., Hilditch, L., Yap, M.W., Rosenthal, P.B., Stoye, J.P., Taylor, I.A., 2014. Structural studies of postentry restriction factors reveal antiparallel dimers that enable avid binding to the HIV-1 capsid lattice. Proceedings of the National Academy of Sciences of the United States of America.

Gossen, M., Freundlieb, S., Bender, G., Muller, G., Hillen, W., Bujard, H., 1995. Transcriptional activation by tetracyclines in mammalian cells. Science 268, 1766-1769.

Gottlieb, M.S., Schroff, R., Schanker, H.M., Weisman, J.D., Fan, P.T., Wolf, R.A., Saxon, A., 1981. Pneumocystis carinii pneumonia and mucosal candidiasis in previously healthy homosexual men: evidence of a new acquired cellular immunodeficiency. The New England journal of medicine 305, 1425-1431.

Goujon, C., Moncorge, O., Bauby, H., Doyle, T., Barclay, W.S., Malim, M.H., 2014. Transfer of the amino-terminal nuclear envelope targeting domain of human MX2 converts MX1 into an HIV-1 resistance factor. Journal of virology.

Goujon, C., Moncorge, O., Bauby, H., Doyle, T., Ward, C.C., Schaller, T., Hue, S., Barclay, W.S., Schulz, R., Malim, M.H., 2013. Human MX2 is an interferon-induced post-entry inhibitor of HIV-1 infection. Nature 502, 559-562.

Gross, I., Hohenberg, H., Huckhagel, C., Krausslich, H.G., 1998. N-Terminal extension of human immunodeficiency virus capsid protein converts the in vitro assembly phenotype from tubular to spherical particles. Journal of virology 72, 4798-4810.

Gross, I., Hohenberg, H., Krausslich, H.G., 1997. In vitro assembly properties of purified bacterially expressed capsid proteins of human immunodeficiency virus. European journal of biochemistry / FEBS 249, 592-600.

Gross, L., 1951. "Spontaneous" leukemia developing in C3H mice following inoculation in infancy, with AK-leukemic extracts, or AK-embrvos. Proceedings of the Society for Experimental Biology and Medicine. Society for Experimental Biology and Medicine 76, 27-32.

Gu, C., Wei, X., Wang, Y., Chen, Y., Liu, J., Wang, H., Sun, G., Yi, D., 2008. No infection with porcine endogenous retrovirus in recipients of acellular porcine aortic valves: a two-year study. Xenotransplantation 15, 121-128.

Guenzel, C.A., Herate, C., Benichou, S., 2014. HIV-1 Vpr-a still "enigmatic multitasker". Frontiers in microbiology 5, 127.

Guntaka, R.V., 1993. Transcription termination and polyadenylation in retroviruses. Microbiological reviews 57, 511-521.

Gupta, S.S., Maetzig, T., Maertens, G.N., Sharif, A., Rothe, M., Weidner-Glunde, M., Galla, M., Schambach, A., Cherepanov, P., Schulz, T.F., 2013. Bromo and ET domain (BET) chromatin regulators serve as co-factors for murine leukemia virus integration. Journal of virology.

Hadravova, R., de Marco, A., Ulbrich, P., Stokrova, J., Dolezal, M., Pichova, I., Ruml, T., Briggs, J.A., Rumlova, M., 2012. In Vitro Assembly of Virus-Like Particles of a Gammaretrovirus, the Murine Leukemia Virus XMRV. Journal of virology 86, 1297-1306.

Han, G.Z., Worobey, M., 2012a. An endogenous foamy-like viral element in the coelacanth genome. PLoS pathogens 8, e1002790.

Han, G.Z., Worobey, M., 2012b. An endogenous foamy virus in the aye-aye (Daubentonia madagascariensis). Journal of virology 86, 7696-7698.

Han, G.Z., Worobey, M., 2012c. Endogenous lentiviral elements in the weasel family (Mustelidae). Molecular biology and evolution 29, 2905-2908.

Han, G.Z., Worobey, M., 2015. A primitive endogenous lentivirus in a colugo: insights into the early evolution of lentiviruses. Molecular biology and evolution 32, 211-215.

Hanly, S.M., Rimsky, L.T., Malim, M.H., Kim, J.H., Hauber, J., Duc Dodon, M., Le, S.Y., Maizel, J.V., Cullen, B.R., Greene, W.C., 1989. Comparative analysis of the HTLV-I Rex and HIV-1 Rev trans-regulatory proteins and their RNA response elements. Genes & development 3, 1534-1544.

Hare, S., Gupta, S.S., Valkov, E., Engelman, A., Cherepanov, P., 2010. Retroviral intasome assembly and inhibition of DNA strand transfer. Nature 464, 232-236.

Hare, S., Shun, M.C., Gupta, S.S., Valkov, E., Engelman, A., Cherepanov, P., 2009. A novel co-crystal structure affords the design of gain-of-function lentiviral integrase mutants in the presence of modified PSIP1/LEDGF/p75. PLoS pathogens 5, e1000259.

Harrison, I.P., McKnight, A., 2011. Cellular entry via an actin and clathrin-dependent route is required for Lv2 restriction of HIV-2. Virology 415, 47-55.

Hartley, J.W., Rowe, W.P., 1975. Clonal cells lines from a feral mouse embryo which lack host-range restrictions for murine leukemia viruses. Virology 65, 128-134.

Hartley, J.W., Rowe, W.P., Huebner, R.J., 1970. Host-range restrictions of murine leukemia viruses in mouse embryo cell cultures. Journal of virology 5, 221-225.

Hatziioannou, T., Cowan, S., Goff, S.P., Bieniasz, P.D., Towers, G.J., 2003. Restriction of multiple divergent retroviruses by Lv1 and Ref1. The EMBO journal 22, 385-394.

Hatziioannou, T., Perez-Caballero, D., Yang, A., Cowan, S., Bieniasz, P.D., 2004. Retrovirus resistance factors Ref1 and Lv1 are species-specific variants of TRIM5alpha. Proceedings of the National Academy of Sciences of the United States of America 101, 10774-10779.

Hauser, H., Lopez, L.A., Yang, S.J., Oldenburg, J.E., Exline, C.M., Guatelli, J.C., Cannon, P.M., 2010. HIV-1 Vpu and HIV-2 Env counteract BST-2/tetherin by sequestration in a perinuclear compartment. Retrovirology 7, 51.

Hayward, J.A., Tachedjian, M., Cui, J., Field, H., Holmes, E.C., Wang, L.F., Tachedjian, G., 2013. Identification of diverse full-length endogenous betaretroviruses in megabats and microbats. Retrovirology 10, 35.

Henderson, B.R., Percipalle, P., 1997. Interactions between HIV Rev and nuclear import and export factors: the Rev nuclear localisation signal mediates specific binding to human importin-beta. Journal of molecular biology 274, 693-707.

Heneine, W., Tibell, A., Switzer, W.M., Sandstrom, P., Rosales, G.V., Mathews, A., Korsgren, O., Chapman, L.E., Folks, T.M., Groth, C.G., 1998. No evidence of infection with porcine endogenous retrovirus in recipients of porcine islet-cell xenografts. Lancet 352, 695-699.

Hilditch, L., 2010. Interactions of host restriction factors with retroviral capsid proteins. PhD Thesis, University College London, London.

Hilditch, L., Matadeen, R., Goldstone, D.C., Rosenthal, P.B., Taylor, I.A., Stoye, J.P., 2011. Ordered assembly of murine leukemia virus capsid protein on lipid nanotubes directs specific binding by the restriction factor, Fv1. Proceedings of the National Academy of Sciences of the United States of America 108, 5771-5776.

Hilditch, L., Towers, G.J., 2014. A model for cofactor use during HIV-1 reverse transcription and nuclear entry. Current opinion in virology 4, 32-36.

Hill, C.P., Worthylake, D., Bancroft, D.P., Christensen, A.M., Sundquist, W.I., 1996. Crystal structures of the trimeric human immunodeficiency virus type 1 matrix protein: implications for membrane association and assembly. Proceedings of the National Academy of Sciences of the United States of America 93, 3099-3104.

Himathongkham, S., Luciw, P.A., 1996. Restriction of HIV-1 (subtype B) replication at the entry step in rhesus macaque cells. Virology 219, 485-488.

Hinnebusch, A.G., Jackson, B.M., Mueller, P.P., 1988. Evidence for regulation of reinitiation in translational control of GCN4 mRNA. Proceedings of the National Academy of Sciences of the United States of America 85, 7279-7283.

Hinz, A., Miguet, N., Natrajan, G., Usami, Y., Yamanaka, H., Renesto, P., Hartlieb, B., McCarthy, A.A., Simorre, J.P., Gottlinger, H., Weissenhorn, W., 2010. Structural basis of HIV-1 tethering to membranes by the BST-2/tetherin ectodomain. Cell host & microbe 7, 314-323.

Hirsch, V.M., Olmsted, R.A., Murphey-Corb, M., Purcell, R.H., Johnson, P.R., 1989. An African primate lentivirus (SIVsm) closely related to HIV-2. Nature 339, 389-392.

Hofmann, W., Schubert, D., LaBonte, J., Munson, L., Gibson, S., Scammell, J., Ferrigno, P., Sodroski, J., 1999. Species-specific, postentry barriers to primate immunodeficiency virus infection. Journal of virology 73, 10020-10028.

Hopkins, N., Schindler, J., Hynes, R., 1977. Six-NB-tropic murine leukemia viruses derived from a B-tropic virus of BALB/c have altered p30. Journal of virology 21, 309-318.

Hotter, D., Sauter, D., Kirchhoff, F., 2013. Emerging role of the host restriction factor tetherin in viral immune sensing. Journal of molecular biology 425, 4956-4964.

Hrecka, K., Hao, C., Gierszewska, M., Swanson, S.K., Kesik-Brodacka, M., Srivastava, S., Florens, L., Washburn, M.P., Skowronski, J., 2011. Vpx relieves inhibition of HIV-1 infection of macrophages mediated by the SAMHD1 protein. Nature 474, 658-661.

Hron, T., Fabryova, H., Pa Es, J., Elleder, D., 2014. Endogenous lentivirus in Malayan colugo (Galeopterus variegatus), a close relative of primates. Retrovirology 11, 84.

Hu, W.S., Hughes, S.H., 2012. HIV-1 reverse transcription. Cold Spring Harbor perspectives in medicine 2.

Huang, A.S., Besmer, P., Chu, L., Baltimore, D., 1973. Growth of pseudotypes of vesicular stomatitis virus with N-tropic murine leukemia virus coats in cells resistant to N-tropic viruses. Journal of virology 12, 659-662.

Huet, T., Cheynier, R., Meyerhans, A., Roelants, G., Wain-Hobson, S., 1990. Genetic organization of a chimpanzee lentivirus related to HIV-1. Nature 345, 356-359.

Hulme, A.E., Perez, O., Hope, T.J., 2011. Complementary assays reveal a relationship between HIV-1 uncoating and reverse transcription. Proceedings of the National Academy of Sciences of the United States of America 108, 9975-9980.

Hunter, E., 1997. Viral entry and receptors, in: Coffin, J.M., Hughes, S.H., Varmus, H.E. (Eds.), Retroviruses. Cold Spring Harbor Laboratory Press, Cold Spring Harbor (NY).

Huseby, D., Barklis, R.L., Alfadhli, A., Barklis, E., 2005. Assembly of human immunodeficiency virus precursor gag proteins. The Journal of biological chemistry 280, 17664-17670.

Hutter, S., Zurnic, I., Lindemann, D., 2013. Foamy virus budding and release. Viruses 5, 1075-1098.

Inaguma, Y., Miyashita, N., Moriwaki, K., Huai, W.C., Jin, M.L., He, X.Q., Ikeda, H., 1991. Acquisition of two endogenous ecotropic murine leukemia viruses in distinct Asian wild mouse populations. Journal of virology 65, 1796-1802.

Iordanskiy, S., Berro, R., Altieri, M., Kashanchi, F., Bukrinsky, M., 2006. Intracytoplasmic maturation of the human immunodeficiency virus type 1 reverse transcription complexes determines their capacity to integrate into chromatin. Retrovirology 3, 4.

Ivanov, D., Tsodikov, O.V., Kasanov, J., Ellenberger, T., Wagner, G., Collins, T., 2007. Domain-swapped dimerization of the HIV-1 capsid C-terminal domain. Proceedings of the National Academy of Sciences of the United States of America 104, 4353-4358.

Iwatani, Y., Chan, D.S., Wang, F., Maynard, K.S., Sugiura, W., Gronenborn, A.M., Rouzina, I., Williams, M.C., Musier-Forsyth, K., Levin, J.G., 2007. Deaminase-independent inhibition of HIV-1 reverse transcription by APOBEC3G. Nucleic acids research 35, 7096-7108.

Jacks, T., Power, M.D., Masiarz, F.R., Luciw, P.A., Barr, P.J., Varmus, H.E., 1988. Characterization of ribosomal frameshifting in HIV-1 gag-pol expression. Nature 331, 280-283.

Jager, S., Kim, D.Y., Hultquist, J.F., Shindo, K., LaRue, R.S., Kwon, E., Li, M., Anderson, B.D., Yen, L., Stanley, D., Mahon, C., Kane, J., Franks-Skiba, K., Cimermancic, P., Burlingame, A., Sali, A., Craik, C.S., Harris, R.S., Gross, J.D., Krogan, N.J., 2012. Vif hijacks CBF-beta to degrade APOBEC3G and promote HIV-1 infection. Nature 481, 371-375.

Jakobsen, M.R., Bak, R.O., Andersen, A., Berg, R.K., Jensen, S.B., Tengchuan, J., Laustsen, A., Hansen, K., Ostergaard, L., Fitzgerald, K.A., Xiao, T.S., Mikkelsen, J.G., Mogensen, T.H., Paludan, S.R., 2013. IFI16 senses DNA forms of the lentiviral replication cycle and controls HIV-1 replication. Proceedings of the National Academy of Sciences of the United States of America 110, E4571-4580.

Jamjoom, G.A., Naso, R.B., Arlinghaus, R.B., 1976. Selective decrease in the rate of cleavage of an intracellular precursor to Rauscher leukemia virus p30 by treatment of infected cells with actinomycin D. Journal of virology 19, 1054-1072.

Jang, S.K., Krausslich, H.G., Nicklin, M.J., Duke, G.M., Palmenberg, A.C., Wimmer, E., 1988. A segment of the 5' nontranslated region of encephalomyocarditis virus RNA directs internal entry of ribosomes during in vitro translation. Journal of virology 62, 2636-2643.

Ji, X., Wu, Y., Yan, J., Mehrens, J., Yang, H., DeLucia, M., Hao, C., Gronenborn, A.M., Skowronski, J., Ahn, J., Xiong, Y., 2013. Mechanism of allosteric activation of SAMHD1 by dGTP. Nature structural & molecular biology 20, 1304-1309.

Jin, X., Turcott, E., Englehardt, S., Mize, G.J., Morris, D.R., 2003. The two upstream open reading frames of oncogene mdm2 have different translational regulatory properties. The Journal of biological chemistry 278, 25716-25721.

Jin, Z., Jin, L., Peterson, D.L., Lawson, C.L., 1999. Model for lentivirus capsid core assembly based on crystal dimers of EIAV p26. Journal of molecular biology 286, 83-93.

John, S.P., Chin, C.R., Perreira, J.M., Feeley, E.M., Aker, A.M., Savidis, G., Smith, S.E., Elia, A.E., Everitt, A.R., Vora, M., Pertel, T., Elledge, S.J., Kellam, P., Brass, A.L., 2013. The CD225 domain of IFITM3 is required for both IFITM protein association and inhibition of influenza A virus and dengue virus replication. Journal of virology 87, 7837-7852.

Johnston, J.A., Ward, C.L., Kopito, R.R., 1998. Aggresomes: a cellular response to misfolded proteins. J Cell Biol 143, 1883-1898.

Jolicoeur, P., Baltimore, D., 1976. Effect of Fv-1 gene product on proviral DNA formation and integration in cells infected with murine leukemia viruses. Proceedings of the National Academy of Sciences of the United States of America 73, 2236-2240.

Jones, C.P., Datta, S.A., Rein, A., Rouzina, I., Musier-Forsyth, K., 2011. Matrix domain modulates HIV-1 Gag's nucleic acid chaperone activity via inositol phosphate binding. J Virol 85, 1594-1603.

Jun, S., Ke, D., Debiec, K., Zhao, G., Meng, X., Ambrose, Z., Gibson, G.A., Watkins, S.C., Zhang, P., 2011. Direct visualization of HIV-1 with correlative live-cell microscopy and cryo-electron tomography. Structure 19, 1573-1581.

Jung, Y.T., Kozak, C.A., 2000. A single amino acid change in the murine leukemia virus capsid gene responsible for the Fv1(nr) phenotype. Journal of virology 74, 5385-5387.

Kafaie, J., Song, R., Abrahamyan, L., Mouland, A.J., Laughrea, M., 2008. Mapping of nucleocapsid residues important for HIV-1 genomic RNA dimerization and packaging. Virology 375, 592-610.

Kalyanaraman, V.S., Sarngadharan, M.G., Robert-Guroff, M., Miyoshi, I., Golde, D., Gallo, R.C., 1982. A new subtype of human T-cell leukemia virus (HTLV-II) associated with a T-cell variant of hairy cell leukemia. Science 218, 571-573.

Kane, M., Yadav, S.S., Bitzegeio, J., Kutluay, S.B., Zang, T., Wilson, S.J., Schoggins, J.W., Rice, C.M., Yamashita, M., Hatziioannou, T., Bieniasz, P.D., 2013. MX2 is an interferon-induced inhibitor of HIV-1 infection. Nature 502, 563-566.

Kar, A.K., Diaz-Griffero, F., Li, Y., Li, X., Sodroski, J., 2008. Biochemical and biophysical characterization of a chimeric TRIM21-TRIM5alpha protein. Journal of virology 82, 11669-11681.

Karageorgos, L., Li, P., Burrell, C., 1993. Characterization of HIV replication complexes early after cell-to-cell infection. AIDS research and human retroviruses 9, 817-823.

Karn, J., Stoltzfus, C.M., 2012. Transcriptional and posttranscriptional regulation of HIV-1 gene expression. Cold Spring Harbor perspectives in medicine 2, a006916.

Kashmiri, S.V., Rein, A., Bassin, R.H., Gerwin, B.I., Gisselbrecht, S., 1977. Donation of N- or B-tropic phenotype to NB-tropic murine leukemia virus during mixed infections. Journal of virology 22, 626-633.

Katzourakis, A., Gifford, R.J., Tristem, M., Gilbert, M.T., Pybus, O.G., 2009. Macroevolution of complex retroviruses. Science 325, 1512.

Katzourakis, A., Tristem, M., Pybus, O.G., Gifford, R.J., 2007. Discovery and analysis of the first endogenous lentivirus. Proceedings of the National Academy of Sciences of the United States of America 104, 6261-6265.

Kavanaugh, M.P., Miller, D.G., Zhang, W., Law, W., Kozak, S.L., Kabat, D., Miller, A.D., 1994. Cell-surface receptors for gibbon ape leukemia virus and amphotropic murine retrovirus are inducible sodium-dependent phosphate symporters. Proceedings of the National Academy of Sciences of the United States of America 91, 7071-7075.

Keckesova, Z., Ylinen, L.M., Towers, G.J., 2004. The human and African green monkey TRIM5alpha genes encode Ref1 and Lv1 retroviral restriction factor activities. Proceedings of the National Academy of Sciences of the United States of America 101, 10780-10785.

Keckesova, Z., Ylinen, L.M., Towers, G.J., Gifford, R.J., Katzourakis, A., 2009. Identification of a RELIK orthologue in the European hare (Lepus europaeus) reveals a minimum age of 12 million years for the lagomorph lentiviruses. Virology 384, 7-11.

Kim, C.H., Tinoco, I., Jr., 2000. A retroviral RNA kissing complex containing only two G.C base pairs. Proceedings of the National Academy of Sciences of the United States of America 97, 9396-9401.

Kim, J., Tipper, C., Sodroski, J., 2011. Role of TRIM5alpha RING domain E3 ubiquitin ligase activity in capsid disassembly, reverse transcription blockade, and restriction of simian immunodeficiency virus. Journal of virology 85, 8116-8132.

Klatzmann, D., Barre-Sinoussi, F., Nugeyre, M.T., Danquet, C., Vilmer, E., Griscelli, C., Brun-Veziret, F., Rouzioux, C., Gluckman, J.C., Chermann, J.C., et al., 1984. Selective tropism of lymphadenopathy associated virus (LAV) for helper-inducer T lymphocytes. Science 225, 59-63.

Kobayashi, M., Takaori-Kondo, A., Miyauchi, Y., Iwai, K., Uchiyama, T., 2005. Ubiquitination of APOBEC3G by an HIV-1 Vif-Cullin5-Elongin B-Elongin C complex is essential for Vif function. The Journal of biological chemistry 280, 18573-18578.

Koh, Y., Wu, X., Ferris, A.L., Matreyek, K.A., Smith, S.J., Lee, K., KewalRamani, V.N., Hughes, S.H., Engelman, A., 2013. Differential effects of human immunodeficiency virus type 1 capsid and cellular factors nucleoporin 153 and LEDGF/p75 on the efficiency and specificity of viral DNA integration. Journal of virology 87, 648-658.

Konig, R., Zhou, Y., Elleder, D., Diamond, T.L., Bonamy, G.M., Irelan, J.T., Chiang, C.Y., Tu, B.P., De Jesus, P.D., Lilley, C.E., Seidel, S., Opaluch, A.M., Caldwell, J.S., Weitzman, M.D., Kuhen, K.L., Bandyopadhyay, S., Ideker, T., Orth, A.P., Miraglia, L.J., Bushman, F.D., Young, J.A., Chanda, S.K., 2008. Global analysis of host-pathogen interactions that regulate early-stage HIV-1 replication. Cell 135, 49-60.

Kono, K., Bozek, K., Domingues, F.S., Shioda, T., Nakayama, E.E., 2009. Impact of a single amino acid in the variable region 2 of the Old World monkey TRIM5alpha SPRY (B30.2) domain on anti-human immunodeficiency virus type 2 activity. Virology 388, 160-168.

Kozak, C.A., 1985. Analysis of wild-derived mice for Fv-1 and Fv-2 murine leukemia virus restriction loci: a novel wild mouse Fv-1 allele responsible for lack of host range restriction. Journal of virology 55, 281-285.

Kozak, C.A., 2010. The mouse "xenotropic" gammaretroviruses and their XPR1 receptor. Retrovirology 7, 101.

Kozak, C.A., 2014. Origins of the Endogenous and Infectious Laboratory Mouse Gammaretroviruses. Viruses 7, 1-26.

Kozak, C.A., Chakraborti, A., 1996. Single amino acid changes in the murine leukemia virus capsid protein gene define the target of Fv1 resistance. Virology 225, 300-305.

Kozak, M., 1986. Point mutations define a sequence flanking the AUG initiator codon that modulates translation by eukaryotic ribosomes. Cell 44, 283-292.

Kozak, M., 1987. Effects of intercistronic length on the efficiency of reinitiation by eucaryotic ribosomes. Molecular and cellular biology 7, 3438-3445.

Kozak, M., 2001. Constraints on reinitiation of translation in mammals. Nucleic acids research 29, 5226-5232.

Kozak, M., 2002. Pushing the limits of the scanning mechanism for initiation of translation. Gene 299, 1-34.

Krishnamoorthy, G., Roques, B., Darlix, J.L., Mely, Y., 2003. DNA condensation by the nucleocapsid protein of HIV-1: a mechanism ensuring DNA protection. Nucleic acids research 31, 5425-5432.

Krontiris, T.G., Soeiro, R., Fields, B.N., 1973. Host restriction of Friend leukemia virus. Role of the viral outer coat. Proceedings of the National Academy of Sciences of the United States of America 70, 2549-2553.

Kubo, Y., Hayashi, H., Matsuyama, T., Sato, H., Yamamoto, N., 2012. Retrovirus entry by endocytosis and cathepsin proteases. Advances in virology 2012, 640894.

Kupzig, S., Korolchuk, V., Rollason, R., Sugden, A., Wilde, A., Banting, G., 2003. Bst-2/HM1.24 is a raft-associated apical membrane protein with an unusual topology. Traffic 4, 694-709.

Kutluay, S.B., Perez-Caballero, D., Bieniasz, P.D., 2013. Fates of Retroviral Core Components during Unrestricted and TRIM5-Restricted Infection. PLoS pathogens 9, e1003214.

Kwong, P.D., Wyatt, R., Robinson, J., Sweet, R.W., Sodroski, J., Hendrickson, W.A., 1998. Structure of an HIV gp120 envelope glycoprotein in complex with the CD4 receptor and a neutralizing human antibody. Nature 393, 648-659.

Kyere, S.K., Joseph, P.R., Summers, M.F., 2008. The p12 domain is unstructured in a murine leukemia virus p12-CA(N) Gag construct. PloS one 3, e1902.

Laguette, N., Sobhian, B., Casartelli, N., Ringeard, M., Chable-Bessia, C., Segeral, E., Yatim, A., Emiliani, S., Schwartz, O., Benkirane, M., 2011a. SAMHD1 is the dendritic- and myeloid-cell-specific HIV-1 restriction factor counteracted by Vpx. Nature 474, 654-657.

Laguette, N., Sobhian, B., Casartelli, N., Ringeard, M., Chable-Bessia, C., Segeral, E., Yatim, A., Emiliani, S., Schwartz, O., Benkirane, M., 2011b. SAMHD1 is the dendritic- and myeloid-cell-specific HIV-1 restriction factor counteracted by Vpx. Nature 474, 654-657.

Lahaye, X., Satoh, T., Gentili, M., Cerboni, S., Conrad, C., Hurbain, I., El Marjou, A., Lacabaratz, C., Lelievre, J.D., Manel, N., 2013. The capsids of HIV-1 and HIV-2 determine immune detection of the viral cDNA by the innate sensor cGAS in dendritic cells. Immunity 39, 1132-1142.

Lai, M.C., Lin, R.I., Tarn, W.Y., 2001. Transportin-SR2 mediates nuclear import of phosphorylated SR proteins. Proceedings of the National Academy of Sciences of the United States of America 98, 10154-10159.

Lander, M.R., Chattopadhyay, S.K., 1984. A Mus dunni cell line that lacks sequences closely related to endogenous murine leukemia viruses and can be infected by ectropic, amphotropic, xenotropic, and mink cell focus-forming viruses. Journal of virology 52, 695-698.

Langelier, C.R., Sandrin, V., Eckert, D.M., Christensen, D.E., Chandrasekaran, V., Alam, S.L., Aiken, C., Olsen, J.C., Kar, A.K., Sodroski, J.G., Sundquist, W.I., 2008. Biochemical characterization of a recombinant TRIM5alpha protein that restricts human immunodeficiency virus type 1 replication. Journal of virology 82, 11682-11694.

Lapatto, R., Blundell, T., Hemmings, A., Overington, J., Wilderspin, A., Wood, S., Merson, J.R., Whittle, P.J., Danley, D.E., Geoghegan, K.F., et al., 1989. X-ray analysis of HIV-1 proteinase at 2.7 A resolution confirms structural homology among retroviral enzymes. Nature 342, 299-302.

Lassaux, A., Sitbon, M., Battini, J.L., 2005. Residues in the murine leukemia virus capsid that differentially govern resistance to mouse Fv1 and human Ref1 restrictions. Journal of virology 79, 6560-6564.

Laughrea, M., Jette, L., 1994. A 19-nucleotide sequence upstream of the 5' major splice donor is part of the dimerization domain of human immunodeficiency virus 1 genomic RNA. Biochemistry 33, 13464-13474.

Lecossier, D., Bouchonnet, F., Clavel, F., Hance, A.J., 2003. Hypermutation of HIV-1 DNA in the absence of the Vif protein. Science 300, 1112.

Lee, K., Mulky, A., Yuen, W., Martin, T.D., Meyerson, N.R., Choi, L., Yu, H., Sawyer, S.L., Kewalramani, V.N., 2012. HIV-1 capsid-targeting domain of cleavage and polyadenylation specificity factor 6. Journal of virology 86, 3851-3860.

Lee, S., Zhao, Y., Anderson, W.F., 1999. Receptor-mediated Moloney murine leukemia virus entry can occur independently of the clathrin-coated-pit-mediated endocytic pathway. Journal of virology 73, 5994-6005.

Lewis, P., Hensel, M., Emerman, M., 1992. Human immunodeficiency virus infection of cells arrested in the cell cycle. The EMBO journal 11, 3053-3058.

Li, K., Markosyan, R.M., Zheng, Y.M., Golfetto, O., Bungart, B., Li, M., Ding, S., He, Y., Liang, C., Lee, J.C., Gratton, E., Cohen, F.S., Liu, S.L., 2013. IFITM proteins restrict viral membrane hemifusion. PLoS pathogens 9, e1003124.

Li, M., Laco, G.S., Jaskolski, M., Rozycki, J., Alexandratos, J., Wlodawer, A., Gustchina, A., 2005. Crystal structure of human T cell leukemia virus protease, a novel target for anticancer drug design. Proceedings of the National Academy of Sciences of the United States of America 102, 18332-18337.

Li, M., Mizuuchi, M., Burke, T.R., Jr., Craigie, R., 2006a. Retroviral DNA integration: reaction pathway and critical intermediates. The EMBO journal 25, 1295-1304.

Li, S., Hill, C.P., Sundquist, W.I., Finch, J.T., 2000. Image reconstructions of helical assemblies of the HIV-1 CA protein. Nature 407, 409-413.

Li, X., Li, Y., Stremlau, M., Yuan, W., Song, B., Perron, M., Sodroski, J., 2006b. Functional replacement of the RING, B-box 2, and coiled-coil domains of tripartite motif 5alpha (TRIM5alpha) by heterologous TRIM domains. Journal of virology 80, 6198-6206.

Li, X., Sodroski, J., 2008. The TRIM5alpha B-box 2 domain promotes cooperative binding to the retroviral capsid by mediating higher-order self-association. Journal of virology 82, 11495-11502.

Li, Y., Li, X., Stremlau, M., Lee, M., Sodroski, J., 2006c. Removal of arginine 332 allows human TRIM5alpha to bind human immunodeficiency virus capsids and to restrict infection. Journal of virology 80, 6738-6744.

Liberatore, R.A., Bieniasz, P.D., 2011. Sensing retroviruses. Immunity 35, 8-10.

Lienlaf, M., Hayashi, F., Di Nunzio, F., Tochio, N., Kigawa, T., Yokoyama, S., Diaz-Griffero, F., 2011. Contribution of E3-ubiquitin ligase activity to HIV-1 restriction by TRIM5alpha(rh): structure of the RING domain of TRIM5alpha. Journal of virology 85, 8725-8737.

Lilly, F., 1970. Fv-2: identification and location of a second gene governing the spleen focus response to Friend leukemia virus in mice. Journal of the National Cancer Institute 45, 163-169.

Lilly, F., Pincus, T., 1973. Genetic control of murine viral leukemogenesis. Adv Cancer Res.

Lilly, F., Steeves, R.A., 1973. B-tropic Friend virus: a host-range pseudotype of spleen focus-forming virus (SFFV). Virology 55, 363-370.

Lin, D.H., Zimmermann, S., Stuwe, T., Stuwe, E., Hoelz, A., 2013. Structural and functional analysis of the C-terminal domain of Nup358/RanBP2. Journal of molecular biology 425, 1318-1329.

Liu, Z., Pan, Q., Ding, S., Qian, J., Xu, F., Zhou, J., Cen, S., Guo, F., Liang, C., 2013. The interferon-inducible MxB protein inhibits HIV-1 infection. Cell host & microbe 14, 398-410.

Loew, R., Heinz, N., Hampf, M., Bujard, H., Gossen, M., 2010. Improved Tet-responsive promoters with minimized background expression. BMC biotechnology 10, 81.

Losey, E.A., Smith, M.D., Meng, M., Best, M.D., 2009. Microplate-based analysis of protein-membrane binding interactions via immobilization of whole liposomes containing a biotinylated anchor. Bioconjugate chemistry 20, 376-383.

Loving, R., Kronqvist, M., Sjoberg, M., Garoff, H., 2011. Cooperative cleavage of the R peptide in the Env trimer of Moloney murine leukemia virus facilitates its maturation for fusion competence. Journal of virology 85, 3262-3269.

Loving, R., Li, K., Wallin, M., Sjoberg, M., Garoff, H., 2008. R-Peptide cleavage potentiates fusion-controlling isomerization of the intersubunit disulfide in Moloney murine leukemia virus Env. Journal of virology 82, 2594-2597.

Loving, R., Wu, S.R., Sjoberg, M., Lindqvist, B., Garoff, H., 2012. Maturation cleavage of the murine leukemia virus Env precursor separates the transmembrane subunits to prime it for receptor triggering. Proceedings of the National Academy of Sciences of the United States of America 109, 7735-7740.

Lowy, D.R., Rowe, W.P., Teich, N., Hartley, J.W., 1971. Murine leukemia virus: high-frequency activation in vitro by 5-iododeoxyuridine and 5-bromodeoxyuridine. Science 174, 155-156.

Lu, J., Pan, Q., Rong, L., He, W., Liu, S.L., Liang, C., 2011. The IFITM proteins inhibit HIV-1 infection. Journal of virology 85, 2126-2137.

Luban, J., Bossolt, K.L., Franke, E.K., Kalpana, G.V., Goff, S.P., 1993. Human immunodeficiency virus type 1 Gag protein binds to cyclophilins A and B. Cell 73, 1067-1078.

Lukic, Z., Hausmann, S., Sebastian, S., Rucci, J., Sastri, J., Robia, S.L., Luban, J., Campbell, E.M., 2011. TRIM5alpha associates with proteasomal subunits in cells while in complex with HIV-1 virions. Retrovirology 8, 93.

Ly, H., Parslow, T.G., 2002. Bipartite signal for genomic RNA dimerization in Moloney murine leukemia virus. Journal of virology 76, 3135-3144.

Maddon, P.J., McDougal, J.S., Clapham, P.R., Dalgleish, A.G., Jamal, S., Weiss, R.A., Axel, R., 1988. HIV infection does not require endocytosis of its receptor, CD4. Cell 54, 865-874.

Maegawa, H., Miyamoto, T., Sakuragi, J., Shioda, T., Nakayama, E.E., 2010. Contribution of RING domain to retrovirus restriction by TRIM5alpha depends on combination of host and virus. Virology 399, 212-220.

Maertens, G., Cherepanov, P., Pluymers, W., Busschots, K., De Clercq, E., Debyser, Z., Engelborghs, Y., 2003. LEDGF/p75 is essential for nuclear and chromosomal targeting of HIV-1 integrase in human cells. The Journal of biological chemistry 278, 33528-33539.

Maertens, G.N., Cook, N.J., Wang, W., Hare, S., Gupta, S.S., Oztop, I., Lee, K., Pye, V.E., Cosnefroy, O., Snijders, A.P., KewalRamani, V.N., Fassati, A., Engelman, A., Cherepanov, P., 2014. Structural basis for nuclear import of splicing factors by human Transportin 3. Proceedings of the National Academy of Sciences of the United States of America 111, 2728-2733.

Maillard, P.V., Reynard, S., Serhan, F., Turelli, P., Trono, D., 2007. Interfering residues narrow the spectrum of MLV restriction by human TRIM5alpha. PLoS pathogens 3, e200.

Malfavon-Borja, R., Wu, L.I., Emerman, M., Malik, H.S., 2013. Birth, decay, and reconstruction of an ancient TRIMCyp gene fusion in primate genomes. Proceedings of the National Academy of Sciences of the United States of America 110, E583-592.

Malim, M.H., Hauber, J., Le, S.Y., Maizel, J.V., Cullen, B.R., 1989. The HIV-1 rev trans-activator acts through a structured target sequence to activate nuclear export of unspliced viral mRNA. Nature 338, 254-257.

Mangeat, B., Turelli, P., Caron, G., Friedli, M., Perrin, L., Trono, D., 2003. Broad antiretroviral defence by human APOBEC3G through lethal editing of nascent reverse transcripts. Nature 424, 99-103.

Marchant, D., Neil, S.J., Aubin, K., Schmitz, C., McKnight, A., 2005. An envelope-determined, pH-independent endocytic route of viral entry determines the susceptibility of human immunodeficiency virus type 1 (HIV-1) and HIV-2 to Lv2 restriction. Journal of virology 79, 9410-9418.

Markovic, I., Stantchev, T.S., Fields, K.H., Tiffany, L.J., Tomic, M., Weiss, C.D., Broder, C.C., Strebel, K., Clouse, K.A., 2004. Thiol/disulfide exchange is a prerequisite for CXCR4-tropic HIV-1 envelope-mediated T-cell fusion during viral entry. Blood 103, 1586-1594.

Marno, K.M., Ogunkolade, B.W., Pade, C., Oliveira, N.M., O'Sullivan, E., McKnight, A., 2014. Novel restriction factor RNA-associated early-stage anti-viral factor (REAF) inhibits human and simian immunodeficiency viruses. Retrovirology 11, 3.

Marshall, H.M., Ronen, K., Berry, C., Llano, M., Sutherland, H., Saenz, D., Bickmore, W., Poeschla, E., Bushman, F.D., 2007. Role of PSIP1/LEDGF/p75 in lentiviral infectivity and integration targeting. PloS one 2, e1340.

Martin-Serrano, J., Eastman, S.W., Chung, W., Bieniasz, P.D., 2005. HECT ubiquitin ligases link viral and cellular PPXY motifs to the vacuolar protein-sorting pathway. The Journal of cell biology 168, 89-101.

Matreyek, K.A., Engelman, A., 2011. The requirement for nucleoporin NUP153 during human immunodeficiency virus type 1 infection is determined by the viral capsid. Journal of virology 85, 7818-7827.

Matreyek, K.A., Engelman, A., 2013. Viral and cellular requirements for the nuclear entry of retroviral preintegration nucleoprotein complexes. Viruses 5, 2483-2511.

Matreyek, K.A., Yucel, S.S., Li, X., Engelman, A., 2013. Nucleoporin NUP153 phenylalanine-glycine motifs engage a common binding pocket within the HIV-1 capsid protein to mediate lentiviral infectivity. PLoS pathogens 9, e1003693.

Mayo, K., Huseby, D., McDermott, J., Arvidson, B., Finlay, L., Barklis, E., 2003. Retrovirus capsid protein assembly arrangements. Journal of molecular biology 325, 225-237.

McClure, M.O., Marsh, M., Weiss, R.A., 1988. Human immunodeficiency virus infection of CD4-bearing cells occurs by a pH-independent mechanism. The EMBO journal 7, 513-518.

McClure, M.O., Sommerfelt, M.A., Marsh, M., Weiss, R.A., 1990. The pH independence of mammalian retrovirus infection. The Journal of general virology 71 (Pt 4), 767-773.

McCullough, J., Colf, L.A., Sundquist, W.I., 2013. Membrane fission reactions of the mammalian ESCRT pathway. Annual review of biochemistry 82, 663-692.

McDonald, D., Vodicka, M.A., Lucero, G., Svitkina, T.M., Borisy, G.G., Emerman, M., Hope, T.J., 2002. Visualization of the intracellular behavior of HIV in living cells. The Journal of cell biology 159, 441-452.

McNatt, M.W., Zang, T., Bieniasz, P.D., 2013. Vpu binds directly to tetherin and displaces it from nascent virions. PLoS pathogens 9, e1003299.

Mellgren, R.L., 1997. Evidence for participation of a calpain-like cysteine protease in cell cycle progression through late G1 phase. Biochemical and biophysical research communications 236, 555-558.

Meng, X., Zhao, G., Yufenyuy, E., Ke, D., Ning, J., Delucia, M., Ahn, J., Gronenborn, A.M., Aiken, C., Zhang, P., 2012. Protease Cleavage Leads to Formation of Mature Trimer Interface in HIV-1 Capsid. PLoS pathogens 8, e1002886.

Mertz, J.A., Simper, M.S., Lozano, M.M., Payne, S.M., Dudley, J.P., 2005. Mouse mammary tumor virus encodes a self-regulatory RNA export protein and is a complex retrovirus. Journal of virology 79, 14737-14747.

Mi, S., Lee, X., Li, X., Veldman, G.M., Finnerty, H., Racie, L., LaVallie, E., Tang, X.Y., Edouard, P., Howes, S., Keith, J.C., Jr., McCoy, J.M., 2000. Syncytin is a captive retroviral envelope protein involved in human placental morphogenesis. Nature 403, 785-789.

Miller, M., Schneider, J., Sathyanarayana, B.K., Toth, M.V., Marshall, G.R., Clawson, L., Selk, L., Kent, S.B., Wlodawer, A., 1989. Structure of complex of synthetic HIV-1 protease with a substrate-based inhibitor at 2.3 A resolution. Science 246, 1149-1152.

Miller, M.D., Farnet, C.M., Bushman, F.D., 1997. Human immunodeficiency virus type 1 preintegration complexes: studies of organization and composition. Journal of virology 71, 5382-5390.

Miyauchi, K., Kim, Y., Latinovic, O., Morozov, V., Melikyan, G.B., 2009. HIV enters cells via endocytosis and dynamin-dependent fusion with endosomes. Cell 137, 433-444.

Mizuguchi, H., Xu, Z., Ishii-Watabe, A., Uchida, E., Hayakawa, T., 2000. IRES-dependent second gene expression is significantly lower than cap-dependent first gene expression in a bicistronic vector. Molecular therapy : the journal of the American Society of Gene Therapy 1, 376-382.

Moebes, A., Enssle, J., Bieniasz, P.D., Heinkelein, M., Lindemann, D., Bock, M., McClure, M.O., Rethwilm, A., 1997. Human foamy virus reverse transcription that occurs late in the viral replication cycle. Journal of virology 71, 7305-7311.

Monette, A., Valiente-Echeverria, F., Rivero, M., Cohen, E.A., Lopez-Lastra, M., Mouland, A.J., 2013. Dual mechanisms of translation initiation of the full-length HIV-1 mRNA contribute to gag synthesis. PloS one 8, e68108.

Moore, M.D., Nikolaitchik, O.A., Chen, J., Hammarskjold, M.L., Rekosh, D., Hu, W.S., 2009. Probing the HIV-1 genomic RNA trafficking pathway and dimerization by genetic recombination and single virion analyses. PLoS pathogens 5, e1000627.

Morellet, N., Druillennec, S., Lenoir, C., Bouaziz, S., Roques, B.P., 2005. Helical structure determined by NMR of the HIV-1 (345-392)Gag sequence, surrounding p2: implications for particle assembly and RNA packaging. Protein science : a publication of the Protein Society 14, 375-386.

Mortuza, G.B., Dodding, M.P., Goldstone, D.C., Haire, L.F., Stoye, J.P., Taylor, I.A., 2008. Structure of B-MLV capsid amino-terminal domain reveals key features of viral tropism, gag assembly and core formation. Journal of molecular biology 376, 1493-1508.

Mortuza, G.B., Goldstone, D.C., Pashley, C., Haire, L.F., Palmarini, M., Taylor, W.R., Stoye, J.P., Taylor, I.A., 2009. Structure of the capsid amino-terminal domain from the betaretrovirus, Jaagsiekte sheep retrovirus. Journal of molecular biology 386, 1179-1192.

Mortuza, G.B., Haire, L.F., Stevens, A., Smerdon, S.J., Stoye, J.P., Taylor, I.A., 2004. High-resolution structure of a retroviral capsid hexameric amino-terminal domain. Nature 431, 481-485.

Mothes, W., Uchil, P.D., 2010. Retroviral entry and uncoating, in: Kurth, R., Bannert, N. (Eds.), Retroviruses: molecular biology, genomics and pathogenesis. Caister Academic Press, Norfolk, UK, pp. 107-128.

Mu, D., Yang, H., Zhu, J.W., Liu, F.L., Tian, R.R., Zheng, H.Y., Han, J.B., Shi, P., Zheng, Y.T., 2014. Independent birth of a novel TRIMCyp in Tupaia belangeri with a divergent function from its paralog TRIM5. Molecular biology and evolution.

Muesing, M.A., Smith, D.H., Capon, D.J., 1987. Regulation of mRNA accumulation by a human immunodeficiency virus trans-activator protein. Cell 48, 691-701.

Munk, C., Brandt, S.M., Lucero, G., Landau, N.R., 2002. A dominant block to HIV-1 replication at reverse transcription in simian cells. Proceedings of the National Academy of Sciences of the United States of America 99, 13843-13848.

Muranyi, W., Malkusch, S., Muller, B., Heilemann, M., Krausslich, H.G., 2013. Super-resolution microscopy reveals specific recruitment of HIV-1 envelope proteins to viral assembly sites dependent on the envelope C-terminal tail. PLoS pathogens 9, e1003198.

Murray, P.S., Li, Z., Wang, J., Tang, C.L., Honig, B., Murray, D., 2005. Retroviral matrix domains share electrostatic homology: models for membrane binding function throughout the viral life cycle. Structure 13, 1521-1531.

Nabel, G., Baltimore, D., 1987. An inducible transcription factor activates expression of human immunodeficiency virus in T cells. Nature 326, 711-713.

Naldini, L., Blomer, U., Gallay, P., Ory, D., Mulligan, R., Gage, F.H., Verma, I.M., Trono, D., 1996. In vivo gene delivery and stable transduction of nondividing cells by a lentiviral vector. Science 272, 263-267.

Navia, M.A., Fitzgerald, P.M., McKeever, B.M., Leu, C.T., Heimbach, J.C., Herber, W.K., Sigal, I.S., Darke, P.L., Springer, J.P., 1989. Three-dimensional structure of aspartyl protease from human immunodeficiency virus HIV-1. Nature 337, 615-620.

Neil, S.J., Zang, T., Bieniasz, P.D., 2008. Tetherin inhibits retrovirus release and is antagonized by HIV-1 Vpu. Nature 451, 425-430.

Neville, M., Stutz, F., Lee, L., Davis, L.I., Rosbash, M., 1997. The importin-beta family member Crm1p bridges the interaction between Rev and the nuclear pore complex during nuclear export. Current biology : CB 7, 767-775.

Newman, R.M., Hall, L., Kirmaier, A., Pozzi, L.A., Pery, E., Farzan, M., O'Neil, S.P., Johnson, W., 2008. Evolution of a TRIM5-CypA splice isoform in old world monkeys. PLoS pathogens 4, e1000003.

Ni, Z., Olsen, J.B., Guo, X., Zhong, G., Ruan, E.D., Marcon, E., Young, P., Guo, H., Li, J., Moffat, J., Emili, A., Greenblatt, J.F., 2011. Control of the RNA polymerase II phosphorylation state in promoter regions by CTD interaction domain-containing proteins RPRD1A and RPRD1B. Transcription 2, 237-242.

Ni, Z., Xu, C., Guo, X., Hunter, G.O., Kuznetsova, O.V., Tempel, W., Marcon, E., Zhong, G., Guo, H., Kuo, W.H., Li, J., Young, P., Olsen, J.B., Wan, C., Loppnau, P., El Bakkouri, M., Senisterra, G.A., He, H., Huang, H., Sidhu, S.S., Emili, A., Murphy, S., Mosley, A.L., Arrowsmith, C.H., Min, J., Greenblatt, J.F., 2014. RPRD1A and RPRD1B are human RNA polymerase II C-terminal domain scaffolds for Ser5 dephosphorylation. Nature structural & molecular biology 21, 686-695.

Nikolaitchik, O.A., Dilley, K.A., Fu, W., Gorelick, R.J., Tai, S.H., Soheilian, F., Ptak, R.G., Nagashima, K., Pathak, V.K., Hu, W.S., 2013. Dimeric RNA recognition regulates HIV-1 genome packaging. PLoS pathogens 9, e1003249.

Nisole, S., Lynch, C., Stoye, J.P., Yap, M.W., 2004. A Trim5-cyclophilin A fusion protein found in owl monkey kidney cells can restrict HIV-1. Proceedings of the National Academy of Sciences of the United States of America 101, 13324-13328.

Ocwieja, K.E., Brady, T.L., Ronen, K., Huegel, A., Roth, S.L., Schaller, T., James, L.C., Towers, G.J., Young, J.A., Chanda, S.K., Konig, R., Malani, N., Berry, C.C., Bushman, F.D., 2011. HIV integration targeting: a pathway involving Transportin-3 and the nuclear pore protein RanBP2. PLoS pathogens 7, e1001313.

Odaka, T., 1969. Inheritance of susceptibility to Friend mouse leukemia virus. V. Introduction of a gene responsible for susceptibility in the genetic complement of resistant mice. Journal of virology 3, 543-548.

Odaka, T., Yamamoto, T., 1965. Inheritance of susceptibility to Friend mouse leukemia virus. 11. Spleen foci method applied to test the susceptibility of crossbred progeny between a sensitive and a resistant strain. The Japanese journal of experimental medicine 35, 311-314.

Ohishi, M., Nakano, T., Sakuragi, S., Shioda, T., Sano, K., Sakuragi, J., 2011. The relationship between HIV-1 genome RNA dimerization, virion maturation and infectivity. Nucleic acids research 39, 3404-3417.

Ohkura, S., Goldstone, D.C., Yap, M.W., Holden-Dye, K., Taylor, I.A., Stoye, J.P., 2011. Novel escape mutants suggest an extensive TRIM5alpha binding site spanning the entire outer surface of the murine leukemia virus capsid protein. PLoS pathogens 7, e1002011.

Ohkura, S., Stoye, J.P., 2013. A Comparison of Murine Leukemia Viruses That Escape from Human and Rhesus Macaque TRIM5alphas. Journal of virology 87, 6455-6468.

Ohkura, S., Yap, M.W., Sheldon, T., Stoye, J.P., 2006. All three variable regions of the TRIM5alpha B30.2 domain can contribute to the specificity of retrovirus restriction. Journal of virology 80, 8554-8565.

Opstelten, D.J., Wallin, M., Garoff, H., 1998. Moloney murine leukemia virus envelope protein subunits, gp70 and Pr15E, form a stable disulfide-linked complex. Journal of virology 72, 6537-6545.

Oshima, M., Muriaux, D., Mirro, J., Nagashima, K., Dryden, K., Yeager, M., Rein, A., 2004. Effects of blocking individual maturation cleavages in murine leukemia virus gag. Journal of virology 78, 1411-1420.

Paradis, K., Langford, G., Long, Z., Heneine, W., Sandstrom, P., Switzer, W.M., Chapman, L.E., Lockey, C., Onions, D., Otto, E., 1999. Search for cross-species transmission of porcine endogenous retrovirus in patients treated with living pig tissue. The XEN 111 Study Group. Science 285, 1236-1241.

Pasquinelli, A.E., Ernst, R.K., Lund, E., Grimm, C., Zapp, M.L., Rekosh, D., Hammarskjold, M.L., Dahlberg, J.E., 1997. The constitutive transport element (CTE) of Mason-Pfizer monkey virus (MPMV) accesses a cellular mRNA export pathway. The EMBO journal 16, 7500-7510.

Patience, C., Patton, G.S., Takeuchi, Y., Weiss, R.A., McClure, M.O., Rydberg, L., Breimer, M.E., 1998. No evidence of pig DNA or retroviral infection in patients with short-term extracorporeal connection to pig kidneys. Lancet 352, 699-701.

Patience, C., Takeuchi, Y., Weiss, R.A., 1997. Infection of human cells by an endogenous retrovirus of pigs. Nature medicine 3, 282-286.

Paulus, C., Hellebrand, S., Tessmer, U., Wolf, H., Krausslich, H.G., Wagner, R., 1999. Competitive inhibition of human immunodeficiency virus type-1 protease by the Gag-Pol transframe protein. The Journal of biological chemistry 274, 21539-21543.

Payne, L.N., Chubb, R.C., 1968. Studies on the nature and genetic control of an antigen in normal chick embryos which reacts in the COFAL test. The Journal of general virology 3, 379-391.

Perreira, J.M., Chin, C.R., Feeley, E.M., Brass, A.L., 2013. IFITMs restrict the replication of multiple pathogenic viruses. Journal of molecular biology 425, 4937-4955.

Perron, M.J., Stremlau, M., Lee, M., Javanbakht, H., Song, B., Sodroski, J., 2007. The human TRIM5alpha restriction factor mediates accelerated uncoating of the N-tropic murine leukemia virus capsid. Journal of virology 81, 2138-2148.

Perron, M.J., Stremlau, M., Sodroski, J., 2006. Two surface-exposed elements of the B30.2/SPRY domain as potency determinants of N-tropic murine leukemia virus restriction by human TRIM5alpha. Journal of virology 80, 5631-5636.

Perron, M.J., Stremlau, M., Song, B., Ulm, W., Mulligan, R.C., Sodroski, J., 2004. TRIM5alpha mediates the postentry block to N-tropic murine leukemia viruses in human cells. Proceedings of the National Academy of Sciences of the United States of America 101, 11827-11832.

Pertel, T., Hausmann, S., Morger, D., Zuger, S., Guerra, J., Lascano, J., Reinhard, C., Santoni, F.A., Uchil, P.D., Chatel, L., Bisiaux, A., Albert, M.L., Strambio-De-Castillia, C., Mothes, W., Pizzato, M., Grutter, M.G., Luban, J., 2011. TRIM5 is an innate immune sensor for the retrovirus capsid lattice. Nature 472, 361-365.

Pessel-Vivares, L., Ferrer, M., Laine, S., Mougel, M., 2014. MLV requires Tap/NXF1-dependent pathway to export its unspliced RNA to the cytoplasm and to express both spliced and unspliced RNAs. Retrovirology 11, 21.

Peters, G., Harada, F., Dahlberg, J.E., Panet, A., Haseltine, W.A., Baltimore, D., 1977. Low-molecular-weight RNAs of Moloney murine leukemia virus: identification of the primer for RNA-directed DNA synthesis. Journal of virology 21, 1031-1041.

Pettit, S.C., Moody, M.D., Wehbie, R.S., Kaplan, A.H., Nantermet, P.V., Klein, C.A., Swanstrom, R., 1994. The p2 domain of human immunodeficiency virus type 1 Gag regulates sequential proteolytic processing and is required to produce fully infectious virions. Journal of virology 68, 8017-8027.

Pham, Q.T., Veillette, M., Brandariz-Nunez, A., Pawlica, P., Thibert-Lefebvre, C., Chandonnet, N., Diaz-Griffero, F., Berthoux, L., 2013. A novel aminoacid determinant of HIV-1 restriction in the TRIM5alpha variable 1 region isolated in a random mutagenic screen. Virus research 173, 306-314.

Pincus, T., Hartley, J.W., Rowe, W.P., 1971. A major genetic locus affecting resistance to infection with murine leukemia viruses. I. Tissue culture studies of naturally occurring viruses. The Journal of experimental medicine 133, 1219-1233.

Pinter, A., Honnen, W.J., 1988. O-linked glycosylation of retroviral envelope gene products. Journal of virology 62, 1016-1021.

Pinter, A., Kopelman, R., Li, Z., Kayman, S.C., Sanders, D.A., 1997. Localization of the labile disulfide bond between SU and TM of the murine leukemia virus envelope protein complex to a highly conserved CWLC motif in SU that resembles the active-site sequence of thiol-disulfide exchange enzymes. Journal of virology 71, 8073-8077.

Pluta, K., Luce, M.J., Bao, L., Agha-Mohammadi, S., Reiser, J., 2005. Tight control of transgene expression by lentivirus vectors containing second-generation tetracycline-responsive promoters. The journal of gene medicine 7, 803-817.

Poiesz, B.J., Ruscetti, F.W., Gazdar, A.F., Bunn, P.A., Minna, J.D., Gallo, R.C., 1980. Detection and isolation of type C retrovirus particles from fresh and cultured lymphocytes of a patient with cutaneous T-cell lymphoma. Proceedings of the National Academy of Sciences of the United States of America 77, 7415-7419.

Pornillos, O., Ganser-Pornillos, B.K., Banumathi, S., Hua, Y., Yeager, M., 2010. Disulfide bond stabilization of the hexameric capsomer of human immunodeficiency virus. Journal of molecular biology 401, 985-995.

Pornillos, O., Ganser-Pornillos, B.K., Kelly, B.N., Hua, Y., Whitby, F.G., Stout, C.D., Sundquist, W.I., Hill, C.P., Yeager, M., 2009. X-ray structures of the hexameric building block of the HIV capsid. Cell 137, 1282-1292.

Pornillos, O., Ganser-Pornillos, B.K., Yeager, M., 2011. Atomic-level modelling of the HIV capsid. Nature 469, 424-427.

Prats, A.C., De Billy, G., Wang, P., Darlix, J.L., 1989. CUG initiation codon used for the synthesis of a cell surface antigen coded by the murine leukemia virus. Journal of molecular biology 205, 363-372.

Price, A.J., Fletcher, A.J., Schaller, T., Elliott, T., Lee, K., KewalRamani, V.N., Chin, J.W., Towers, G.J., James, L.C., 2012. CPSF6 defines a conserved capsid interface that modulates HIV-1 replication. PLoS pathogens 8, e1002896.

Price, A.J., Marzetta, F., Lammers, M., Ylinen, L.M., Schaller, T., Wilson, S.J., Towers, G.J., James, L.C., 2009. Active site remodeling switches HIV specificity of antiretroviral TRIMCyp. Nature structural & molecular biology 16, 1036-1042.

Prizan-Ravid, A., Elis, E., Laham-Karam, N., Selig, S., Ehrlich, M., Bacharach, E., 2010. The Gag cleavage product, p12, is a functional constituent of the murine leukemia virus pre-integration complex. PLoS pathogens 6, e1001183.

Pryciak, P.M., Varmus, H.E., 1992. Fv-1 restriction and its effects on murine leukemia virus integration in vivo and in vitro. Journal of virology 66, 5959-5966.

Purcell, D.F., Martin, M.A., 1993. Alternative splicing of human immunodeficiency virus type 1 mRNA modulates viral protein expression, replication, and infectivity. Journal of virology 67, 6365-6378.

Qi, C.F., Bonhomme, F., Buckler-White, A., Buckler, C., Orth, A., Lander, M.R., Chattopadhyay, S.K., Morse 3rd, H.C., 1998a. Molecular phylogeny of Fv1. Mammalian genome : official journal of the International Mammalian Genome Society 9, 1049-1055.

Qi, C.F., Bonhomme, F., Buckler-White, A., Buckler, C., Orth, A., Lander, M.R., Chattopadhyay, S.K., Morse, H.C., 3rd, 1998b. Molecular phylogeny of Fv1. Mammalian genome : official journal of the International Mammalian Genome Society 9, 1049-1055.

Rahm, N., Yap, M., Snoeck, J., Zoete, V., Munoz, M., Radespiel, U., Zimmermann, E., Michielin, O., Stoye, J.P., Ciuffi, A., Telenti, A., 2011. Unique spectrum of activity of prosimian TRIM5alpha against exogenous and endogenous retroviruses. Journal of virology 85, 4173-4183.

Rasaiyaah, J., Tan, C.P., Fletcher, A.J., Price, A.J., Blondeau, C., Hilditch, L., Jacques, D.A., Selwood, D.L., James, L.C., Noursadeghi, M., Towers, G.J., 2013. HIV-1 evades innate immune recognition through specific cofactor recruitment. Nature 503, 402-405.

Rasmussen, S., Pedersen, F.S., 2004. Complementarity between RNA dimerization elements favors formation of functional heterozygous murine leukemia viruses. Virology 329, 440-453.

Ratner, L., Haseltine, W., Patarca, R., Livak, K.J., Starcich, B., Josephs, S.F., Doran, E.R., Rafalski, J.A., Whitehorn, E.A., Baumeister, K., et al., 1985. Complete nucleotide sequence of the AIDS virus, HTLV-III. Nature 313, 277-284.

Rein, A., 2010. Nucleic acid chaperone activity of retroviral Gag proteins. RNA biology 7, 700-705.

Rein, A., Kashmiri, S.V., Bassin, R.H., Gerwin, B.L., Duran-Troise, G., 1976. Phenotypic mixing between N- and B-tropic murine leukemia viruses: infectious particles with dual sensitivity to Fv-1 restriction. Cell 7, 373-379.

Rein, A., McClure, M.R., Rice, N.R., Luftig, R.B., Schultz, A.M., 1986. Myristylation site in Pr65gag is essential for virus particle formation by Moloney murine leukemia virus. Proceedings of the National Academy of Sciences of the United States of America 83, 7246-7250.

Rethwilm, A., Bodem, J., 2013. Evolution of foamy viruses: the most ancient of all retroviruses. Viruses 5, 2349-2374.

Reymond, A., Meroni, G., Fantozzi, A., Merla, G., Cairo, S., Luzi, L., Riganelli, D., Zanaria, E., Messali, S., Cainarca, S., Guffanti, A., Minucci, S., Pelicci, P.G., Ballabio, A., 2001. The tripartite motif family identifies cell compartments. The EMBO journal 20, 2140-2151.

Riffel, N., Harlos, K., Iourin, O., Rao, Z., Kingsman, A., Stuart, D., Fry, E., 2002. Atomic resolution structure of Moloney murine leukemia virus matrix protein and its relationship to other retroviral matrix proteins. Structure 10, 1627-1636.

Risco, C., Menendez-Arias, L., Copeland, T.D., Pinto da Silva, P., Oroszlan, S., 1995. Intracellular transport of the murine leukemia virus during acute infection of NIH 3T3 cells: nuclear import of nucleocapsid protein and integrase. Journal of cell science 108 (Pt 9), 3039-3050.

Roe, T., Reynolds, T.C., Yu, G., Brown, P.O., 1993a. Integration of murine leukemia virus DNA depends on mitosis. The EMBO journal 12, 2099-2108.

Roe, T., Reynolds, T.C., Yu, G., Brown, P.O., 1993b. Integration of murine leukemia virus DNA depends on mitosis. EMBO J 12, 2099-2108.

Rold, C.J., Aiken, C., 2008. Proteasomal degradation of TRIM5alpha during retrovirus restriction. PLoS pathogens 4, e1000074.

Rous, P., 1911. A Sarcoma of the Fowl Transmissible by an Agent Separable from the Tumor Cells. The Journal of experimental medicine 13, 397-411.

Rowe, W.P., Sato, H., 1973. Genetic mapping of the Fv-1 lcous of the mouse. Science 180, 640-641.

Rulli, S.J., Jr., Mirro, J., Hill, S.A., Lloyd, P., Gorelick, R.J., Coffin, J.M., Derse, D., Rein, A., 2008. Interactions of murine APOBEC3 and human APOBEC3G with murine leukemia viruses. Journal of virology 82, 6566-6575.

Rustigian, R., Johnston, P., Reihart, H., 1955. Infection of monkey kidney tissue cultures with virus-like agents. Proceedings of the Society for Experimental Biology and Medicine. Society for Experimental Biology and Medicine 88, 8-16.

Saad, J.S., Miller, J., Tai, J., Kim, A., Ghanam, R.H., Summers, M.F., 2006. Structural basis for targeting HIV-1 Gag proteins to the plasma membrane for virus assembly. Proceedings of the National Academy of Sciences of the United States of America 103, 11364-11369.

Saenz, D.T., Teo, W., Olsen, J.C., Poeschla, E.M., 2005. Restriction of feline immunodeficiency virus by Ref1, Lv1, and primate TRIM5alpha proteins. Journal of virology 79, 15175-15188.

Sakuma, T., Davila, J.I., Malcolm, J.A., Kocher, J.P., Tonne, J.M., Ikeda, Y., 2014. Murine leukemia virus uses NXF1 for nuclear export of spliced and unspliced viral transcripts. Journal of virology 88, 4069-4082.

Sakuragi, J., Sakuragi, S., Shioda, T., 2007. Minimal region sufficient for genome dimerization in the human immunodeficiency virus type 1 virion and its potential roles in the early stages of viral replication. Journal of virology 81, 7985-7992.

Salgado, G.F., Marquant, R., Vogel, A., Alves, I.D., Feller, S.E., Morellet, N., Bouaziz, S., 2009. Structural studies of HIV-1 Gag p6ct and its interaction with Vpr determined by solution nuclear magnetic resonance. Biochemistry 48, 2355-2367.

Sanchez, J.G., Okreglicka, K., Chandrasekaran, V., Welker, J.M., Sundquist, W.I., Pornillos, O., 2014. The tripartite motif coiled-coil is an elongated antiparallel hairpin dimer. Proceedings of the National Academy of Sciences of the United States of America 111, 2494-2499.

Saphire, A.C., Bobardt, M.D., Zhang, Z., David, G., Gallay, P.A., 2001. Syndecans serve as attachment receptors for human immunodeficiency virus type 1 on macrophages. Journal of virology 75, 9187-9200.

Sarafianos, S.G., Das, K., Tantillo, C., Clark, A.D., Jr., Ding, J., Whitcomb, J.M., Boyer, P.L., Hughes, S.H., Arnold, E., 2001. Crystal structure of HIV-1 reverse transcriptase in complex with a polypurine tract RNA:DNA. The EMBO journal 20, 1449-1461.

Sastri, J., O'Connor, C., Danielson, C.M., McRaven, M., Perez, P., Diaz-Griffero, F., Campbell, E.M., 2010. Identification of residues within the L2 region of rhesus TRIM5alpha that are required for retroviral restriction and cytoplasmic body localization. Virology 405, 259-266.

Sawyer, S.L., Emerman, M., Malik, H.S., 2004. Ancient adaptive evolution of the primate antiviral DNA-editing enzyme APOBEC3G. PLoS biology 2, E275.

Sawyer, S.L., Wu, L.I., Emerman, M., Malik, H.S., 2005. Positive selection of primate TRIM5alpha identifies a critical species-specific retroviral restriction domain. Proceedings of the National Academy of Sciences of the United States of America 102, 2832-2837.

Sayah, D.M., Sokolskaja, E., Berthoux, L., Luban, J., 2004. Cyclophilin A retrotransposition into TRIM5 explains owl monkey resistance to HIV-1. Nature 430, 569-573.

Schaller, T., Ocwieja, K.E., Rasaiyaah, J., Price, A.J., Brady, T.L., Roth, S.L., Hue, S., Fletcher, A.J., Lee, K., KewalRamani, V.N., Noursadeghi, M., Jenner, R.G., James, L.C., Bushman, F.D., Towers, G.J., 2011. HIV-1 capsid-cyclophilin interactions determine nuclear import pathway, integration targeting and replication efficiency. PLoS pathogens 7, e1002439.

Schaller, T., Ylinen, L.M., Webb, B.L., Singh, S., Towers, G.J., 2007. Fusion of cyclophilin A to Fv1 enables cyclosporine-sensitive restriction of human and feline immunodeficiency viruses. Journal of virology 81, 10055-10063.

Schlesinger, S., Lee, A.H., Wang, G.Z., Green, L., Goff, S.P., 2013. Proviral silencing in embryonic cells is regulated by Yin Yang 1. Cell reports 4, 50-58.

Schmitz, C., Marchant, D., Neil, S.J., Aubin, K., Reuter, S., Dittmar, M.T., McKnight, A., 2004. Lv2, a novel postentry restriction, is mediated by both capsid and envelope. Journal of virology 78, 2006-2016.

Schneider, W.M., Brzezinski, J.D., Aiyer, S., Malani, N., Gyuricza, M., Bushman, F.D., Roth, M.J., 2013. Viral DNA tethering domains complement replication-defective mutations in the p12 protein of MuLV Gag. Proceedings of the National Academy of Sciences of the United States of America 110, 9487-9492.

Schubert, H.L., Zhai, Q., Sandrin, V., Eckert, D.M., Garcia-Maya, M., Saul, L., Sundquist, W.I., Steiner, R.A., Hill, C.P., 2010. Structural and functional studies on the extracellular domain of BST2/tetherin in reduced and oxidized conformations. Proceedings of the National Academy of Sciences of the United States of America 107, 17951-17956.

Schuler, W., Dong, C., Wecker, K., Roques, B.P., 1999. NMR structure of the complex between the zinc finger protein NCp10 of Moloney murine leukemia virus and the single-stranded pentanucleotide d(ACGCC): comparison with HIV-NCp7 complexes. Biochemistry 38, 12984-12994.

Schwartz, S., Felber, B.K., Fenyo, E.M., Pavlakis, G.N., 1990. Env and Vpu proteins of human immunodeficiency virus type 1 are produced from multiple bicistronic mRNAs. Journal of virology 64, 5448-5456.

Schwefel, D., Groom, H.C., Boucherit, V.C., Christodoulou, E., Walker, P.A., Stoye, J.P., Bishop, K.N., Taylor, I.A., 2014. Structural basis of lentiviral subversion of a cellular protein degradation pathway. Nature 505, 234-238.

Scobie, L., Padler-Karavani, V., Le Bas-Bernardet, S., Crossan, C., Blaha, J., Matouskova, M., Hector, R.D., Cozzi, E., Vanhove, B., Charreau, B., Blancho, G., Bourdais, L., Tallacchini, M., Ribes, J.M., Yu, H., Chen, X., Kracikova, J., Broz, L., Hejnar, J., Vesely, P., Takeuchi, Y., Varki, A., Soulillou, J.P., 2013. Long-term IgG response to porcine Neu5Gc antigens without transmission of PERV in burn patients treated with porcine skin xenografts. Journal of immunology 191, 2907-2915.

Sebastian, S., Grutter, C., Strambio de Castillia, C., Pertel, T., Olivari, S., Grutter, M.G., Luban, J., 2009. An invariant surface patch on the TRIM5alpha PRYSPRY domain is required for retroviral restriction but dispensable for capsid binding. Journal of virology 83, 3365-3373.

Sebastian, S., Luban, J., 2005. TRIM5alpha selectively binds a restriction-sensitive retroviral capsid. Retrovirology 2, 40.

Segura-Morales, C., Pescia, C., Chatellard-Causse, C., Sadoul, R., Bertrand, E., Basyuk, E., 2005. Tsg101 and Alix interact with murine leukemia virus Gag and cooperate with Nedd4 ubiquitin ligases during budding. The Journal of biological chemistry 280, 27004-27012.

Serra-Moreno, R., Zimmermann, K., Stern, L.J., Evans, D.T., 2013. Tetherin/BST-2 antagonism by Nef depends on a direct physical interaction between Nef and tetherin, and on clathrin-mediated endocytosis. PLoS pathogens 9, e1003487.

Sette, P., Dussupt, V., Bouamr, F., 2012. Identification of the HIV-1 NC binding interface in Alix Bro1 reveals a role for RNA. Journal of virology 86, 11608-11615.

Sharma, A., Larue, R.C., Plumb, M.R., Malani, N., Male, F., Slaughter, A., Kessl, J.J., Shkriabai, N., Coward, E., Aiyer, S.S., Green, P.L., Wu, L., Roth, M.J., Bushman, F.D., Kvaratskhelia, M., 2013. BET proteins promote efficient murine leukemia virus integration at transcription start sites. Proceedings of the National Academy of Sciences of the United States of America 110, 12036-12041.

Sharp, P.M., Hahn, B.H., 2011. Origins of HIV and the AIDS pandemic. Cold Spring Harbor perspectives in medicine 1, a006841.

Sheehy, A.M., Gaddis, N.C., Choi, J.D., Malim, M.H., 2002. Isolation of a human gene that inhibits HIV-1 infection and is suppressed by the viral Vif protein. Nature 418, 646-650.

Shi, J., Friedman, D.B., Aiken, C., 2013. Retrovirus Restriction by TRIM5 Proteins Requires Recognition of Only a Small Fraction of Viral Capsid Subunits. Journal of virology 87, 9271-9278.

Shibata, R., Kawamura, M., Sakai, H., Hayami, M., Ishimoto, A., Adachi, A., 1991. Generation of a chimeric human and simian immunodeficiency virus infectious to monkey peripheral blood mononuclear cells. Journal of virology 65, 3514-3520.

Shun, M.C., Raghavendra, N.K., Vandegraaff, N., Daigle, J.E., Hughes, S., Kellam, P., Cherepanov, P., Engelman, A., 2007. LEDGF/p75 functions downstream from preintegration complex formation to effect gene-specific HIV-1 integration. Genes & development 21, 1767-1778.

Sironi, M., Biasin, M., Cagliani, R., Gnudi, F., Saulle, I., Ibba, S., Filippi, G., Yahyaei, S., Tresoldi, C., Riva, S., Trabattoni, D., De Gioia, L., Lo Caputo, S., Mazzotta, F., Forni, D., Pontremoli, C., Pineda, J.A., Pozzoli, U., Rivero-Juarez, A., Caruz, A., Clerici, M., 2014. Evolutionary Analysis Identifies an MX2 Haplotype Associated with Natural Resistance to HIV-1 Infection. Molecular biology and evolution 31, 2402-2414.

Sodroski, J.G., Rosen, C.A., Haseltine, W.A., 1984. Trans-acting transcriptional activation of the long terminal repeat of human T lymphotropic viruses in infected cells. Science 225, 381-385.

Solbak, S.M., Reksten, T.R., Hahn, F., Wray, V., Henklein, P., Henklein, P., Halskau, O., Schubert, U., Fossen, T., 2013. HIV-1 p6 - a structured to flexible multifunctional membrane-interacting protein. Biochimica et biophysica acta 1828, 816-823.

Soll, S.J., Wilson, S.J., Kutluay, S.B., Hatziioannou, T., Bieniasz, P.D., 2013. Assisted Evolution Enables HIV-1 to Overcome a High TRIM5alpha-Imposed Genetic Barrier to Rhesus Macaque Tropism. PLoS pathogens 9, e1003667.

Soneoka, Y., Cannon, P.M., Ramsdale, E.E., Griffiths, J.C., Romano, G., Kingsman, S.M., Kingsman, A.J., 1995. A transient three-plasmid expression system for the production of high titer retroviral vectors. Nucleic acids research 23, 628-633.

Song, B., Diaz-Griffero, F., Park, D.H., Rogers, T., Stremlau, M., Sodroski, J., 2005a. TRIM5alpha association with cytoplasmic bodies is not required for antiretroviral activity. Virology 343, 201-211.

Song, B., Gold, B., O'Huigin, C., Javanbakht, H., Li, X., Stremlau, M., Winkler, C., Dean, M., Sodroski, J., 2005b. The B30.2(SPRY) domain of the retroviral restriction factor TRIM5alpha exhibits lineage-specific length and sequence variation in primates. Journal of virology 79, 6111-6121.

Song, B., Javanbakht, H., Perron, M., Park, D.H., Stremlau, M., Sodroski, J., 2005c. Retrovirus restriction by TRIM5alpha variants from Old World and New World primates. Journal of virology 79, 3930-3937.

Spearman, P., Wang, J.J., Vander Heyden, N., Ratner, L., 1994. Identification of human immunodeficiency virus type 1 Gag protein domains essential to membrane binding and particle assembly. Journal of virology 68, 3232-3242.

Steeves, R., Lilly, F., 1977. Interactions between host and viral genomes in mouse leukemia. Annual review of genetics 11, 277-296.

Stevens, A., Bock, M., Ellis, S., LeTissier, P., Bishop, K.N., Yap, M.W., Taylor, W., Stoye, J.P., 2004. Retroviral capsid determinants of Fv1 NB and NR tropism. Journal of virology 78, 9592-9598.

Stoye, J.P., 2012. Studies of endogenous retroviruses reveal a continuing evolutionary saga. Nature reviews. Microbiology 10, 395-406.

Stoye, J.P., Blomberg, J., Coffin, J.M., Fan, H., Hahn, B., Neil, J., Quackenbush, S., Rethwilm, A., Tristem, M., 2011. Retroviridae, in: King, A.M.Q., Adams, M.J., Carstens, E.B., Lefkowitz, E.J. (Eds.), Virus taxonomy: classification and nomemclature of retroviruses: Ninth Report of the International Committee on Taxonomy of Viruses. Elsevier, San Diego, CA, pp. 477-495.

Strack, B., Calistri, A., Craig, S., Popova, E., Gottlinger, H.G., 2003. AIP1/ALIX is a binding partner for HIV-1 p6 and EIAV p9 functioning in virus budding. Cell 114, 689-699.

Stremlau, M., Owens, C.M., Perron, M.J., Kiessling, M., Autissier, P., Sodroski, J., 2004. The cytoplasmic body component TRIM5alpha restricts HIV-1 infection in Old World monkeys. Nature 427, 848-853.

Stremlau, M., Perron, M., Lee, M., Li, Y., Song, B., Javanbakht, H., Diaz-Griffero, F., Anderson, D.J., Sundquist, W.I., Sodroski, J., 2006. Specific recognition and accelerated uncoating of retroviral capsids by the TRIM5alpha restriction factor. Proceedings of the National Academy of Sciences of the United States of America 103, 5514-5519.

Stremlau, M., Perron, M., Welikala, S., Sodroski, J., 2005. Species-specific variation in the B30.2(SPRY) domain of TRIM5alpha determines the potency of human immunodeficiency virus restriction. Journal of virology 79, 3139-3145.

Summers, M.F., Henderson, L.E., Chance, M.R., Bess, J.W., Jr., South, T.L., Blake, P.R., Sagi, I., Perez-Alvarado, G., Sowder, R.C., 3rd, Hare, D.R., et al., 1992. Nucleocapsid zinc fingers detected in retroviruses: EXAFS studies of intact viruses and the solution-state structure of the nucleocapsid protein from HIV-1. Protein science : a publication of the Protein Society 1, 563-574.

Sun, L., Wu, J., Du, F., Chen, X., Chen, Z.J., 2013. Cyclic GMP-AMP synthase is a cytosolic DNA sensor that activates the type I interferon pathway. Science 339, 786-791.

Sun, X., Yau, V.K., Briggs, B.J., Whittaker, G.R., 2005. Role of clathrin-mediated endocytosis during vesicular stomatitis virus entry into host cells. Virology 338, 53-60.

Sundquist, W.I., Krausslich, H.G., 2012. HIV-1 assembly, budding, and maturation. Cold Spring Harbor perspectives in medicine 2, a006924.

Suzuki, Y., Chew, M.L., Suzuki, Y., 2012. Role of host-encoded proteins in restriction of retroviral integration. Frontiers in microbiology 3, 227.

Sveda, M.M., Soeiro, R., 1976. Host restriction of Friend leukemia virus: synthesis and integration of the provirus. Proceedings of the National Academy of Sciences of the United States of America 73, 2356-2360.

Tang, C., Ndassa, Y., Summers, M.F., 2002. Structure of the N-terminal 283-residue fragment of the immature HIV-1 Gag polyprotein. Nature structural biology 9, 537-543.

Temin, H.M., Mizutani, S., 1970. RNA-dependent DNA polymerase in virions of Rous sarcoma virus. Nature 226, 1211-1213.

Thompson, M.R., Sharma, S., Atianand, M., Jensen, S.B., Carpenter, S., Knipe, D.M., Fitzgerald, K.A., Kurt-Jones, E.A., 2014. Interferon Gamma Inducible protein (IFI)16 transcriptionally regulates type I interferons and other interferon stimulated genes and controls the interferon response to both DNA and RNA viruses. The Journal of biological chemistry.

Tipper, C., Sodroski, J.G., 2014. Contribution of glutamine residues in the helix 4-5 loop to capsid-capsid interactions in simian immunodeficiency virus of macaques. Journal of virology 88, 10289-10302.

Tounekti, N., Mougel, M., Roy, C., Marquet, R., Darlix, J.L., Paoletti, J., Ehresmann, B., Ehresmann, C., 1992. Effect of dimerization on the conformation of the encapsidation Psi domain of Moloney murine leukemia virus RNA. Journal of molecular biology 223, 205-220.

Towers, G., Bock, M., Martin, S., Takeuchi, Y., Stoye, J.P., Danos, O., 2000. A conserved mechanism of retrovirus restriction in mammals. Proceedings of the National Academy of Sciences of the United States of America 97, 12295-12299.

Towers, G., Collins, M., Takeuchi, Y., 2002. Abrogation of Ref1 retrovirus restriction in human cells. Journal of virology 76, 2548-2550.

Towers, G.J., Hatziioannou, T., Cowan, S., Goff, S.P., Luban, J., Bieniasz, P.D., 2003. Cyclophilin A modulates the sensitivity of HIV-1 to host restriction factors. Nature medicine 9, 1138-1143.

Towers, G.J., Noursadeghi, M., 2014. Interactions between HIV-1 and the cell-autonomous innate immune system. Cell host & microbe 16, 10-18.

Triezenberg, S.J., Kingsbury, R.C., McKnight, S.L., 1988. Functional dissection of VP16, the trans-activator of herpes simplex virus immediate early gene expression. Genes & development 2, 718-729.

Urlinger, S., Baron, U., Thellmann, M., Hasan, M.T., Bujard, H., Hillen, W., 2000. Exploring the sequence space for tetracycline-dependent transcriptional activators: novel mutations yield expanded range and sensitivity. Proceedings of the National Academy of Sciences of the United States of America 97, 7963-7968.

Vallée, H., Carré, H., 1904. Sur la nature infectieuse de l'anémie du cheval. C. R. Acad. Sci. 139, 331-333.

van der Loo, W., Abrantes, J., Esteves, P.J., 2009. Sharing of endogenous lentiviral gene fragments among leporid lineages separated for more than 12 million years. Journal of virology 83, 2386-2388.

Vaughan, A.E., Mendoza, R., Aranda, R., Battini, J.L., Miller, A.D., 2012. Xpr1 is an atypical G-protein-coupled receptor that mediates xenotropic and polytropic murine retrovirus neurotoxicity. Journal of virology 86, 1661-1669.

Virgen, C.A., Kratovac, Z., Bieniasz, P.D., Hatziioannou, T., 2008. Independent genesis of chimeric TRIM5-cyclophilin proteins in two primate species. Proceedings of the National Academy of Sciences of the United States of America 105, 3563-3568.

Vogt, V.M., 1997. Purification, Composition, and Morphology of Virions, in: Coffin, J.M., Hughes, S.H., Varmus, H.E. (Eds.), Retroviruses. Cold Spring Harbor Laboratory Press, Cold Spring Harbor (NY).

Voisset, C., Weiss, R.A., Griffiths, D.J., 2008. Human RNA "rumor" viruses: the search for novel human retroviruses in chronic disease. Microbiology and molecular biology reviews : MMBR 72, 157-196.

von Schwedler, U.K., Stemmler, T.L., Klishko, V.Y., Li, S., Albertine, K.H., Davis, D.R., Sundquist, W.I., 1998. Proteolytic refolding of the HIV-1 capsid protein amino-terminus facilitates viral core assembly. The EMBO journal 17, 1555-1568.

von Schwedler, U.K., Stray, K.M., Garrus, J.E., Sundquist, W.I., 2003. Functional surfaces of the human immunodeficiency virus type 1 capsid protein. Journal of virology 77, 5439-5450.

Votteler, J., Sundquist, W.I., 2013. Virus budding and the ESCRT pathway. Cell host & microbe 14, 232-241.

Walker, R., 1969. Virus associated with epidermal hyperplasia in fish. National Cancer Institute monograph 31, 195-207.

Walker, S.J., Pizzato, M., Takeuchi, Y., Devereux, S., 2002. Heparin binds to murine leukemia virus and inhibits Env-independent attachment and infection. Journal of virology 76, 6909-6918.

Wallin, M., Ekstrom, M., Garoff, H., 2004. Isomerization of the intersubunit disulphide-bond in Env controls retrovirus fusion. The EMBO journal 23, 54-65.

Weber, I.T., Miller, M., Jaskolski, M., Leis, J., Skalka, A.M., Wlodawer, A., 1989. Molecular modeling of the HIV-1 protease and its substrate binding site. Science 243, 928-931.

Wei, P., Garber, M.E., Fang, S.M., Fischer, W.H., Jones, K.A., 1998. A novel CDK9-associated C-type cyclin interacts directly with HIV-1 Tat and mediates its high-affinity, loop-specific binding to TAR RNA. Cell 92, 451-462.

Weinberg, J.B., Matthews, T.J., Cullen, B.R., Malim, M.H., 1991. Productive human immunodeficiency virus type 1 (HIV-1) infection of nonproliferating human monocytes. The Journal of experimental medicine 174, 1477-1482.

Weiss, R.A., 2006. The discovery of endogenous retroviruses. Retrovirology 3, 67.

White, J.M., Delos, S.E., Brecher, M., Schornberg, K., 2008. Structures and mechanisms of viral membrane fusion proteins: multiple variations on a common theme. Critical reviews in biochemistry and molecular biology 43, 189-219.

Wight, D.J., Boucherit, V.C., Nader, M., Allen, D.J., Taylor, I.A., Bishop, K.N., 2012. The Gammaretroviral p12 protein has multiple domains that function during the early stages of replication. Retrovirology 9, 83.

Wildum, S., Schindler, M., Munch, J., Kirchhoff, F., 2006. Contribution of Vpu, Env, and Nef to CD4 down-modulation and resistance of human immunodeficiency virus type 1-infected T cells to superinfection. Journal of virology 80, 8047-8059.

Wills, N.M., Gesteland, R.F., Atkins, J.F., 1991. Evidence that a downstream pseudoknot is required for translational read-through of the Moloney murine leukemia virus gag stop codon. Proceedings of the National Academy of Sciences of the United States of America 88, 6991-6995.

Wilson-Kubalek, E.M., Chappie, J.S., Arthur, C.P., 2010. Helical crystallization of soluble and membrane binding proteins. Methods in enzymology 481, 45-62.

Wilson, S.J., Webb, B.L., Ylinen, L.M., Verschoor, E., Heeney, J.L., Towers, G.J., 2008. Independent evolution of an antiviral TRIMCyp in rhesus macaques. Proceedings of the National Academy of Sciences of the United States of America 105, 3557-3562.

Wolf, D., Goff, S.P., 2009. Embryonic stem cells use ZFP809 to silence retroviral DNAs. Nature 458, 1201-1204.

Wolf, D., Hug, K., Goff, S.P., 2008. TRIM28 mediates primer binding site-targeted silencing of Lys1,2 tRNA-utilizing retroviruses in embryonic cells. Proceedings of the National Academy of Sciences of the United States of America 105, 12521-12526.

Wolfe, N.D., Heneine, W., Carr, J.K., Garcia, A.D., Shanmugam, V., Tamoufe, U., Torimiro, J.N., Prosser, A.T., Lebreton, M., Mpoudi-Ngole, E., McCutchan, F.E., Birx, D.L., Folks, T.M., Burke, D.S., Switzer, W.M., 2005. Emergence of unique primate T-lymphotropic viruses among central African bushmeat hunters. Proceedings of the National Academy of Sciences of the United States of America 102, 7994-7999.

Woodward, C.L., Prakobwanakit, S., Mosessian, S., Chow, S.A., 2009. Integrase interacts with nucleoporin NUP153 to mediate the nuclear import of human immunodeficiency virus type 1. Journal of virology 83, 6522-6533.

Worthylake, D.K., Wang, H., Yoo, S., Sundquist, W.I., Hill, C.P., 1999. Structures of the HIV-1 capsid protein dimerization domain at 2.6 A resolution. Acta crystallographica. Section D, Biological crystallography 55, 85-92.

Wright, E.R., Schooler, J.B., Ding, H.J., Kieffer, C., Fillmore, C., Sundquist, W.I., Jensen, G.J., 2007. Electron cryotomography of immature HIV-1 virions reveals the structure of the CA and SP1 Gag shells. The EMBO journal 26, 2218-2226.

Wu, J., Matunis, M.J., Kraemer, D., Blobel, G., Coutavas, E., 1995. Nup358, a cytoplasmically exposed nucleoporin with peptide repeats, Ran-GTP binding sites, zinc fingers, a cyclophilin A homologous domain, and a leucine-rich region. The Journal of biological chemistry 270, 14209-14213.

Wu, X., Anderson, J.L., Campbell, E.M., Joseph, A.M., Hope, T.J., 2006. Proteasome inhibitors uncouple rhesus TRIM5alpha restriction of HIV-1 reverse transcription and infection. Proceedings of the National Academy of Sciences of the United States of America 103, 7465-7470.

Wyma, D.J., Jiang, J., Shi, J., Zhou, J., Lineberger, J.E., Miller, M.D., Aiken, C., 2004. Coupling of human immunodeficiency virus type 1 fusion to virion maturation: a novel role of the gp41 cytoplasmic tail. Journal of virology 78, 3429-3435.

Xu, H., Franks, T., Gibson, G., Huber, K., Rahm, N., De Castillia, C.S., Luban, J., Aiken, C., Watkins, S., Sluis-Cremer, N., Ambrose, Z., 2013. Evidence for biphasic uncoating during HIV-1 infection from a novel imaging assay. Retrovirology 10, 70.

Yamashita, M., Emerman, M., 2004. Capsid is a dominant determinant of retrovirus infectivity in nondividing cells. Journal of virology 78, 5670-5678.

Yamauchi, K., Wada, K., Tanji, K., Tanaka, M., Kamitani, T., 2008. Ubiquitination of E3 ubiquitin ligase TRIM5 alpha and its potential role. The FEBS journal 275, 1540-1555.

Yan, N., Regalado-Magdos, A.D., Stiggelbout, B., Lee-Kirsch, M.A., Lieberman, J., 2010. The cytosolic exonuclease TREX1 inhibits the innate immune response to human immunodeficiency virus type 1. Nature immunology 11, 1005-1013.

Yan, Y., Buckler-White, A., Wollenberg, K., Kozak, C.A., 2009. Origin, antiviral function and evidence for positive selection of the gammaretrovirus restriction gene Fv1 in the genus Mus. Proceedings of the National Academy of Sciences of the United States of America 106, 3259-3263.

Yang, H., Ji, X., Zhao, G., Ning, J., Zhao, Q., Aiken, C., Gronenborn, A.M., Zhang, P., Xiong, Y., 2012. Structural insight into HIV-1 capsid recognition by rhesus TRIM5alpha. Proceedings of the National Academy of Sciences of the United States of America 109, 18372-18377.

Yang, H., Wang, J., Jia, X., McNatt, M.W., Zang, T., Pan, B., Meng, W., Wang, H.W., Bieniasz, P.D., Xiong, Y., 2010. Structural insight into the mechanisms of enveloped virus tethering by tetherin. Proceedings of the National Academy of Sciences of the United States of America 107, 18428-18432.

Yang, Y., Brandariz-Nunez, A., Fricke, T., Ivanov, D.N., Sarnak, Z., Diaz-Griffero, F., 2014. Binding of the rhesus TRIM5alpha PRYSPRY domain to capsid is necessary but not sufficient for HIV-1 restriction. Virology 448, 217-228.

Yang, Y., Fricke, T., Diaz-Griffero, F., 2013. Inhibition of reverse transcriptase activity increases stability of the HIV-1 core. Journal of virology 87, 683-687.

Yap, M.W., Colbeck, E., Ellis, S.A., Stoye, J.P., 2014. Evolution of the retroviral restriction gene Fv1: inhibition of non-MLV retroviruses. PLoS pathogens 10, e1003968.

Yap, M.W., Lindemann, D., Stanke, N., Reh, J., Westphal, D., Hanenberg, H., Ohkura, S., Stoye, J.P., 2008. Restriction of foamy viruses by primate Trim5alpha. Journal of virology 82, 5429-5439.

Yap, M.W., Mortuza, G.B., Taylor, I.A., Stoye, J.P., 2007. The design of artificial retroviral restriction factors. Virology 365, 302-314.

Yap, M.W., Nisole, S., Lynch, C., Stoye, J.P., 2004. Trim5alpha protein restricts both HIV-1 and murine leukemia virus. Proceedings of the National Academy of Sciences of the United States of America 101, 10786-10791.

Yap, M.W., Nisole, S., Stoye, J.P., 2005. A single amino acid change in the SPRY domain of human Trim5alpha leads to HIV-1 restriction. Current biology : CB 15, 73-78.

Yap, M.W., Stoye, J.P., 2003. Intracellular localisation of Fv1. Virology 307, 76-89.

Yeager, M., 2011. Design of in vitro symmetric complexes and analysis by hybrid methods reveal mechanisms of HIV capsid assembly. Journal of molecular biology 410, 534-552.

Yeager, M., Wilson-Kubalek, E.M., Weiner, S.G., Brown, P.O., Rein, A., 1998. Supramolecular organization of immature and mature murine leukemia virus revealed by electron cryo-microscopy: implications for retroviral assembly mechanisms. Proceedings of the National Academy of Sciences of the United States of America 95, 7299-7304.

Yee, J.K., Miyanohara, A., LaPorte, P., Bouic, K., Burns, J.C., Friedmann, T., 1994. A general method for the generation of high-titer, pantropic retroviral vectors: highly efficient infection of primary hepatocytes. Proceedings of the National Academy of Sciences of the United States of America 91, 9564-9568.

Yeung, M.L., Houzet, L., Yedavalli, V.S., Jeang, K.T., 2009. A genome-wide short hairpin RNA screening of jurkat T-cells for human proteins contributing to productive HIV-1 replication. The Journal of biological chemistry 284, 19463-19473.

Yokoyama, N., Hayashi, N., Seki, T., Pante, N., Ohba, T., Nishii, K., Kuma, K., Hayashida, T., Miyata, T., Aebi, U., et al., 1995. A giant nucleopore protein that binds Ran/TC4. Nature 376, 184-188.

Yoshinaka, Y., Katoh, I., Copeland, T.D., Oroszlan, S., 1985. Murine leukemia virus protease is encoded by the gag-pol gene and is synthesized through suppression of an amber termination codon. Proceedings of the National Academy of Sciences of the United States of America 82, 1618-1622.

Yu, S.F., von Ruden, T., Kantoff, P.W., Garber, C., Seiberg, M., Ruther, U., Anderson, W.F., Wagner, E.F., Gilboa, E., 1986. Self-inactivating retroviral vectors designed for transfer of whole genes into mammalian cells. Proceedings of the National Academy of Sciences of the United States of America 83, 3194-3198.

Yu, X., Yu, Y., Liu, B., Luo, K., Kong, W., Mao, P., Yu, X.F., 2003. Induction of APOBEC3G ubiquitination and degradation by an HIV-1 Vif-Cul5-SCF complex. Science 302, 1056-1060.

Yuan, B., Campbell, S., Bacharach, E., Rein, A., Goff, S.P., 2000. Infectivity of Moloney murine leukemia virus defective in late assembly events is restored by late assembly domains of other retroviruses. Journal of virology 74, 7250-7260.

Yuan, B., Li, X., Goff, S.P., 1999. Mutations altering the moloney murine leukemia virus p12 Gag protein affect virion production and early events of the virus life cycle. The EMBO journal 18, 4700-4710.

Zhang, C., de Silva, S., Wang, J.H., Wu, L., 2012a. Co-evolution of primate SAMHD1 and lentivirus Vpx leads to the loss of the vpx gene in HIV-1 ancestor. PloS one 7, e37477.

Zhang, F., Zang, T., Wilson, S.J., Johnson, M.C., Bieniasz, P.D., 2011. Clathrin facilitates the morphogenesis of retrovirus particles. PLoS pathogens 7, e1002119.

Zhang, G., Gurtu, V., Kain, S.R., 1996. An enhanced green fluorescent protein allows sensitive detection of gene transfer in mammalian cells. Biochemical and biophysical research communications 227, 707-711.

Zhang, Z., Harrison, P.M., Liu, Y., Gerstein, M., 2003. Millions of years of evolution preserved: a comprehensive catalog of the processed pseudogenes in the human genome. Genome research 13, 2541-2558.

Zhang, Z., Liu, J., Li, M., Yang, H., Zhang, C., 2012b. Evolutionary dynamics of the interferon-induced transmembrane gene family in vertebrates. PloS one 7, e49265.

Zhao, G., Ke, D., Vu, T., Ahn, J., Shah, V.B., Yang, R., Aiken, C., Charlton, L.M., Gronenborn, A.M., Zhang, P., 2011. Rhesus TRIM5alpha disrupts the HIV-1 capsid at the inter-hexamer interfaces. PLoS pathogens 7, e1002009.

Zhao, G., Perilla, J.R., Yufenyuy, E.L., Meng, X., Chen, B., Ning, J., Ahn, J., Gronenborn, A.M., Schulten, K., Aiken, C., Zhang, P., 2013. Mature HIV-1 capsid structure by cryo-electron microscopy and all-atom molecular dynamics. Nature 497, 643-646.

Zhou, H., Xu, M., Huang, Q., Gates, A.T., Zhang, X.D., Castle, J.C., Stec, E., Ferrer, M., Strulovici, B., Hazuda, D.J., Espeseth, A.S., 2008. Genome-scale RNAi screen for host factors required for HIV replication. Cell host & microbe 4, 495-504.

Zhou, X., Vink, M., Klaver, B., Berkhout, B., Das, A.T., 2006. Optimization of the Tet-On system for regulated gene expression through viral evolution. Gene therapy 13, 1382-1390.

Zhu, H., Jian, H., Zhao, L.J., 2004. Identification of the 15FRFG domain in HIV-1 Gag p6 essential for Vpr packaging into the virion. Retrovirology 1, 26.

Zuber, G., McDermott, J., Karanjia, S., Zhao, W., Schmid, M.F., Barklis, E., 2000. Assembly of retrovirus capsid-nucleocapsid proteins in the presence of membranes or RNA. Journal of virology 74, 7431-7441.

Zybarth, G., Carter, C., 1995. Domains upstream of the protease (PR) in human immunodeficiency virus type 1 Gag-Pol influence PR autoprocessing. Journal of virology 69, 3878-3884.